J/ψ DECAYS

L. KÖPKE and N. WERMES

CERN, CH-1211 Geneva 23, Switzerland

NORTH-HOLLAND – AMSTERDAM

PHYSICS REPORTS (Review Section of Physics Letters) 174, Nos. 2 & 3 (1989) 67–227. North-Holland, Amsterdam

J/ψ DECAYS

L. KÖPKE and N. WERMES

CERN, CH-1211 Geneva 23, Switzerland

Received August 1988

Contents:

Abstract:

A total of nearly 20 million J/ψ decays have been analysed by various experiments that have operated at the J/ψ energy in e^+e^- storage rings. Their results are comprehensively reviewed in this report. Special emphasis is given to the aspect of gluon bound states, which are believed to be copiously produced in radiative decays of the J/ψ. A key feature to the understanding of the different candidate states is the systematic comparison of radiative and non-radiative J/ψ decays. It is argued that excellent candidates for 0^{-+} and 2^{++} gluonium states exist. A brief outlook to the future of J/ψ physics expected at the BEPC storage ring in China is given in the summary.

Single orders for this issue

PHYSICS REPORTS (Review Section of Physics Letters) 174, Nos. 2 & 3 (1989) 67–227.

Copies of this issue may be obtained at the price given below. All orders should be sent directly to the Publisher. Orders must be accompanied by check.

Single issue price Dfl. 121.00, postage included.

1. Introduction

1.1. The discovery of the J/ψ

A fourth quark named "charm" was proposed by Bjorken and Glashow [1] in 1964 following the ideas of the "eightfold way" by Gell-Mann and Ne'eman [2]. The concept of the charm quark then found its first real application in the 1970 paper by Glashow, Iliopoulos and Maiani [3], providing a mechanism to explain the suppression of strangeness changing neutral currents. The mass of the c quark was suggested by Gaillard and Lee [4] to be in the region of 1–2 GeV by calculating the rate for the process $K_L^0 \to \mu\mu$.

In the so-called "November Revolution of Particle Physics" [5] the 1^{--} ground state of the charmonium family, the J/ψ particle, was discovered at Brookhaven [6] and SLAC [7] in 1974. At Brookhaven a narrow resonance at 3.1 GeV was observed in the e^+e^- invariant mass spectrum of

$$p + Be \to e^+e^- + X, \tag{1}$$

whereas at the e^+e^- storage ring SPEAR at SLAC the same resonance was seen in the reactions

$$e^+e^- \to \text{hadrons}, \ \mu^+\mu^-, \text{ and } e^+e^- . \tag{2}$$

Figure 1 shows the signals for the J/ψ as observed in reactions (1) and (2), respectively. The MIT–BNL

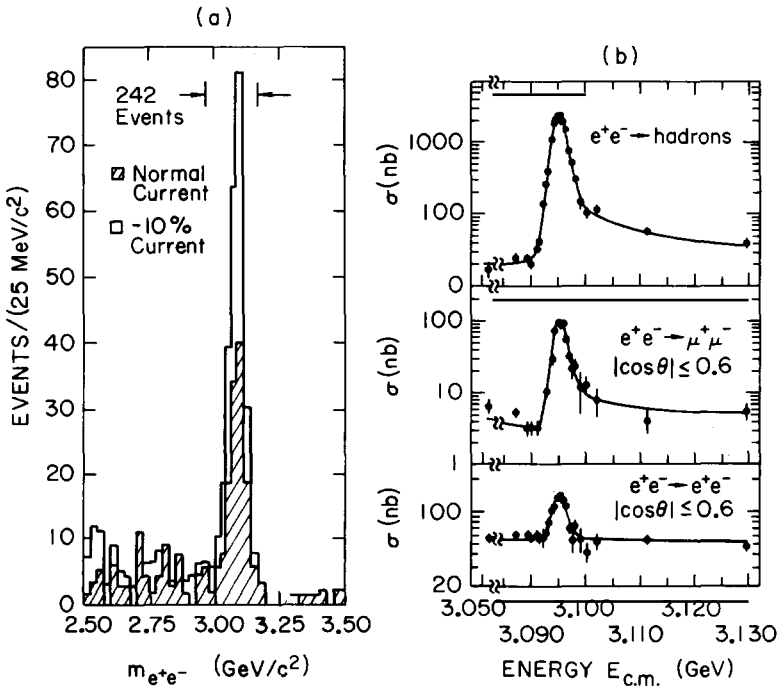

Fig. 1. Discovery of the J/ψ particle at BNL and at SLAC. (a) J discovery at BNL, showing the e^+e^- invariant mass distribution of the reaction $p + Be \to e^+e^- + X$. The unshaded area is the result after a deliberate 10% shift in the spectrometer momentum [6]. (b) ψ discovery at SLAC. A very strong rise of the cross sections for hadron, μμ, and e^+e^- final states is observed [7].

group at Brookhaven used an extremely intense beam of $\sim 10^{12}$ protons/pulse at $\sqrt{s} = 7.6$ GeV and observed the J as a narrow peak at 3.1 GeV in the e^+e^- invariant mass.

The SLAC–LBL Collaboration observed an enormous increase in the cross section for multihadron, e^+e^-, and $\mu\mu$ production. This finding was confirmed [8, 9] immediately afterwards at the ADONE and DORIS storage rings.

The most surprising feature of this resonance, apart from its enormous cross section ($\int \sigma(E)\,dE \approx 12\,\mu b\,MeV$), is its small decay width (74 ± 8 keV),*) which indicates that decays of the J/ψ to lighter hadrons are suppressed. The determination of the J/ψ resonance parameters and quantum numbers is described in chapter 4.

Soon after the discovery of the J/ψ(3100), first the ψ'(3685) [10] and then a complete family of $c\bar{c}$ states [11], very similar to the energy levels of positronium, were observed. The charmonium family, as it is known today, is shown in fig. 2.

The reason for the extremely small decay width of the J/ψ is very relevant to this report. It is usually referred to by the phenomenological OZI (Okubo–Zweig–Iizuka) rule [12], which states that processes in which the initial quark pairs cannot appear as part of the final state particles are suppressed. Or, stated more simply, processes with "detached" quark lines are suppressed. The meaning of this rule is graphically depicted in fig. 3 for decays of the φ(1020) and the J/ψ. The decay of the J/ψ is hindered because it is too light to decay into mesons which contain a c quark (D or D_s mesons).

Within the framework of QCD, OZI suppression is described in terms of the annihilation of quark lines into hard gluons. The Zweig rule violating processes are of higher order in the (small) quark–gluon coupling $\alpha_s(Q^2)$ and are therefore suppressed. The J/ψ decay diagrams are shown in figs. 4a and c classifying the decays of the J/ψ into non-radiative (direct) hadronic decays and radiative decays into hadrons. The strength of the OZI suppression puts the electromagnetic decay rate (fig. 4b) into the same order of magnitude as its strong decay rate—a remarkable situation for a meson with a mass around 3 GeV.

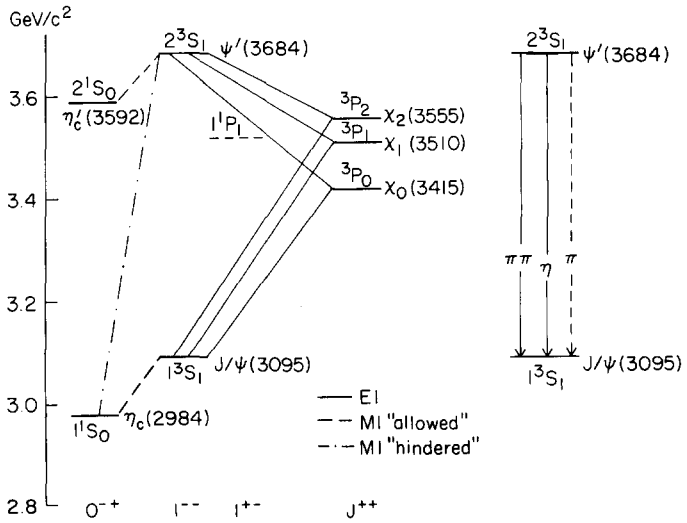

Fig. 2. The charmonium family. Shown are the observed charmonium levels below charm threshold and the transitions between them.

*) This value [23, 24] is different from the one quoted by the Particle Data Group [14] (see also sections 2.1 and 4.1).

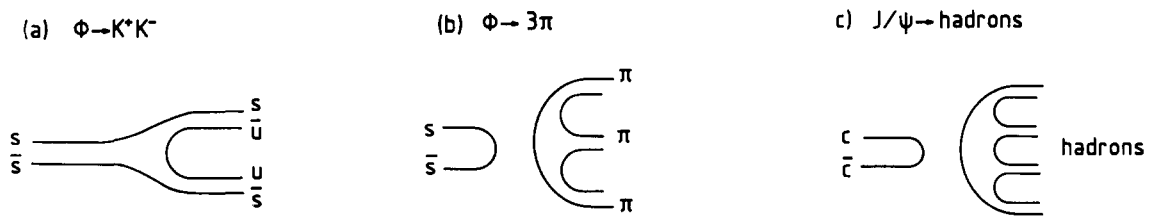

Fig. 3. OZI allowed and forbidden decays. Diagrams of $\phi(1020)$ and J/ψ decays which are (a) OZI allowed and (b), (c) OZI suppressed.

Although the J/ψ was discovered almost 15 years ago and its decays have been studied ever since, experiments operating at the J/ψ still attract both experimentalists and theorists due to the unique constellations of this resonance. The attention given to the study of J/ψ decays received an additional impetus in recent years due to the possibility of finding bound states of gluons (glueballs, gluonia) in radiative decays of the J/ψ. This question has been addressed in studies using large-statistics data samples in the so-called "second- or third-generation" experiments such as Crystal Ball and Mark III at SPEAR or DM2 at DCI/Orsay.

If the gluons of fig. 4c form a bound state, a resonance peak in the energy distribution of the inclusive photon or in the final state hadron invariant mass distribution should be observed. Since the gluons can, in principle, form a glueball at any mass between 0 and M_ψ, the radiative decay process is ideal to scan the predicted glueball mass spectrum (see section 2.4) and to search for glueball candidates. In this vein the hadronic and electromagnetic J/ψ decays have regained attention because, together with the observations in radiative decays, they provide additional information about the quark/glue nature of a glueball candidate resonance.

Data on J/ψ decays are available since 1974. The authors of this report do not intend to review in full detail all the data and the analysis results that have been published by the various experiments since then and have already been previously reviewed [13]. Instead, wherever possible, the more recent results are given priority over older publications unless different experiments come to contradicting or inconsistent conclusions. Also, whenever new discoveries are reported, the original publication will be referenced.

The emphasis of this report is on reviewing the data which have a strong connection to the physics of glueballs. The studies which were very important to establish the nature of the J/ψ particle and which are reviewed in great detail elsewhere [13] are treated here only briefly.

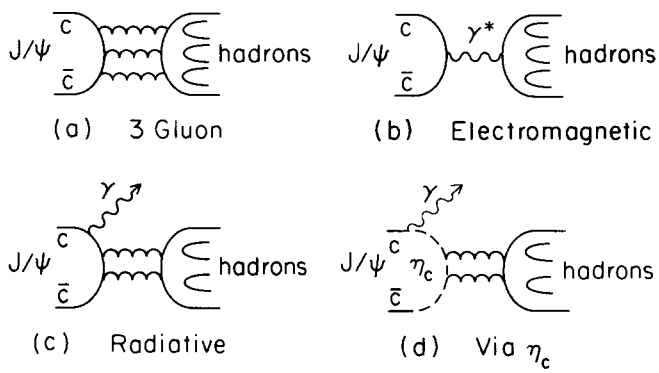

Fig. 4. J/ψ decays into hadrons in lowest order. (a) The hadronic decay, (b) the electromagnetic decay, (c) the radiative decay into hadrons, and (d) the radiative M1 transition to the η_c.

1.2. Organization of the paper

In chapter 2 some basic concepts on the physics of J/ψ decays are recalled and an introduction to the spectroscopy of $q\bar{q}$ states, gluonia, and other exotic phenomena is given. The experiments which have operated at the J/ψ energy in e^+e^- storage rings are introduced in chapter 3 and some techniques to analyse the data are discussed. After a brief review on J/ψ resonance parameters in chapter 4, the wealth of experimental data on the decays of the J/ψ is reviewed, in chapter 5 for the non-radiative decays and in chapter 6 for the radiative decays. Because the question of the existence of gluonic bound states is extremely relevant to the experimental program of J/ψ decays, chapter 7 is specifically devoted to this topic by confronting the "glueball phenomenology" with the available experimental information. Chapter 7 also includes comparisons and connections with the results from other reactions such as γγ collisions or hadroproduction. Finally, a summary and an outlook into the future of the still continuing analyses of J/ψ decays is presented in chapter 8.

A word should be said on the use of particle names in this report. We adopt the naming convention proposed by the Particle Data Group [14] in 1986. Although this is an obviously cogent choice it can lead to some confusion in the context of the new resonances "iota"/η(1440) and "theta"/f_2(1720). We have therefore taken the liberty to also refer to these states as "iota" and "theta", respectively, whenever it seems appropriate to distinguish them from standard quark-based states.

2. The physics of J/ψ decays

2.1. J/ψ decay mechanisms

The lowest-order diagrams for the decays of the J/ψ are shown in fig. 4, representing (a) the hadronic decay via $c\bar{c}$ annihilation into three gluons, (b) the electromagnetic decay via $c\bar{c}$ annihilation to a virtual photon, (c) the radiative J/ψ decay with $c\bar{c}$ annihilation into a photon and two gluons, and (d) the magnetic dipole transition to the $c\bar{c}$ $^1S_0$ state $\eta_c(2980)$. The decay rates are readily calculated in perturbative QCD using lowest-order expressions [15] and first-order QCD corrections [16–18, 20].

The choice of Q^2 at which to evaluate α_s is to some extent arbitrary. In the literature one commonly finds the use of $Q^2 = M_\psi^2$ [17] or $Q^2 = m_c^2$ [18]. Brodsky, Lepage, and Mackenzie [19] have argued for a particular choice which absorbs the dependence on the number of light quark flavours, n_f, into the lowest-order α_s term. The particular choice of the Q^2 scale does not affect the corrections to the electromagnetic processes like $J/\psi \to \mu\mu$ or 3γ. The rates that depend on α_s to lowest order are, however, affected. Predictions for ratios of rates are expected to be more reliable than individual predictions involving $|\Psi(0)|^2$ [17]. In this chapter we shall use the first-order corrections evaluated at $Q^2 = M_\psi^2$ following ref. [17].

Starting with the Van Royen–Weisskopf formula [21] for the *electromagnetic decay into leptons* one finds, neglecting lepton mass effects [20, 21]

$$\Gamma(J/\psi \to \ell^+\ell^-) = \tfrac{16}{3}\pi\alpha^2 e_c^2 N_c \frac{|\Psi(0)|^2}{M_\psi^2}\left(1 - \tfrac{16}{3}\alpha_s/\pi\right), \tag{3}$$

where e_c is the charm quark charge, N_c the number of colours, and $\Psi(0)$ the value of the radial wave

function at the J/ψ origin. M_ψ is the J/ψ mass and α_s is the strong coupling constant evaluated at $Q^2 = M_\psi^2$. Note that in the literature one often finds the convention $|R(0)|^2 = 4\pi|\Psi(0)|^2$.

The three-gluon decay width (fig. 4a) can be calculated [15] in close analogy to the 3γ decay of orthopositronium, for which the decay rate [22] is given by

$$\Gamma(^1S_0 \to 3\gamma) = \tfrac{16}{9}(\pi^2 - 9)\alpha^3 e_c^6 N_c \frac{|\Psi(0)|^2}{m_c^2}(1 - 12.6\alpha_s/\pi), \tag{4}$$

where $m_c \approx M_\psi/2$ is the charm quark mass.

The prescription to obtain the lowest-order part of the formula for the *three-gluon decay* of the J/ψ is obtained substituting

$$\alpha^3 e_c^6 N_c \to \tfrac{5}{18}\alpha_s^3 . \tag{5}$$

Including the first-order corrections [16] one obtains

$$\Gamma(J/\psi \to ggg) = \tfrac{40}{81}(\pi^2 - 9)\alpha_s^3 \frac{|\Psi(0)|^2}{m_c^2}(1 + 4.9\alpha_s/\pi) . \tag{6}$$

Substituting (3) into (6), together with a proper treatment of the first-order terms, results in [17–19]

$$\Gamma(J/\psi \to ggg) = \frac{5}{18\pi}(\pi^2 - 9)\frac{\alpha_s^3}{\alpha^2}\Gamma(J/\psi \to \ell^+\ell^-)(1 + 10.3\alpha_s/\pi) \approx 48\,\text{keV} , \tag{7}$$

using the experimental value*) of $\Gamma(J/\psi \to \ell^+\ell^-) = (5.1 \pm 0.3)$ keV [23, 99] and $\alpha_s = 0.16$ (see chapter 6). Equation (7) represents the hadronic decay width of the J/ψ to first order if one assumes that the gluons couple to the final state hadrons with unit probability. Note that the first-order correction corresponds to a sizeable fraction of the total rate.

The *electromagnetic decay* width for an individual quark pair (fig. 4b) is identical to (3) when one corrects for the quark charge and neglects quark mass effects [15]. Summing over u, d and s this results into

$$\Gamma_{elm}(J/\psi \to q\bar{q}) = 3\sum e_q^2 \cdot \Gamma(J/\psi \to \ell^+\ell^-) = (10.2 \pm 0.6)\,\text{keV} . \tag{8}$$

Alternatively one finds

$$\Gamma_{elm}(J/\psi \to \text{hadrons}) = R(\text{off-resonance})\Gamma(J/\psi \to e^+e^-) = (13.2 \pm 1.1)\,\text{keV} , \tag{9}$$

where [25] R(off-resonance) $= (2.59 \pm 0.15 \pm 0.08)$ is the ratio of hadronic and μμ cross sections, $\sigma_{had}/\sigma_{\mu\mu}$, at 3 GeV. Compared to the total width of the J/ψ, 13 keV is a very large width for an electromagnetic transition. This is due to the strong suppression of the three-gluon hadronic decay as a consequence of the OZI rule.

*) A better understanding of QED radiative corrections has recently led to a modification of the J/ψ resonance parameters [23, 24, 99] (see also section 5.2.2).

The *radiative width* (fig. 4c) in first-order QCD is proportional to $\alpha_s^2\alpha$,

$$\Gamma(J/\psi\to\gamma gg) = \tfrac{32}{9}(\pi^2-9)\alpha_s^2\alpha e_c^2\,\frac{|\Psi(0)|^2}{m_c^2}\,(1-0.9\alpha_s/\pi)\,, \tag{10}$$

assuming on-shell gluons [15–18]. The ratio of the radiative decay to the three-gluon decay of the J/ψ is

$$\frac{\Gamma(J/\psi\to\gamma gg)}{\Gamma(J/\psi\to ggg)} = \tfrac{16}{5}(\alpha/\alpha_s)(1-5.8\alpha_s/\pi)\approx 10.3\%\,. \tag{11}$$

With (7) we find

$$\Gamma(J/\psi\to\gamma gg)\approx 5\,\text{keV}\,. \tag{12}$$

Finally, the *transition to the* $\eta_c(2980)$ (fig. 4d) has been measured by the Crystal Ball experiment [26] using the inclusive photon spectrum. The partial decay width is

$$\Gamma(J/\psi\to\gamma\eta_c) = (940\pm 285)\,\text{eV}\,, \tag{13}$$

corresponding to a branching fraction [26] of $(1.27\pm 0.36)\%$.

Summarizing, we note that the decay modes of the J/ψ into hadrons, calculated including first-order corrections, roughly contribute the fractions

$$\frac{\Gamma_{had}}{\Gamma_{non\text{-}lept}} : \frac{\Gamma_{elm}}{\Gamma_{non\text{-}lept}} : \frac{\Gamma_{rad}}{\Gamma_{non\text{-}lept}} : \frac{\Gamma_{\eta_c}}{\Gamma_{non\text{-}lept}} \approx 75\% : 16\% : 8\% : 1\% \tag{14}$$

to the non-leptonic decay width into hadrons. The total non-leptonic width is $(63.8\pm 9.0)\,\text{keV} = (74\pm 8)\,\text{keV} - \Gamma_{ee,\mu\mu}$ [23, 99]. Electromagnetic and radiative decays are thus only suppressed by factors of about 5 to 10 with respect to the hadronic decays and not by several orders of magnitude as one would naively expect on the basis of the coupling constant ratios.

2.2. *Light-quark meson spectroscopy at the* J/ψ

The spin 1/2 quarks and antiquarks lie in **6** and $\bar{\mathbf{6}}$ representations of SU(6) (u, d, s quarks, two spin states). For a $q\bar{q}$ meson the SU(6) representations are

$$\mathbf{6}\otimes\bar{\mathbf{6}} = \mathbf{1}\oplus\mathbf{35}\,. \tag{15}$$

Decomposing the SU(6) representations **1** and **35** into $SU(3)_{flavour}$ and $SU(3)_{spin}$ representations, one finds the results of table 1. The ground state $q\bar{q}$ mesons (u, d, s) are assigned to places in these irreducible representations. In addition there exist radial and orbital excitations for each representation.

Let us consider, for example, the ground state $q\bar{q}$ mesons with no orbital angular momentum (s wave), which form the pseudoscalar and the vector mesons. The classification is shown in table 2. The $SU(3)_{flavour}$ singlet eigenstates η_1, η_8 and ω_1, ω_8 frequently mix to become the physical mesons (mass eigenstates). For the vector mesons, as for most SU(3) representations, this mixing is almost ideal, i.e.,

Table 1
SU(6) decomposition into $SU(3)_{flavour}$ and $SU(3)_{spin}$ multiplets. For the spin part the notation $2s+1$, where s is the quark spin, is used.

SU(6)	(SU(3),2s + 1)
1	(1, 1)
35	(8, 1), (8, 3), (1, 3)

Table 2
Classification of the ground state mesons.

(SU(3),2s + 1)	$SU(2)_{flavour}$	peudoscalar mesons	vector mesons	quark flavour decomposition
(1, 1), (1, 3)	1	η_1	ω_1	$(u\bar{u}+d\bar{d}+s\bar{s})/\sqrt{3}$
(8, 1), (8, 3)	3	π^+, π^0, π^-	ρ^+, ρ^0, ρ^-	$u\bar{d}$, $(u\bar{u}+d\bar{d})/\sqrt{2}$
	2	K^+, K^0	K^{*+}, K^{*0}	$u\bar{s}$, $d\bar{s}$
	2	$\bar{K}^0, K^-$	$\bar{K}^{*0}, K^{*-}$	$s\bar{d}$, $s\bar{u}$
	1	η_8	ω_8	$(u\bar{u}+d\bar{d}-2s\bar{s})/\sqrt{6}$

the mass eigenstates are (almost) diagonal in the quark flavour. Because of this it is common to group the mesons into nonets, rather than octets and singlets. One should note, however, that the pseudoscalar nonet is *not* ideally mixed.

A common notation in terms of SU(2) representations is (*triplet*, *singlet*, *singlet*, *doublet*). Thus the pseudoscalar nonet will be denoted (π, η, η', K), the vector nonet will read (ρ, ω, ϕ, K*(892)), and the tensor meson nonet with orbital angular momentum $L=1$ (p wave) is ($a_2(1320)$, $f_2(1270)$, $f_2'(1525)$, $K_2^*(1430)$).

The assignment of experimentally observed states to this scheme is done in fig. 5, showing the orbital and radial quantum numbers of $q\bar{q}$ states. Note that the parity, P, and charge conjugation, C, of $q\bar{q}$ states are given by $P=(-1)^{l+1}$ and $C=(-1)^{l+s}$.

2.3. *SU*(3) *and Zweig's rule*

The quark flavour symmetry group that is explicitly tested in J/ψ decays is $SU(3)_{flavour}$. Since the J/ψ is a $c\bar{c}$ bound state it behaves as a singlet with respect to a symmetry of three quark flavours.

A very important rule can be derived from charge conjugation invariance (C) applied to the different meson nonets. Under C, a meson nonet N^α transforms [27] as $N^\alpha \rightarrow \mathscr{C}\varepsilon^\alpha N^\alpha$ (no sum over α), where $\mathscr{C}$ is the C parity of N^3, the centre member of the nonet (the π^0-like state), $\varepsilon^2=\varepsilon^5=\varepsilon^7=-1$, and all other $\varepsilon^\alpha=+1$. We shall regard $\mathscr{C}$ as the C parity of the nonet. Since the J/ψ has $C=-1$, $\mathscr{C}$ invariance implies that the two nonets (octets, singlets) to which it can decay must have opposite $\mathscr{C}$ parity. Of course, this rule only holds in the SU(3) symmetry limit. As an example, the decay $J/\psi \rightarrow \pi^0\pi^0$ is explicitly forbidden by C parity, while $J/\psi \rightarrow K^0\bar{K}^0$ is forbidden by $\mathscr{C}$ only in the SU(3) symmetric limit. Table 3 shows which multiplet combinations are allowed or forbidden by $\mathscr{C}$ invariance.

Table 3
Selection rules for J/ψ and η_c decays under generalized C parity. S, P, V, T denote Scalar, Pseudoscalar, Vector and Tensor meson multiplets, respectively. A^+ and A^- denote the two axial vector nonets with opposite $\mathscr{C}$ parity. For three-particle final states only one example is given. "Yes" refers to allowed and "–" refers to forbidden decays.

Decay	PP	PS	PV	PT	SS	SV	ST	VV	VT	TT	PPP
$J/\psi \rightarrow X$	–	–	yes	–	–	yes	–	–	yes	–	–
$J/\psi \rightarrow \gamma X$	yes	yes	–	yes	yes	–	yes	yes	–	yes	yes
$\eta_c \rightarrow X$	yes	yes	–	yes	yes	–	yes	yes	–	yes	yes

Decay	PA^+	PA^-	SA^+	SA^-	VA^+	VA^-	TA^+	TA^-	A^+A^+	A^-A^-	A^+A^-
$J/\psi \rightarrow X$	yes	–	–	yes	yes	–	–	yes	–	–	yes
$J/\psi \rightarrow \gamma X$	–	yes	yes	–	–	yes	yes	–	yes	yes	–
$\eta_c \rightarrow X$	–	yes	yes	–	–	yes	yes	–	yes	yes	–

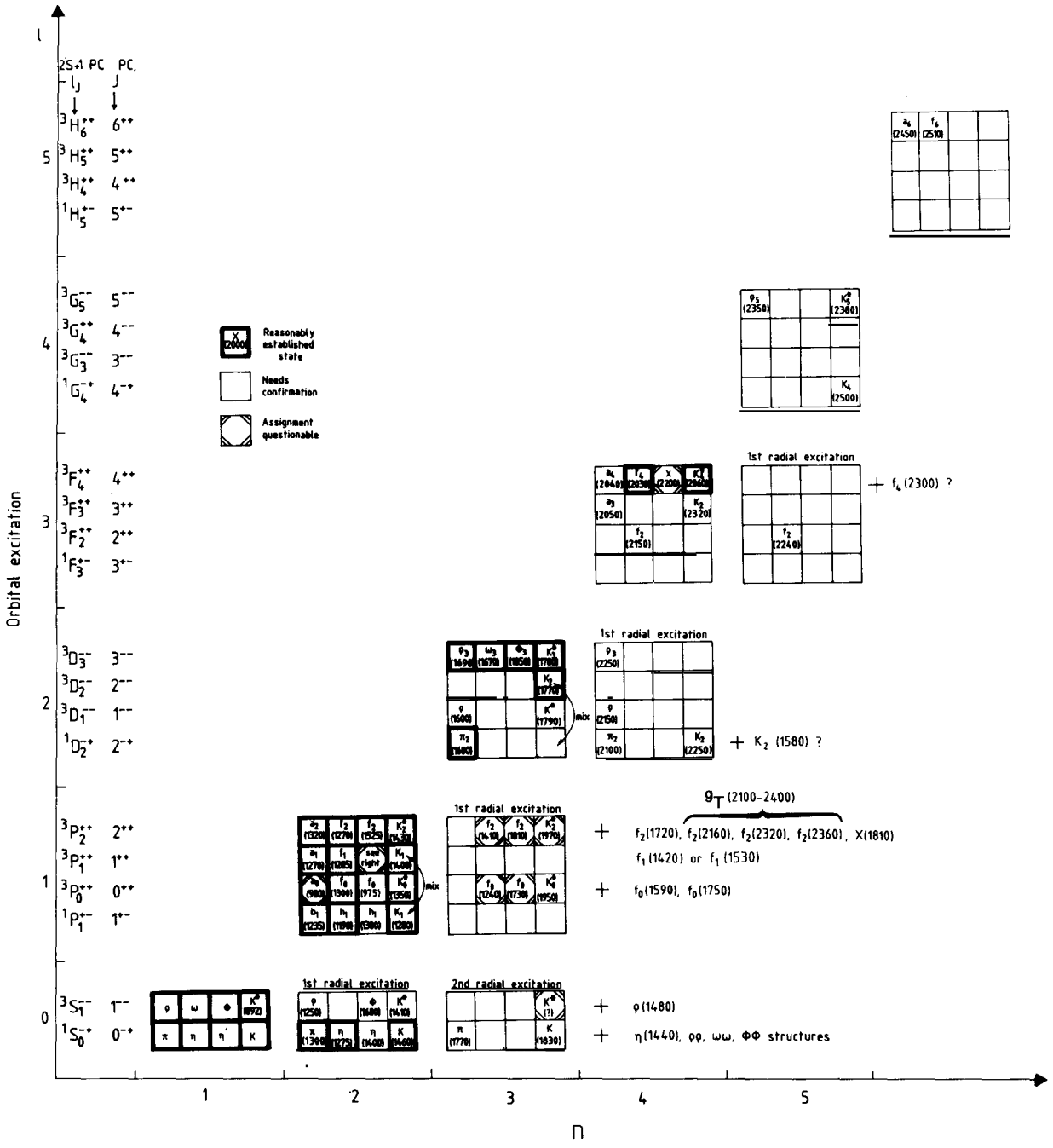

Fig. 5. The present experimental knowledge of $q\bar{q}$ states.

Of course, the same rule can be applied to radiative J/ψ decays and to hadronic decays of the η_c. Here the η_c or the system X recoiling against the radiative photon have $C = +1$. This requires that the decay products come from nonets with the same $\mathscr{C}$.

This rule is valid only in the SU(3) symmetry limit, and SU(3) breaking effects as well as the OZI rule spoil the strict predictions of table 3. On the other hand, one can determine the amount of SU(3) breaking from the measured branching fractions (see section 5.3.1). To give an example how strong this suppression can be, one may compare the ratios

$$\frac{B(J/\psi \to K^+K^-)}{\frac{1}{2}B(J/\psi \to K^{*+}K^- + \text{c.c.})} = \frac{(2.36 \pm 0.30) \times 10^{-4}}{(2.58 \pm 0.22) \times 10^{-3}} \approx \frac{1}{11}, \tag{16}$$

$$\frac{B(J/\psi \to \rho^+\rho^-)}{B(J/\psi \to \omega f_2(1270))} = \frac{(9.4 \pm 1.8) \times 10^{-4}}{(4.15 \pm 0.51) \times 10^{-3}} \approx \frac{1}{5}. \tag{17}$$

The production of isovector states in radiative J/ψ decays is strongly suppressed because the two gluons emitted from the $c\bar{c}$ quark line (fig. 4c) form a singlet in SU(3) and isospin is a conserved quantum number in hadronic interactions. Radiative decays to isovectors arise from a process where the photon is radiated from a final state quark line.

Implications of Zweig's rule. Apart from explaining the narrowness of the J/ψ, the OZI rule [12] plays an important role in the evaluation of hadronic J/ψ decays. Although all of the hadronic decays of the J/ψ are singly OZI suppressed (cf. fig. 4a), some decays suffer yet another OZI suppression in the formation of the final state quarks. This is demonstrated in fig. 6.

The decays $J/\psi \to \omega f_2'(1525)$ or $J/\psi \to \phi f_2(1270)$ are doubly OZI suppressed as compared to $J/\psi \to \omega f_2(1270)$ or $J/\psi \to \phi f_2'(1525)$ because they require disconnected quark lines in the final state, too.

Experimentally one observes (see table 17 in section 5.3.4)

$$\frac{J/\psi \to \omega f_2'(1525)}{J/\psi \to \omega f_2(1270)} < \frac{1}{30}, \tag{18}$$

$$\frac{J/\psi \to \phi f_2(1270)}{J/\psi \to \phi f_2'(1525)} < \frac{1}{1.25}. \tag{19}$$

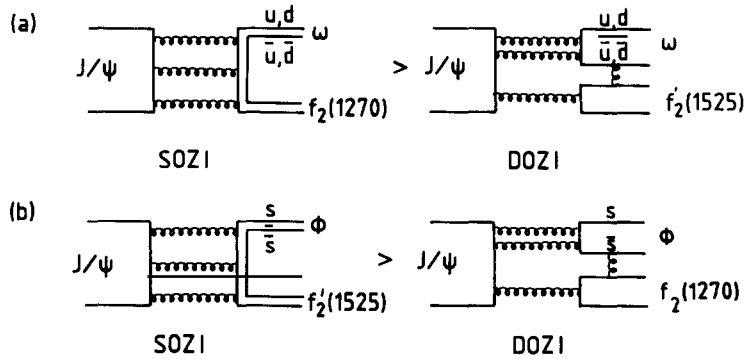

Fig. 6. Singly and doubly OZI suppressed decays. $f_2(1270)$, $f_2'(1525)$ recoiling (a) against an ω, and (b) against a φ.

2.4. Glueballs, hybrids, and four-quark states

The colour force carried by the gluon is the central feature of the strong interaction. Most directly, the existence of this force would manifest itself in particles that have gluon constituents like glueballs or hybrid states, which can only exist because the gluon carries a colour charge. The unambiguous identification of such states would be an essential proof of the validity of QCD. As of today, this identification has not been achieved; the difficulty is largely due to the complexity of the particle spectrum in the 1–2.5 GeV region, where $q\bar{q}$, gg, $q\bar{q}g$, and $q\bar{q}q\bar{q}$ states are expected to exist. In addition, states with different constituents may overlap in mass or mix with each other. Therefore it is very important to find criteria by which one can distinguish the nature of the different objects. The J^{PC} values possible for five alternatives are listed in table 4. Naturally, states with quantum numbers inaccessible for $q\bar{q}$ states are of particular interest in the search for "exotic" phenomena.

In the following sections we outline by which means theoretical models and QCD inspired phenomenology may identify these quark and gluon compound states. The discussion is not intended to be an exhaustive review of all models since excellent reviews [29] have been written on the subject.

2.4.1. Bound states of gluons

Glueballs, being singlet states in $SU(3)_{colour}$ and $SU(3)_{flavour}$, can neither carry isospin, nor charge, nor flavour. Although there are indications that bound states made of gluons exist, masses, widths, and mixing with other states cannot be rigorously calculated yet. Glueball masses have been estimated in the context of several models: lattice Monte Carlo calculations [30, 32, 33], bag models [36, 37], potential models [38], effective lagrangian models [39], and QCD sum rules [40]. These models are in approximate agreement on the general scale of the mass spectrum (see fig. 7); however, none is devoid of problems. Of all approaches, the lattice technique [31], an attempt to perform true QCD calculations

Table 4
Allowed $q\bar{q}$, $qq\bar{q}\bar{q}$, hybrid, and glueball states. Listed are the J^{PC} combinations that are allowed for the various states. If the valence gluons are massless, the states marked by [a] are forbidden by Yang's theorem [228]. A 0^{+-} hybrid state is only allowed with one unit of angular momentum between the $q\bar{q}$ system and the gluon[b].

J^{PC}	$q\bar{q}$	$qq\bar{q}\bar{q}$	$q\bar{q}g$	gg	ggg
0^{++}	yes	yes	yes	yes	yes
0^{+-}	–	yes	yes[b]	–	yes
0^{-+}	yes	yes	yes	yes	yes
0^{--}	–	yes	yes	–	yes
1^{++}	yes	yes	yes	yes[a]	yes
1^{+-}	yes	yes	yes	–	yes
1^{-+}	–	yes	yes	yes[a]	yes
1^{--}	yes	yes	yes	–	yes
2^{++}	yes	yes	yes	yes	yes
2^{+-}	–	yes	yes	–	yes
2^{-+}	yes	yes	yes	yes	yes
2^{--}	yes	yes	yes	–	yes
3^{++}	yes	yes	yes	yes	yes
3^{+-}	yes	yes	yes	–	yes
3^{-+}	–	yes	yes	yes[a]	yes
3^{--}	yes	yes	yes	–	yes

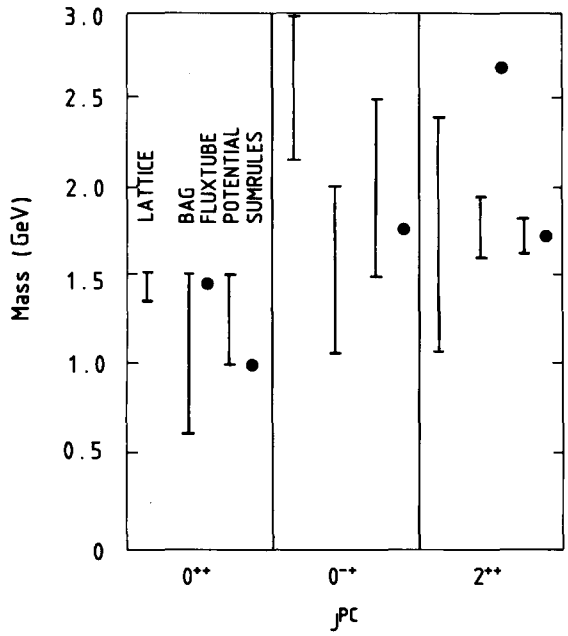

Fig. 7. Predictions for glueball masses. The figure is based on a—non-comprehensive—compilation by A. Le Yaouanc et al. [34]. The value for the 0^{++} glueball mass is taken from ref. [35].

in a non-perturbative manner by employing Monte Carlo techniques, has the best chance to eventually give accurate quantitative results. Until now, quantum corrections due to fermion loops are not included in the calculations so that the effect of mixing with $q\bar{q}$ states is not incorporated in the results.*) It is commonly accepted that the lowest lying glueball states are those with $J^{PC} = 0^{++}$, 0^{-+} and 2^{++}. Spin 1 glueballs can only be produced by off-shell gluons due to Yang's theorem. There have been arguments about which of these is the lowest in mass [32]. Most recent lattice calculations compute that the 0^{++} state is close to or lower in mass than the 2^{++} state. For more convincing mass predictions one will have to wait until more powerful computing methods and computers have been introduced. It has been estimated [51] that computing speeds of 30 gigaflops for a reduced and 3 teraflops for a full calculation are necessary for a definite prediction of glueball masses, several orders of magnitude more than current supercomputers and dedicated number crunching farms can achieve.

A word should be said concerning the expected width of gluonic states. According to the glueball lore, the width of glueballs should follow the "$\sqrt{\text{OZI}}$" rule [52]. This rule is derived from the observation that in OZI forbidden meson decays the quarks annihilate into gluons which then mediate the decay to the final state hadrons. In contrast, a glueball decay does not have to proceed through quark annihilation. The rate should therefore typically be given by the geometric mean between the rate of an OZI forbidden and an OZI allowed transition, i.e., $\sim\sqrt{\Gamma_{\eta_c}\Gamma_\rho} \approx 10$–$50$ MeV. This naive argument has been criticized on several grounds [53] and, lacking any detailed calculation, one can only state that the width cannot be used to provide any guidance, not even qualitative, in the search for gluonium states.

For the purpose of guiding experimental searches for glueballs it is better to rely on rather general

*) Attempts to estimate the mixing between $q\bar{q}$ states and gluonia have been made; see, e.g., refs. [50].

properties of glueballs which are based on their singlet nature and preferable production in gluon favoured reactions such as radiative J/ψ decays, pomeron–pomeron scattering, and OZI suppressed processes. Semi-quantitative criteria along these lines will be discussed in chapter 7. These criteria should always be employed with a critical mind as will be discussed below for the example of flavour symmetry in the decays of glueballs.

Naively, the decays of glueballs should reflect their singlet nature of $SU(3)_{flavour}$ and thus show a flavour-symmetric pattern. However, several authors have argued for various reasons that an SU(3)-symmetric decay pattern on the quark/gluon level is not expected to be maintained on the hadron level. For (TM) gluons in a spherical bag Chanowitz and Sharpe [54, 56] find that decay modes to kaons are substantially enhanced, a result also obtained in models using QCD sum rules [55]. In addition, helicity conservation may favour final states with strangeness. For $J = 0$ glueballs, for instance, this mechanism can suppress decays into two massless spin 1/2 fermions and can enhance $s\bar{s}$ production by a factor of m_s^2/m_u^2 [54, 55]. Finally, form factor effects [57] or mixing with ordinary quark states [58, 59] have been invoked to explain a suppression of $\pi\pi$ decays.

2.4.2. Hybrid states

Hybrid states [44], also called meiktons or hermaphrodites, have been predicted in bag models [45], lattice gauge calculations [46], chromodynamic flux tube models [41], and in models based on QCD sum rules [47]. In hybrid states, the colour octet component of a $3 \times \bar{3}$ quark–antiquark pair is neutralized by a constituent gluon. Unlike glueballs, hybrids appear also as isodoublet and isovector states. The states lowest in mass are made from quarks and gluons in relative s waves. In the bag model the valence gluon can either be transverse electric (TE, $J^P = 1^+$) or tranverse magnetic (TM, $J^P = 1^-$) with positive and negative parity, respectively. Since gluons carry one unit of spin, four ground state nonets each can be formed,

$$|q\bar{q}g_{TE}\rangle: \quad 0^{-+} \times g_{TE} = 1^{--}, \quad 1^{--} \times g_{TE} = \{0^{-+}, 1^{-+}, 2^{-+}\}, \tag{20}$$

$$|q\bar{q}g_{TM}\rangle: \quad 0^{-+} \times g_{TM} = 1^{+-}, \quad 1^{--} \times g_{TM} = \{0^{++}, 1^{++}, 2^{++}\}. \tag{21}$$

Bag model calculations [45] agree on the mass scale of the hybrid spectrum (1.2–2.5 GeV). In particular they predict the mass ordering

$$m(0^{-+}) < m(1^{-+}) < m(1^{--}) < m(2^{-+}). \tag{22}$$

Two typical sets of mass predictions [45] are displayed in fig. 8. Hybrid states with a transverse magnetic gluon are expected to be several hundred MeV heavier than the ones with a transverse electric gluon. While results obtained on the lattice [46] are in fair agreement with bag model calculations, the corresponding mass predictions are higher in flux tube models [42].

Following Chanowitz [48], two general comments can be made regarding the decays of hybrid mesons. The first comment concerns hybrid states which contain a non-strange $q\bar{q}$ pair (denoted as $\ell\bar{\ell}$ below) but decay into final states with strangeness. The decay chain

$$(\bar{\ell}\ell')_8 g \to (\bar{\ell}\ell')_8(\bar{s}s)_8 \to \begin{cases} (\bar{\ell}s)_1(\bar{s}\ell')_1 \\ (\bar{\ell}\ell')_1(\bar{s}s)_1 \end{cases} \tag{23}$$

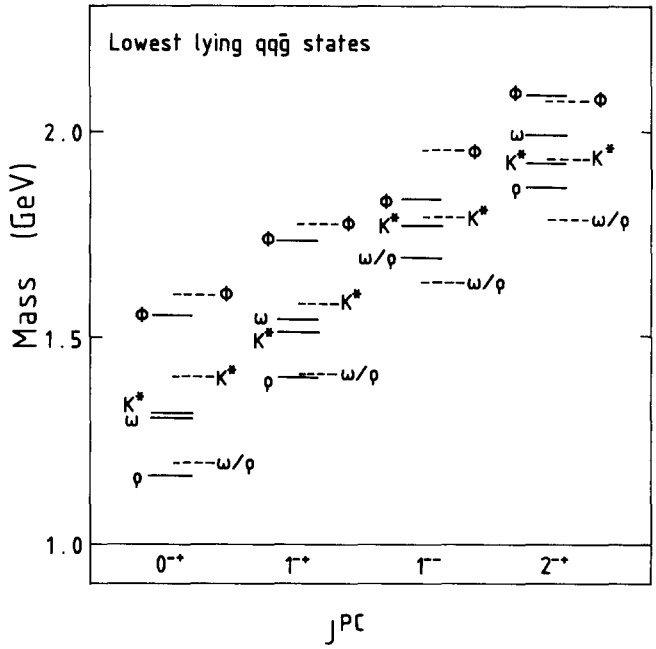

Fig. 8. Predictions for the masses of hybrid states. Shown are predictions from Barnes and Close (solid) and Chanowitz and Sharpe (dashed) for $C_{TE}/C_{TM} = 0.5$ (both ref. [45]).

can lead to colour singlet final states either by rearrangement of the quarks or by soft gluon exchange. If the latter occurs at an appreciable rate, final states like $\phi\pi$ or $\omega\phi$ may be a signature of a hybrid decay since such final states are OZI forbidden for all $q\bar{q}$ mesons.

The second comment concerns the possible preference for final states containing one meson in an orbitally excited state. The decay of a hybrid state into two mesons can either lead to a relative s wave,

$$|\bar{q}qg\rangle \rightarrow |q\bar{q}\rangle^{l=0}|\bar{q}'q'\rangle^{l=1} \quad \text{(s wave)}, \tag{24}$$

or relative p wave,

$$|\bar{q}qg\rangle \rightarrow |q\bar{q}\rangle^{l=0}|\bar{q}'q'\rangle^{l=0} \quad \text{(p wave)}, \tag{25}$$

between the final state mesons by transferring the $q\bar{q}$ angular momentum to an orbital momentum between the final state particles. Using a chromodynamic flux tube model Isgur, Kokoski, and Paton [42] have argued that the sequence of eq. (24) dominates, leading preferentially to final states with one meson being excited, such as $b_1(1235)\pi$, $f_1(1285)\pi$, and $K_2^*(1430)K$. This, and the prediction that hybrid states generally have fairly large widths of typically 0.5–2 GeV [42], may be the reason why they have so far escaped detection.

2.4.3. Four-quark states

The fact that most mesonic resonance states can be accommodated for in the simple $q\bar{q}$ classification is quite remarkable, since the light mesons constitute relativistic systems. If $qq\bar{q}\bar{q}$, $qqq\bar{q}\bar{q}\bar{q}$, etc. wave functions were important for meson spectroscopy, it would have been much more intricate to establish

the quark model and QCD. In principle, evidence for four-quark states could easily be found by searching for exotic quantum numbers, e.g. states with charge or strangeness 2. However, no tell-tale candidates for $qq\bar{q}\bar{q}$ states have yet been found. Bag model calculations [43] offer an explanation to this fact by predicting that

- the lowest lying $qq\bar{q}\bar{q}$ states do not carry exotic quantum numbers and form nonets carrying the same quantum numbers as $q\bar{q}$ nonets, and
- most $qq\bar{q}\bar{q}$ can fall apart into two colour single mesons and thus have a decay width in the order of their mass, too wide to be detected as a resonance.

The four-quark states which one may hope to observe are those whose nominal masses lie below the thresholds of their principal fall-apart modes. It has been argued [43] that $f_0(975)$ and $a_0(980)$ are candidates for the $I=0$ $s\bar{s}(u\bar{u}+d\bar{d})$ and $I=1$ $s\bar{s}d\bar{u}$ states of the lowest lying scalar four-quark nonet. Because of their quark content these states will couple strongly to $K\bar{K}$. However, being below the $K\bar{K}$ threshold these decays are strongly suppressed by phase space. For the $f_0(975)$ the remaining dominant channel is $\pi\pi$, which requires an OZI violation to annihilate the $s\bar{s}$ quark pair. The quark content and the estimated masses for the lightest $qq\bar{q}\bar{q}$ nonet with $J^{PC}=0^{++}$ is shown in fig. 9.

As discussed above, most $qq\bar{q}\bar{q}$ states are expected to be essentially unconfined and therefore will not be observable as resonance peaks with reasonably narrow widths. Those few four-quark states whose mass is below their principal fall apart mode will feature an unusually large fraction of decays into pseudoscalar and vector meson pairs.

2.4.4. *Production of mesons, hybrids, and glueballs in J/ψ decays*

A naive estimate of the production rate of the various particle species based simply on counting powers of the electromagnetic and strong coupling constants yields [48]

$$\begin{aligned}
&\Gamma(J/\psi\to\gamma G)\approx O(\alpha\alpha_s^2)\,, \quad \Gamma(J/\psi\to\gamma H)\approx O(\alpha\alpha_s^3)\,, \quad \Gamma(J/\psi\to\gamma M)\approx O(\alpha\alpha_s^4)\,,\\
&\Gamma(J/\psi\to MH)\approx O(\alpha_s^5)\,, \quad \Gamma(J/\psi\to MM')\approx O(\alpha_s^6)\,, \quad \Gamma(J/\psi\to MG)\approx O(\alpha_s^6)\,,
\end{aligned} \tag{26}$$

where M, H, and G denote mesons, hybrids, and glueballs, respectively. From these estimates one obtains the hierarchies

$$\begin{aligned}
&\Gamma(J/\psi\to\gamma G)>\Gamma(J/\psi\to\gamma H)>\Gamma(J/\psi\to\gamma M)\,,\\
&\Gamma(J/\psi\to MH)>\Gamma(J/\psi\to MM')\approx\Gamma(J/\psi\to MG)\,.
\end{aligned} \tag{27}$$

While these simple estimates are certainly too naive to be trusted without a detailed calculation, one

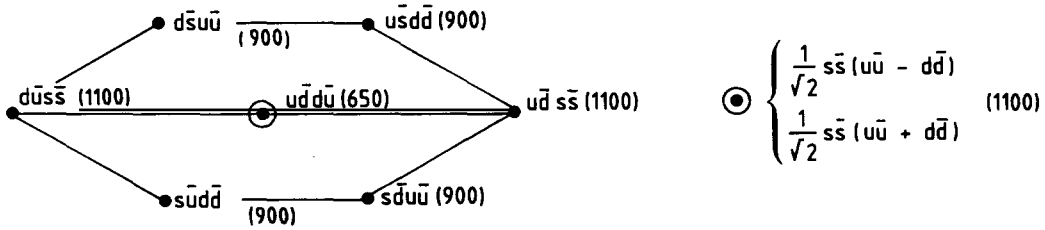

Fig. 9. The lightest $qq\bar{q}\bar{q}$ nonet. Quark content and mass estimates of the scalar $qq\bar{q}\bar{q}$ states [37].

can nevertheless see why the radiative decay channel has been considered a "hunting ground" for gluonic bound states. Note that hybrid states, if they exist, should be produced with a fairly large production rate in J/ψ decays. A possible production of $qq\bar{q}\bar{q}$ mesons in J/ψ is discussed in refs. [49, 319].

3. The experiments

Results on J/ψ decays are almost exclusively obtained from experiments operating at e^+e^- storage rings, such as SPEAR [60] at Stanford, ADONE [61] at Frascati, DORIS [62] at Hamburg, and DCI [63] at Orsay. The BEPC storage ring in Beijing, China, is expected to start operation in 1989. Some of the machine features relevant for the study of decays of the J/ψ and the performance of the detectors are listed in table 5.

One may divide the set of detectors that provided measurements of J/ψ decays into three generations (table 6). Under the label "*first-generation*" detectors we gathered detectors that were operational around the time of the J/ψ discovery or soon after. The list includes the SLAC–LBL (Mark I) detector, the prototype of modern multipurpose e^+e^- storage ring experiments covering a large solid angle.

The "*second-generation*" detectors came into operation in the late seventies and introduced new detector elements like central drift chambers (Mark II), superconducting solenoids (PLUTO), or high-resolution photon detectors with large solid angle coverage (Crystal Ball). The quality of these detectors may be judged from the observation that most of them have subsequently been used at other storage ring facilities such as PEP, SLC (Mark II), PETRA (PLUTO), or DORIS (Crystal Ball).

The "*third generation*" finally started to come into operation at the beginning of the 1980s, its design

Table 5
Machine parameters of the e^+e^- storage rings SPEAR, DORIS, DCI, and BEPC (projected) that are relevant for the study of the J/ψ parameters and decays are listed. The values are given for $E_{beam} = m_\psi/2$. Some of the values have changed during the time the rings were in operation.

	SPEAR	DORIS	DCI	BEPC
energy spread ΔE (MeV)	1.7	1.0	1.4	0.6
bunch length σ_z (mm)	26	30	190	22
peak luminosity ($cm^{-2}s^{-1}$)	0.5×10^{30}	2×10^{30}	1.3×10^{30}	5×10^{30}

Table 6
e^+e^- detectors operating at the J/ψ. Detectors that are written in bold face are described in some detail below.

First generation (mid 1970s)	Second generation (late 1970s)	Third generation (1980s)
Mark I [65] (SPEAR)	PLUTO [76] (DORIS)	**DM2** [75] (DCI)
MEA, 2γ, BB [64] (ADONE)	**Crystal Ball** [68] (SPEAR)	**Mark III** [74] (SPEAR)
DASP [67] (DORIS)	**Mark II** [66] (SPEAR)	BES [77] (BEPC)
DESY–Heidelberg [69] (DORIS)	OLYA [70] (VEPP4)	
SP-14 [73] (SPEAR)		
BONANZA [71] (DORIS)		
SP-27 [72] (SPEAR)		
LGW [78] (SPEAR)[a]		

[a] The Mark I detector was augmented by a lead glass wall for electron and photon detection [78].

profiting from several years of analysing complex J/ψ decays. One of the lessons learned was to increase efficiencies and reduce the level of background events by enlarging the solid angle coverage, improving particle identification, and guaranteeing a high efficiency for both charged and neutral tracks over as large a momentum range as possible. The other lesson learned was that by employing kinematic fits, good energy resolution of neutral showers proves to be less important than good spatial resolution, uniformity, and detection efficiency at low energy. In the following sections we will describe some of the detectors in more detail.

3.1. First-generation detectors

Within days after the discovery of the J/ψ at BNL and at SLAC the existence of the J/ψ resonance was confirmed by the Gamma Gamma, MEA, and Baryon Antibaryon Collaborations at ADONE and by DASP at DORIS. (To reach 3.1 GeV, the energy of the storage ring ADONE was pushed beyond its nominal limit.)

The *SLAC–LBL detector (Mark I)* [65] was the first solenoidal e^+e^- detector covering a large solid angle. The momenta and directions of charged particles are measured in two cylindrical proportional chambers and four sets of spark chambers in a magnetic field of 4 kG extending over a region 3 m in diameter and 3 m in length. A set of 48 scintillation counters at a radial distance of 1.5 m provides TOF information with a resolution of 0.4 ns. Outside the coil a cylindrical array of 24 lead scintillator shower counters, covering the polar angle range from 50°–130°, is used for electron identification and triggering. Outside the 20 cm thick iron magnetic flux return, planar spark chambers cover roughly 70% of the azimuth. Additional muon detection for 15% of the azimuth is provided by a tower above the main detector, consisting of concrete slabs interleaved with spark chambers. In total approximately 150 000 hadronic J/ψ decays were recorded by the SLAC–LBL detector.

The two-arm spectrometer *DASP* [67] combines a non-magnetic inner detector covering 70% of the solid angle and two identical magnetic spectrometers symmetrically positioned with respect to the interaction point. The spectrometer arms, covering 0.9 sr, provide high momentum resolution of $\sigma_p/p = 0.007p$ (GeV), particle identification by means of gas Cerenkov and shower counters with $\sigma_E/E = 30\%/\sqrt{E}$ (GeV), and time-of-flight measurements ($\sigma_\tau = 260$ ps over a flight path of 5 m).

3.2. Second-generation detectors

The non-magnetic *Crystal Ball* detector [68] is optimized for high-resolution measurements of electromagnetically showering particles and is therefore ideal for the study of inclusive and exclusive events containing photons. A schematic view of the detector is displayed in fig. 10 and the main features are listed in table 7. During operation at SPEAR the central tracking system consisted of one proportional chamber sandwiched between two spark chambers, covering 94% of 4π for the innermost chamber and 71% of 4π for the outermost chamber. While tracks in all chambers are required for chamber-reconstructed trajectories, information from the innermost chambers may be enough to reject events with charged tracks. The main part of the detector is a spherical shell made of 672 individual crystals of 16 radiation lengths thick sodium iodide doped with thallium (NaI(Tl)). The resulting energy resolution is about 4.8 MeV at 100 MeV, and the efficiency for detecting photons is 100% for energies as small as 1 MeV. The main ball covers 93% of the solid angle; including the end caps increases the coverage to 98%. While energies of muons and charged hadrons cannot be determined, a separation between hadrons, muons and electrons is to some extent possible due to their different transverse

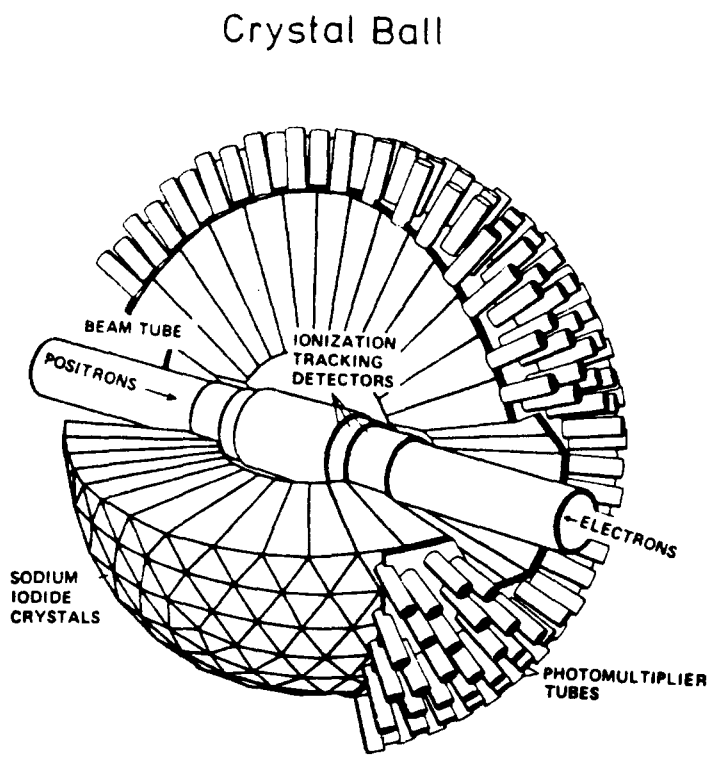

Fig. 10. Schematic view of the Crystal Ball detector.

Table 7
List of features of some second- and third-generation detectors

	Mark III	DM2	Crystal Ball	Mark II
charged tracking:				
σ_p/p at 1 GeV	2.1%	3.5%	–	1.7%
solid angle	84%	87%	71–94%	75%
shower counters:				
σ_E/E at 1 GeV	17%	35%	2.6%	11%
E(eff ≈ 100%) (MeV)	~100	~100	<1	~400
solid angle	94%	70% + 12%	93 + 5%	70% + 20%
longitudinal sampling	0.5–1.5 r.l.	0.25–0.5 r.l.	–	0.7–1.8 r.l.
σ_θ (polar)	15 mr	7 mr	17–35 mr	7 mr
σ_ϕ (azimuthal)	7 mr	10 mr	$\sigma_\theta/\sin\theta$	7 mr
particle identification:				
TOF resolution	190 ps	540 ps	–	300 ps
3σ π/K separation	0.85 GeV	0.42 GeV	–	0.8 GeV
solid angle	80%	80%	–	75%
# of J/ψ decays	5.8×10^6	8.6×10^6	2.2×10^6	1.3×10^6

energy deposition patterns in the crystals. For fully detected J/ψ decays energy and momentum constraints can be used to completely reconstruct the event even if charged particles are present.

The main features of the *Mark II detector* [66] are listed in table 7. The momenta of charged tracks are measured in a cylindrical drift chamber containing 16 sense wire layers of radii from 0.41 to 1.45 m. The magnetic field of 4.1 kG allows a measurement of particle momenta over 75% of 4π with an accuracy of $\sigma_p/p = [(0.010p)^2 + (0.0145)^2]^{1/2}$, where p is the track momentum in GeV. The drift chamber is surrounded by 48 scintillation counters, 2.54 cm thick, providing a time-of-flight resolution of 300 ps. The liquid argon calorimeter behind 1.36 radiation lengths of solenoidal coil covers 70% of the solid angle and contains about 14 radiation lengths of lead and argon with readout strips parallel, perpendicular, and at 45° to the beam axis. The energy resolution above 0.5 GeV is $\sigma_E/E = 0.11/\sqrt{E}$ and the angular resolution is about 8 mrad, both in azimuth and polar angle. The measured photon efficiencies are 15% at 100 MeV, 50% at 200 MeV, and >90% above 400 MeV. Additional shower counters at small angles relative to the beam extend the solid angle coverage to 90% of 4π. Finally, two steel walls each followed by one layer of proportional tubes are used for the detection of muons with momenta above 700 MeV, covering an angular range of 55% of 4π.

3.3. Third-generation detectors

The *DM2 magnetic detector* [75] is depicted in fig. 11 and its main features are listed in table 7. A 5 kG magnetic field is produced by a 2 m diameter and 3 m length solenoid with a 1 X_0 aluminium coil. Charged track momenta are measured by two layers of cylindrical proportional and 13 layers of drift chambers over 87% of the solid angle with a momentum resolution of 3.5% at 1 GeV. Inside the solenoid coil, 36 scintillator counters measure the time of flight of charged particles; the resolution of 540 ps is dominated by the uncertainty on the interaction time (440 ps) introduced by the longitudinal beam spread. A 3σ π/K separation is obtained up to 420 MeV and 3σ π/p separation up to 830 MeV. The photon detector, placed outside the coil, is segmented into 8 octants of 5 radiation lengths thickness. Each octant consists of 14 planes of delay line streamer tubes interleaved with lead and 5 planes of scintillators. The barrel covers 70% of the solid angle with a detection efficiency greater than 96% for $E_\gamma > 110$ MeV; the resolution in the photon detection is 10 mrad in azimuth and 7 mrad in polar angle. The resolution in energy scales as $\sigma_E/E = 0.19/\sqrt{E}$ (GeV) below 300 MeV and stays at the level of 35% above. The two end cap detectors, covering an additional 12% of the solid angle, have mostly only been used as veto counters since they do not provide an energy measurement. The granularity of the shower detector allows a measurement of the shower apex with an accuracy of the order of 1 cm and to reconstruct the track direction for both charged particles and photon showers.

The *Mark III detector* [74] (fig. 12) is a general purpose solenoidal detector optimized for the reconstruction of exclusive hadronic final states in the SPEAR energy range. A low-mass inner drift chamber surrounding the beryllium beam pipe provides tracking and a first-level trigger. The main drift chamber system, in a 4 kG magnetic field, measures the momentum of charged particles over 84% of the solid angle with a resolution of $\sigma_p/p = 0.015\sqrt{1+p^2}$ (p in GeV). Two stereo layers and charge division on four of the axial layers provide a measurement of the polar angle. Charged particle identification is obtained with a system of 48 time-of-flight counters of 5 cm thick scintillator, covering 80% of the solid angle and featuring a time resolution of 190 ps for hadrons. Between the TOF counters and the solenoidal coil is a highly segmented gas sampling calorimeter consisting of 24 layers of alternating 0.5 radiation length lead sheets and proportional counters. End cap counters of similar

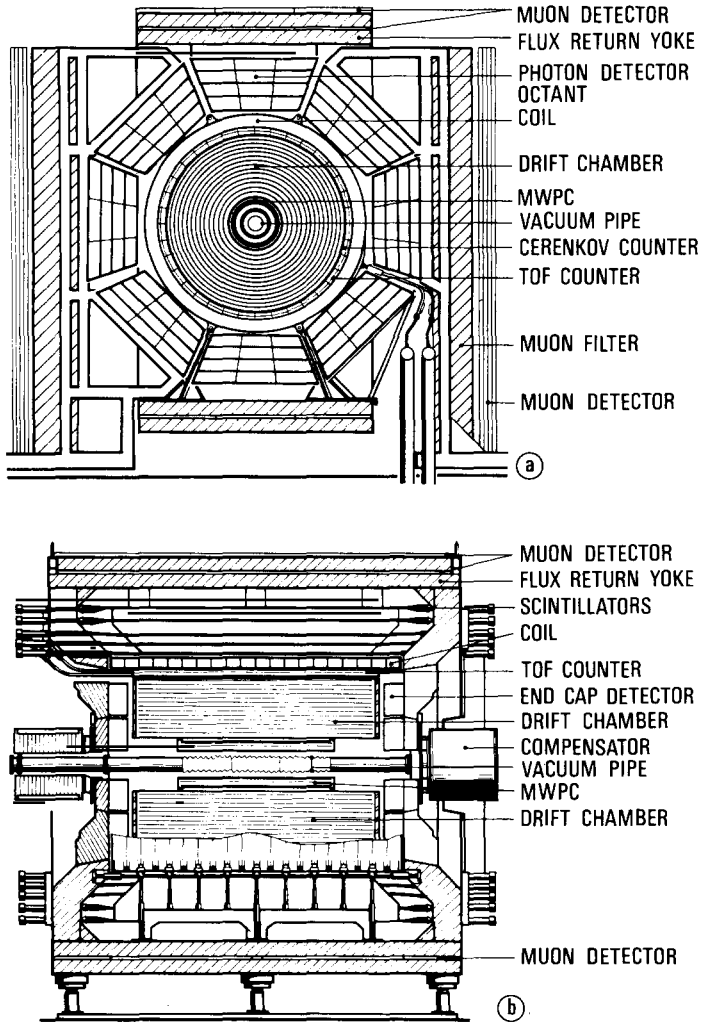

Fig. 11. Axial and transverse view of the DM2 detector.

design extend the photon detection to 94% of the solid angle. For 100 MeV photons, the shower counters are fully efficient and have an angular resolution of approximately 10 mrad and an energy resolution of $\sigma_E/E = 0.17/\sqrt{E}$ (GeV).

3.4. *Analysis techniques*

The techniques for analysing J/ψ decays have evolved over the years based on the experience gained by many experiments. They are optimized for analysing data collected by e^+e^- multi-purpose detectors and reflect the characteristics of J/ψ decays leading to low-multiplicity events with rather low particle momenta (typically less than one GeV). The necessity to reconstruct π^0's over a large momentum range requires optimized procedures to detect very low-energy photons in the presence of spurious

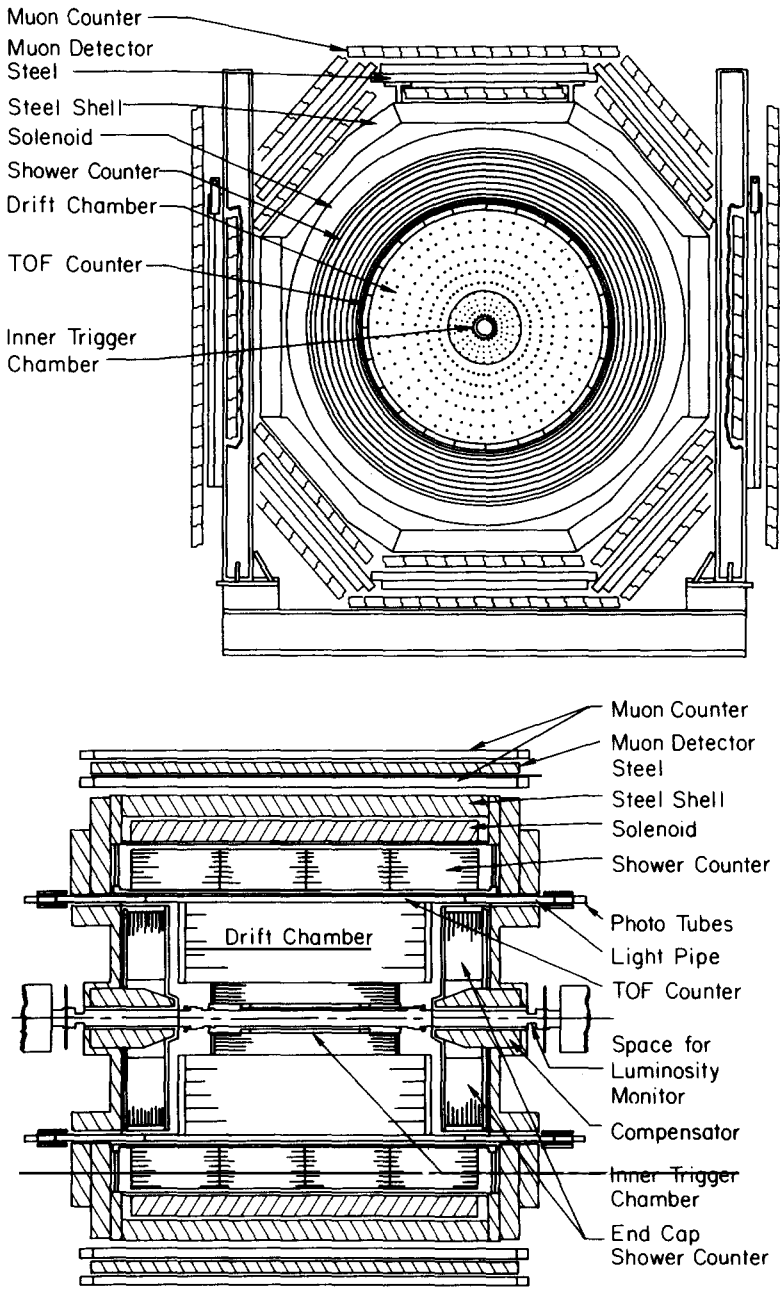

Fig. 12. Axial and transverse view of the Mark III detector.

backgrounds*) as well as high momentum π^0's where the two photons have merged into one shower cluster.**) Kaons and protons have to be safely identified without substantial deterioration in the acceptance (see fig. 13).

The analysis techniques for detecting J/ψ decays have some common features for different final states and even for different experiments. The event selection for a desired final state usually begins with the requirement of a compatible topology (exact number of charged tracks and a number of showers equal to or larger than that required by the final state). Additional showers are allowed, since the identification of photons is complicated by the fact that charged particles often interact in the material of the shower counters, producing spurious clusters of hits, which can be mistaken for photon signals. Analyses which eliminate showers inside a cone around charged tracks or require a minimum photon energy help to cope with this source of background. The first-generation detectors (section 3.1), handicapped by relatively meager statistics and inferior photon detection capabilities, sometimes employed techniques allowing for missing particles. Similar methods have been employed for the detection of final states including K_L^0's and neutrons.

Particle identification, mostly by time of flight, is used whenever possible to distinguish pions, kaons, and protons. To avoid efficiency losses due to K decays or geometrical acceptance, the cuts are chosen as loose as allowed by background.

The events are often kinematically fitted by imposing constraints from energy and momentum conservation and from final state invariant masses. This serves to improve the resolution of the measured quantities, especially those which are poorly determined. In the case of the DM2 and Mark III experiments, with good momentum resolution for charged particles but only average shower counter energy resolutions, the fit substantially improves the photon energy estimation, which in turn improves

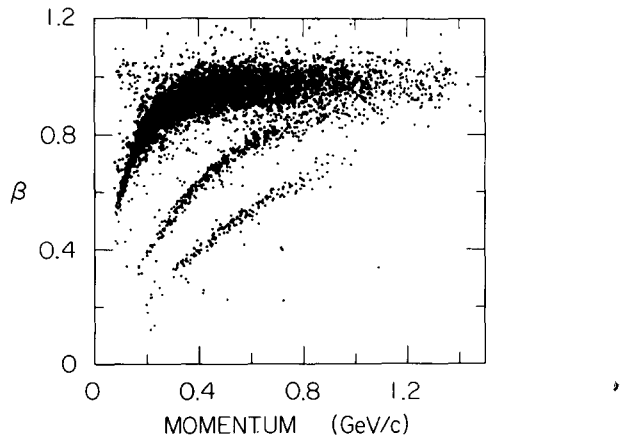

Fig. 13. Identification of charged particles by TOF. Plotted is the particle velocity as obtained by a time-of-flight measurement versus the particle momentum (Mark III).

*) Calorimeters that are highly segmented in lateral direction allow for a direction measurement of a shower. This can be used to distinguish photons coming from the interaction region from spurious showers that originate from backscattered secondary particles. To remove background events in which a π^0 is falsely reconstructed from a high-energy photon and a second spurious shower a cut on the energy asymmetry $|(E_{\gamma_1} - E_{\gamma_2})/p_{\pi^0}|$, which is uniformly distributed for π^0 decays, is often introduced.

**) Crystal Ball has employed a technique based on the second moment of the energy distribution of a shower to disentangle photons from merged π^0 showers and to estimate a global shower invariant mass [79].

the determination of the invariant masses of subgroups of particles in the final state. After fitting, the mass resolution is typically 1%. In the case of the non-magnetic Crystal Ball detector, with excellent photon energy resolution but no momentum measurement for charged particles, the kinematic constraints are essential for the reconstruction of events containing charged tracks. Furthermore, the kinematic fits help in the reconstruction of events with spurious photons or ambiguous particle type assignments. In such events, all possible combinations are tried in the fit and the confidence level is used to identify the most probable set of photons and particle mass assignments.

The yield for a specific decay mode is determined from resonant peaks in the invariant mass distributions. Signal events are extracted using fits of appropriate Breit–Wigner shapes, folded with the resolution, and a parametrization of the background. To study the background, mass sidebands surrounding the resonance are often selected.

The detection efficiency for a specific decay mode is estimated by generating events of the desired type by Monte Carlo and passing them through the entire analysis chain. A systematic error arises from uncertainties in the Monte Carlo simulation (typically 5%–20%), insufficient knowledge of the underlying physics process, uncertainties in the branching fractions of the observed particles, and from the determination of the total number of produced J/ψ's (typically 5%–10%).

Among the variables that have been introduced for selecting radiative J/ψ decays, the quantities U and $p_{t_\gamma}^2$ are worth mentioning. Both variables are particularly suited for the case where the four-momentum of the hadronic system recoiling against the radiative photon is precisely determined, which is, for example, fulfilled if the hadronic final state contains only charged tracks. The variable

$$U = |E_{\text{missing}} - P_{\text{missing}}| , \tag{28}$$

where E_{missing} denotes the missing energy from the system recoiling against the radiative photon and P_{missing} is the missing momentum, gives a more precise estimate on the mass of the missing particle than the missing mass $M^2_{\text{missing}} = (E_{\text{missing}} + P_{\text{missing}})U$, when M_{missing} is small. Since U is linear in E_{missing}, the error in U does not depend to first order on the magnitude of the missing energy. In common e^+e^- detectors, the resolution in U is good enough to be able to reject events where more than one π^0 escaped detection.

The variable [80]

$$p_{t_\gamma}^2 = 4|\boldsymbol{p}_X|^2 \sin^2\delta/2 , \tag{29}$$

where $\boldsymbol{p}_X$ is the momentum vector of the radiatively produced system X and δ is the angle between $\boldsymbol{p}_X$ and the radiative photon, depends on the angle measurement but not on the energy measurement of the photon. Consequently it is a very sensitive quantity when the directions of the photon and the recoiling hadronic system are precisely determined. The observation that this variable has approximately constant resolution as a function of the energy of the radiative photon makes it particularly useful to statistically separate radiative from non-radiative channels. An application for the $J/\psi \to \gamma 2(\pi^+\pi^-)$ reaction, which is contaminated by $J/\psi \to \pi^0 2(\pi^+\pi^-)$ decays, is shown in fig. 14. While the background reaction produces a smooth distribution in $p_{t_\gamma}^2$ the radiative decay process is sharply peaked at $p_{t_\gamma}^2 = 0$. (This technique was first employed by Himel et al. [80].)

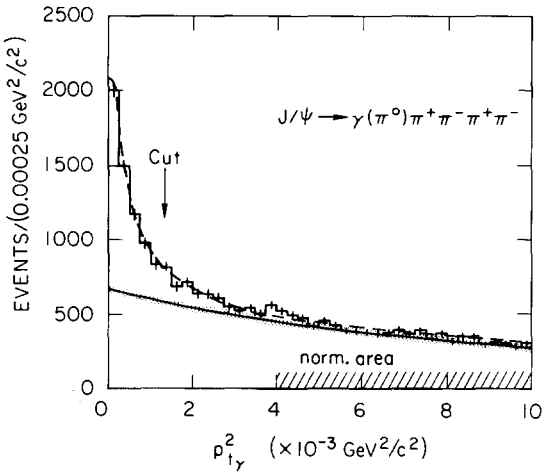

Fig. 14. Statistical separation of radiative and non-radiative decays. $p^2_{t_\gamma}$ distribution for $\gamma(\pi^0)\pi^+\pi^-\pi^+\pi^-$ final states. The band represents the background distribution from $J/\psi \to 5\pi$ extrapolated from above (Mark III [345]).

4. The resonance parameters of the J/ψ

4.1. Mass determination

The mass of the J/ψ has been measured quite precisely in the Novosibirsk e^+e^- storage ring [81] and in collisions of a stochastically cooled [82] antiproton beam with an internal jet target at the ISR at CERN [83]. The precision of the mass determination in e^+e^- storage rings is limited by the uncertainty in the calibration of the absolute energy scale ($\approx$1 MeV). This can be overcome by exploiting the resonance depolarization method, which has been perfected by the Novosibirsk group [84]. The method is based on the measurement of the spin precession frequency Ω of the polarized beam electrons, which is related to the beam energy by the relation

$$\frac{E_e}{m_e} = \kappa^{-1}\left(\frac{\Omega}{\omega} - 1\right). \tag{30}$$

Here κ is the ratio of the anomalous and normal parts of the electron's magnetic moment and ω is the beam revolution frequency, which is known to an accuracy of better than 10^{-6}. The spin precession frequency Ω is determined by slowly varying the frequency ω_d of a depolarizing field, leading to an actual depolarization when $\omega_d = \Omega$. This method allows the determination of the beam energy to a relative accuracy of 3×10^{-5}, which is 10 times more precise than previous measurements and 5 times more accurate than the beam energy spread. The final result for the J/ψ mass, taking into account radiative corrections [93], is

$$m_\psi = (3096.93 \pm 0.09)\ \text{MeV}. \tag{31}$$

At the ISR it was possible to control a $\bar{p}$ beam to a high precision allowing for an absolute calibration of the centre of mass energy to a fraction of an MeV. The CERN ISR experiment R704 has studied the process

$$p\bar{p} \rightarrow J/\psi \rightarrow e^+e^- \tag{32}$$

to precisely determine the mass of the J/ψ. They obtain

$$m_\psi = (3096.96 \pm 0.10 \pm 0.30)\,\text{MeV}\,, \tag{33}$$

where the systematic error arises from uncertainties in the beam momentum calibration.

4.2. Measurement of the total width

The total width has not been measured directly since the energy spread in both e^+e^- ($\Delta E \approx 1.7$ MeV at SPEAR) and $p\bar{p}$ machines ($\Delta E \approx 0.7$ MeV) is too large. It can, however, be inferred from the integrated leptonic reaction rate and the leptonic branching ratio employing the formula

$$\Sigma_\psi^{ee} \equiv \int_{-\infty}^{\infty} \sigma(E)\,\mathrm{d}E = \frac{6\pi^2\hbar^2c^2}{m_\psi^2}\left(\frac{\Gamma_{ee}}{\Gamma_{\text{total}}}\right)^2 \Gamma_{\text{total}} \approx 900\,\text{nb MeV}\,. \tag{34}$$

Here, the left-hand side of the equation has been corrected for the effect of initial state radiation, which constitutes a significant correction (see section 5.2.2). From the average of all measurements one then finds [23]*)

$$\Gamma_{\text{total}} = (74 \pm 8)\,\text{keV}\,. \tag{35}$$

It should be pointed out that this result has been obtained by first-generation experiments using relatively small data samples, thus it could be easily improved in a relatively short amount of running time.

4.3. The quantum numbers of the J/ψ

One of the early investigations of J/ψ decays was the determination of its quantum numbers [85, 86]. The study of the leptonic $\mu^+\mu^-$ final state, showing interference with the non-resonant amplitude, leads to the conclusion that the J/ψ carries the quantum numbers of the photon, i.e., $J^{PC} = 1^{--}$ (see fig. 1b). The G parity has been established by studying multi-pion final states. The G parity of a pion is defined as

$$\begin{aligned} G|\pi^\pm\rangle &= C\,e^{i\pi I_2}|\pi^\pm\rangle = C(-|-\pi^\mp\rangle) = -|\pi^\pm\rangle\,, \\ G|\pi^0\rangle &= C\,e^{i\pi I_2}|\pi^0\rangle = C(-|\pi^0\rangle) = -|\pi^0\rangle\,, \end{aligned} \tag{36}$$

leading to the general expression for a system of n pions

$$G|n\pi\rangle = (-1)^n|n\pi\rangle\,.$$

*) This value is obtained from the expression $\Gamma_{\text{tot}} = \Gamma_{ee}/B_{ee} = (5.1 \pm 0.3)/(0.069 \pm 0.006)$ keV, assuming lepton universality.

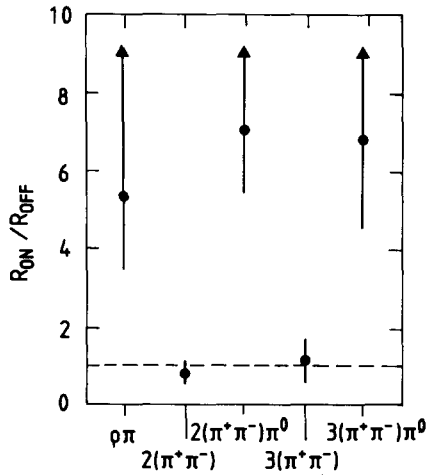

Fig. 15. Determination of the G parity of the J/ψ. Comparison of the ratio of multi-pion to μ pair production on and off resonance, for various multi-pion channels [85].

Consequently, G parity invariance for strong decays implies odd and even numbers of pions in the final state for $G=-1$ and $G=+1$, respectively. In fig. 15 the ratio $R^{on}_{n\pi}/R^{off}_{n\pi}$, where $R_{n\pi}=\sigma_{n\pi}/\sigma_{\mu\mu}$, is plotted for several final states with different n. The cross sections σ^{on} and σ^{off} refer to the cross sections obtained on and off the J/ψ resonance, respectively. The formation of μ pairs and the off-resonance production of hadrons proceed via a virtual photon (fig. 4b), an electromagnetic process where isospin or G parity is generally not conserved. From the observation [85] that the J/ψ preferably decays into an odd number of pions, the G parity is determined to be $G=-1$. The data are consistent with the hypothesis that all final states of even numbers of pions are produced by one photon annihilation, while the access of final states with odd numbers of pions is due to the direct decay of the J/ψ, fragmenting into three gluons (fig. 4a). Since $G=C(-1)^I$, the isospin must be even.

The observation of the decays

$$J/\psi \rightarrow \Lambda\bar{\Lambda},\ p\bar{p},\ K^*\bar{K}, \tag{37}$$

which cannot occur if the J/ψ is an isotensor, and the ratio of $B(J/\psi\rightarrow\pi^0\rho^0)/B(J/\psi\rightarrow\pi^{\pm}\rho^{\mp})=0.49\pm0.01\pm0.03$ [127], which should be 0.5 (2.0) for $I=0$ ($I=2$), determine the J/ψ to be an isosinglet state. The decay pattern of the J/ψ into pairs of mesons (see sections 5.3.2 to 5.4) establishes that the J/ψ is also consistent with being an SU(3) singlet.

5. Non-radiative decays of the J/ψ

The study of non-radiative J/ψ decays is rewarding because a multitude of leptonic, mesonic, and baryonic final states is produced by fairly well-defined electromagnetic and hadronic decay mechanisms.

The *leptonic decays*, electromagnetic in origin, give an estimate of the J/ψ wave function at the origin, and thus serve as a normalization for other decays (sections 5.2 and 2.1).

Electromagnetic decays of the J/ψ into hadrons allow one to measure the form factor of the final

state particles at $Q^2 = m_\psi^2$ and complement measurements made at lower momentum transfers (section 5.4).

At first sight, the set of measured *hadronic decay channels* may appear overly complex. However, simple ideas, such as $SU(3)_{flavour}$ invariance and Zweig's rule (section 2.3), represent powerful tools to classify mesonic and baryonic final states (see sections 5.3.2 to 5.3.5, and 5.6). A particular application is the possibility to tag the flavour of final states X in two-body J/ψ decays like $J/\psi \to \phi + X$ and $J/\psi \to \omega + X$. Dominance of the SOZI diagrams of fig. 6 implies that the quarks of the final state hadrons are correlated so that the $s\bar{s}$ meson φ acts as a probe to detect final states with strangeness, while the $u\bar{u} + d\bar{d}$ meson ω goes with non-strange systems. These ideas serve as a qualitative guide to understand the spectrum of J/ψ hadronic decays. A more detailed quantitative treatment must account for electromagnetic transitions, SU(3) breaking effects, and contributions from disconnected diagrams. Phenomenological models trying to incorporate all of these effects have been put forward by several authors both for mesonic [118, 199, 256, 257] and baryonic final states [186]. For the case of $\mathcal{C}$-allowed decays to two mesons we will follow the prescription of Seiden et al. [256], which is outlined in section 5.3. The corresponding models for the $\mathcal{C}$-forbidden two-body decays [199] and baryonic decays are introduced in sections 5.4 and 5.6.1, respectively.

5.1. *Inclusive studies of* J/ψ *decays*

The J/ψ energy is too low to show distinct jets of particles and a large fraction of its decays are few-body decays. The average number of charged and neutral pions per decay is 3.8 ± 0.3 and 3.1 ± 0.8, respectively [87]. Due to the large angular coverage of e^+e^- detectors, good particle identification capability, and good resolution obtained by kinematic fitting, the full reconstruction of these final states has been routinely achieved even for topologies like $J/\psi \to \gamma\omega\omega$ with four charged and five neutral particles. Because of these reasons only a few studies of inclusive J/ψ decays have been done so far [87–90].

Figure 16 shows the momentum distribution of charged pions, kaons, and antiprotons in J/ψ decays obtained by DASP [89]. Integrating over all momenta one finds the charged particle fractions

$$R_{\pi^\pm} = (87.5 \pm 1.3)\% , \qquad R_{K^\pm} = (8.9 \pm 1.0)\% , \qquad R_{2\cdot\bar{p}} = (3.6 \pm 0.9)\% . \tag{38}$$

The behaviour of the inclusive spectra and particle multiplicities for J/ψ decays is very similar to that found in the non-resonant region of e^+e^- reactions or in central $p\bar{p}$ collisions [91].

That it nevertheless makes sense to make use of the enormous data samples of J/ψ decays in inclusive studies has been shown by the Mark II Collaboration [90]. Figure 17 shows the inclusive $\pi^+\pi^-$ mass spectrum in J/ψ decays, based on a sample of 1.3×10^6 J/ψ decays. The combinatorial background, which can be estimated from the same-sign combinations $\pi^+\pi^+$ and $\pi^-\pi^-$, has been subtracted. The spectrum shows clear indications for the ρ(770), the ω(783) (shoulder at the high side of the ρ peak), the $f_0(975)$, and the $f_2(1270)$. The solid curve shows the result of a fit composed of four incoherent*) Breit–Wigner functions.

A slightly better fit in the 1 GeV region has been achieved by using a coupled channel parametrization for the $f_0(975)$ (see section 5.3.3). The fitted pole position in the complex mass plane is determined to be

*) Since the G parity of the J/ψ is odd, the allowed strong decays are $\omega + 2n$ pions and $\rho + (2n-1)$ pions, in different final states.

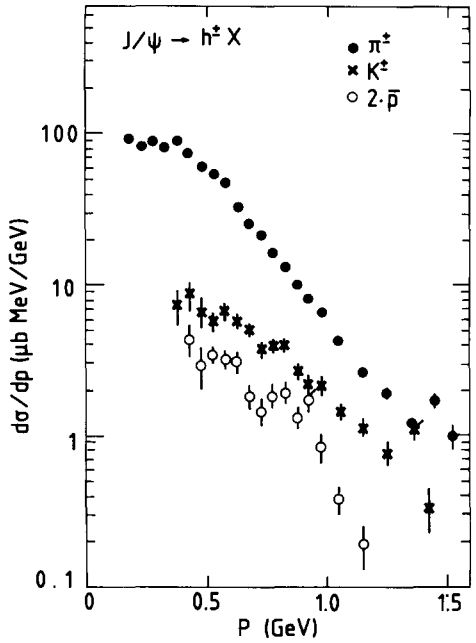

Fig. 16. Differential cross sections for inclusively produced particles. The cross section $d\sigma/dp$ is plotted for $\pi^{\pm}$, $K^{\pm}$, and $2\cdot\bar{p}$ inclusive final states [89].

$$m_{\text{pole}} = (974 \pm 4 - i(14 \pm 5))\,\text{MeV}\,. \tag{39}$$

The *inclusive* branching ratios, obtained from the fit of fig. 17, are listed in table 8 and compared to the sum of *exclusively* reconstructed events containing a ρ, ω, $f_0(975)$, or $f_2(1270)$, which account for (10–30)% of the inclusively measured single-particle production. The observed ratios of ω/ρ^0 and $f_2(1270)/\rho^0$ are consistent with the values measured in πp, pp, and $p\bar{p}$ interactions [92].

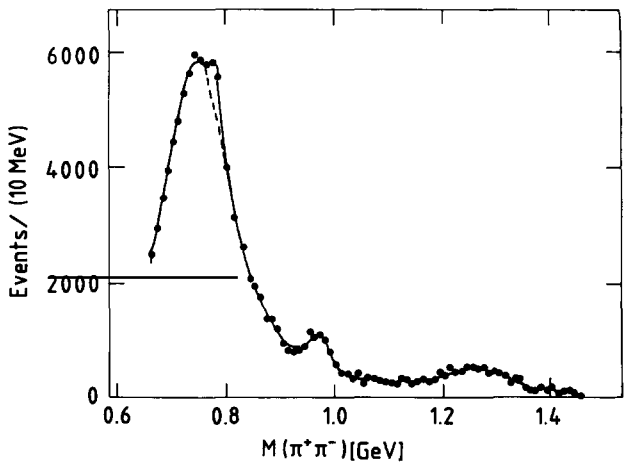

Fig. 17. Inclusive $\pi^+\pi^-$ invariant mass spectrum in J/ψ decays. The non-resonant background has been subtracted [90].

Table 8
Measured branching fractions of inclusive J/ψ decays. Listed are results from the Mark II Collaboration [90]. The branching fractions for each of the resonances R in the $J/\psi \to R + X$ reaction are corrected for unobserved decay modes. In particular $B(\omega \to \pi^+\pi^-) = 0.014 \pm 0.004$ and $B(f_0(975) \to \pi\pi) = 0.78 \pm 0.03$ have been assumed.

R	$B(J/\psi \to R + X)$ (inclusive) (%)	$B(J/\psi \to R + X)$ (exclusive) (%)	exclusive channels considered
ρ^0	8.3 ± 0.8	$>1.0 \pm 0.1$	$\rho^0\pi$, $\rho^0 a_2$, $\gamma\rho^0\rho^0$
ω	13.4 ± 4.7	$>4.9 \pm 0.9$	$\omega\pi\pi$, $\omega 4\pi$, $\omega K\bar{K}$, $\omega K\bar{K}\pi$, $\omega p\bar{p}$, $\omega\eta$, $\omega\pi^0$, $\gamma\omega\omega$
$f_0(975)$	0.54 ± 0.10	$>0.042 \pm 0.005$	ϕf_0, ωf_0
$f_2(1270)$	1.6 ± 0.2	$>0.58 \pm 0.05$	ωf_2, γf_2

Many of the inclusive $f_0(975)$ events result from multi-body final states or cascade decays. This can be seen from fig. 18, where the mass of the system recoiling against an $f_0(975)$ is displayed. The spectrum is peaked towards higher masses, indicating high multiplicity.

5.2. *Decays of the J/ψ into leptons and photons*

Leptonic decays of the J/ψ provide a very clear signature and have been used in hadroproduction and e^+e^- storage ring experiments to identify charm or beauty. The measurement of the leptonic decay rates gives an estimate for the J/ψ wave function at the origin and may therefore serve as a normalization for other decays. Because the J/ψ mass is below the $\tau^+\tau^-$ threshold, only the leptonic decays $J/\psi \to e^+e^-$, $\mu^+\mu^-$ can be investigated in lowest order. While the $J/\psi \to \gamma\gamma$ decay is forbidden by C parity conservation, the photonic decay $J/\psi \to \gamma\gamma\gamma$ is allowed by the selection rules.

5.2.1. $J/\psi \to \gamma\gamma\gamma$

The $J/\psi \to \gamma\gamma\gamma$ decay has been studied by the DASP [67, 107], Crystal Ball [109], and DM2 [110] experiments, which feature triggers for final states with neutral particles only. The decay is dominated by intermediate $\gamma\pi^0$, $\gamma\eta$, $\gamma\eta'$ final states (see fig. 62, section 6.3.1). The DASP [67, 107] and Crystal

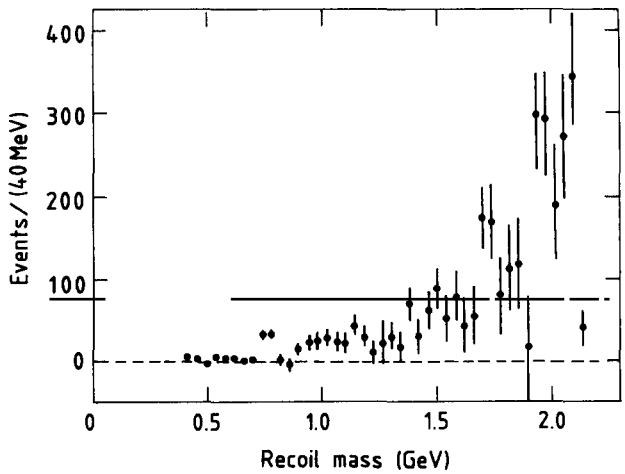

Fig. 18. Recoil mass spectrum against $f_0(975)$. The mass spectrum is background subtracted.

Ball [109] Collaborations have studied the part of 3γ production that does not proceed via intermediate resonance states. The upper limit by Crystal Ball of

$$B(J/\psi \to 3\gamma) < 5.5 \times 10^{-5} \quad (90\%\ \text{C.L.}) \tag{40}$$

is still a factor ≈3 above the QED expectation [see eq. (4) in section 2.1].

5.2.2. $J/\psi \to e^+e^-$, $J/\psi \to \mu^+\mu^-$

The leptonic branching ratios have been determined with the SLAC–LBL detector (Mark I) [111] to be

$$B(J/\psi \to e^+e^-) = 0.069 \pm 0.009\,, \qquad B(J/\psi \to \mu^+\mu^-) = 0.069 \pm 0.009\,. \tag{41}$$

For the ratio of the electronic and muonic widths other experiments [112, 115] contributed as well, yielding the averaged result of

$$\frac{B(J/\psi \to e^+e^-)}{B(J/\psi \to \mu^+\mu^-)} = 0.980 \pm 0.043\,. \tag{42}$$

This value is consistent with unity as expected for e–μ universality.

When determining the e^+e^- and $\mu^+\mu^-$ partial widths one has to consider the effect of interference with the much*) smaller non-resonant amplitude. For the muonic decay one finds ($m_\mu = 0$)

$$\left(\frac{d\sigma}{d\Omega}\right)_{\mu\mu} = \frac{\alpha^2}{4s}(1+\cos^2\Theta_\mu)[1+|A_R^{e\mu}|^2 - 2\,\mathrm{Re}(A_R^{e\mu})]\,, \quad A_R^{e\mu} = \frac{3}{2\alpha}\,\frac{\sqrt{\Gamma_e\Gamma_\mu}}{M_\psi - \sqrt{s} - i\Gamma_{tot}/2}\,, \tag{43}$$

where in addition the machine energy spread and the effect of initial state radiation have to be taken into account. The interference effect for the $\mu^+\mu^-$ final state is sizeable (see fig. 1b in section 1.1) and is well described by the QED calculation, demonstrating that the quantum numbers of the J/ψ are those of the photon.

The effect of interference is much less pronounced in the case of the e^+e^- final state because of the additional *t*-channel diagram of Bhabha scattering,

$$\left(\frac{d\sigma}{d\Omega}\right)_{ee} = \frac{\alpha^2}{4s}\left[\left(\frac{3+\cos^2\Theta_e}{1-\cos\Theta_e}\right)^2 + (1+\cos^2\Theta_e)|A_R^{ee}|^2 + \text{interference term}\right]. \tag{44}$$

In this expression the small *t*-channel contribution to the resonance production has been neglected; A_R^{ee} is defined according to eq. (43). The values for the leptonic and hadronic widths can then be obtained

*) The peak cross section at the nominal mass of the J/ψ is $\sigma_{\mu\mu}$(resonant) ≈ 8700 nb if one includes radiative corrections and interference effects. Due to the finite energy resolution of the storage rings, the visible peak cross section is typically 40 times lower. For comparison, $\sigma_{\mu\mu}$(non-resonant) ≈ 9 nb.

by integrating over the resonance region and applying the formula

$$\Sigma_{\psi}^{\text{final}} \equiv \int_{-\infty}^{\infty} \sigma(E)\,\mathrm{d}E = \frac{6\pi^2\hbar^2c^2}{m_{\psi}^2}\,\frac{\Gamma_{ee}\Gamma_{\text{final}}}{\Gamma_{\text{total}}} \tag{45}$$

to the e^+e^-, $\mu^+\mu^-$, and hadronic final states in e^+e^- collisions. The J/ψ is produced with a strength proportional to its leptonic partial width.

In order to compare the experimental results with theoretical predictions, a proper treatment of QED radiative corrections has to be performed. The original work, published at the beginning of J/ψ research, employed various methods to correct for radiative effects [93, 95, 97]. Since then, more sophisticated tools for radiative correction calculations have been developed to cope with the much more critical situation of Υ and Z^0 decays [24, 96]. In this context, Baru et al. [98] have shown that the Jackson and Scharre formalism [93] yields a 9% lower leptonic width than the Kuraev–Fadin method [94]. Whether or not to include the effect of vacuum polarization [93, 95] depends on what needs to be determined. To be consistent with the experimental $B(J/\psi\to e^+e^-) = \Gamma_{ee}/\Gamma_{tot}$ measurement, which by definition includes the effect of vacuum polarization (Π), one should also include this effect in the radiative corrections. On the other hand, theoretical estimates for the leptonic widths are usually not corrected for vacuum polarization and therefore have to be compared with the equivalent experimental numbers. For the J/ψ, Tsai [97] finds that the two quantities are related by the expression

$$\Gamma_{ee}^0 = \Gamma_{ee} \times (1-\Pi)^2 = \Gamma_{ee}\cdot 0.958\,, \tag{46}$$

where Γ_{ee}^0 does *not* include the vacuum polarization term.

Along these lines, Königsmann [23] and Alexander et al. [24] have corrected the early determinations of the leptonic widths obtained at the SPEAR [113], ADONE [87, 114, 115], and DORIS [67, 116] storage rings in a consistent way. Following ref. [23] one obtains*) the average values of

$$\Gamma_{ee}^0 = (4.9\pm 0.3)\ \text{keV}\,, \qquad \Gamma_{ee} = (5.1\pm 0.3)\ \text{keV}\,. \tag{47}$$

The measurements of the leptonic widths are of interest since they can be compared to theoretical calculations including higher-order QCD corrections [see eq. (3) in section 2.1].

Table 9 lists various results on Γ_{ee}^0. The lowest-order calculations [100, 101] clearly demonstrate the need for the inclusion of first-order QCD corrections [102, 105, 106]. It is found that relativistic corrections increase the leptonic width by ~20% [103], while QCD radiative effects decrease it [106]. It should be noted that QCD sum rules also predict leptonic widths rather accurately [104]. The value for Γ_{ee} fits nicely into the empirical finding [117] that the ratio $\Gamma_{ee}/\langle q_{\text{quark}}\rangle^2$ is approximately constant for all vector mesons, indicating that the assignment $q_c = \frac{2}{3}$ is correct (see fig. 19).

A last remark concerns the possibility of determining α_s from the ratio of leptonic and hadronic widths, which is independent of wave function ambiguities. A theoretical expression has been derived [17–19] in a non-relativistic approximation [see eq. (7) of section 2.1] including first-order α_s correction terms. The large $O(\alpha_s)$ correction corresponds to a substantial fraction of the total rate, suggesting that

*) The electromagnetic width has been calculated from the experimentally measured quantities $\Gamma_{ee}\Gamma_{had}/\Gamma_{tot} = (4.4\pm 0.2)$ keV, and $B_{had} = \Gamma_{had}/\Gamma_{tot} = 1\text{–}2\times B(J/\psi\to \ell^+\ell^-)$ assuming lepton universality.

Table 9
Predictions for Γ^0_{ee}.

Author	Reference	Γ^0_{ee} (keV)	Remarks
Bander et al.	[100]	9.0	lowest order in QCD
Falkensteiner et al.	[101]	13.3	lowest order in QCD
Eichten et al.	[102]	4.8	
Jacobs et al.	[103]	5.4	
Sum rules	[104]	4.3	
Gupta et al.	[105]	4.8	
Buchmüller et al.	[106]	3.7 ± 3.1	
Experiment		4.9 ± 0.3	

higher-order corrections cannot be neglected.*) As a result, perturbative QCD is only a qualitative guide to the decay rate of the J/ψ into hadrons. If one would simply ignore the QCD corrections of eq. (7), one would infer $\alpha_s \approx 0.18$ (see section 6.1).

5.3. Decays into meson pairs allowed by generalized C parity

In this section, the $\mathcal{C}$-allowed decays J/ψ→PV, TV, SV, and AV are discussed, where P, V, T, S, A denote members of the pseudoscalar, vector, tensor, scalar, and axialvector nonets, respectively. The results will be compared to an SU(3) inspired model [256], which is briefly outlined below.

5.3.1. A model for two-body J/ψ decays into meson pairs

In this chapter decays of the type J/ψ→NN′ are considered, where N denotes a member of an ideally mixed meson nonet (e.g. vector mesons) and N′ denotes a member of another meson multiplet.

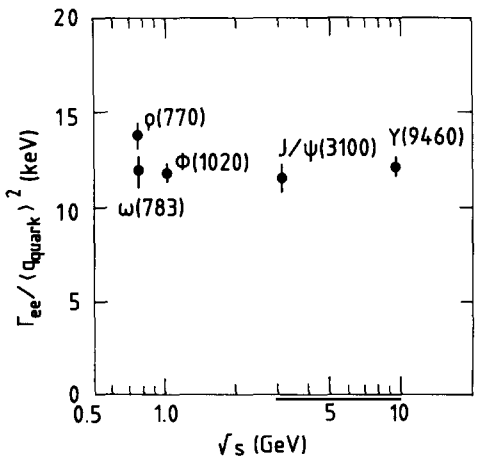

Fig. 19. Electromagnetic widths of vector mesons. Shown is the ratio of the leptonic width and the mean quark charge squared for the vector mesons $\rho = (u\bar{u} - d\bar{d})/\sqrt{2}$, $\omega = (u\bar{u} + d\bar{d})/\sqrt{2}$, $\phi = s\bar{s}$, $J/\psi = c\bar{c}$, and $\Upsilon = b\bar{b}$.

*) At the energy of the J/ψ the three gluons are not energetic enough to appear as three distinct jets, indicating that non-perturbative effects play a major role.

We restrict ourselves to decays allowed by generalized $\mathscr{C}$ parity (cf. table 3). A general prescription for all two- and three-body decays of J/ψ and η_c can be found in ref. [199]. As an example, we shall use the decays into a pair of a pseudoscalar and a vector meson (P + V); the model can be extended to other mesons by appropriate change of labeling. We follow here the prescription of ref. [256].

The wave functions of the two isosinglet mesons of the pseudoscalar nonet can be written [119] in terms of the non-strange and strange components X, Y*),

$$|\eta\rangle = (X_\eta/\sqrt{2})|u\bar{u} + d\bar{d}\rangle + Y_\eta|s\bar{s}\rangle + Z_\eta|\text{other components}\rangle\,,$$
$$|\eta'\rangle = (X_{\eta'}/\sqrt{2})|u\bar{u} + d\bar{d}\rangle + Y_{\eta'}|s\bar{s}\rangle + Z_{\eta'}|\text{other components}\rangle\,, \tag{48}$$

where we allow for additional contributions from other states like glueballs. In the absence of such additional components one obtains the constraints

$$X_\eta^2 + Y_\eta^2 = X_{\eta'}^2 + Y_{\eta'}^2 = 1\,, \qquad X_{\eta'} = -Y_\eta\,, \quad Y_{\eta'} = X_\eta\,; \tag{49}$$

however, we do not make this assumption in the following discussion.

The parametrization of the amplitudes for J/ψ two-body decays up to first order in the SU(3) breaking is done by the following terms [256] (compare to fig. 20):

- the SU(3) symmetric singly OZI violating (SOZI) amplitude represented by g,
- the nonet symmetry breaking, doubly OZI violating (DOZI) amplitude r, which is expressed relative to g, and
- the electromagnetic amplitude e.
- To account for SU(3) violations the following additional factors are applied:
  - a factor $(1 - s_g)$ for every strange quark contributing to g,
  - a factor $(1 - s_{V,P})$ for a strange member of the V or P nonet contributing to r, and
  - a factor $(1 - s_e)$ for every strange quark contributing to e.

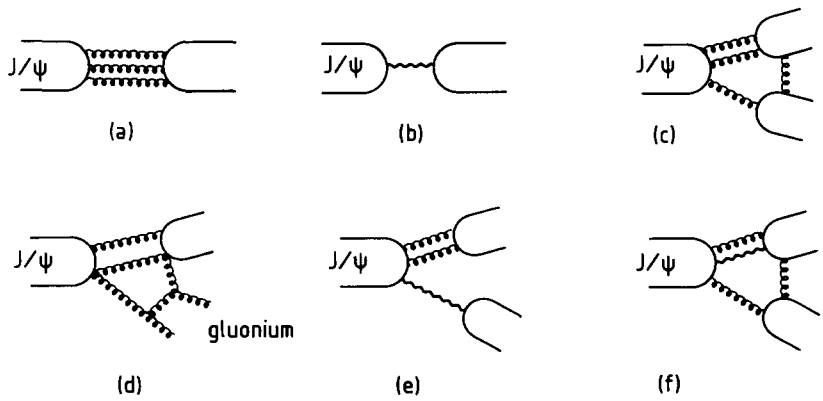

Fig. 20. J/ψ decay mechanisms. Shown are diagrams for (a) SOZI suppressed strong decays, (b) electromagnetic decays, (c) DOZI suppressed decays into mesons, (d) glueball production in DOZI suppressed decays, and (e), (f) DOZI suppressed electromagnetic decays.

*) If η and η′ were unmixed octet and singlet states, then $\eta = (u\bar{u} + d\bar{d} - 2s\bar{s})/\sqrt{6}$ and $\eta' = (u\bar{u} + d\bar{d} + s\bar{s})/\sqrt{3}$ corresponding to the quark components $X_{\eta'} = -Y_\eta = \sqrt{2/3}$, $X_\eta = Y_{\eta'} = \sqrt{1/3}$.

The DOZI amplitude is taken to be r times the SOZI amplitude times a coupling factor depending on the flavour content of the final state mesons. The coupling of the DOZI amplitude to the sum of u and d quarks is $\sqrt{2}$ times the coupling to strange quarks. In principle one has to account for corrections equivalent to the DOZI decays also for the electromagnetic amplitudes. The electromagnetic DOZI diagrams of figs. 20e and f can lead to corrections of 30% and 20% to the amplitude e of the one-photon exchange graph, respectively [256].

The model also tries to account for possible glueball production in J/ψ two-body decays. The DOZI graph provides a way to produce glueballs associated with hadrons, as can be seen from fig. 20. The corresponding expression in table 10 reflects the SU(3) singlet nature of gluonia; an additional parameter f accounts for the difference in the coupling of two gluons to glueballs as compared to quark states. With a similar ansatz, a possible gluonium admixture to quark states can also be accounted for.

The total amplitudes following these prescriptions are given in table 10. In order to simplify the expressions one can exploit the fact that e, r, s_g, s_V, and s_P are small numbers. Without desisting from the required precision one can drop any product of those quantities when compared with g or unity. This results in the expressions of table 14 of section 5.3.2. Note that DM2 [124] and earlier publications by Mark III [121] use an explicit SU(3) breaking term for the electromagnetic amplitude. Since the rate for this transition is proportional to the quark magnetic moments, which in turn depend on m_q^{-1}, the contribution of s quarks to the electromagnetic amplitude is suppressed by an amount characterized by the ratio of constituent quark masses, $x = m_u/m_s$ [120]. This second-order correction, if left out, does not dramatically change the results [121].

The expressions of table 14 are equivalent [256] to those calculated by Haber and Perrier [199], who use a somewhat less intuitive group theoretical approach. Note that, in a group theoretical language, the existence of DOZI contributions corresponds to nonet symmetry breaking.

5.3.2. *Decays into vector–pseudoscalar meson pairs*

The states assigned to the ground state pseudoscalar $q\bar{q}$ nonet with $J^{PC} = 0^{-+}$ are identified as $\eta(539)$, $\eta'(958)$, π, and K. The complete set of decay rates of the eleven possible pairings of

Table 10

Parametrization of amplitudes for J/ψ two-body decays. For clarity, the decays into pairs of vector and pseudoscalar mesons are taken as an example. The table can be used for any other decay of the J/ψ into two mesons that is allowed by generalized $\mathscr{C}$ parity by appropriate change of labeling.

Final state	SOZI amplitude	DOZI correction
$\rho^+\pi^-$, $\rho^0\pi^0$, $\rho^-\pi^+$	$g+e$	
$K^{*+}K^-$, $K^{*-}K^+$	$g(1-s_g)+e(1+s_e)$	
$K^{*0}\bar{K}^0$, $\bar{K}^{*0}K^0$	$g(1-s_g)-e(2-s_e)$	
$\omega\eta$	$(g+e)X_\eta$	$+\ \sqrt{2}rg[\sqrt{2}X_\eta+(1-s_P)Y_\eta]$
$\omega\eta'$	$(g+e)X_{\eta'}$	$+\ \sqrt{2}rg[\sqrt{2}X_{\eta'}+(1-s_P)Y_{\eta'}]$
$\phi\eta$	$[g(1-2s_g)-2e(1-s_e)]Y_\eta$	$+\ rg(1-s_V)[\sqrt{2}X_\eta+(1-s_P)Y_\eta]$
$\phi\eta'$	$[g(1-2s_g)-2e(1-s_e)]Y_{\eta'}$	$+\ rg(1-s_V)[\sqrt{2}X_{\eta'}+(1-s_P)Y_{\eta'}]$
$\rho\eta$	$3eX_\eta$	
$\rho\eta'$	$3eX_{\eta'}$	
$\omega\pi^0$	$3e$	
$\phi\pi^0$	0	
ω + glueball		$\sqrt{6}rgf$
ϕ + glueball		$\sqrt{3}rgf$

pseudoscalar and vector mesons that are allowed in strong and electromagnetic reactions has been determined. Since the pseudoscalar ground state mesons are either stable or narrow and tend to be produced relatively background free, it has been possible to examine many $J/\psi \to VP$ reactions in different final states. Most of the measurements stem from detailed studies undertaken by Mark III [121, 127] and DM2 [124, 125].

The decay matrix element in the J/ψ rest frame is proportional to

$$\hat{e}_\psi \cdot \hat{e}_V \times \boldsymbol{P}_V \,, \tag{50}$$

where $\hat{e}_\psi$ and $\hat{e}_V$ are the respective polarization vectors of the J/ψ and the vector mesons, and $\boldsymbol{P}_V$ is the momentum vector of V. The angular distribution of the decay sequence

$$\begin{aligned} J/\psi \to\ & \text{vector} + \text{pseudoscalar} \\ & \quad\ \big\lfloor \to 2 \text{ or } 3 \text{ pseudoscalars} \end{aligned} \tag{51}$$

is uniquely determined by the expression

$$\frac{d^3\sigma}{d\cos\theta_V\, d\cos\theta_1\, d\phi_1} \propto \sin^2\theta_1[1 + \cos^2\theta_V + \sin^2\theta_V \cos(2\phi_1)] \,, \tag{52}$$

where θ_V is the angle between the vector meson and the positron direction, and θ_1 and ϕ_1 describe the decay products of the vector meson in its helicity frame. For two-body decays, such as $\phi \to K^+K^-$, θ_1 and ϕ_1 are the polar and azimuthal angles of the momentum of the K^+ with respect to the helicity direction of the ϕ. For three-body decays like $\omega \to \pi^+\pi^-\pi^0$, they represent the angles of the normal to the decay plane with respect to the helicity direction. In the following paragraphs we will briefly describe the evidence for the final states that have been studied. The results are summarized in table 11, table 12, and table 13.

Table 11
Results on $J/\psi \to VP$ branching ratios (I). Shown are the results of the Mark I [167], DESY-Heidelberg [122], Pluto [123], DASP [67, 86], and Mark III [127] experiments for $I = 1$ and $I = 1/2$ pseudoscalars. All results are corrected for unobserved decay modes. The results of Mark I on the K*K final states have not been used in the average since they are incompatible with newer data.

Decay $J/\psi \to PV$	Final state	Branching ratio (units of 10^{-4})	Reference
$\rho^+\pi^-$, $\rho^0\pi^0$, $\rho^-\pi^+$	$\pi^\pm + X$	133 ± 21	DASP [67]
	$\pi^0\pi^+\pi^-$	100 ± 20	DESY-Heidelberg [122]
	$\pi^0\pi^+\pi^-$	130 ± 30	Mark I [167]
	$\pi^0\pi^+\pi^-$	160 ± 40	Pluto [123]
	$\pi^0\pi^+\pi^-$	$142 \pm 1 \pm 19$	Mark III [127]
		128 ± 10	⟨average⟩
$K^{*+}K^-$, $K^{*-}K^+$	$K^\pm + X$	41 ± 12	DASP [86]
	$K^+K^-\pi^0$	$56.6 \pm 1.2 \pm 8.3$	Mark III [127]
	$K^\pm K_S^0 \pi^\mp$	32 ± 6	Mark I [167]
	$K^\pm K_S^0 \pi^\mp$	$51.6 \pm 1.6 \pm 5.4$	Mark III [127]
		51.6 ± 4.4	⟨average⟩
$K^{*0}\bar{K}^0$, $\bar{K}^{*0}K^0$	$K^\pm K_S^0 \pi^\mp$	27 ± 6	Mark I [167]
	$K^\pm K_S^0 \pi^\mp$	$43.3 \pm 1.2 \pm 4.5$	Mark III [127]

Table 12
Results on J/ψ→VP branching ratios (II). Shown are the results of the Mark I [167], Mark III [127, 156] and DM2 [124] experiments for $I = 0$ pseudoscalars that can be produced by strong interactions. The preliminary results of DM2 are averaged over the indicated final states. With the exception of the iota/η(1440), all results are corrected for unobserved decay modes.

Decay J/ψ→PV	Final state	Branching ratio (units of 10^{-4})	Reference
ωη	$\pi^+\pi^-\pi^0\gamma\gamma$	$18.6 \pm 0.6 \pm 2.5$	Mark III [127]
	$\pi^+\pi^-\pi^0\pi^+\pi^-\gamma$	$14.9 \pm 1.7 \pm 2.2$	Mark III [127]
	$\pi^+\pi^-\pi^0\gamma\gamma$ $\pi^+\pi^-\pi^0\pi^+\pi^-\pi^0$	14.4 ± 1.4	DM2 [124]
		15.3 ± 1.1	⟨average⟩
ωη′	$\pi^+\pi^-\pi^0\pi^+\pi^0\gamma$	$1.67 \pm 0.25 \pm 0.24$	Mark III [127]
	$\pi^+\pi^-\pi^0\pi^+\pi^0\gamma$	1.9 ± 0.5	DM2 [124]
	$\pi^+\pi^-\pi^0\pi^+\pi^-\gamma\gamma$	$1.69 \pm 0.27 \pm 0.25$	Mark III [127]
	$3(\pi^+\pi^-)2\pi^0$	$1.54 \pm 0.51 \pm 0.26$	Mark III [127]
		1.70 ± 0.21	⟨average⟩
φη	$K^+K^-\pi^+\pi^-\pi^0$	10 ± 6	Mark I [167]
	$K^+K^-\pi^+\pi^-\pi^0$	$6.77 \pm 0.88 \pm 0.96$	Mark III [127]
	$K^+K^-\gamma\gamma$	$6.51 \pm 0.49 \pm 0.92$	Mark III [127]
	$K^+K^-\pi^+\pi^-\pi^0$ $K^+K^-\gamma\gamma$ $K^+K^-\pi^+\pi^-\gamma$	6.4 ± 0.6	DM2 [124]
		6.50 ± 0.48	⟨average⟩
φη′	$K^+K^-\pi^+\pi^-\gamma\gamma$ $K^+K^-\pi^+\pi^-\gamma$	4.05 ± 0.45	DM2 [124]
	$K^+K^-\pi^+\pi^-\gamma\gamma$	$2.90 \pm 0.50 \pm 0.39$	Mark III [127]
	$K^+K^-\pi^+\pi^-\gamma\gamma$	$3.27 \pm 0.46 \pm 0.49$	Mark III [127]
		3.57 ± 0.32	⟨average⟩
φι→φKK̄π	$K\bar{K}\pi$	<2.1 (90% C.L.)	Mark III [127]
	$K^\pm K_S^0 \pi^\mp$	<2.5 (90% C.L.)	DM2 [126]

Table 13
Results on J/ψ→VP branching ratios (III). Shown are the results of the Mark III [127, 156] and DM2 [124] experiments for $I = 0$ pseudoscalars that can only be produced electromagnetically. The results of DM2 are preliminary. All results are corrected for unobserved decay modes.

Decay J/ψ→PV	Final state	Branching ratio (units of 10^{-4})	Reference
$\omega\pi^0$	$\pi^+\pi^-\pi^0\pi^0$	5.1 ± 0.5	DM2 [124]
	$\pi^+\pi^-\pi^0\pi^0$	$4.82 \pm 0.19 \pm 0.64$	Mark III [127]
		5.00 ± 0.40	⟨average⟩
$\rho^0\eta$	$\pi^+\pi^-\gamma\gamma$	$1.91 \pm 0.13 \pm 0.34$	Mark III [127]
	$\pi^+\pi^-\pi^+\pi^-\pi^0$	1.9 ± 0.5	DM2 [124]
	$\pi^+\pi^-\pi^+\pi^-\pi^0$	$1.96 \pm 0.29 \pm 0.40$	Mark III [127]
		1.92 ± 0.25	⟨average⟩
$\rho^0\eta'$	$\pi^+\pi^-\pi^+\pi^-\gamma$	0.83 ± 0.3	DM2 [124]
	$\pi^+\pi^-\pi^+\pi^-\gamma$	$1.33 \pm 0.18 \pm 0.24$	Mark III [127]
	$\pi^+\pi^-\pi^+\pi^-\gamma\gamma$	$0.97 \pm 0.22 \pm 0.17$	Mark III [127]
		1.04 ± 0.17	⟨average⟩
$\phi\pi^0$	$K^+K^-\pi^0$	<0.068 (90% C.L.)	Mark III [127]

Figure 21 shows the Dalitz plots of the decays $J/\psi \to \pi^+\pi^-\pi^0$ and $J/\psi \to K\bar{K}\pi$. The decays are dominated by the $J/\psi \to \rho\pi$ and $J/\psi \to K^*\bar{K}$ reactions, respectively. The ratio $B(J/\psi \to \rho^0\pi^0)/B(J/\psi \to \rho^{\pm}\pi^{\mp}) = 0.49 \pm 0.01 \pm 0.03$ agrees well with the value 0.5 expected from isospin invariance. Similarly, the ratio $B(J/\psi \to K^{*0}\bar{K}^0)/B(J/\psi \to K^{*\pm}K^{\mp})$ is predicted to be 1. The measured value of $0.82 \pm 0.05 \pm 0.09$ can be taken as direct evidence for the presence of an isospin violating electromagnetic term in the decay amplitude, which, unlike the case of $\rho\pi$, contributes differently to the charged and neutral states (see table 11).

Evidence for $J/\psi \to \omega\eta$ and the isospin violating $J/\psi \to \omega\pi^0$ decay is presented in fig. 22. From the $J/\psi \to \omega\pi^0$ reaction, which can be considered purely electromagnetic in nature, one can determine the $\omega\pi^0$ form factor at $Q^2 = m_\psi^2$. Normalizing to the form factor at $Q^2 = 0$ by using the crossed channel decay $\omega \to \gamma\pi^0$ [14], one finds

$$\frac{|F(m_\psi^2)|}{|F(0)|} = \sqrt{\frac{\alpha}{3}\left(\frac{P_\gamma}{P_\omega}\right)^3 \frac{m_\psi \Gamma(J/\psi \to \omega\pi^0)}{\Gamma(J/\psi \to \gamma\pi^0)\Gamma(J/\psi \to \mu\mu)}} = 0.0335 \pm 0.0059 . \tag{53}$$

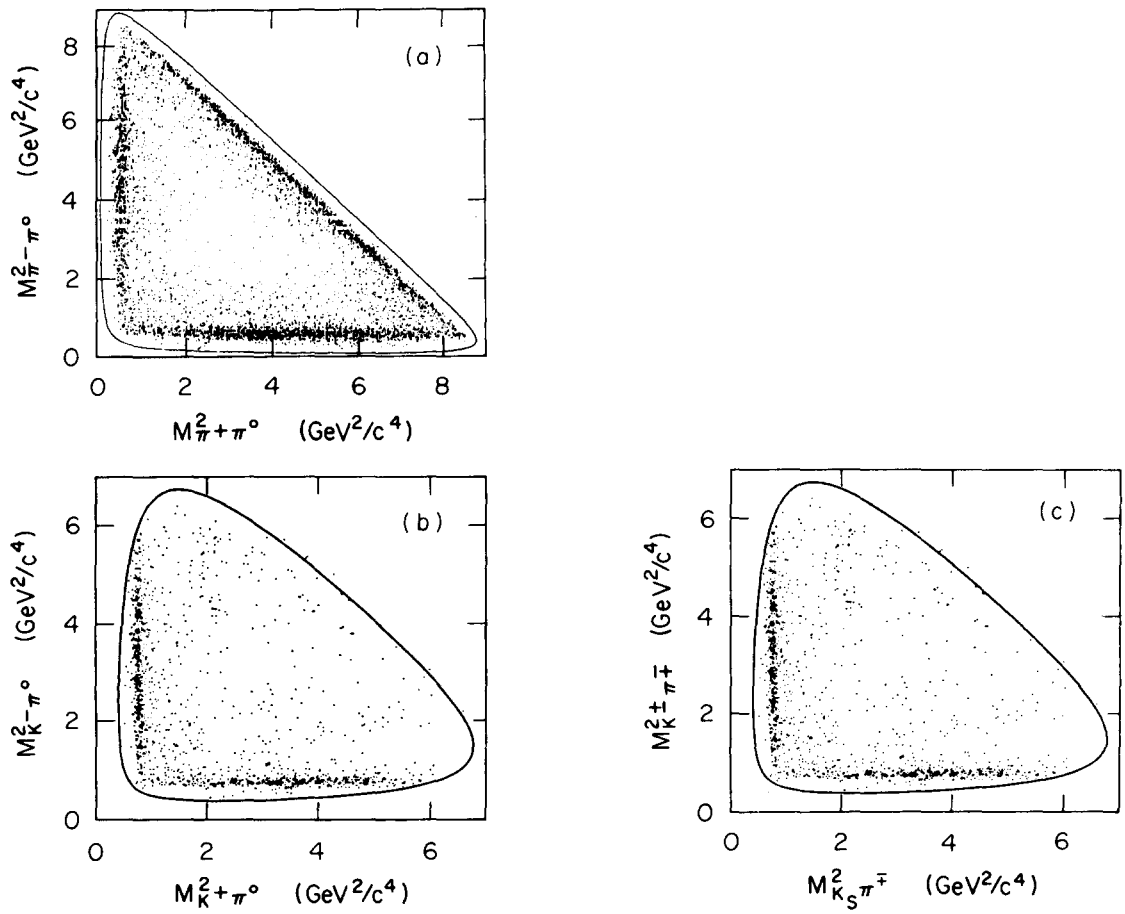

Fig. 21. Dalitz plots of the $\pi^+\pi^-\pi^0$ and $K\bar{K}\pi$ final states. Shown are the Dalitz plots corresponding to (a) the $J/\psi \to \pi^+\pi^-\pi^0$, (b) $J/\psi \to K^+K^-\pi^0$ and (c) $J/\psi \to K^{\pm}K^0_S\pi^{\mp}$ reactions (Mark III [121]). Note the bands corresponding to ρ's and K*'s, respectively.

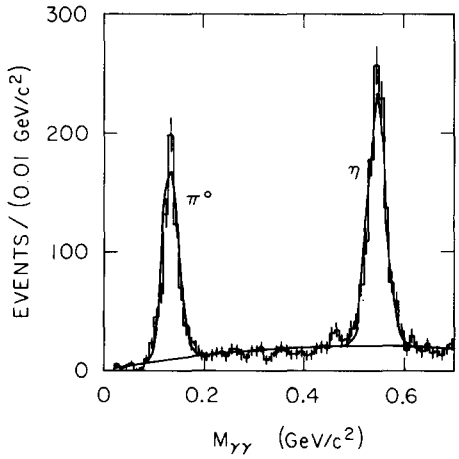

Fig. 22. Evidence for $J/\psi \to \omega\pi^0$ and $J/\psi \to \omega\eta$. Shown is the invariant mass distribution of the $\gamma\gamma$ system from the $J/\psi \to \omega\gamma\gamma$, $\omega \to \pi^+\pi^-\pi^0$ reaction (Mark III [127]).

Here P_γ (P_ω) is the photon (ω) momentum in the ω (J/ψ) rest frame. Comparing this result with that for the $\pi^+\pi^-$ electromagnetic form factor at $Q^2 = m_\psi^2$ (see section 5.4), one notices a suppression by roughly a factor 3. This difference in energy dependence agrees qualitatively with the prediction that hadronic helicity conservation requires the $\omega\pi^0$ form factor to be suppressed by $O(Q^2)$ relative to that for $\pi^+\pi^-$ [164].

It has been pointed out [128] that even a small $\rho^0 \to \pi^+\pi^-\pi^0$ decay mode could change the true $J/\psi \to \omega\pi^0$ branching ratio significantly due to an interference effect similar to the $J/\psi \to \{\omega, \rho\} + \eta$ case which is discussed below.

Evidence for the very clean $J/\psi \to \phi\eta$ decay is obtained from fig. 23. No sign is found for the $J/\psi \to \phi\pi^0$ reaction, which can only proceed by an electromagnetic, doubly OZI violating process (see fig. 20), or if the vector meson nonet were not ideally mixed. The upper limit of $B(J/\psi \to \phi\pi^0) <$

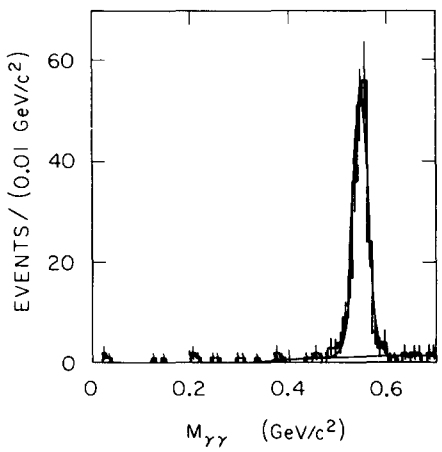

Fig. 23. Distribution of $\gamma\gamma$ invariant masses in $J/\psi \to \phi\gamma\gamma$ decay. The $\gamma\gamma$ system, produced in association with a ϕ meson, shows clear evidence for an η but not a π^0 (Mark III).

6.8×10^{-6} at 90% confidence level demonstrates that electromagnetic DOZI processes play a negligible role in $J/\psi \to PV$ decays.

Clear signals for the $J/\psi \to \omega\eta'$ and $J/\psi \to \phi\eta'$ reactions can be seen in fig. 24 and fig. 25. One should emphasize that finding the $\omega\eta'$ signal in the $2(\pi^+\pi^-)4\gamma$ and $3(\pi^+\pi^-)4\gamma$ channels, with, respectively, 24 and 54 possible permutations to form the $\omega \to \pi^+\pi^-\pi^0$, $\eta \to \gamma\gamma$ ($\eta \to \pi^+\pi^-\pi^0$), and $\eta' \to \eta\pi^+\pi^-$ subsystems, constitutes a challenge to experimentalists, indeed. Still, the reaction can clearly be separated from background by employing 6C kinematic fits and exploiting that ω, η, and η' all are narrow resonances.

Like the $J/\psi \to \omega\pi^0$ decay, the $J/\psi \to \rho\eta$ and $J/\psi \to \rho\eta'$ decays violate isospin and thus are electromagnetic in nature. When studying the $\pi^+\pi^-$ mass spectrum of the $\eta\pi^+\pi^-$ final state, one notices that the ρ peak at 0.77 GeV does not resemble the shape of an ordinary Breit–Wigner resonance (fig. 26). This effect can be attributed to interference [128] between the electromagnetic $J/\psi \to \rho\eta$ decay and the much more abundant $J/\psi \to \omega\eta$ decay, which, even for the relatively rare $\omega \to \pi^+\pi^-$ decay, gives a sizeable contribution. This is demonstrated by the fitted curve in fig. 26, which is based on the ansatz

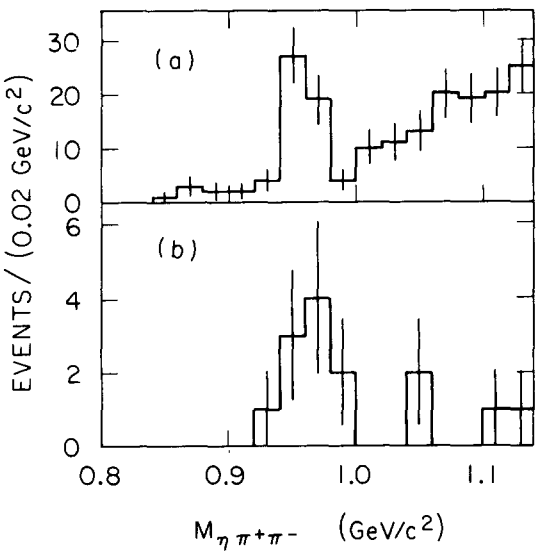

Fig. 24. Evidence for $J/\psi \to \omega\eta'$. Shown are $\eta\pi^+\pi^-$ invariant mass distributions, where the η is detected in its (a) $\gamma\gamma$ and (b) $\pi^+\pi^-\pi^0$ decay mode (Mark III [127]).

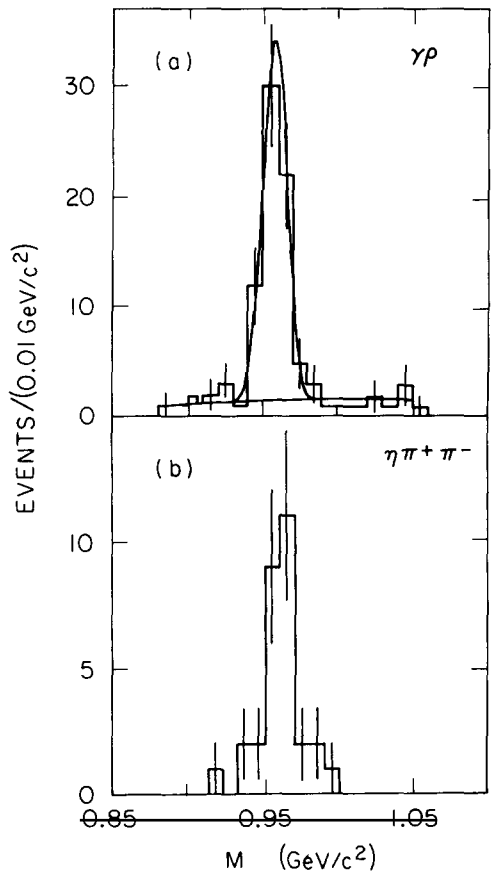

Fig. 25. Evidence for $J/\psi \to \phi\eta'$. Shown are (a) $\gamma\rho$ and (b) $\eta\pi^+\pi^-$ invariant mass distributions. The ϕ is detected in its K^+K^- decay mode (Mark III [127]).

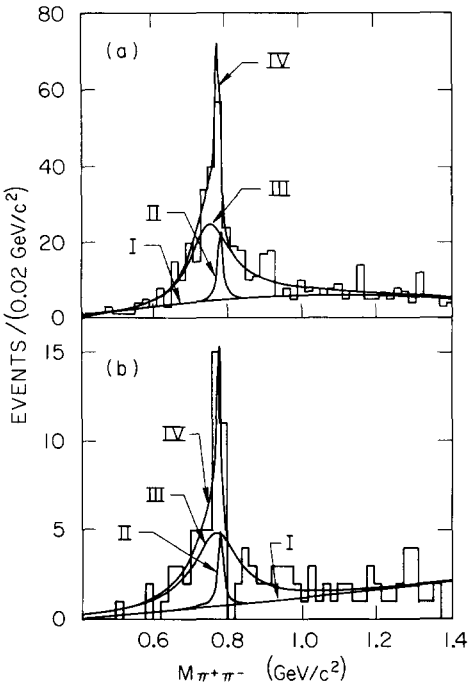

Fig. 26. Interference effects in the $J/\psi \to \pi^+\pi^-\eta$ reaction. Shown is the $\pi^+\pi^-$ invariant mass distribution for events of the type $J/\psi \to \pi^+\pi^-\eta$ with (a) $\eta \to \gamma\gamma$ and (b) $\eta \to \pi^+\pi^-\pi^0$. The curves represent (I) background, (II) ω, (III) ρ^0, and (IV) coherent sum of ρ^0 and ω contributions, each with the background term included (Mark III [121]).

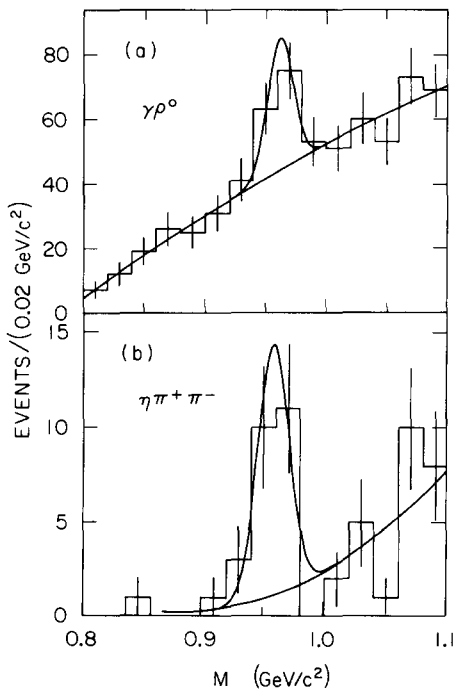

Fig. 27. Evidence for the $J/\psi \to \rho\eta'$ reaction. Shown is the distribution of the (a) $\gamma\pi^+\pi^-$ and (b) $\eta\pi^+\pi^-$ invariant mass spectra (Mark III [127]).

$$N(m_{\pi\pi}) = \text{background} + \left|\sqrt{N_\rho}\,\mathrm{BW}_\rho(m_{\pi\pi}) + \sqrt{N_\omega}\,\mathrm{BW}_\omega(m_{\pi\pi})\,e^{i\phi}\right|^2 . \tag{54}$$

The number of ρ's and ω's (N_ρ and N_ω, respectively) as well as the relative phase ϕ are treated as free parameters. BW_i denotes the appropriate Breit–Wigner amplitude for ρ and ω, respectively. Evidence for the $J/\psi \to \rho\eta'$ reaction is presented in fig. 27.

Interpretation of the results. The well-measured set of all possible decays of the J/ψ into pairs of vector and pseudoscalar mesons allows one to systematically study quark and gluon contents of the pseudoscalar mesons, as well as the effect of SU(3) breaking and electromagnetic amplitudes in two-body decays of the J/ψ. For this end, the decay rates have been compared to the model outlined in section 5.3, neglecting second-order effects (see table 14). The matrix element contains an explicit momentum factor [see eq. (50)], which can be factored out to define the reduced branching ratio $\tilde{B}$,

$$B(J/\psi \to \text{vector} + \text{pseudoscalar}) = \tilde{B}P_V^3 , \tag{55}$$

where the third power reflects the p wave between the two final state mesons. The amplitude decompositions for the various final states as well as the reduced branching ratios determined by Mark III [127] and DM2 [124] are compiled in table 14. For the following discussion only the relative

magnitudes of the various amplitudes are important. Common systematic errors that affect only the absolute normalization in the experiments have therefore been disregarded. Even without a full determination of the various amplitudes by means of fitting it is clear that the SU(3) breaking and electromagnetic amplitudes play a non-negligible role. Not only is the $K^*\bar{K}$ mode suppressed compared to $\rho\pi$, the rates for charged and neutral K^*K systems differ, too. The need for a doubly OZI violating amplitude (DOZI) can be inferred from a comparison of the ratios (Mark III)

$$\frac{\tilde{B}(J/\psi\to\omega\eta)}{\tilde{B}(J/\psi\to\omega\eta')}=6.4\pm1.2 \quad \text{and} \quad \frac{\tilde{B}(J/\psi\to\rho^0\eta)}{\tilde{B}(J/\psi\to\rho^0\eta')}=1.3\pm0.3\,, \tag{56}$$

which, for a negligible DOZI contribution, should both be equal (see table 14).

In order to determine both the strange and non-strange components of η and η', as well as the effect of SU(3) breaking, electromagnetic, and doubly OZI violating amplitudes, it is necessary to perform a global fit to the amplitudes listed in table 14. In the first analysis of this kind, performed by Mark III [121], dominance of singly OZI violating diagrams has been assumed. This early study has led to the conclusion that, while the η meson wave function is almost saturated by its quark components, there may be an additional singlet contribution to the η' wave function introduced by mixing with other pseudoscalars or glue components. As pointed out by Pinsky and others [129], the principal deficiency of the Mark III analysis is the assumption that doubly disconnected diagrams do not contribute. A small doubly OZI violating amplitude can produce a large effect due to interference with the dominant SOZI amplitude.

Subsequently, Mark III [256] and DM2 [124] repeated the analysis allowing for a contribution of the doubly disconnected diagram (DOZI), which is parametrized by the relative coupling constant r (table 14). Leaving the quark components X_η, $X_{\eta'}$, Y_η and $Y_{\eta'}$ unconstrained and with twice as many data as before, Mark III [256] now finds that

$$X_\eta^2+Y_\eta^2=1.00\pm0.16\,, \qquad X_{\eta'}^2+Y_{\eta'}^2=1.44\pm0.25\,. \tag{57}$$

Table 14

Parametrization of amplitudes for $J/\psi\to PV$. The results of the Mark III [127] and DM2 [124] Collaborations on the reduced branching ratio $\tilde{B}=B/p^3$ are compared to the parametrization of the amplitude described in section 5.3. As an approximation, all terms quadratic in small amplitudes have been dropped. In the determination of $\tilde{B}$ common systematic errors due to the normalization have been omitted and the remaining statistical and systematic errors have been added in quadrature. The SOZI amplitude is g, the relative DOZI amplitude is r, s_g characterizes the SU(3) violation, and e is the electromagnetic amplitude.

Process $J/\psi\to PV$	SOZI amplitude		DOZI correction	$\tilde{B}$ (Mark III) (units of 10^{-3})	$\tilde{B}$ (DM2) (units of 10^{-3})
$\rho^+\pi^-$, $\rho^0\pi^0$, $\rho^-\pi^+$	$g+e$			1.556 ± 0.161	
$K^{*+}K^-$, $K^{*-}K^+$	$g(1-s_g)+e$			1.017 ± 0.061	
$K^{*0}\bar{K}^0$, $\bar{K}^{*0}K^0$	$g(1-s_g)-2e$			0.836 ± 0.055	
$\omega\eta$	$(g+e)X_\eta$	+	$\sqrt{2}rg(\sqrt{2}X_\eta+Y_\eta)$	0.632 ± 0.058	0.531 ± 0.052
$\omega\eta'$	$(g+e)X_{\eta'}$	+	$\sqrt{2}rg(\sqrt{2}X_{\eta'}+Y_{\eta'})$	0.079 ± 0.010	0.091 ± 0.024
$\phi\eta$	$[g(1-2s_g)-2e]Y_\eta$	+	$rg(\sqrt{2}X_\eta+Y_\eta)$	0.287 ± 0.031	0.278 ± 0.026
$\phi\eta'$	$[g(1-2s_g)-2e]Y_{\eta'}$	+	$rg(\sqrt{2}X_{\eta'}+Y_{\eta'})$	0.182 ± 0.025	0.239 ± 0.027
$\rho\eta$	$3eX_\eta$			0.071 ± 0.010	0.070 ± 0.018
$\rho\eta'$	$3eX_{\eta'}$			0.054 ± 0.009	0.039 ± 0.014
$\omega\pi^0$	$3e$			0.159 ± 0.017	0.169 ± 0.016
$\phi\pi^0$	0			<0.0026	

A graphical presentation of the different measurements on the non-strange and strange quark components of η and η′ is given in the "Rosner plot" [119] of fig. 28. When allowing for a doubly OZI violating contribution, both η and η′ are consistent with being solely composed of u, d, s quarks, with no need for other components. The values for the coupling constants obtained from fits to the Mark III and DM2 data are listed in table 15. The results of the two experiments are in fair agreement, reaffirming that the SU(3) breaking term $|s|$, the electromagnetic term $|e|$, and the DOZI term $|r|$ are all small, equaling 16%, 11%, and 10% of $|g|$, respectively. Setting $r = 0$ results in non-acceptable fits with typically χ^2/d.o.f. $\approx 25/2$ [256]. Changing the constraints on the η, η′ quark contents or using additional information from two-photon decays and radiative J/ψ decays does not significantly affect the results.

To decrease the number of free parameters DM2 and Mark III repeated the fits assuming only $q\bar{q}$ components in the η and η′ wave functions ($X^2 + Y^2 = 1$). The η–η′ mixing angle, θ_p, is then related to X_η, $X_{\eta'}$, Y_η, and $Y_{\eta'}$ according to the expressions

$$X_\eta = Y_{\eta'} = \sqrt{1/3}\cos\theta_p - \sqrt{2/3}\sin\theta_p\,, \tag{58}$$

$$X_{\eta'} = -Y_\eta = \sqrt{1/3}\sin\theta_p + \sqrt{2/3}\cos\theta_p\,, \tag{59}$$

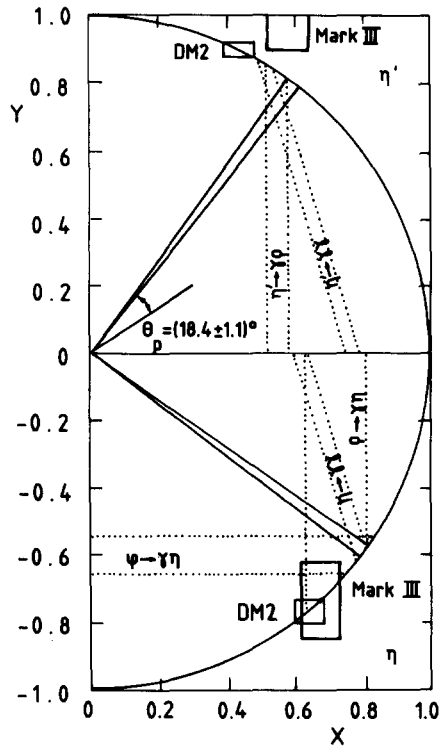

Fig. 28. Rosner plot for η and η′. The results of the Mark III [127] and DM2 [124] experiments are compared to two-photon results and measurements of the radiative widths of pseudoscalar mesons [131]. X and Y represent the non-strange and strange quark fractions of the states. The circle corresponds to $X^2 + Y^2 = 1$. Note that the DM2 results have been obtained using additional constraints on the η, η′ quark contents (table 15).

Table 15
Results from a global fit to J/ψ→PV decays. Shown are the results of the Mark III [256] and DM2 [124] Collaborations on fits allowing for doubly OZI violating contributions. While the quark contents of η, η′ are left unconstrained in the Mark III fits, the DM2 results are constrained by the conditions $X_\eta^2 + Y_\eta^2 = 1$ and $X_{\eta'}^2 + Y_{\eta'}^2 = 1$.

Coupling	Mark III	DM2
$\|g\|$	1.21 ± 0.05	1.120 ± 0.041
$\|s_g\|$	0.21 ± 0.04	0.176 ± 0.030
$\|e\|$	0.13 ± 0.01	0.137 ± 0.006
θ_e	1.26 ± 0.11	1.170 ± 0.090
r	−0.14 ± 0.02	−0.088 ± 0.019
X_η	0.67 ± 0.05	0.637 ± 0.044
Y_η	−0.74 ± 0.10	−0.771 ± 0.037
$X_{\eta'}$	0.58 ± 0.06	0.436 ± 0.044
$Y_{\eta'}$	1.05 ± 0.12	0.900 ± 0.021
χ^2/d.o.f.	0.02	0.047

or equivalently,

$$\tan\theta_p = -\frac{\sqrt{2}X_\eta + Y_\eta}{X_\eta - \sqrt{2}Y_\eta} = \frac{X_{\eta'} - \sqrt{2}Y_{\eta'}}{\sqrt{2}X_{\eta'} + Y_{\eta'}} . \tag{60}$$

An evaluation of the formulae yields [124, 127]

$$\theta_p = (-19.0 \pm 1.0)^\circ \quad \text{Mark III}, \qquad \theta_p = (-20.0 \pm 1.6)^\circ \quad \text{DM2}, \tag{61}$$

in agreement with two-photon results [130, 131], $(-18.4 \pm 1.1)^\circ$, and other determinations [241].

DM2 [124] has addressed the question whether a glue content of the η′ is excluded from the measured branching ratios in table 14. A gluonic component in the η′ ($Z_{\eta'}$) could couple to the singlet parts of ω and φ through the disconnected diagram of fig. 20c. The results on the quark content of η, η′ are essentially left unchanged, and the allowed gluonic part of the η′ is found to be very small ($|Z_{\eta'}|^2 \approx 1\%$).

Finally, one may ask oneself whether *gluonic states* are expected to be observed in two-body hadronic J/ψ decays. Glueballs could be produced either by mixing with other pseudoscalars or directly via the doubly OZI forbidden diagram of fig. 20 (see also table 10). The data do not show evidence for the excitation of the "iota"/η(1440) in hadronic J/ψ decays (see table 12). In chapter 7 the experimental observation is confronted with the prediction of Seiden et al. [256].

5.3.3. Decays into vector–scalar meson pairs

The states traditionally assigned to the scalar $q\bar{q}$ nonet are the $f_0(975)$, $f_0(1300)$, $a_0(980)$, and $K_0^*(1350)$, formerly called S*, ε, δ, and κ. While the evidence for the broad $f_0(1300)$ is weak, the $f_0(975)$ and the $a_0(980)$ have been firmly established for quite some time. In the quark model their natural assignment is that of the singlet and triplet states of the $^3P_0$ nonet with $J^{PC} = 0^{++}$. However,

there are problems with this interpretation (see, e.g., mini review in ref. [132]). Other than $q\bar{q}$ states*), the $f_0(975)$ and $a_0(980)$ have been speculated to be four-quark states [134], loosely bound $K\bar{K}$ molecules [135], or to be mixed with scalar gluonia [136]. A phase shift analysis of central $p\bar{p} \to \pi\pi(K\bar{K})$ production [137] suggests more than one isoscalar resonance around 1 GeV, one of which could be a glueball [138].

Depending on the interpretation one obtains different predictions for the production of $f_0(975)$ and $a_0(980)$ in hadronic J/ψ decays. The classification of the $f_0(975)$ as an $s\bar{s}$ state implies that

$$B(J/\psi \to \omega f_0(975)) \approx 0\,, \tag{62}$$

and, neglecting phase space and SU(3) breaking effects,

$$B(J/\psi \to \rho a_0(980)) = 3 \times B(J/\psi \to \phi f_0(975))\,. \tag{63}$$

If, however, $f_0(975)$ and $a_0(980)$ are $K\bar{K}$ molecules, the expected $J/\psi \to \rho a_0(980)$ rate is much smaller than for the $q\bar{q}$ case. In the SU(3) symmetric limit one predicts that [130]

$$B(J/\psi \to \rho a_0(980)) = \tfrac{3}{2} \times B(J/\psi \to \phi f_0(975)) = 3 \times B(J/\psi \to \omega f_0(975))\,. \tag{64}$$

The $K\bar{K}$ molecule predictions are expected to be relatively immune to SU(3) breaking effects since both final states contain the same number of s quarks from the "sea". This is not the case if $f_0(975)$ and $a_0(980)$ are $q\bar{q}$ states, where SU(3) breaking effects are expected to suppress the $J/\psi \to \phi f_0(975)$ decay, similar to the case of the tensor mesons**) (see section 5.3.3).

The $f_0(975)$ has been searched for in the $\pi\pi$ and $K\bar{K}$ final states recoiling against ω and φ by the Mark II [140], DM2 [141], and Mark III [142] experiments, as well as in an inclusive study of $\pi^+\pi^-$ pairs [140] (see section 5.1). Figure 29a,b shows the slightly asymmetrical signal for the $f_0(975) \to \pi^+\pi^-$ decay associated with a recoiling φ meson. The observed angular distribution is consistent with that of a scalar state [126]. The K^+K^- mass spectrum recoiling against the φ, on the other hand, does not show a narrow peak at the $f_0(975)$ mass and instead exhibits a wide threshold enhancement as shown in fig. 29c.

These observations, together with the fact that the $f_0(975)$ mass is close to the $K\bar{K}$ threshold, can be explained by a coupled channel effect. In this scheme a wide and low-mass $f_0(975)$ prefers to decay into $K\bar{K}$. However, being partly below $K\bar{K}$ threshold, only its high-mass tail will be visible in the $K\bar{K}$ channel. In the $\pi\pi$ channel unitarity effects lead to a narrow "cusp" at $K\bar{K}$ threshold and a sharp fall-off on the high-mass side of the $f_0(975)$. The branching ratios, which were determined using the simple coupled channel parametrization à la Flatté [143] as well as more refined relativistic parametrizations [144], are listed in table 16. In the framework of these models, the fitted parameters for the $\pi^+\pi^-$ spectrum can be used to predict the corresponding rate in the K^+K^- channel. The Flatté parametrization is in rough agreement with the data. In a model [141] that couples $f_0(975)$ and $f_0(1300)$ to $\pi\pi$, $K\bar{K}$, 4π, 4K, etc., the fit to the $f_0(975)$ in $\pi\pi$ is improved (fig. 29a) and the shape of the K^+K^- spectrum is correctly predicted (fig. 29c).

*) Shabalin [133] and Törnqvist [133] find that f_0 and a_0 are unitarized remnants of conventional $q\bar{q}$ states with large components of $q\bar{q}q\bar{q}$, mainly in the form of virtual $K\bar{K}$ states.

**) In the case of the tensor mesons one finds that $B(J/\psi \to \rho^0 a_2^0(1320)) \approx 5 \times B(J/\psi \to \phi f') \times B(f' \to K\bar{K})$.

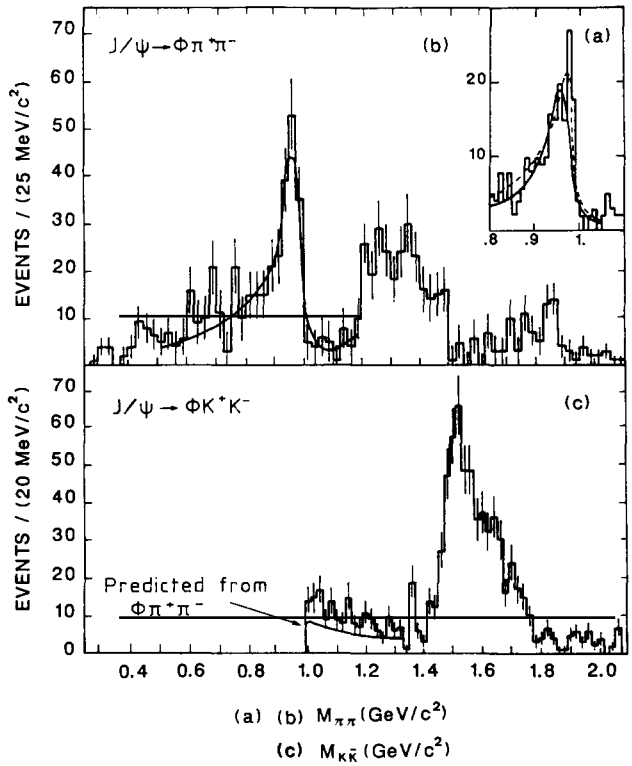

Fig. 29. Evidence for the $J/\psi \to \phi f_0(975)$ decay. In (a) and (b) the $\pi^+\pi^-$ invariant mass spectrum from the $J/\psi \to K^+K^-\pi^+\pi^-$ decay as obtained by DM2 [141] is shown. The solid line in (a) corresponds to a fit using a Flatté-type coupled channel Breit–Wigner parametrization [143], the dashed curve refers to the Menessier model [144]. The K^+K^- mass spectrum associated with a ϕ is displayed in (c). The expectation from the fit to the $\pi\pi$ spectrum is given by the solid line.

Table 16

Scalar resonances observed in two-body J/ψ decays. Listed are published results from the Mark II [140], and preliminary results from the DM2 [141] and Mark III [142] experiments. The decay rates of the isoscalar $f_0(975)$ are corrected for the unobserved $\pi^0\pi^0$ mode. In addition, in the calculation of the average the unobserved decay modes of the $f_0(975)$ are taken into account using the value $B(f_0(975) \to \pi\pi) = 0.78 \pm 0.03$ [14]. Note, that the $\eta\pi$ decay of the $a_0(980)$ is presumably dominant [147].

Final state	Decay mode of scalar	Branching ratio (units of 10^{-4})	Experiment
$\phi f_0(975)$	$\pi\pi$	2.0 ± 0.5	Mark II [140]
	$\pi\pi$	$3.4 \pm 0.5 \pm 0.8$	Mark III [142]
	$\pi\pi$	$3.6 \pm 0.3 \pm 0.6$	DM2 [126]
	all	3.5 ± 0.5	⟨average⟩
$\omega f_0(975)$	$\pi\pi$	$0.95 \pm 0.10 \pm 0.22$	DM2 [141]
	all	1.22 ± 0.31	
$\rho a_0(980)$	$\eta\pi$	<4.4 (90% C.L.)	Mark III [142]

The DM2 Collaboration [141] has also searched for the $J/\psi \to \omega f_0(975)$ decay. The $\pi^+\pi^-$ mass spectrum (fig. 30) exhibits a small signal at $m = (0.9544 \pm 0.0034)$ GeV. The actual fit parameters depend heavily on the kind of parametrization used for the $f_0(975)$ and the $f_2(1270)$, the dominant state in this channel. If the structure is interpreted as being due to the $f_0(975)$, the branching ratio listed in table 16 is obtained.

The Mark III Collaboration [145] has searched for the isovector partner of the $f_0(975)$, the $a_0(980)$, in the $J/\psi \to \rho\eta\pi$ reaction. While a peak at the $a_2(1320)$ mass is apparent (see also section 5.3.4), fig. 31 shows little evidence for an $a_0(980)$ signal in conjunction with the ρ. The corresponding upper limit for the branching ratio (see table 16) is approximately 25 times smaller than that of other decays to isovector pairs. If $B(a_0(980) \to \eta\pi)$ is sufficiently large,*) the observations are in contradiction to the interpretation of $f_0(975)$ and $a_0(980)$ as $s\bar{s}$ and $(1/\sqrt{2})(u\bar{u} - d\bar{d})$ states of the 0^{++} nonet. The $K\bar{K}$

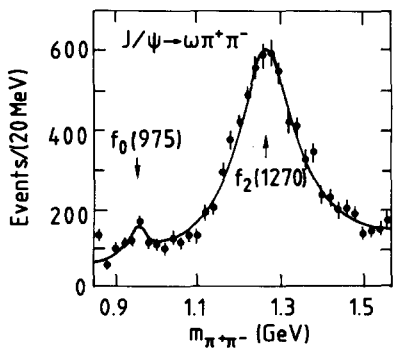

Fig. 30. Evidence for the $J/\psi \to \omega f_0(975)$ reaction. Shown is the $\pi^+\pi^-$ invariant mass spectrum from the $J/\psi \to \omega\pi^+\pi^-$ reaction as observed by DM2 [141]. The accumulation of events around 0.954 GeV is interpreted as the $f_0(975)$.

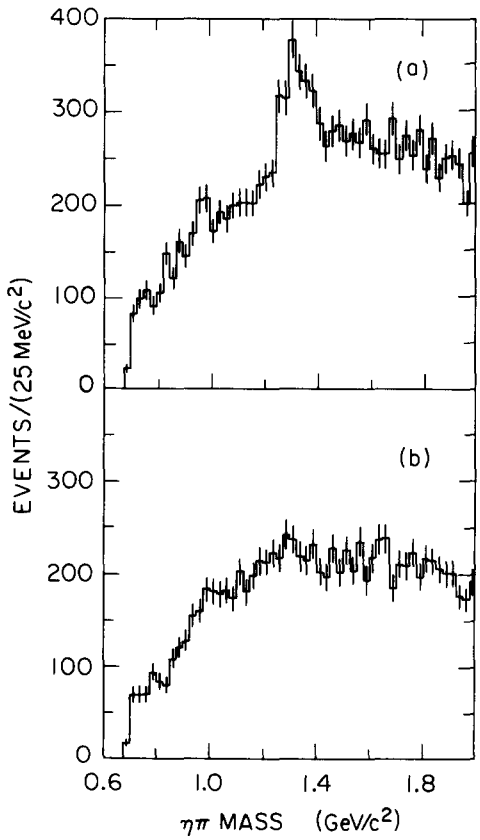

Fig. 31. Search for the $J/\psi \to \rho a_0(980)$ reaction. Shown in (a) are the combined $\eta\pi^+$, $\eta\pi^-$, and $\eta\pi^0$ mass spectra associated with ρ^-, ρ^+, ρ^0, respectively (Mark III [145]). The peak corresponds to the reaction $J/\psi \to \rho a_2(1320)$. An estimate of events not containing a ρ, obtained from the ρ sidebands is shown in (b).

*) From a fit to the $f_1(1285) \to a_0(980)\pi \to K\bar{K}\pi$, $\eta\pi\pi$ reaction, Achasov et al. [146] have determined the ratio of coupling constants to be $3/4 < g^2(a_0 \to K^+K^-)/g^2(a_0 \to \eta\pi) < 4.2$. It has been pointed out by Barnes [147] that the corresponding ratio of branching ratios is much smaller $[B(a_0 \to K\bar{K})/B(a_0 \to \eta\pi) \approx O(10^{-1})]$, since an additional phase space factor p_K/p_η has to be applied.

molecule hypothesis appears to be more attractive and the observation of $J/\psi \to \omega f_0(975)$, if confirmed, would support this hypothesis.

5.3.4. Decays into vector–tensor meson pairs

All members of the lowest lying tensor multiplet with the quantum numbers $^3P_2$, $J^{PC} = 2^{++}$ are identified beyond doubt (see fig. 5). Still, the observed deviation from ideal mixing by 7° has prompted some speculation of whether this is due to mixing with additional tensor states [148], outside the ground state nonet. One may hope that a systematic study of all $J/\psi \to V + T$ decays, including the search [59, 149] for the glueball candidate $f_2(1720)$, gives additional insight, like in the case of the pseudoscalar mesons. However, the analysis of $J/\psi \to V + T$ decays is more involved than that for $J/\psi \to V + P$ since neither the angular distributions nor the momentum dependence of the five matrix elements are uniquely determined. The matrix elements can be expressed in terms of Lorentz invariant amplitudes that explicitly include the momentum factors in the production [150].

Even though *vector–tensor* final states have been studied by various experiments, Mark I [167], Pluto [157], DM2 [110, 141], and Mark III [142, 145, 150, 171], the set of measured branching ratios is far from being complete (see table 17). In particular, the purely electromagnetic decays have not been investigated, forbidding a comprehensive analysis as performed for the $J/\psi \to V + P$ decays.

Clear evidence for the isoscalar $f_2(1270)$ in the $J/\psi \to \omega\pi^+\pi^-$ decay is depicted in fig. 32 (Mark III) and fig. 47 (DM2). The broad enhancement around 0.5 GeV is discussed in section 5.5, the small enhancement near 1 GeV may be due to the $f_0(975)$ as mentioned in section 5.3.3. Part of the background underneath the $f_2(1270)$ peak arises from the decay $J/\psi \to b_1(1235)^{\pm}\pi^{\mp} \to \omega\pi^+\pi^-$, which populates the same final state (see fig. 38).

Evidence for the $s\bar{s}$ state $f_2'(1525)$ in the K^+K^- and $K_S^0K_S^0$ systems produced in association with a ϕ is

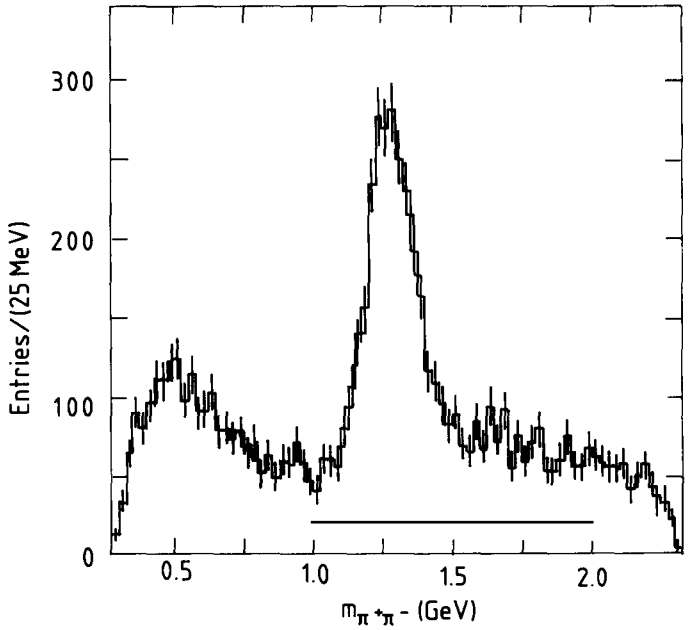

Fig. 32. Evidence for the $f_2(1270)$ in hadronic J/ψ decays. Shown is the $\pi^+\pi^-$ invariant mass distribution recoiling against an ω from the $J/\psi \to \omega\pi^+\pi^-$ decay (Mark III [145]).

Table 17
Tensor resonances seen in two-body J/ψ decays. Listed are results from the Mark I [167], Mark II [90], Pluto [157], DM2 [110, 126], and Mark III [142, 145, 150, 171] experiments. The results by Mark III are preliminary. The Mark I measurement of $J/\psi \to \omega f$ is not included in the average. Isospin corrections assume $I = 0$. Upper limits are given at the 90% confidence limits.

Decay J/ψ→ vector + X	Mode X→	Branching ratio (units of 10^{-4})	Experiment
$\omega f_2(1270)$	all	19 ± 8	Mark I [167]
	all	40 ± 14	Pluto [157]
	all	40 ± 6	DM2 [110]
	all	$49.3 \pm 2.5 \pm 12.5$	Mark III [142]
	all	41.5 ± 5.1	⟨average⟩
$\phi f_2(1270)$	all	<3.7	Mark I [167]
	all	<4.5	DM2 [126]
$\omega f_2'(1525)$	$K\bar{K}$	<2.0	DM2 [126]
	$K\bar{K}$	<1.2	Mark III [142]
$\phi f_2'(1525)$	$K\bar{K}$	8.0 ± 5.0	Mark I [167]
	$K\bar{K}$	3.4 ± 1.3	Mark II [90]
	$K\bar{K}$	$8.8 \pm 0.4 \pm 1.4$	DM2 [126]
	$K\bar{K}$	$4.85 \pm 0.26 \pm 1.05$	Mark III [150]
	$K\bar{K}$	5.4 ± 0.7	⟨average⟩
ωX(1730)	$K\bar{K}$	$4.0 \pm 1.2 \pm 0.6$	DM2 [126]
	$K\bar{K}$	$4.5 \pm 1.2 \pm 1.0$	Mark III [142]
	$K\bar{K}$	4.2 ± 1.0	⟨average⟩
φX(1730)	$K\bar{K}$	$3.6 \pm 0.2 \pm 0.6$	DM2 [126]
	$K\bar{K}$	$3.08 \pm 0.48 \pm 0.67$	Mark III [142]
	$K\bar{K}$	3.5 ± 0.3	⟨average⟩
$\rho a_2(1320)$ $(a_2 \to \rho\pi)$	all	84 ± 45	Mark I [167]
$(a_2 \to \rho\pi)$	all	$86 \pm 3 \pm 13$	DM2 [110]
$(a_2 \to \eta\pi)$	all	$118 \pm 8 \pm 29$	Mark III [145]
	all	91 ± 12	⟨average⟩
$K^{*0}(892)\bar{K}_2^{*0}(1430) + cc$	all	67 ± 26	Mark I [167]
	all	$76 \pm 11 \pm 13$	Mark III [171]
	all	73 ± 14	⟨average⟩
$K^{*+}(892)K_2^{*-}(1430) + cc$	all	$81 \pm 12 \pm 12$	Mark III [171]

presented in fig. 33 and in fig. 29c. In addition a shoulder at the high-mass side of the $f_2'(1525)$ is evident. It is tempting to identify the source of this shoulder with the $f_2(1720)$, a tensor glueball candidate seen in radiative J/ψ decays. To verify that the events near 1.7 GeV come from a 2^{++} object rather than a 0^{++} state [14], the Mark III Collaboration [150] has investigated the angular distribution of $\cos\theta_K$, the angle between the positive kaon in the tensor meson rest system with respect to its direction of flight. The probability that the distribution agrees with that of a scalar is 8% in the 1.55–1.63 GeV and only 0.5% in the 1.63–1.80 GeV mass region, in accordance with the $f_2(1720)$, which has $J^{PC} = 2^{++}$. The helicity amplitudes describing the production of $f_2'(1525)$ and $f_2(1720)$ were extracted from the data in two almost interference free regions in the invariant K^+K^- mass by means of a maximum likelihood fit. It is found that all partial waves contribute, implying large variations in the angular distributions and rates when compared to other J/ψ→V + T decays. For example, a factor of seven suppression of $B(J/\psi \to \phi f_2')$ relative to $B(J/\psi \to \omega f_2)$ solely due to kinematic factors is found.

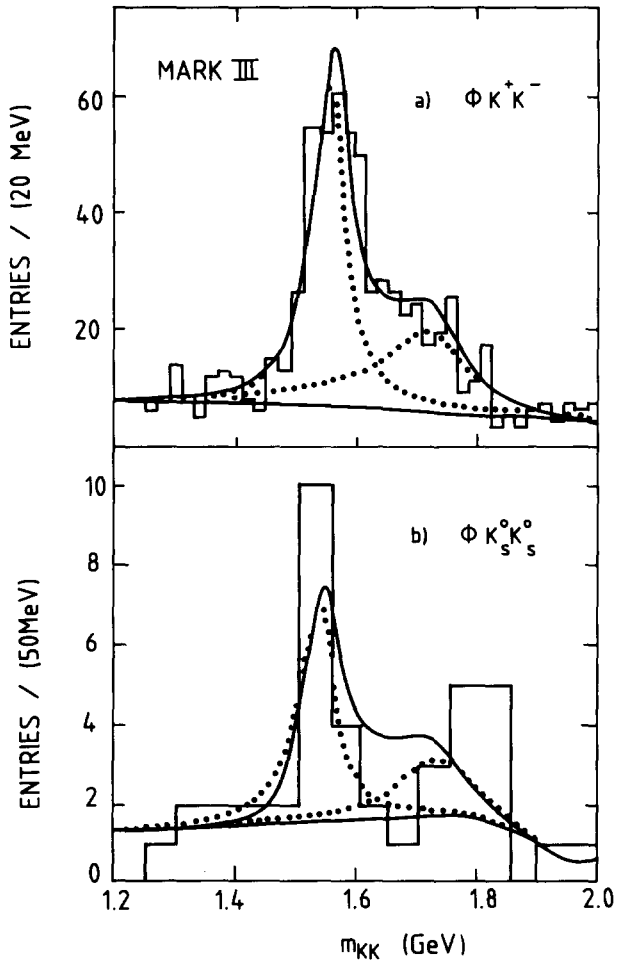

Fig. 33. Result of the fit for $J/\psi \to \phi X$. Shown in (a) is the best fit to the K^+K^- mass spectrum (Mark III) recoiling against a ϕ. In (b) the result of this fit is overlaid on the $K_S^0K_S^0$ mass distribution.

Uncertainties in this factor, which critically depends on the admixture of decay amplitudes, can mask the presence of other phenomena such as explicit SU(3) violations or electromagnetic contributions.

As in the case of radiative production from the J/ψ, the polarization structure is observed to be different in the $f_2(1720)$ and $f_2'(1525)$ mass regions. This leads to coherent interference between the two objects. The K^+K^- mass distribution has been fit [150] fixing the $f_2'(1525)$ parameters [14], but allowing for arbitrary mass and width of the $f_2(1720)$. The curve corresponding to the best fit is compared to the data for the K^+K^- and $K_S^0K_S^0$ final states in figs. 33a and b, respectively. The resulting branching ratios (table 17) are consistent with an isoscalar assignment for the two resonances; the mass and width of the "theta"/$f_2(1720)$ [150],

$$m = 1730 \pm 13\,\text{MeV}\,, \qquad \Gamma = 163 \pm 30\,\text{MeV}\,, \tag{65}$$

are consistent with the values obtained in radiative J/ψ decays (see table 35). A similar result is obtained by DM2 [126].

While non-resonant $J/\psi \to \omega K\bar{K}$ production is only singly OZI suppressed, intermediate resonances in the $K\bar{K}$ system must contain a non-strange component or be produced in a doubly OZI violating process. Figure 34 (DM2) and fig. 101b (Mark III) show mass spectra of the K^+K^- systems produced in association with an ω. A resonance near 1.73 GeV is clearly seen in both cases. A background arising from non-resonant $\omega K\bar{K}$ production is also present. In particular one notices a rapid rise of the $K\bar{K}$ spectrum near 1 GeV which could be due to a threshold effect similar to that seen in the corresponding ππ system (see section 5.5). The fitted parameters of the resonance at 1.73 GeV (see table 17) are again consistent with those of the "theta"/$f_2(1720)$. Spin parity analyses have not yet yielded unambiguous results due to the large number of parameters involved and the significant non-resonant background.

The doubly OZI violating decay $J/\psi \to \phi\pi\pi$ has been investigated by many experiments [140–142]. The $\pi^+\pi^-$ mass spectrum, which is shown in fig. 35 and fig. 102c, shows several interesting features. The dominant signal near 1 GeV is attributed to the $f_0(975)$ and is discussed in section 5.3.3. Furthermore one notices a box-like structure between 1.1 and 1.5 GeV and a small signal around 1.75 GeV, which one may speculate to be the "theta"/$f_2(1720)$. Whether the $f_2(1270)$, $f_0(1300)$, $f_2'(1525)$, or more exotic states like the 2^{++} X(1410) [151], or even a scalar glueball contribute to this box-like enhancement is still under investigation. Additional information from a spin parity analysis may prove to be essential for a definite conclusion.

DM2 [126] has taken a look at the angular distributions of the $\pi^+\pi^-$ system. Figure 36 shows three distributions of $\cos\theta_\pi^*$, the angle of the π^+ with respect to the $\pi^+\pi^-$ direction in the $\pi^+\pi^-$ rest system

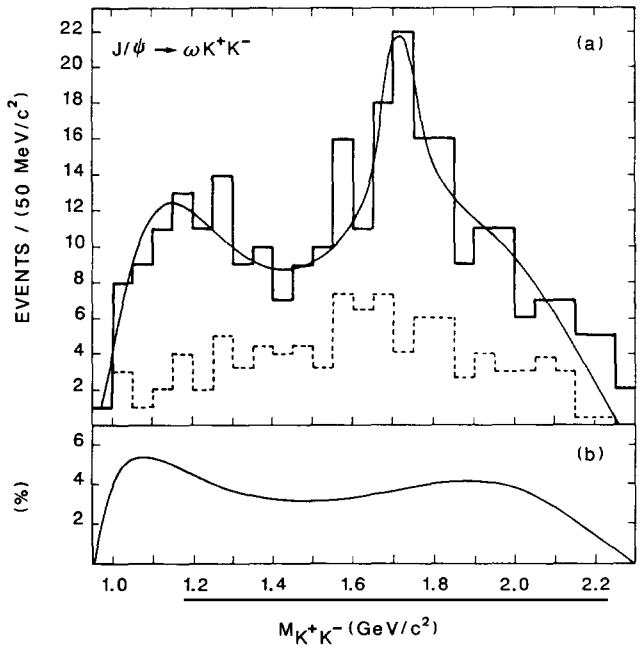

Fig. 34. Mass spectrum of K^+K^- system recoiling against an ω (DM2). The mass spectrum in (a) still contains background from events not containing a real ω, which is estimated by the dashed histogram. The detection efficiency for the DM2 detector is plotted in (b).

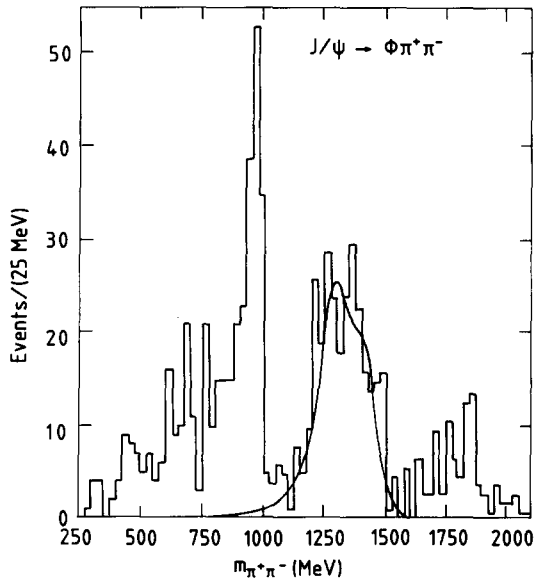

Fig. 35. $\pi^+\pi^-$ mass spectrum recoiling against a ϕ. The distribution is background subtracted (DM2). The solid line is a fit to two interfering resonances as described in the text.

for events in the $f_0(975)$, in the (1.20–1.32) GeV [$f_2(1270)$], and in the (1.32–1.50) GeV mass regions. While the angular distribution in the $f_2(1270)$ mass region is not compatible with $J = 0$ as expected, the corresponding distributions in the high- and low-mass regions are consistent with $J = 0$. From a fit to the structure at ~1300 MeV including the $f_2(1270)$ plus a second Breit–Wigner amplitude (see fig. 35) DM2 [152]*) obtains values of $m = (1372 \pm 10)$ MeV, $\Gamma_X = (106 \pm 13)$ MeV, and $m = (1445 \pm 9 \pm 9)$ MeV, $\Gamma_X = (139 \pm 16)$ MeV for coherent and incoherent resonance production, respectively. In both cases the

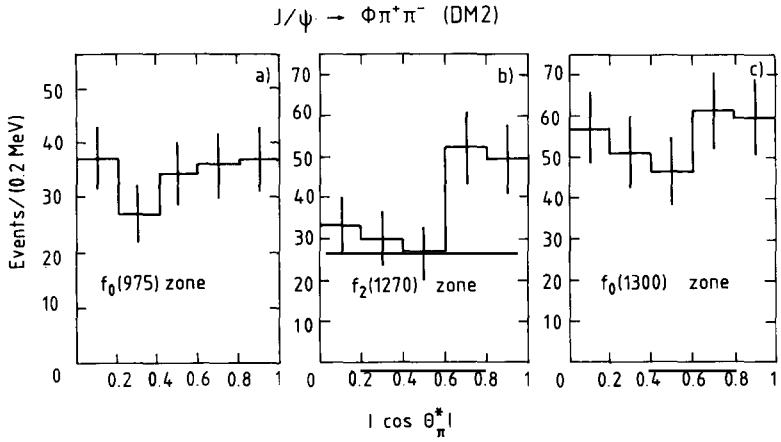

Fig. 36. Angular distributions of the $\pi\pi$ system recoiling against a ϕ. Shown are the distributions of $\cos\theta^*_\pi$ for events in the mass region (a) of the $f_0(975)$, (b) between 1.2 and 1.32 GeV, and (c) between 1.32 and 1.50 GeV (DM2 [126]). While (b) shows non-uniform behaviour, as expected for non-zero spin, the low- and high-mass regions (a) and (c) are consistent with flat distributions.

*) The parameters of the $f_2(1270)$ were kept fixed at their nominal values [14].

fit gives a rather poor description of the data. While the above mass values are clearly below the nominal $f_2'(1525)$ mass, it may still be possible to explain the box-like structure in terms of $f_2(1270)$ and $f_2'(1525)$ if in addition the effect of interference with the "theta"/$f_2(1720)$ is taken into account. Constructive interference is expected between $f_2(1270)$ and $f_2'(1525)$ and destructive interference between $f_2'(1525)$ and "theta"/$f_2(1720)$.*) Such an interference pattern could explain the observed mass shifts.

One may note that, while no sign of the 1.4 GeV structure is apparent in the $J/\psi \to \omega\pi^+\pi^-$ reaction, the radiatively produced $f_2(1270)$ exhibits an interesting shoulder in this mass range (compare fig. 102 of chapter 7). This shoulder could be an indication of $f_2(1270)$–$f_2'(1525)$ interference in the "flavour independent" radiative channel or a manifestation of the enhancement seen in the doubly OZI violating $J/\psi \to \phi\pi\pi$ reaction. This subject is further discussed in chapter 7.

The isovector state $a_2(1320)$ is observed in associated production with a ρ in the ρπ [110, 167] and ηπ decay modes [145]. Figure 37 shows the summed $\rho^+\pi^-$, $\rho^0\pi^0$, and $\rho^-\pi^+$ mass spectra recoiling against charged and neutral ρ's. A clear $a_2(1320)$ signal is seen on top of a large background. A similar situation is found for the ηπ final state (see fig. 31).

To study tensor meson states with open strangeness, the systems recoiling against charged and neutral K*(892)'s have been studied. Clear signals for the $J/\psi \to K^*(892)K_2^*(1430)$ reactions have been observed [167, 171] (see fig. 45). The ratio of decays to neutral and charged final states of $K^*(892)K_2^*(1430)$ is measured to be 0.90 ± 0.30, consistent with the corresponding value obtained for the *pseudoscalar + vector* case (see section 5.3.2). In the presence of an isospin violating term in the decay amplitude it is expected that the value of this ratio deviates from unity.

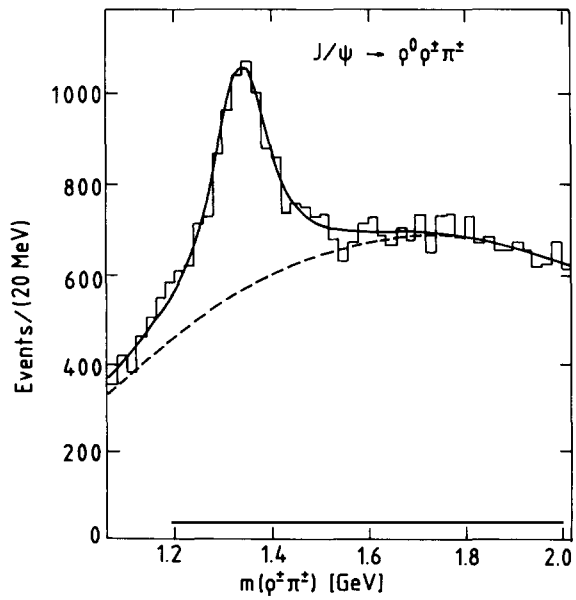

Fig. 37. Evidence for the $a_2(1320)$ in J/ψ two-body decays. Summed $\rho^+\pi^-$, $\rho^0\pi^0$, and $\rho^-\pi^+$ mass spectra recoiling against a ρ (DM2 [110]).

*) Because $X_{f'}$ is negative, for the ππ mode the interference of $f_2(1270)$ and $f_2'(1525)$ is constructive at masses in between the states, opposite to what is expected for the $K\bar{K}$ final state. In the case of the $f_2(1720)$, constructive interference with the $f_2'(1525)$ in the $K\bar{K}$ final state has been observed experimentally [150]. One therefore expects destructive interference between these states in the ππ mode.

Even though the set of measured $J/\psi \to V + T$ decays is not complete, a few remarks can be made based on a comparison with the SU(3) based model described in chapter 5. The ratio

$$B(J/\psi \to \omega f_2(1270))/B(J/\psi \to \rho^0 a_2^0(1320)) = 1.4 \pm 0.3 \tag{66}$$

deviates from unity, again indicating that doubly OZI violating effects play a role. The DOZI amplitude has to be in phase with the connected diagram, contrary to what has been observed for pseudoscalars (see table 10).

Seiden et al. [256] find reasonable agreement of all measured branching ratios in a model allowing for a doubly OZI violating contribution of 14% which is in phase with the SU(3) allowed amplitude. They are also able to roughly explain the measured rates of the "theta"/$f_2(1720)$ if it is assumed to be a pure glueball state. For a $SU(3)_{\text{flavour}}$ singlet, G(1730), one expects that

$$B(J/\psi \to \omega G(1730))/B(J/\psi \to \phi G(1730)) = 2 \times (P_\omega/P_\phi)^n \approx 2.5\text{–}5.9\,, \tag{67}$$

where the lower bound corresponds to predominance of an s wave ($n = 1$) and the higher bound corresponds to a d wave ($n = 5$) between the vector meson and G. The experimental value of 1.2 ± 0.3 is smaller than the range given by (67), pointing to some flavour symmetry breaking. If G(1730) is identified with the glueball candidate "theta"/$f_2(1720)$, this observation complies qualitatively with the observed preference for decay modes with strangeness.

5.3.5. Axial-vector states in two-body J/ψ decays

The quark model predicts two distinct ground state axial-vector nonets, the $^1P_1$, $J^{PC} = 1^{+-}$ multiplet with negative, and the $^3P_1$, $J^{PC} = 1^{++}$ multiplet with positive charge conjugation. While candidates for all states have been found, some assignments are ambiguous or need confirmation (see fig. 5). This is in particular true for the heavier isosinglet state in the 1^{++} nonet, for which two candidates exist, the $f_1(1420)$ and the $f_1(1530)$ [153, 154, 411]. The situation is further complicated by the fact that states with open strangeness (K_A, K_B) are not eigenstates of C and may therefore mix. The search for axial-vector mesons in J/ψ two-body decays has started only recently. The first results, some of which are still ambiguous, are described in the following sections.

5.3.5.1. Axial-vector mesons with negative charge conjugation. Mesons with $J^{PC} = 1^{+-}$ can be produced in association with pseudoscalar mesons in $\mathcal{C}$-allowed processes. So far only the $J/\psi \to b_1(1235)\pi$ decay has been measured by the PLUTO Collaboration [157], and seen by others [110, 145]. The Dalitz plot of the $J/\psi \to \omega\pi^+\pi^-$ reaction shows diagonal bands due to the low-mass $\pi^+\pi^-$ and the $f_2(1270)$ enhancements as well as bands arising from the $b_1(1235)$ in the $\omega\pi$ channel (fig. 38a).

The branching ratio has been determined to be [157]

$$B(J/\psi \to b_1^{\pm}\pi^{\mp}) \times B(b_1^{\pm} \to \omega\pi^{\pm}) = (2.8 \pm 0.7) \times 10^{-3}\,. \tag{68}$$

The measured mass of the $b_1(1235)$, $m = (1.188 \pm 0.032)$ GeV, is below the averaged value obtained in other experiments, $m = (1.233 \pm 0.010)$ GeV. This may be due to interference between the $b_1(1235)$ and the structures seen in the $\pi^+\pi^-$ channel (fig. 38), or is due to problems in estimating the background shape.

The PLUTO Collaboration has also investigated the angular dependence of the production angle θ_b

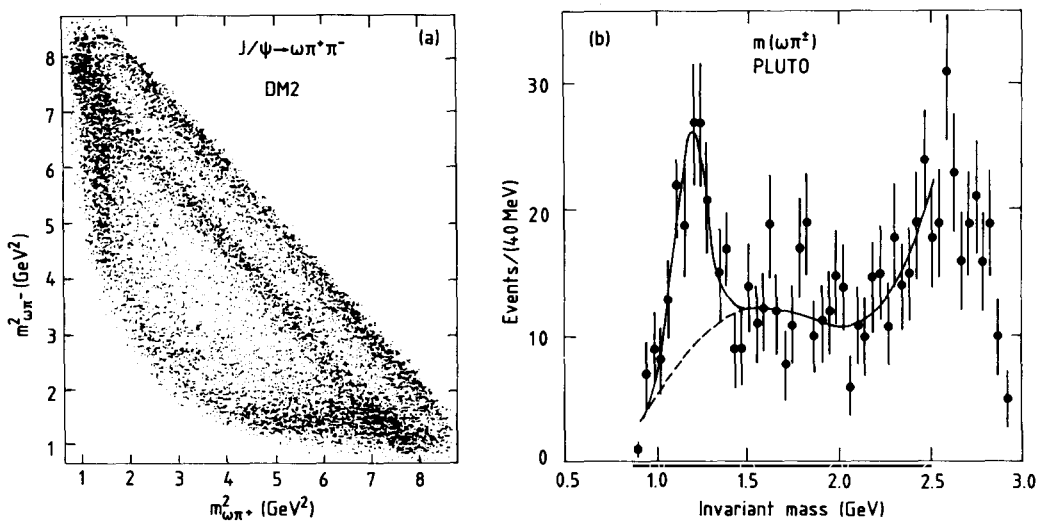

Fig. 38. Evidence for the $J/\psi \to b_1(1235)\,\pi$ reaction. Shown is (a) the $\omega\pi^+\pi^-$ Dalitz plot (DM2 [110]) and (b) the projected $\omega\pi^+$ mass distribution (both charge combinations added), as obtained by PLUTO [157].

of the b_1 relative to the beam axis. Fitting $dN/d\cos\theta_b$ with the form $1 + A\cos^2\theta_b$, they obtain $A = 1.1 \pm 1.1$. For production of the $b_1(1235)$ with helicity $\lambda = 1$ one expects $A = +1$, while $\lambda = 0$ would result in $A = -1$.

Since the production rate of the isovector $b_1(1235)$ is relatively large in two-body J/ψ decays, one may also expect observable signals for the isoscalar $h_1(1170)$ and $h_1'(1380)$ states. Of special interest is the mainly $s\bar{s}$ state $h_1'(1380)$ since it is poorly understood [154]; it could be studied in J/ψ decays by examining the $K\bar{K}\pi$ channel [155] in association with η and η'.

5.3.5.2. Axial-vector mesons with positive charge conjugation. The DM2 [141] and Mark III Collaborations [142, 156] have studied the $\eta\pi$, $K\bar{K}\pi$, and 4π final states associated with ω and ϕ to search for $I = 0$ axial-vector states. Structures have been found in the 1.28 GeV and 1.42 GeV mass regions, consistent with the $f_1(1285)$ and $f_1(1420)$, respectively (table 18). However, this interpretation is not imperative since in most cases no spin determinations have been done and the observed structures may have both 0^{-+} and 1^{++} contributions [161]*) rather than being dominated by single resonances. In addition, Chanowitz [162] has discussed the possibility of an exotic 1^{-+} hybrid state in the 1.4 GeV mass range. Below we will describe the experimental results in more detail.

The $K\bar{K}\pi$ system in association with an ω has been studied by Mark III [156] in the $K^+K^-\pi^0$ and $K^\pm K_S^0\pi^\mp$ final states. In both modes, a peak at 1.44 GeV is apparent (fig. 39). The width, which is given as $24\ \text{MeV} < \Gamma < 84\ \text{MeV}$ at 90% C.L., is not consistent with that of the $\eta(1440)$ (see table 32 in section 6.4.1). The angular distribution of the ω was studied to distinguish between the spin parities 0^- and 1^+ of the $K\bar{K}\pi$ system. Figure 39d shows the distribution of the normal to the ω decay plane in the helicity system of the ω. The uniquely determined prediction for $J^P = 0^-$ (solid curve) does not follow the data;

*) Depending on experiment and reaction, spin parity measurements of the 1.4 GeV mass region have yielded pseudoscalar or axial-vector assignments [161]. It has been speculated that these seemingly contradictory results can be accommodated in a scenario where up to three resonances populate the 1.4 GeV/c^2 mass region (see, e.g., refs. [198]).

Table 18

Candidates for 1^{++} states in J/ψ two-body decays. Shown are preliminary results from the Mark III [142, 156] and DM2 [141] Collaborations. Except for the $J/\psi \to \omega K\bar{K}\pi$ decay, no spin determinations have been attempted as yet. Since the 1.28 GeV and 1.40 GeV mass regions may have both pseudoscalar and axial vector contributions rather than being dominated by single resonances, an assignment of the observed structures to particular resonances is not made.

Final state	Mass (MeV)	Width (MeV)	Product branching ratio (units of 10^{-4})	Experiment
X(1280):				
$\omega\eta\pi^+\pi^-$	$1283 \pm 6 \pm 10$	$14^{+19}_{-14} \pm 10$	$B(J/\psi \to \omega X \to \omega\eta\pi\pi) = 4.3 \pm 1.2 \pm 1.3$	Mark III [142]
$\omega K\bar{K}\pi$	1285 fixed	24 fixed	$B(J/\psi \to \omega X \to \omega K\bar{K}\pi) < 1.1$ (90% C.L.)	Mark III [156]
$\phi\eta\pi^+\pi^-$	$1283 \pm 6 \pm 10$	$24^{+20}_{-10} \pm 10$	$B(J/\psi \to \phi X \to \phi\eta\pi\pi) = 1.6^{+0.6}_{-0.5} \pm 0.4$	Mark III [142]
$\phi\eta\pi^+\pi^-$	1285 fixed	24 fixed	$B(J/\psi \to \phi X \to \phi\eta\pi\pi) = 1.83 \pm 0.60$	DM2 [141]
$\phi 2(\pi^+\pi^-)$	1287 ± 7	16^{+26}_{-10}	$B(J/\psi \to \phi X \to \phi 4\pi^\pm) = 0.34 \pm 0.09$	Mark III [142]
$\phi 2(\pi^+\pi^-)$	1285 fixed	24 fixed	$B(J/\psi \to \phi X \to \phi 4\pi^\pm) = 0.43 \pm 0.13$	DM2 [141]
$\phi K\bar{K}\pi$	$1279 \pm 6 \pm 10$	$14^{+20}_{-14} \pm 10$	$B(J/\psi \to \phi X \to \phi K\bar{K}\pi) = 0.6 \pm 0.2 \pm 0.1$	Mark III [156]
X(1420):				
$\omega\eta\pi^+\pi^-$	$1421 \pm 8 \pm 10$	$45^{+32}_{-23} \pm 15$	$B(J/\psi \to \omega X \to \omega\eta\pi\pi) = 9.2 \pm 2.4 \pm 2.8$	Mark III [142]
$\omega K\bar{K}\pi$	$1442 \pm 5^{+10}_{-17}$	$40^{+17}_{-13} \pm 5$	$B(J/\psi \to \omega X \to \omega K\bar{K}\pi) = 6.8^{+1.9}_{-1.6} \pm 1.7$	Mark III [156]
$\phi K^\pm K^0_S \pi^\mp$	1420–1440	40–60	$B(J/\psi \to \omega X \to \phi K\bar{K}\pi) < 1.2$ (90% C.L.)	Mark III [156]

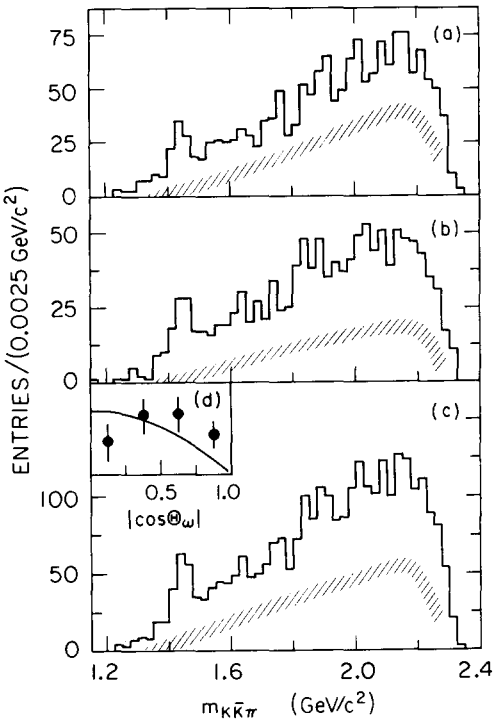

Fig. 39. Distribution of $m(K\bar{K}\pi)$ in $J/\psi \to \omega K\bar{K}\pi$ decays. (a) $K^\pm K^0_S \pi^\mp$ invariant mass distribution from the reaction $J/\psi \to \omega K^\pm K^0_S \pi^\mp$, (b) $K^+K^-\pi^0$ invariant mass distribution from $J/\psi \to \omega K^+K^-\pi^0$, and (c) sum. The shaded bands show the estimate of the background. (d) Distribution of $|\cos\theta_\omega|$ with prediction for $J^P = 0^-$ (solid line). The data are from Mark III [156].

a fit yields a probability of only 6% for the hypothesis that all signal events arise from a pseudoscalar resonance. The result is supported by a three-channel analysis where the $K\bar{K}\pi$ system is assumed to be composed of a $J^P = 0^-$ state decaying via the $a_0(980)\pi$ intermediate state, a $J^P = 1^+$ particle decaying via $K^*\bar{K}$, and an isotropic distribution. The analysis assigns the resonant structure to the axial-vector component.

The $K\bar{K}\pi$ system in association with a ϕ has been studied by Mark III [156] and DM2 [141] in several final states. The $K\bar{K}\pi$ mass spectrum (fig. 40, fig. 42) is dominated by phase space distributed $J/\psi \to \phi K^*\bar{K}$ events. No enhancement in the 1.4 GeV mass region is seen. A small signal at 1.28 GeV is seen by requiring that the $K\bar{K}$ invariant mass of the $K\bar{K}\pi$ system is below 1.15 GeV (fig. 42c). This observation is consistent with the $f_1(1280)$, which is known [160] to decay dominantly via the $a_0(980)\pi$ intermediate state.

A similar structure at 1.28 GeV has also been seen in the $\pi^+\pi^-\pi^+\pi^-$ system produced in association with a ϕ, as displayed in fig. 42 (DM2) and fig. 105c (Mark III) in section 7.1. In contrast to the doubly OZI violating $J/\psi \to \phi\pi^+\pi^-\pi^+\pi^-$ decay, the $J/\psi \to \omega\pi^+\pi^-\pi^+\pi^-$ decay has a large rate and shows no strucures on top of a large non-resonant component (see fig. 105b).

The $\eta\pi^+\pi^-$ system has been studied both in association with an ω [142] and a ϕ [141, 142]. Figure 41a displays the background subtracted $\eta\pi^+\pi^-$ mass spectrum of events having a recoiling ω and requiring that at least one $\eta\pi$ submass be consistent with an $a_0(980)$ within 50 MeV. The latter cut strongly reduces the background while not affecting the 1.28 GeV peak and retaining most of the events of the 1.4 GeV structure [145].

The $\eta\pi^+\pi^-$ system recoiling against the ϕ features a narrow structure around 1.28 GeV, which is seen both by Mark III (fig. 41b) and DM2 (fig. 42a). The enhancement is correlated with an $a_0(980)$ in the $\eta\pi^\pm$ subsystem. The one-bin fluctuation in fig. 41, slightly below 1.4 GeV, is not seen by DM2 (fig. 42a).

Interpretation of the results. One can summarize the experimental situation by stating that a structure at 1.44 GeV is observed in association with an ω, but not with a ϕ, while a peak at 1.28 GeV is observed in association with both ω and ϕ. Lacking definite spin parity assignments for the observed states one may still ask whether this peculiar pattern can be understood *at all* in terms of the axial-vector states $f_1(1285)$ and $f_1(1420)$.

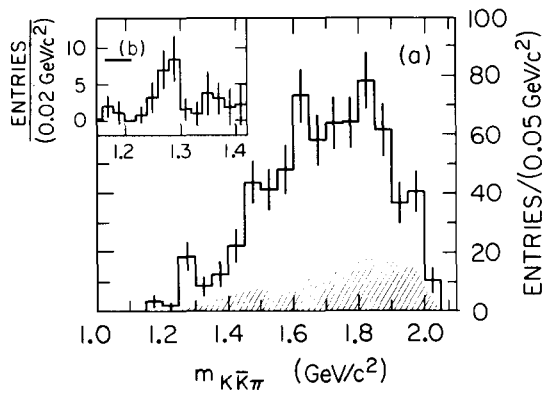

Fig. 40. Distribution of $m(K\bar{K}\pi)$ in $J/\psi \to \phi K\bar{K}\pi$ decays. (a) Summed $K^+K^-\pi^0$ and $K^\pm K_S^0\pi^\mp$ invariant mass distributions. (b) Detail of 1.2 GeV mass region after selection of $m(K\bar{K}) < 1.15$ GeV. The shaded area shows the estimate of the background. The data are from Mark III [156].

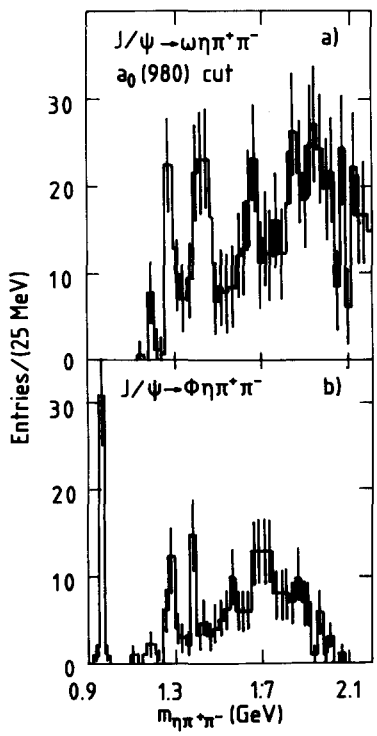

Fig. 41. Distribution of $m(\eta\pi^+\pi^-)$ in $J/\psi \to \{\omega, \phi\}\eta\pi^+\pi^-$ decays. The background subtracted $\eta\pi^+\pi^-$ invariant mass spectra from the reactions (a) $J/\psi \to \omega\eta\pi^+\pi^-$ and (b) $J/\psi \to \phi\eta\pi^+\pi^-$. A $a_0(980)$ cut (see text) has been applied in (a). The data are from Mark III [142].

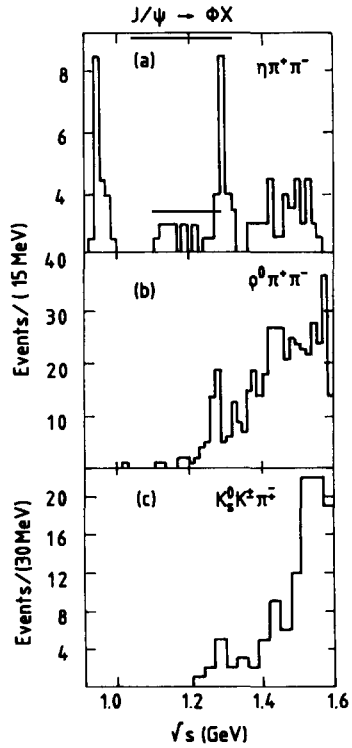

Fig. 42. Evidence for the $J/\psi \to \phi f_1(1280)/\eta(1275)$ decay. (a) $\eta\pi^+\pi^-$, (b) $\rho^0\pi^+\pi^-$, and (c) $K^\pm K_S^0\pi^\mp$ invariant mass spectra. The data are from DM2 [141].

While the measured branching fractions of X(1.28) recoiling against a ϕ (table 18) are consistent with that of the $f_1(1285)$ [14],

$$\text{X(1285):}\quad K\bar{K}\pi : \eta\pi\pi : 4\pi = \begin{cases} 0.19 \pm 0.07 : 0.50 \pm 0.21 : 0.32 \pm 0.08 & \text{(Mark III)}, \\ 0.11 \pm 0.03 : 0.49 \pm 0.06 : 0.40 \pm 0.07 & \text{(world average)}, \end{cases} \tag{69}$$

the $\eta\pi\pi$ branching fraction of X(1420) recoiling against an ω is rather large compared to the value obtained for the $f_1(1420)$ in 2γ reactions by Mark II [163],

$$\text{X(1420):}\quad \eta\pi\pi : K\bar{K}\pi = \begin{cases} 1.35 \pm 0.75 & \text{(Mark III)}, \\ <0.6 & (f_1(1420), \text{ obtained in } 2\gamma \text{ measurements}). \end{cases} \tag{70}$$

This may indicate that at least part of the observed $\eta\pi\pi$ structure at 1.4 GeV is due to the pseudoscalar $\eta(1400)$.

More striking even is the lack of observation of a signal at 1.4 GeV in association with a ϕ. The opposite pattern is expected from quark correlations since the $f_1(1420)$, being heavier than the $f_1(1285)$, should contain a larger fraction of strange quarks if both states are the isosinglet members of the *same* 1^{++} $q\bar{q}$ nonet. However, one has to note that the concept of quark correlations breaks down in the presence of a large interference term between singly and doubly OZI violating amplitudes. For

example, even in the case of a particle containing *only* strange quarks the decay rate for the $J/\psi \to \phi X$ will vanish if (see table 14)

$$r = -(1 - 2s_g - 2e/g) \approx O(0.5) . \tag{71}$$

Along these lines and allowing for non-ideal mixing in the 1^{++} nonet, Seiden et al. [256] have found that the observed branching ratios of table 18 can qualitatively be explained in terms of the axial-vectors $f_1(1280)$ and $f_1(1420)$. However, since the spins of the structures have not been determined, it is equally possible that the data contain contributions from several states with nearly identical masses.

It is interesting to note that the data do not show any evidence for the $f_1(1530)$, which has been observed by experiments studying $K^- p \to K_S^0 K^{\pm} \pi^{\mp}$ + *hyperon* reactions [153, 154].

5.4. Decays into meson pairs violating generalized $\mathscr{C}$ parity

The direct hadronic decays of the J/ψ to particle pairs belonging to the same SU(3) multiplet are forbidden in the limit of perfect SU(3) symmetry. Consequently they are expected to have a large electromagnetic component, described, to first order, by the virtual photon diagram. This constitutes a rather unique opportunity to probe the hadron structure using a 3 GeV virtual photon by studying form factors and the spin structure of the produced particles. While the creation of the primary $q\bar{q}$ pair is a well-known electromagnetic process, the creation of the quark pair from the "sea" is governed by QCD fragmentation processes at low energies. Models have been put forward by several authors based on QCD [164, 165], vector meson dominance [169], and mixing of the J/ψ with other vector mesons [166], predicting helicity suppression rules and form factors.

5.4.1. Decays of the J/ψ into pairs of pseudoscalar mesons

Among the J/ψ decays that violate generalized $\mathscr{C}$ parity the decays into two pseudoscalar mesons,

$$J/\psi \to \pi^+\pi^-,\ K^+K^-,\ K_S^0 K_L^0 , \tag{72}$$

have been most explicitly measured. The G parity violating $J/\psi \to \pi^+\pi^-$ decay and the $SU(3)_{\text{flavour}}$ forbidden $J/\psi \to K^+K^-$ decay have been observed by several experiments [67, 167, 168, 170] with branching ratios in the order of 10^{-4} (see table 19).

The $\pi^+\pi^-$ and K^+K^- final states have to be selected in the presence of a 300 times larger background of leptonic $J/\psi \to e^+e^-$ and $J/\psi \to \mu^+\mu^-$ events. While the momenta of the final state π's and K's are too high (~1.5 GeV) to allow for particle separation by time-of-flight measurements, $e^{\pm}$ and μ's can well be detected in electromagnetic shower counters and muon filters, respectively. Almost background free signals for $J/\psi \to \pi^+\pi^-$ and $J/\psi \to K^+K^-$ are obtained by additionally employing energy–momentum constraints of the reaction (4C fits) [168].

The SU(3) forbidden decay $J/\psi \to K_S^0 K_L^0$ is identified by the reconstruction of the decay $K_S^0 \to \pi^+\pi^-$ with the correct K_S^0 momentum of 1.468 GeV. The topology of a typical event as detected by the Mark III detector is displayed in fig. 43; here the K_L^0 has produced a detectable signal in the shower counter, as is expected for ≈50% of all events. A major background arises from the reaction $J/\psi \to K_S^0 K^{*0}(892) \to K_S^0 K_L^0 \pi^0$, where the K_S^0 has a recoil momentum of 1.373 GeV. Figure 44 shows the K_S^0 momentum spectrum for different cuts on the number of final state photons; the contamination by

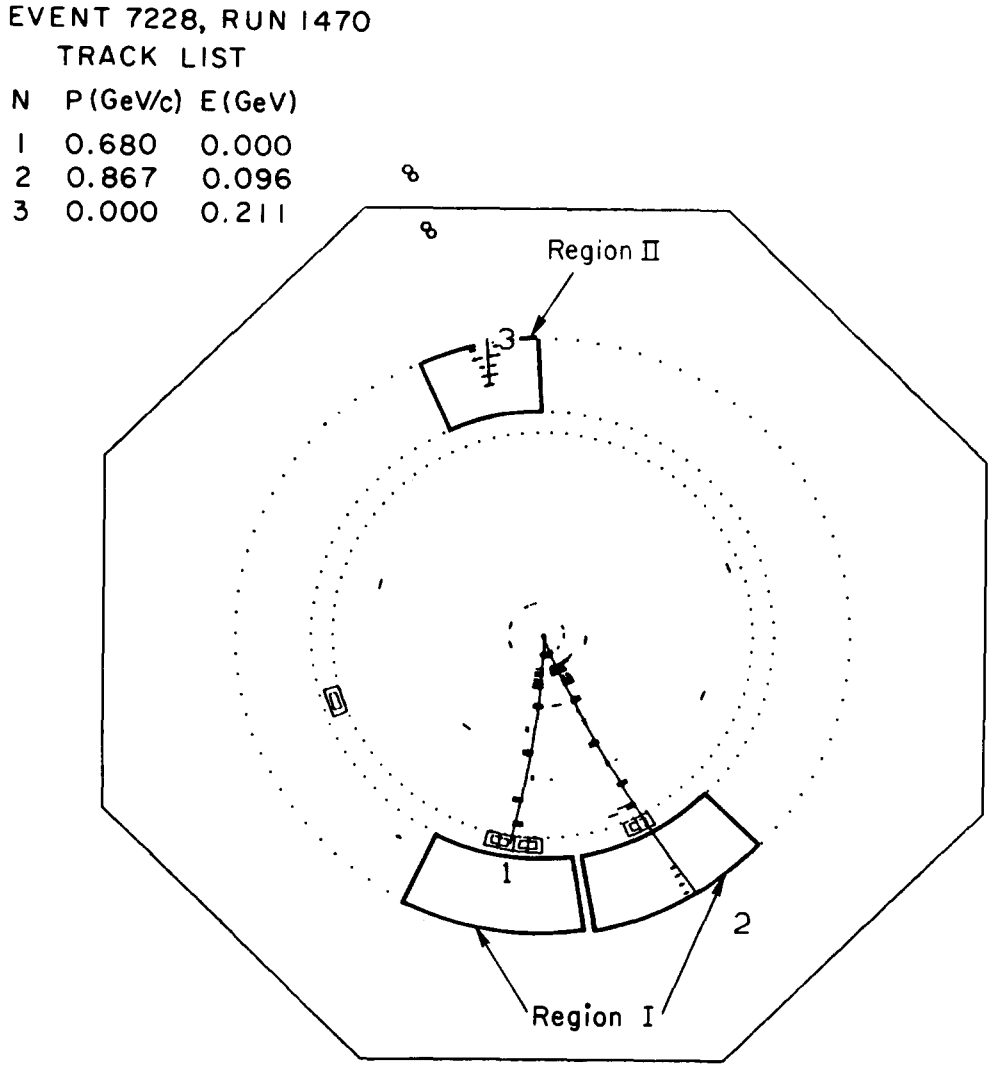

Fig. 43. Example of a $J/\psi \to K_S K_L$ event (Mark III). Note the traces of a hadronic interaction of the K_L^0 in region II.

the background reaction is greatly reduced by requiring that no more than one shower is detected in the electromagnetic calorimeter.

5.4.2. Decays of the J/ψ into pairs of vector mesons

In a preliminary analysis the Mark III Collaboration [171] has studied the decays

$$J/\psi \to \begin{cases} \rho^+\rho^- & \to \pi^+\pi^0\pi^-\pi^0, \\ K^{*+}(892)K^{*-}(892) & \to K^+\pi^0K^-\pi^0, \\ K^{*0}(892)\bar{K}^{*0}(892) & \to K^+\pi^-K^-\pi^+. \end{cases} \tag{73}$$

Evidence for the $J/\psi \to K^{*0}(892)\bar{K}^{*0}(892)$ reaction is presented in fig. 45, showing the correlation of the $K^+\pi^-$ invariant masses and the recoiling $K^-\pi^+$ system. Two bands are clearly seen at the K^{*0} mass,

Table 19
Decays of the J/ψ into pairs of pseudoscalar mesons. Listed are results from Mark I, DASP, Mark III, and DM2 (preliminary). The results have been averaged assuming uncorrelated errors. The first-order expression in terms of electromagnetic (E), and strong SU(3) breaking amplitudes (M) [199] can be compared to the reduced branching ratio $\tilde{B} = B/p^3$ (GeV^{-3}).

Final state	Amplitude	Branching ratio (units of 10^{-4})	$\tilde{B}$ (units of 10^{-4})	Experiment
$\pi^+\pi^-$	E	1.6 ± 1.6		Mark I [167]
		1.0 ± 0.5		DASP [67]
		$1.58 \pm 0.20 \pm 0.15$		Mark III [168]
		1.47 ± 0.22	0.401 ± 0.060	⟨average⟩
K^+K^-	$E + \frac{1}{2}\sqrt{3}M$	2.0 ± 1.6		Mark I [167]
		2.2 ± 0.9		DASP [67]
		$2.39 \pm 0.24 \pm 0.22$		Mark III [168]
		2.36 ± 0.30	0.746 ± 0.095	⟨average⟩
$K_S^0K_L^0$	$\frac{1}{2}\sqrt{3}M$	$1.01 \pm 0.16 \pm 0.09$		Mark III [168]
		$1.18 \pm 0.12 \pm 0.18$		DM2 [170]
		1.08 ± 0.14	0.343 ± 0.044	⟨average⟩

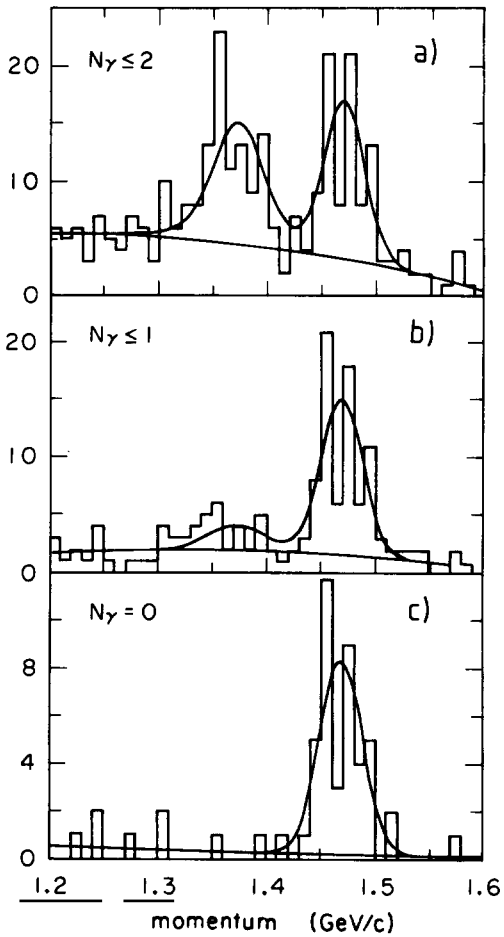

Fig. 44. K_S momentum spectrum (Mark III). The peak at the left, due to $J/\psi \to K_S^0 K^{*0}(892)$ contamination, is strongly reduced when the correct topology of ≤1 detected showers is required.

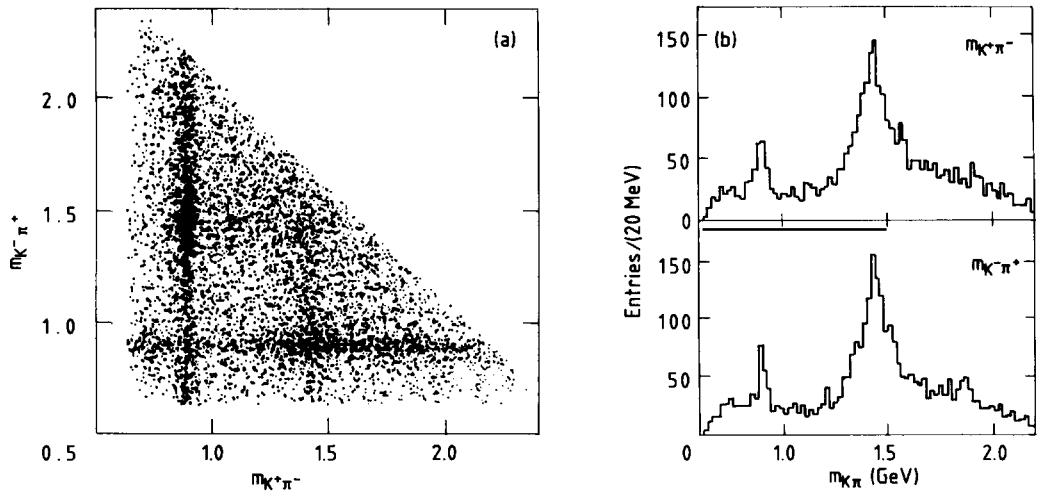

Fig. 45. The decay $J/\psi \to K^+\pi^-K^-\pi^+$. (a) Triangle plot of $m(K^+\pi^-)$ versus $m(K^-\pi^+)$ showing clear K*(892) and $K_2^*(1430)$ bands. (b) Kπ mass spectra recoiling against a K*(892) (Mark III [171]).

featuring a denser population at mass values where the $K^{*0}(892)\bar{K}_2^{*0}(1430)$ and $K^{*0}(892)\bar{K}^{*0}(892)$ final states are expected. The shape of the $K^{\pm}\pi^{\mp}$ mass spectra, after demanding that the recoiling system be consistent with a $K^{*0}(892)$, is shown in fig. 45b.

The number of events due to the $J/\psi \to \rho^+\rho^- \to \pi^+\pi^-\pi^0\pi^0$ and $J/\psi \to K^{*+}(892)K^{*-}(892) \to K^+K^-\pi^0\pi^0$ channels were obtained by employing the method of likelihood fits to signal and background channels. This method accounts for the combinatorial background caused by the two indistinguishable π^0's and the finite width of the ρ and K*(892) resonances. The resulting branching fractions for the channels studied are listed in table 20.

The well-measured $J/\psi \to K^{*0}(892)\bar{K}^{*0}(892)$ reaction was further analysed [171] to determine the three production helicity amplitudes A_{00}, A_{11}, and A_{10}, where the subscript denotes the helicities of the final state vector mesons. The study of angular correlations shows that A_{00} is dominant, which is equivalent to a longitudinal polarization of the vector mesons. This result is in agreement with QCD predictions and confirms the vector nature of the gluon [164].

5.4.3. Determination of electromagnetic and strong SU(3) breaking amplitudes

In table 19 and table 20 the experimental results are compared with the theoretical predictions of an SU(3) based model allowing for first-order SU(3) breaking effects [199]. While only an electromagnetic amplitude is responsible for the isospin violating $J/\psi \to \pi^+\pi^-$ decay, the electromagnetic amplitude

Table 20
Decays of the J/ψ into pairs of vector mesons. Listed are preliminary results from the Mark III experiment [171]. The reduced branching ratio is defined as $\tilde{B} = B/p^3$ (GeV^{-3}).

Final state	Amplitude	Branching ratio (units of 10^{-4})	$\tilde{B}$ (units of 10^{-4})
$\rho^+\rho^-$	E	$9.4 \pm 1.0 \pm 1.5$	3.9 ± 0.7
$K^{*+}\bar{K}^{*-}$	$E + \frac{1}{2}\sqrt{3}M$	$6.7 \pm 1.2 \pm 2.5$	3.3 ± 1.4
$K^{*0}\bar{K}^{*0}$	$\frac{1}{2}\sqrt{3}M$	$2.9 \pm 0.4 \pm 0.6$	1.4 ± 0.4

vanishes for $J/\psi \to K_S^0 K_L^0$ due to a cancellation of $I=0$ and $I=1$ amplitudes of the $K^0\bar{K}^0$ system.*) Although the latter is strictly valid only in the limit of exact $SU(3)_{flavour}$, the electromagnetic contribution to the $J/\psi \to K_S^0 K_L^0$ reaction is expected to be small; a calculation based on a pole model inspired by vector meson dominance [169] yields the estimate $|E_{K_S K_L}/E_{\pi\pi}| < 0.1$ [168]. From table 19 and table 20 one can determine the amplitudes $|E|$, $|M|$ and their phase relative to each other for the $J/\psi \to 0^-0^-$ and for the $J/\psi \to 1^-1^-$ reactions. The results (table 21) do not change significantly if one allows for a second-order mass dependence of the electromagnetic component.

As can be seen from table 19, table 20, and table 21, the patterns observed for $J/\psi \to 0^-0^-$ and $J/\psi \to 1^-1^-$ decays look roughly similar. Electromagnetic and direct mass breaking effects are of the same order for both decay types, showing that interpretations based solely on electromagnetic transitions are not justified. The ratio of reduced branching fractions for charged and neutral kaons is in excellent agreement with that for charged and neutral K*'s, while the effect of SU(3) breaking is more pronounced in the case of the vector mesons.

5.4.4. *The determination of meson form factors*

In order to compare the measured branching ratios with theoretical predictions and experimental results obtained at lower energies, it is useful to introduce the concept of electromagnetic form factors. For the pair production of spin 1 mesons, M_λ, with helicity λ, the form factors $F_{\lambda,\bar{\lambda}}(Q^2)$ are defined according to the formula [172]

$$\frac{(d\sigma/d\Omega)(e^+e^- \to \gamma^* \to M_\lambda \bar{M}_{\bar{\lambda}})}{\sigma(e^+e^- \to \mu^+\mu^-)}$$

$$\equiv C_1 \times \sin^2\theta\,[|F_{0,0}|^2 + C_2|F_{1,1}|^2 + C_3\,\mathrm{Re}(F_{1,1}F_{0,1}^*) + C_4|F_{0,1}|^2] + C_5 \times (1+\cos^2\theta)|F_{0,1}|^2\,, \qquad (74)$$

where the coefficients C_i are functions of the meson velocity $\beta = \sqrt{1-4m_M^2/s}$,

$$C_1 = \frac{3}{32\pi}\beta^3\,,\quad C_2 = \frac{3-2\beta^2+3\beta^4}{(1-\beta^2)^2}\,,\quad C_3 = -4\,\frac{1+\beta^2}{(1-\beta^2)^2}\,,\quad C_4 = \frac{4}{(1-\beta^2)^2}\,,$$

$$C_5 = \frac{9\beta^3}{32\pi(1-\beta^2)}\,.$$

Table 21
Fitted amplitudes for $J/\psi \to 0^-0^-$ and $J/\psi \to 1^-1^-$ decays

Final state	Electromagnetic amplitude $\lvert E\rvert$	SU(3) breaking amplitude $\lvert M\rvert$	Phase angle
0^-0^-	0.65 ± 0.04	0.68 ± 0.03	$92° \pm 11°$
1^-1^-	1.97 ± 0.14	1.38 ± 0.15	$138° \pm 37°$

*) Since the virtual photon has both isoscalar and isovector components, the electromagnetic amplitude for the $K\bar{K}$ system contributes proportional to

$$(K\bar{K} - \bar{K}K)_{I=1} + \alpha(K\bar{K} + \bar{K}K)_{I=0} = (1/\sqrt{2})[(K^+K^- - K^-K^+)(1+\alpha) + (K^0\bar{K}^0 - \bar{K}^0K^0)(1-\alpha)]\,.$$

If SU(3) symmetry holds ($\alpha = 1$) the amplitude for the neutral kaon final state vanishes.

Asymptotic QCD ($Q^2 \to \infty$) predicts [164] that vector mesons are preferably produced with longitudinal polarization, i.e., $F_{0,0}$ dominates. This has been confirmed in the $J/\psi \to K^{*0}(892)\bar{K}^{*0}(892)$ reaction, and for the following discussion we assume that this is valid for all *vector–vector* final states. Under this assumption one then obtains the simplified expression

$$|F_{0,0}(Q^2)|^2 = \frac{4}{\beta^3} \frac{\sigma(e^+e^- \to \gamma^* \to M_0\bar{M}_0)}{\sigma(e^+e^- \to \mu^+\mu^-)} . \tag{75}$$

Applying (75) to the results from the $J/\psi \to \pi^+\pi^-$ and $J/\psi \to \rho^+\rho^-$ decays, Mark III [168, 171] finds for the charge form factors [173]

$$\begin{aligned} |F_\pi(m_\psi^2)|^2 &\equiv |F_{0,0}^\pi(m_\psi^2)|^2 = (11.85 \pm 1.50 \pm 0.91) \times 10^{-3} , \\ |F_\rho(m_\psi^2)|^2 &\equiv \tfrac{1}{3} |F_{0,0}^\rho(m_\psi^2)|^2 = (26.0 \pm 2.7 \pm 4.0) \times 10^{-3} . \end{aligned} \tag{76}$$

The result for the F_π form factor can be compared to measured values at lower centre of mass energies (fig. 46). Also shown are theoretical predictions based on the simplest possible VMD ansatz [169] allowing only for ρ, ω, and φ meson contributions (solid line). The theoretical curves do not describe the experimental data very well, indicating that contributions of higher-mass vector states, such as ρ(1600), cannot be neglected [175].*)

First-order QCD calculations for large Q^2 predict that meson form factors are related to the meson decay constants by the relation [172]

$$\lim_{Q^2 \to \infty} F_M(Q^2) = 16\pi\alpha_s(Q^2) f_M^2 / Q^2 . \tag{77}$$

Using $f_\pi = 0.093$ GeV and $f_\rho = 0.107$ GeV, one requires a magnitude of $\alpha_s \approx 2$–3 for the $\pi^+\pi^-$ and $\rho^+\rho^-$ final states to explain the magnitude of the measured form factors, which clearly shows the inadequacy of the model assumptions.

5.5. Decays into three mesons

It is an experimental fact that most J/ψ decays leading to three stable or unstable particles proceed dominantly via two-body intermediate states (see table 22). For example, the fraction of $J/\psi \to \pi^+\pi^-\pi^0$ decays that do not form intermediate ρπ systems is very small as can readily be seen from the Dalitz plot depicted in fig. 21.

Few reactions, such as $J/\psi \to \omega K^*\bar{K}$ and $J/\psi \to \phi K^*\bar{K}$, have been identified as candidates for "true" three-body decays, with no structure being observed in the two-body subsystems, being instead distributed according to phase space. The ratio of branching ratios,

$$B(J/\psi \to \omega K^*\bar{K} + \text{c.c.}) / B(J/\psi \to \phi K^*\bar{K} + \text{c.c.}) = 2.6 \pm 1.0 , \tag{78}$$

*) The distribution of the π, K and $K_S^0K_L^0$ form factors have been fitted by several authors by including the effect of the ρ(1600) and φ(1680) vector mesons. See, e.g., refs. [175].

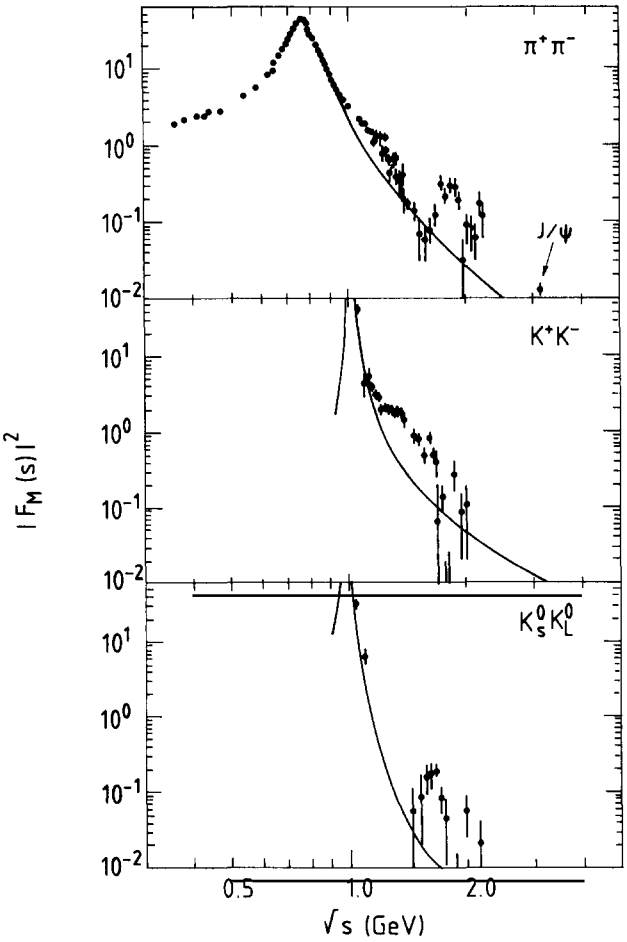

Fig. 46. Pion and kaon form factors. Shown are the meson form factors for $\pi^+\pi^-$, K^+K^-, and $K^0_S K^0_L$ pair production [174]. For clarity, only non-overlapping $|F_\pi|^2$ data from the CMD, OLYA and DM2 experiments are displayed; see Barkov et al. and Bisello et al. [174]. The data for the $K^0_S K^0_L$ form factor were taken from Mané et al. [174], those for the K^+K^- form factor from Delcourt et al. and Ivanov et al. [174]. The solid lines are predictions from a simple VMD model [169].

is larger than expected in the SU(3) symmetric limit $(0.93)^{*)}$ [199], demonstrating again the importance of SU(3) breaking amplitudes.

Other reactions, such as $J/\psi \to \omega\pi\pi$, have both resonant and non-resonant components. The distribution of $m_{\pi\pi}$, as observed by DM2 [176], exhibits a distinct enhancement near threshold (fig. 47). Its branching ratio has been determined to be [176]

$$B(J/\psi \to \omega X(500)) \cdot B(X \to \pi^+\pi^-) = (21 \pm 2 \pm 3) \times 10^{-4}\,. \tag{79}$$

A similar structure is also observed in the corresponding $\pi^0\pi^0$ system with a rate consistent with zero isospin [141].

Only recently has more attention been given to this low-mass enhancement because the scalar

*) s-wave phase space has been taken into account.

Table 22
J/ψ three-body decays into mesons. The averages have been obtained assuming $I = 0$ for the two-meson subsystems.

Final state	Branching ratio (units of 10^{-4})	Experiment	Intermediate two-body systems
$\pi^+\pi^-\pi^0$	150 ± 15	PDG [14]	$\rho\pi$
$K\bar{K}\pi$	61 ± 10	PDG [14]	K^*K
$\omega\pi^+\pi^-$	78 ± 16	PLUTO [157]	
	68 ± 19	Mark I [167]	
	$52 \pm 0.7 \pm 11$	Mark III [177]	
$\omega\pi\pi$	92.7 ± 12.5	⟨average⟩	$\omega f_2(1270)$
ωK^+K^-	8.0 ± 5.0	Mark I [405]	
	$8.6 \pm 0.6 \pm 1.7$	Mark III [177]	
	$7.4 \pm 0.7 \pm 2.3$	DM2 [126]	
$\omega K^0\bar{K}^0$	$12.4 \pm 2.0 \pm 3.1$	DM2 [126]	
$\omega K\bar{K}$	17.4 ± 2.6	⟨average⟩	$\omega f_2(1720)$
$\phi\pi^+\pi^-$	10.5 ± 4.5	Mark I [405]	
	$9.0 \pm 0.4 \pm 2.3$	Mark III [177]	
	$7.8 \pm 0.3 \pm 1.2$	DM2 [126]	
$\phi\pi\pi$	12.3 ± 1.6	⟨average⟩	$\phi f_0(975)$, $\phi f_2(1270)$, $\phi f_0(1300)$, $\phi f_2(1720)$
ϕK^+K^-	9.0 ± 4.0	Mark I [405]	
	$8.3 \pm 0.3 \pm 1.3$	DM2 [126]	
$\phi K^0\bar{K}^0$	$6.3 \pm 0.7 \pm 1.6$	DM2 [126]	
$\phi K\bar{K}$	15.3 ± 2.0	⟨average⟩	$\phi f_2'(1525)$, $\phi f_2(1720)$
$\omega K^*\bar{K}$ + c.c.	$53 \pm 14 \pm 14$	Mark III [156]	phase space distributed
$\phi K^*\bar{K}$ + c.c.	$20.0 \pm 3.0 \pm 3.0$	Mark III [156]	
	$20.7 \pm 2.4 \pm 3.0$	DM2 [126]	
	20.4 ± 2.8	⟨average⟩	phase space distributed

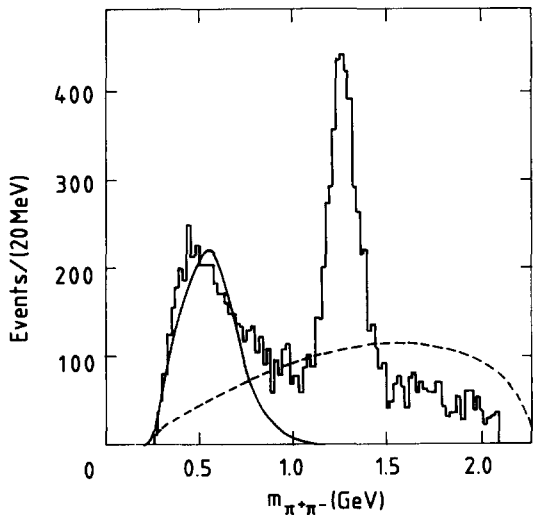

Fig. 47. Invariant mass of the $\pi^+\pi^-$ system produced in association with an ω. The solid curve shows the prediction of the model of ref. [178], the dashed curve represents a phase space distribution. The data are from DM2 [176].

glueball may lie below 1 GeV. However, this speculation has been rejected by an analysis performed by DM2 [176]. Neither is the enhancement well reproduced by a Breit–Wigner shape, nor do the angular distributions indicate the excitation of a single scalar resonance. This is demonstrated in fig. 48.

For a scalar resonance, the decay angle of the π's in the $\pi\pi$ rest system, θ_π, should follow a uniform distribution. However, the experimentally observed θ_π distribution shows some deviation from uniformity depending on the invariant mass of the system X.

An interesting explanation of the low-mass enhancement has been given by Dosch and Gromes [178]. In the discussion of the basic (connected) diagram for meson pair production (fig. 20a), a momentum dependence which can arise by the mechanism for the spontaneous creation of a quark pair from the "sea" has generally been neglected. Using an explicit expression for the spontaneous creation amplitude [179], the authors can qualitatively describe the shape of the low-mass $\pi\pi$ enhancement (solid curve in fig. 47). While the enhancement is not expected to be seen in the OZI forbidden $J/\psi \to \phi\pi\pi$ channel, the model predicts a similar but less pronounced effect for $J/\psi \to \phi K\bar{K}$. Both predictions are consistent with the experimental observation*) (see fig. 32 and fig. 35). It remains to be seen whether this interesting concept can be applied to the $J/\psi \to \omega K\bar{K}$ reaction, where the experimentally observed $K\bar{K}$ spectra (fig. 34 and fig. 101b) can accommodate a significant non-resonant component (see section 5.3.4).

The mechanism for the formation of exclusive final states in the decay of heavy quarkonia has also been discussed by Karl and Tuan [180], who point out the importance of measuring the non-resonant $J/\psi \to \{\omega, \phi\} + \{\pi\pi, K\bar{K}\}$ branching fractions. The proposed mechanism of sequential pair creation [181] may explain the puzzle that the decay $\psi(3685) \to \rho\pi$ is suppressed while $J/\psi \to \rho\pi$ is the largest hadronic decay of the J/ψ.**)

5.6. J/ψ decays into baryons

Under $SU(3)_{\text{flavour}}$ the baryons can be arranged in singlet, octet, and decuplet irreducible representations,

$$\mathbf{3} \otimes \mathbf{3} \otimes \mathbf{3} = \mathbf{1}_A \oplus \mathbf{8}_M \oplus \mathbf{8}_{M'} \oplus \mathbf{10}_S \,. \tag{80}$$

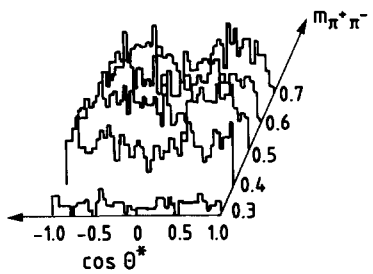

Fig. 48. Angular distributions of events from the low-mass $\pi^+\pi^-$ enhancement. Shown is the distribution of the pion polar angle in the $\pi\pi$ rest frame as a function of $m_{\pi\pi}$ (DM2).

*) The fraction of $J/\psi \to \phi K\bar{K}$ decays that do not proceed via intermediate resonances is small and has been determined by Mark III [150] to be $B(J/\psi \to \phi K\bar{K}) = (2.2 \pm 0.4) \times 10^{-4}$.

**) Another explanation for the comparatively large rates of the J/ψ into the pseudoscalar vector final states $K^*\bar{K}$ and $\rho\pi$ calls for the existence of an intermediate gluonium state around 3.1 GeV; see refs. [182].

The subscripts indicate symmetric, mixed-symmetric, or antisymmetric multiplets under interchange of flavour labels of any two quarks. Each multiplet corresponds to a unique baryon number, spin, and parity and its members are classified by I, I_3, and S. The lowest lying singlet, octet, and decuplet states, denoted B_1, B_8, and B_{10}, correspond to $J^P = \frac{1}{2}^-$, $\frac{1}{2}^+$, and $\frac{3}{2}^+$, respectively. Figure 49 shows the lowest lying multiplets in the S–I_3 space. For brevity we will refer to $\Sigma(1385)$, $\Xi(1530)$, and N(1440–1530) as Σ^*, Ξ^*, and N^*, respectively.

Decays of J/ψ into final states containing baryons have been intensively studied by the BONANZA [71, 183], Mark I [184], DASP [67], Mark II [185], DM2 [188, 186], and Mark III [189] experiments, among which the systematic investigations of the Mark II and DM2 groups are most noteworthy. Good angular coverage, particle identification over a large momentum range by time of flight or Cerenkov counters, as well as the possibility of missing mass measurements due to the well-defined initial state in e^+e^- collisions, allow one to reconstruct complex decay chains, such as

$$J/\psi \to \Xi^-\bar{\Xi}^+ \to \Lambda\pi^-\bar{\Lambda}\pi^+ , \quad \Lambda \to p\pi^-, n\pi^0 . \tag{81}$$

5.6.1. Two-body decays into baryons

The majority of J/ψ baryonic decays proceeds via two-body intermediate states. As in the case of J/ψ decays into meson pairs the decay rates can be compared with theoretical models that exploit the $SU(3)_{flavour}$ singlet nature of the J/ψ. In a SU(3) symmetric world only the decays

$$J/\psi \to B_1\bar{B}_1,\ B_8\bar{B}_8,\ B_{10}\bar{B}_{10} \tag{82}$$

are allowed, with the same decay amplitudes for a given decay family if electromagnetic contributions are neglected.

As indicated in fig. 50, the SU(3) symmetry can be broken in several ways:

- Since the photon contains both SU(3) singlet and octet pieces, the decay (fig. 50a)

$$c\bar{c} \to \gamma_{1\oplus 8} \to B_n\bar{B}_m , \quad n \neq m , \tag{83}$$

is possible via the octet component of the photon, because the direct product $8 \otimes \overline{10}$ contains an octet contribution. In the direct electromagnetic decay (fig. 50c) the photon replaces one of the three

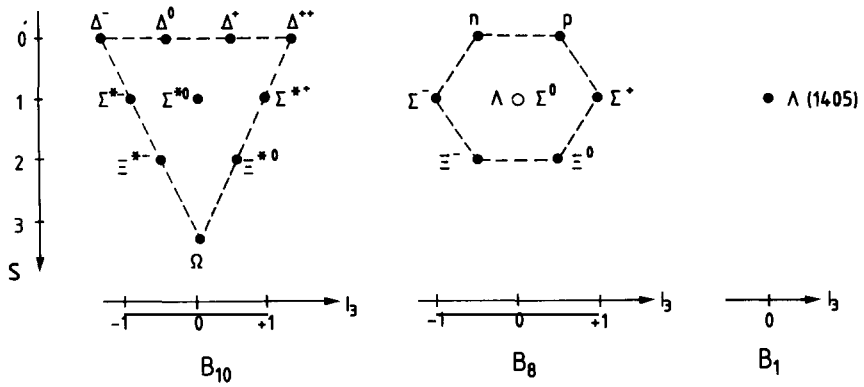

Fig. 49. The lowest lying SU(3) multiplets of baryons.

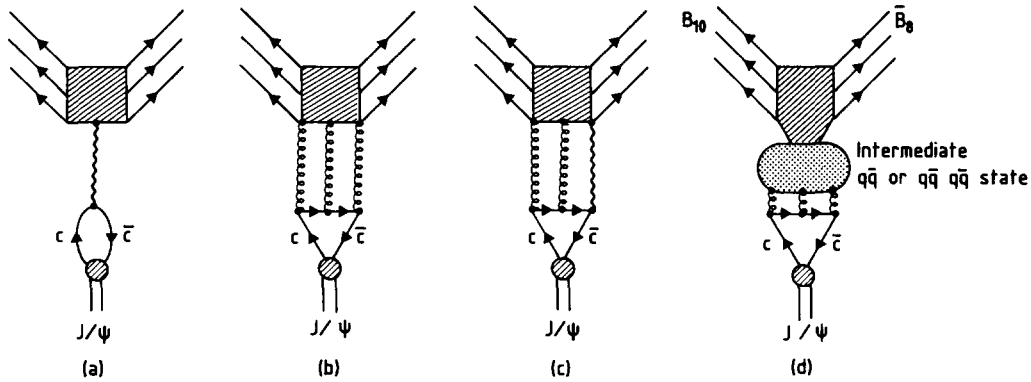

Fig. 50. Diagrams contributing to $J/\psi \to B\bar{B}$ decays. Shown are diagrams representing (a) the one-photon electromagnetic, (b) the direct hadronic, (c) the direct electromagnetic decay, and (d) possible intermediate four-quark or baryonium contributions.

exchanged gluons of fig. 50b, which represents the direct hadronic decay. The ratio R of the corresponding decay amplitude relative to that of the three-gluon decay has been calculated [196] in the framework of perturbative QCD, $R_{\mathrm{QCD}} = -4\alpha/(5\alpha_s)$, and also in the framework of vector meson dominance, $R_{\mathrm{VMD}} = 24\alpha/(5\alpha_s)$.

- A second SU(3) breaking mechanism arises from the mass difference of light and strange quarks.*) That is, the decay chain

$$c\bar{c} \to (u\bar{u} + d\bar{d} + s\bar{s})_1 \to \alpha(u\bar{u} + d\bar{d})_{1\oplus 8} + \beta(s\bar{s})_{1\oplus 8} \to B_{10}\bar{B}_8 \tag{84}$$

can occur if the couplings α and β differ. The mass breaking can equivalently be described by an octet [199] or 27-plet contribution to the J/ψ wave function [186].

- As a last possibility it has been pointed out [200] that $q\bar{q}$, $q\bar{q}q\bar{q}$ or *baryonium* intermediate states in octet or 27-plet representations**) can lead to SU(3) breaking by adding a non-singlet piece to the wave function.

In order to test to what extent SU(3) invariance holds the decays $J/\psi \to B_8\bar{B}_8$, $J/\psi \to B_8\bar{B}_{10}$, and $J/\psi \to B_{10}\bar{B}_{10}$ have been systematically studied. In the following subsections the results are compared to a simple model based on SU(3) symmetry that incorporates the symmetry breaking effects discussed above using the appropriate SU(3) isoscalar coefficients [187]. The (complex) amplitudes considered are

- A, the SU(3) symmetric amplitude due to the strong interaction;
- D (F), symmetric (antisymmetric) electromagnetic contributions (fig. 50a,c);
- D' (F'), symmetric (antisymmetric) SU(3) breaking effects that arise from the strange and light quark mass difference;
- D'', the 27-plet contribution, which, for simplicity, is only taken into account in the SU(3) forbidden $B_8\bar{B}_{10}$ decays.

The question of the phase between one-photon and direct hadronic decays is not settled, neither

*) For an estimate of constituent quark masses, see, e.g., ref. [155] ($m_u \approx m_d \approx 0.6 m_s$).

**) In principle also decuplet and 35-plet contributions may be considered ($8 \otimes \overline{10} = 8 \oplus 27 \oplus \overline{10} \oplus \overline{35}$); however, the $\overline{10}$ and $\overline{35}$ multiplets do not contain isosinglet states, prohibiting their contribution if SU(2) invariance is conserved.

theoretically*) nor experimentally (see, e.g., table 15) and the phase is therefore allowed to vary. The absolute magnitude of the electromagnetic contributions can be calculated in the framework of a GVDM model (Generalized Vector Dominance Model) [66, 196, 197], and is found to be small for SU(3) allowed decays. It depends on the number of strange quarks in the final state and the magnetic baryon form factors [191]. Effects that are of second order in the SU(3) breaking (see section 5.3.1) will be neglected in the following discussion, and for clarity we will assume that the amplitudes considered above are invariants for each class of $B_n\bar{B}_m$ final states.

Finally, we would like to add a remark concerning the treatment of charge conjugate final states. Applying the operator for charge conjugation to a *baryon–antibaryon* system,

$$C|B_n\bar{B}_m\rangle = |\bar{B}_nB_m\rangle \begin{cases} = |B_n\bar{B}_m\rangle & \text{for } n = m\,, \\ \neq |B_n\bar{B}_m\rangle & \text{for } n \neq m\,, \end{cases} \tag{85}$$

generally leads to a different state. Charge conjugate states will nevertheless be produced with the *same* branching ratio if *isospin* is conserved in the decay of the final state particles. We therefore adopt the convention that charge conjugate states are implicitly included in the measurement of branching ratios.

5.6.1.1. Decays into pairs of octet baryons. Decay rates of the J/ψ into pairs of octet baryons have been measured with high precision. The quality of the data can be deduced from fig. 51a,b and fig. 54, showing evidence for the $J/\psi \to p\bar{p}$, $J/\psi \to \Lambda\bar{\Lambda}$, and $\Xi^-\bar{\Xi}^+$ reactions. The so far measured branching ratios of $J/\psi \to B_8\bar{B}_8$ decays are listed in table 23. The phase space corrected branching ratio**), $\tilde{B}$, is

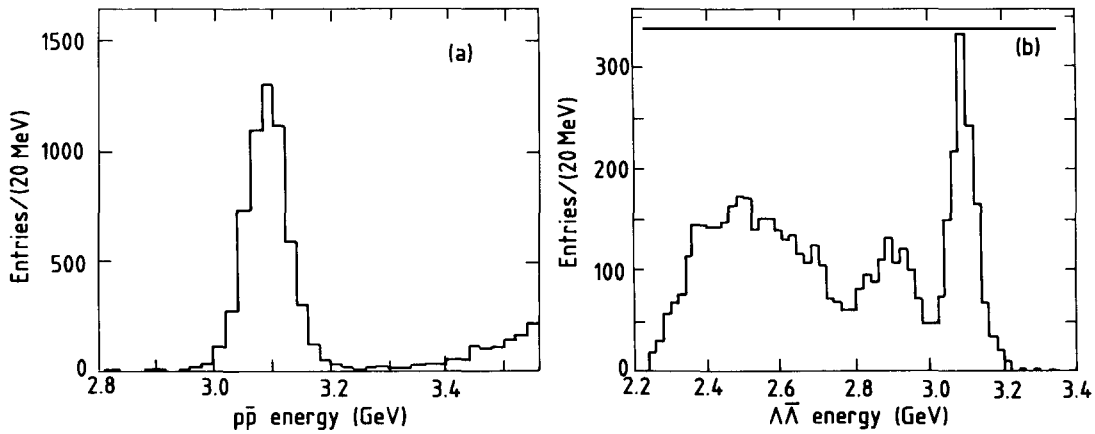

Fig. 51. Examples of J/ψ decays into pairs of octet baryons. Shown in (a) is the energy of the $p\bar{p}$ system showing a peak at the J/ψ mass with negligible background. In (b) the corresponding spectrum for the $\Lambda\bar{\Lambda}$ system is displayed; the enhancement centred at 2.9 GeV comes from the decay $J/\psi \to \Sigma^0\bar{\Sigma}^0$ (DM2 [188]).

*) A QCD analysis fixes the ratio of the direct and one-photon contributions to be positively real (Chernyak and Zhitnitski [201]), while a dispersion approach determines this ratio to be purely imaginary (Fukugita and Kwiecinski [201]).

**) We define the N-body s wave phase space factor R_N by the expression

$$R_N = \int \prod_{i=1}^{N} \frac{d^3p_i}{2E_i}\, \delta^4(P_{\text{final}} - P_{\text{initial}})\,.$$

For the special case of two-body decays one obtains $R_2 = \pi p^*/\sqrt{s}$, where p^* is the momentum of either particle in the centre of mass system. The centre of mass energy is $\sqrt{s}$. Note, that the Particle Data Group [14] uses an additional factor $2\pi^{-3N}$ to define N-body phase space.

Table 23
Decays of the J/ψ into a pair of octet baryons. Listed are results from Mark I [184], DASP [67], BONANZA [183, 71], Mark II [185], DM2 [188, 186], and Mark III [189, 190] (preliminary). The results have been averaged assuming uncorrelated errors. General expressions in terms of singlet (A), as well as symmetric and antisymmetric one-photon (D, F), and octet SU(3) breaking terms (D', F') can be compared with the reduced branching ratio $\tilde{B} = \sqrt{3}/(\pi \cdot p^*) \times B(J/\psi \to X)$. Upper limits are given at the 90% C.L.

Final state	Amplitude	Branching ratio (units of 10^{-4})	$\tilde{B}$ (units of 10^{-4})	Experiment
$p\bar{p}$	$A + D + F + D' + F'$	$22.0 \pm 2.0 \pm 3.3$		Mark I [184]
		20.0 ± 5.0		Bonanza [183]
		25.0 ± 4.0		DASP [67]
		$21.6 \pm 0.7 \pm 1.5$		Mark II [185]
		$19.1 \pm 0.4 \pm 3.0$		DM2 [188]
		$19.1 \pm 0.3 \pm 1.6$		Mark III [189]
		20.6 ± 1.0	16.5 ± 0.8	⟨average⟩
$\Lambda\bar{\Lambda}$	$A - D + 2D'$	$11.0 \pm 2.0 \pm 1.7$		Mark I [184]
		26.0 ± 16.0		Bonanza [71]
		$15.8 \pm 0.8 \pm 1.9$		Mark II [185]
		$13.8 \pm 0.5 \pm 2.0$		DM2 [188]
		14.0 ± 1.3	12.9 ± 1.2	⟨average⟩
$n\bar{n}$	$A - 2D + D' + F'$	18.0 ± 9.0	14.2 ± 7.2	Bonanza [183]
$\Sigma^0\bar{\Sigma}^0$	$A + D - 2D'$	$13.0 \pm 4.0 \pm 2.0$		Mark I [184]
		$15.8 \pm 1.6 \pm 2.5$		Mark II [185]
		$10.6 \pm 0.4 \pm 2.3$		DM2 [188]
		12.6 ± 1.7	12.6 ± 1.7	⟨average⟩
$\Xi^-\bar{\Xi}^+$	$A + D - F + D' - F'$	$14.0 \pm 0.5 \pm 2.1$		Mark I [184]
		$11.4 \pm 0.8 \pm 2.0$		Mark II [185]
		$7.0 \pm 0.6 \pm 1.2$		DM2 [186]
		$8.6 \pm 0.5 \pm 2.0$		Mark III [190]
		9.3 ± 0.9	11.3 ± 1.1	⟨average⟩
$\Sigma^0\bar{\Lambda}$	$\sqrt{3}D$	<1.5		Mark I [1854]
		<0.9	<0.86	DM2 [1186]

calculated assuming no angular momentum (s wave) between the final state baryons. $\tilde{B}$ is roughly the same for all decays since the SU(3) symmetric amplitude is dominant. The available experimental data do not allow a fit for the different amplitudes. However, the upper limit for the isospin violating, purely electromagnetic process $J/\psi \to \Sigma^0\bar{\Lambda}$ infers that the electromagnetic component is small.

In addition to the experimentally measured branching ratios, also information regarding the angular distribution of the decay products has been published. This is especially interesting since theoretical models based on first-order QCD calculations give predictions for the angular distributions of two baryon final states. In these models it is assumed that the decays $J/\psi \to B\bar{B}$ proceed via the diagram shown in fig. 52, and that the amplitude can be factorized in a hard scattering part, calculable in first-order QCD, and a "soft" part that describes the hadronization of the outgoing quarks. The vector nature of the gluon implies quark helicity conservation at each $q\bar{q}g$ vertex if quark masses are neglected.

In general the angular distribution can be written as

$$dN/d\cos\theta_B \propto 1 + \alpha \cos^2\theta_B \,, \tag{86}$$

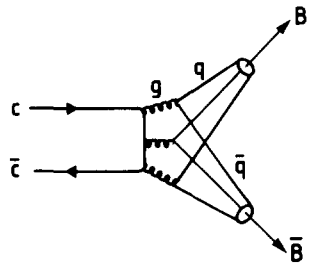

Fig. 52. Dominant diagram for $J/\psi \to B\bar{B}$ in QCD calculations.

where θ_B is the angle between the baryon and the positron beam direction. The experimentally observed angular distributions for $p\bar{p}$, $\Lambda\bar{\Lambda}$, and $\Sigma^0\bar{\Sigma}^0$ final states are shown in fig. 53; the corresponding values for α are compared with the theoretical predictions in table 24. The effect of quark masses has been studied in ref. [192] by setting $m_{quark} = m_{baryon}/3$. Electromagnetic corrections change the results only slightly. It is clear that the data are becoming sensitive enough to test the different models.

It has been suggested [193] to use the decay $J/\psi \to \Lambda\bar{\Lambda} \to \pi^- p \pi^+ \bar{p}$ as an Einstein–Podolski–Rosen experiment [194]. By employing the Λ decays as spin analysers, quantum mechanical correlations at

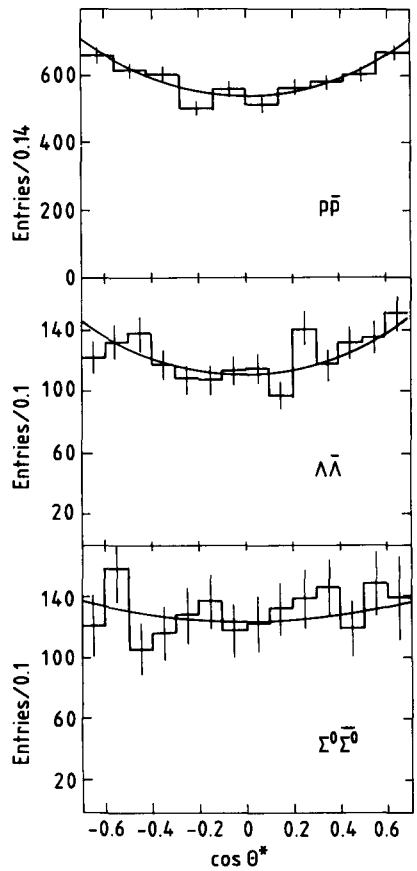

Fig. 53. Angular distribution of the system of two octet baryons. Polar angle distribution of (a) proton, (b) Λ, and (c) Σ^0 with respect to the positron direction. The curves result from fits as described in the text. The data are from DM2 [188].

Table 24
Results on the angular distribution of baryons. The results from the Mark I [184], DASP [67], Mark II [185], DM2 [188], and Mark III [189] experiments are compared with theoretical predictions. Baryon masses have been included in the calculation of ref. [191], significantly changing the predictions for massless baryons [164]. The effect of non-zero quark masses has been studied in ref. [192].

Final state	α	Experiment	Ref. [164] vector gluon ($m_B = 0$)	Ref. [191]	Ref. [192] no e.m. correction	Ref. [192] with e.m. correction
$p\bar{p}$	1.45 ± 0.56	Mark I [184]				
	1.70 ± 1.70	DASP [67]				
	0.61 ± 0.23	Mark II [185]				
	0.62 ± 0.11	DM2 [188]				
	0.58 ± 0.14	Mark III [189]				
	0.63 ± 0.08	⟨average⟩	1	0.46	0.69	0.70
$\Lambda\bar{\Lambda}$	0.72 ± 0.36	Mark II [185]				
	0.62 ± 0.22	DM2 [188]				
	0.65 ± 0.19	⟨average⟩	1	0.32	0.51	–
$\Sigma^0\bar{\Sigma}^0$	0.70 ± 1.10	Mark II [185]				
	0.22 ± 0.31	DM2 [188]				
	0.26 ± 0.30	⟨average⟩	1	0.31	0.43	–

macroscopic distances can be tested and compared to the bounds given by Bell's inequality for hidden variable theories. In a first evaluation, the DM2 Collaboration finds [195] that their data are consistent with the quantum mechanical expectation. However, due to the limited statistics, the significance of the result is still poor.

5.6.1.2. Decays into pairs of decuplet baryons. Several branching ratios have been measured for the $J/\psi \to B_{10}\bar{B}_{10}$ decay. As an example, fig. 54 shows evidence for the $J/\psi \to \Sigma^{-*}\bar{\Sigma}^{+*}$ decay. Since the wave function of decuplet baryons is symmetric with respect to the interchange of any two quarks, the expressions in terms of SU(3) allowed and SU(3) forbidden amplitudes turn out to be simpler than in the case of the octet baryons. For simplicity, possible 27-plet and 64-plet amplitudes have been neglected in the compilation of table 25. The measured branching ratios agree fairly well with each

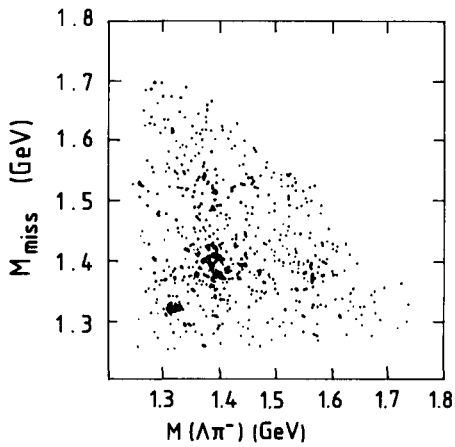

Fig. 54. Evidence for the $J/\psi \to \Sigma^{-*}\bar{\Sigma}^{+*}$ and $J/\psi \to \Xi^-\bar{\Xi}^+$ reactions. Scatterplot of $\Lambda\pi^-$ mass and the recoiling missing invariant mass. The cluster at 1.32 GeV is due to the decay $J/\psi \to \Xi^-\bar{\Xi}^+$ while the cluster at 1.38 GeV is due to $J/\psi \to \Sigma^{-*}\bar{\Sigma}^{+*}$ (DM2 [186]).

Table 25
Decays of the J/ψ into pairs of decuplet baryons. Listed are results from the Mark I [184], Mark II [185], and DM2 [186] experiments. The results have been averaged assuming uncorrelated errors. General expressions in terms of singlet (A), one-photon (D), and octet SU(3) breaking terms (D') can be compared with the reduced branching ration $\tilde{B} = \sqrt{s}/(\pi \cdot p^*) \times B(J/\psi \to X)$.

Final state	Amplitude	Branching ratio (units of 10^{-4})	$\tilde{B}$ (units of 10^{-4})	Experiment
$\Delta^{++}\bar{\Delta}^{--}$	$A+2D+D'$	$11.0 \pm 0.9 \pm 2.8$	11.6 ± 3.1	Mark II [185]
$\Sigma^{-*}\bar{\Sigma}^{+*}$	$A-D$	$8.6 \pm 1.8 \pm 2.2$		Mark II [185]
		$10.0 \pm 0.4 \pm 2.1$		DM2 [186]
		9.5 ± 1.7	13.5 ± 2.4	⟨average⟩
$\Sigma^{+*}\bar{\Sigma}^{-*}$	$A+D$	$10.3 \pm 2.4 \pm 2.5$		Mark II [185]
		$11.9 \pm 0.4 \pm 2.5$		DM2 [186]
		11.3 ± 2.0	16.1 ± 2.8	⟨average⟩

other, indicating that also here SU(3) breaking effects are of minor importance. Specifically, one finds from the ratio of reduced branching fractions,

$$\frac{\tilde{B}(J/\psi \to \Sigma^{+*}\bar{\Sigma}^{-*})}{\tilde{B}(J/\psi \to \Sigma^{-*}\bar{\Sigma}^{+*})} \propto \left|\frac{A+D}{A-D}\right|^2 = 1.19 \pm 0.30\,, \tag{87}$$

that either the electromagnetic amplitude is small or its phase with respect to the strong amplitude is close to 90°.

5.6.1.3. Decays into octet–decuplet baryon pairs. The detection of SU(3) forbidden decays with relatively large branching ratios first published by the Mark II Collaboration [185] came as a surprise, prompting several attempts to explain the effect. The DM2 [186] and Mark III [190] Collaborations have confirmed this result and measured additional $J/\psi \to B_8\bar{B}_{10}$ decays (table 26). Several ratios of decay rates can be formed to test the predictions of various models, assuming for the moment that the amplitudes D, D', D'' are quark mass independent,

$$\begin{aligned}
R_1 &= \frac{\tilde{B}(J/\psi \to \Xi^{0*}\bar{\Xi}^{0})}{\tilde{B}(J/\psi \to \Sigma^{+*}\bar{\Sigma}^{-})} \propto \left|\frac{2D+D'+\frac{3}{2}D''}{2D+D'-D''}\right|^2,\\
R_2 &= \frac{\tilde{B}(J/\psi \to \Xi^{-*}\bar{\Xi}^{+})}{\tilde{B}(J/\psi \to \Sigma^{-*}\bar{\Sigma}^{+})} \propto \left|\frac{D'+\frac{3}{2}D''}{D'-D''}\right|^2,\\
R_3 &= \frac{\tilde{B}(J/\psi \to \Sigma^{+*}\bar{\Sigma}^{-}) - \tilde{B}(J/\psi \to \Sigma^{-*}\bar{\Sigma}^{+})}{\tilde{B}(J/\psi \to \Xi^{0*}\bar{\Xi}^{0}) - \tilde{B}(J/\psi \to \Xi^{-*}\bar{\Xi}^{+})} \propto \frac{|2D+D'-D''|^2 - |D'-D''|^2}{|2D+D'+\frac{3}{2}D''|^2 - |D'+\frac{3}{2}D''|^2}\,.
\end{aligned} \tag{88}$$

Experimentally one finds, using the DM2 value for $\tilde{B}(J/\psi \to \Xi^{0*}\bar{\Xi}^{0})$,

$$R_1 = 1.3 \pm 0.6\,, \qquad R_2 = 2.8 \pm 1.0\,, \qquad R_3 = -0.1 \pm 0.3\,. \tag{89}$$

Genz et al. [200] have put forward the hypothesis that an intermediate $q\bar{q}$ octet state could lead to the

Table 26
SU(3) forbidden decays of the J/ψ into baryons. Listed are results from the Mark II [185], DM2 [186], and Mark III [190] experiments. The results have been averaged assuming uncorrelated errors. General expressions in terms of singlet (A), one-photon (D), octet SU(3) breaking (D'), and 27-plet terms (D'') can be compared with the reduced branching ratio $\tilde{B} = \sqrt{3}/(\pi \cdot p^*) \times B(J/\psi \to X)$. Upper limits are given at the 90% C.L.

Final state	Amplitude	Branching ratio (units of 10^{-4})	$\tilde{B}$ (units of 10^{-4})	Experiment
$\Sigma^{-}\bar{\Sigma}^{+}$	$-D' + D''$	$2.9 \pm 1.1 \pm 1.0$		Mark II [185]
		$3.0 \pm 0.3 \pm 0.8$		DM2 [186]
		3.0 ± 0.7	3.5 ± 0.8	⟨average⟩
$\Sigma^{+}\bar{\Sigma}^{-}$	$-2D - D' + D''$	$3.1 \pm 1.1 \pm 1.1$		Mark II [185]
		$3.4 \pm 0.4 \pm 0.8$		DM2 [186]
		$3.7 \pm 0.4 \pm 0.9$		Mark III [190]
		3.5 ± 0.6	4.0 ± 0.7	⟨average⟩
$\Xi^{-}\bar{\Xi}^{+}$	$D' + \frac{1}{2}D''$	$5.9 \pm 0.9 \pm 1.2$	9.8 ± 2.5	DM2 [186]
$\Xi^{0}\bar{\Xi}^{0}$	$2D + D' + \frac{1}{2}D''$	$3.2 \pm 1.2 \pm 0.7$	5.2 ± 2.2	DM2 [186]
		<4.1	<6.6	Mark III [190]
$\Sigma^{0}\bar{\Lambda}$	$\sqrt{3}D$	<2.0	<2.2	DM2 [186]
$\Delta^{+}\bar{p}$	$2D$	<1.0	<0.9	DM2 [186]

apparent SU(3) breaking. A generalization to multi-quark intermediate states would also make the contribution of a 27-plet possible. As can be seen from the amplitude decomposition, octet dominance ($D' \gg D''$) would predict that $R_1 = R_2 = R_3 = 1$, in contradiction with the measurements. The more sophisticated model of Körner [196], which allows for strong mass breaking effects and final state dependent electromagnetic amplitudes but neglects a 27-plet contribution, runs into similar problems. While a model allowing electromagnetic contributions is ruled out, some electromagnetic component seems to be required, since $\tilde{B}(J/\psi \to \Xi^{0}\bar{\Xi}^{0}) \neq \tilde{B}(J/\psi \to \Xi^{-}\bar{\Xi}^{+})$. In the framework of the given model, the data can well be described if both electromagnetic and strong isospin breaking effects are taken into account.*)

5.6.2. *Three-body decays involving baryons*

The phenomenological model outlined in the previous paragraphs gets very complex when applied to three-body final states with many parameters to be determined. In addition, since most J/ψ decays proceed via two-body intermediate states, including wide resonances, it is hard to experimentally extract the non-resonant three-body contribution. Specific models based on proton and N* pole diagrams (fig. 55) have been introduced [202] to deal with these problems.

Here we discuss only a few of the results and, to guide the eye, furnish reduced branching ratios by dividing out the three-particle s wave phase space factor (see table 27).

By studying table 27, the following observations can be made:

- The ratio

$$\tilde{B}(J/\psi \to p n \pi^{-}) : \tilde{B}(J/\psi \to \bar{p} n \pi^{+}) : \tilde{B}(J/\psi \to \bar{p} p \pi^{0}) = (58.9 \pm 4.7) : (56.2 \pm 4.6) : (31.4 \pm 3.1)$$

is consistent with SU(2) symmetry, which predicts the ratio of 1 : 1 : 0.5.

*) The data can be well fitted even if the octet breaking term is neglected; in this case $|D/D''| \approx 0.05$ with a phase of roughly 180°.

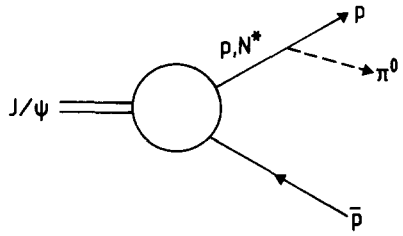

Fig. 55. Example of a baryon pole diagram.

Table 27

Three-body J/ψ decays into baryons. The results have been averaged assuming uncorrelated errors. The reduced branching ratio $\tilde{B}$ is obtained by dividing out the three-body s wave phase space. Upper limits are given at the 90% C.L. The reactions marked by [a] largely proceed via N(1440–1535)π.

Final state	Branching ratio (units of 10^{-4})	$\tilde{B}$ (units of 10^{-4})	Experiment
$p\bar{p}\pi^0$	$10.0 \pm 1.5 \pm 1.5$		Mark I [184]
	$11.3 \pm 0.9 \pm 0.9$		Mark II [185]
	11.0 ± 1.1	31.4 ± 3.1	⟨average⟩
$\Lambda\bar{\Lambda}\pi^0$	$2.2 \pm 0.5 \pm 0.5$	15.4 ± 5.0	DM2 [186]
$p\bar{p}\eta$	$23.0 \pm 4.0 \pm 3.5$		Mark I [184]
	$20.3 \pm 1.3 \pm 1.5$		Mark II [185]
	20.6 ± 1.9	133 ± 12	⟨average⟩
$p\bar{p}\eta'$	$18.0 \pm 6.0 \pm 2.7$		Mark I [184]
	$6.8 \pm 2.3 \pm 1.7$	407 ± 171	Mark II [185]
$\Delta^{++}\bar{p}\pi^-$	$15.8 \pm 2.3 \pm 4.0$	94 ± 27	Mark II [185]
$p\bar{\Lambda}K^-$	$8.9 \pm 0.7 \pm 1.4$	93 ± 16	Mark II [185]
$\bar{p}\Lambda K^+$	$7.1 \pm 0.2 \pm 1.5$	74 ± 16	DM2 [187]
$p\bar{\Sigma}^0K^-$	$2.9 \pm 0.6 \pm 0.5$	42 ± 11	Mark II [185]
$\bar{p}\Sigma^0K^+$	$2.6 \pm 0.3 \pm 0.6$	38 ± 10	DM2 [187]
$p\bar{\Sigma}^{0*}K^-$	$5.1 \pm 2.6 \pm 1.8$	283 ± 176	Mark II [185]
$pn\pi^-$	$21.6 \pm 2.9 \pm 3.3$		Mark I [184][a]
	$20.2 \pm 0.7 \pm 1.6$		Mark II [185][a]
	20.4 ± 1.6	58.9 ± 4.7	⟨average⟩[a]
$\bar{p}n\pi^+$	$20.4 \pm 2.7 \pm 3.1$		Mark I [184][a]
	$19.3 \pm 0.7 \pm 1.6$		Mark II [185][a]
	19.5 ± 1.6	56.2 ± 4.6	⟨average⟩[a]
$\Lambda\bar{\Sigma}^+\pi^-$	$15.3 \pm 1.7 \pm 3.8$		Mark II [185]
	$9.0 \pm 0.6 \pm 1.6$		DM2
	9.9 ± 1.6	90 ± 15	⟨average⟩
$\Lambda\bar{\Sigma}^-\pi^+$	$13.8 \pm 2.1 \pm 3.5$		Mark II [185]
	$11.1 \pm 0.6 \pm 1.6$		DM2 [186]
	11.5 ± 1.9	105 ± 17	⟨average⟩
$p\bar{p}\omega$	$16.0 \pm 3.0 \pm 2.4$		Mark I [184]
	$11.0 \pm 1.7 \pm 1.8$		Mark II [185]
	12.5 ± 2.1	204 ± 34	⟨average⟩
$p\bar{p}\rho$	<0.31	<4.7	Mark II [185]
$p\bar{p}\phi$	$0.45 \pm 0.13 \pm 0.07$	60 ± 20	DM2 [126]

- However, electromagnetic amplitudes *can* play a major role as may be seen from the SU(2) breaking decay $J/\psi \to \Lambda\bar{\Lambda}\pi^0$, whose reduced branching fraction $\tilde{B}$ is half as large as that of the SU(3) allowed decay $J/\psi \to p\bar{p}\pi^0$.
- By comparing the decays

$$J/\psi \to p\bar{p}\begin{cases}\pi^0\\ \eta\\ \eta'\end{cases} \quad \text{and} \quad J/\psi \to p\bar{p}\begin{cases}\rho^0\\ \phi\\ \omega\end{cases} \tag{90}$$

one finds that final states including isovector mesons are relatively suppressed. Considering only the proton pole diagram of fig. 55, assuming the exact validity of the OZI rule and $SU(3)_{\text{flavour}}$, one predicts [202] the ratios ($\theta_{\text{ideal}} = 35.3°$)

$$\tilde{B}(J/\psi \to p\bar{p}\eta) : \tilde{B}(J/\psi \to p\bar{p}\eta') : \tilde{B}(J/\psi \to p\bar{p}\pi^0) = a^2\sin^2(\theta_{\text{ideal}} - \theta_P) : a^2\cos^2(\theta_{\text{ideal}} - \theta_P) : 1$$
$$= 0.004 : 0.002 : 1\,, \tag{91}$$
$$\tilde{B}(J/\psi \to p\bar{p}\omega) : \tilde{B}(J/\psi \to p\bar{p}\phi) : \tilde{B}(J/\psi \to p\bar{p}\rho^0) = 9 : 0 : 1\,.$$

The factor a can be calculated [202, 203]. For definiteness we assume a pseudoscalar mixing angle of $\theta_P = -20°$ and set $a \approx 2.08$ [202, 203]. While this simple model explains the suppression of the $J/\psi \to p\bar{p}\rho^0$ rate, it fails to account for the large $J/\psi \to \eta p\bar{p}$ and $J/\psi \to \omega p\bar{p}$ rates. Sinha and Okubo [202] have included in their calculations the effect of an intermediate N* pole and find reasonable agreement with the relative and absolute $J/\psi \to$ pseudoscalar + $p\bar{p}$ rates. The assumption of large N(1440), N(1535) contributions is verified by experiment, since the reaction $J/\psi \to \pi^0 p\bar{p}$ and $J/\psi \to \eta p\bar{p}$ are found to proceed mainly via the N*p intermediate state [204].

5.7. Rare decays

One reason for the longevity of J/ψ research is that each successive experiment has increased its sensitivity over previous experiments, either by improving the detection efficiency or by increasing the statistics. Branching ratios of order 10^{-4}–10^{-5} are routinely studied, and upper limits have been pushed to the 10^{-6} level. Future experiments at the Beijing Electron Positron Collider (BEPC) [77, 206] have the potential of increasing the sensitivity by one or two orders of magnitude.

5.7.1. Weak decays

The J/ψ can couple to the weak neutral current through the annihilation diagram shown in fig. 56. A simple minded estimate of the branching ratio for weak decays is

$$B(J/\psi \to Z^0 \to X) \approx (m_\psi/m_Z)^4 \times B(J/\psi \to e^+e^-) \approx 10^{-7}\,. \tag{92}$$

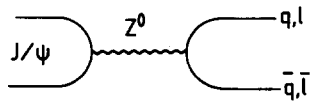

Fig. 56. Feynman diagram for weak J/ψ decays.

Due to the quartic mass factor, the Υ(9460) is favoured compared to the J/ψ by roughly a factor 30, compensating for the advantage of high statistics available at the J/ψ. Still, predictions for exclusive channels have been made for several final states including $J/\psi \to \nu\bar{\nu}$ [207], the C parity violating decay $J/\psi \to \phi\phi$ [208], and $J/\psi \to K_S^0 \bar{K}_S^0$ [209], which is forbidden by the spin statistics theorem. The $J/\psi \to \nu\bar{\nu}$ decay, which can in principle be tagged via $\psi' \to \pi^+\pi^- J/\psi \to \pi^+\pi^-$ + nothing, occurs with a rate of ($\sin^2\theta_W = 0.22$)

$$B(J/\psi \to \nu\bar{\nu}) = N_\nu \frac{9(1-\frac{8}{3}\sin^2\theta_W)^2}{512 \sin^4\theta_W \cos^4\theta_W} \left(\frac{M_\psi}{M_Z}\right)^4 B(J/\psi \to e^+e^-) \approx 10^{-8} \times N_\nu . \tag{93}$$

Given the backgrounds, this is too small to lead to an interesting bound on the number of neutrino generations N_ν. The predictions for $J/\psi \to \phi\phi$ ($<10^{-8}$) and $J/\psi \to K_S^0 \bar{K}_S^0$ ($<10^{-9}$) are even smaller. Electroweak interference effects in decays like $J/\psi \to \mu\mu$ are small and only observable if the helicity of the muon can be detected [205].

Although in the minimal standard model (one Higgs doublet) the Linde–Weinberg bound [210] constrains the Higgs mass to be well above the J/ψ mass,*) this does not necessarily apply to theories with more than one Higgs doublet. The signature for the Higgs would be an extremely narrow, spinless state, decaying primarily into final states involving kaons. The claimed evidence for the ξ(2230) by Mark III has, among others, also generated speculations that it might be a Higgs boson (see discussion in section 6.4.3).

5.7.2. New fudamental couplings

New fundamental couplings, such as in supersymmetric or composite models, may produce observable effects in J/ψ decays if the mass scale is low enough. For example, if the supersymmetric partner of the gluon, the gluino, has sufficiently low mass, a two-gluino state might be observable in J/ψ radiative decays [211]. From the apparent absence of such a signal, the authors conclude that $m_{\text{gluino}} > 1$ GeV, independent of its lifetime and the squark mass. For most signatures, however, measurements at PETRA/PEP are, despite the lower statistics, more sensitive to new couplings than at the J/ψ.

5.7.3. Axion searches

The axion is a Goldstone boson resulting from the breaking [213] of a U(1) symmetry. The apparent lack of large P and CP violations in strong interactions can be explained if such a symmetry is imposed [214] on the QCD Lagrangian. The standard axion has a small mass of the order of 100 keV and a rather long lifetime $\tau_a \approx 10^{-2\pm2}$ s. Early experiments on axion production and/or decay were controversial, either observing [215] the decay of an axion-like particle of mass $m_a \approx 250$ keV, or ruling out [217] the existence of a standard axion.

The predicted radiative decay rate for a vector meson into an axion contains a free parameter x, the ratio of the vacuum expectation values of the two Higgs fields in the theory. For the J/ψ one predicts [218]

$$\frac{B(J/\psi \to \gamma a)}{B(J/\psi \to \mu^+\mu^-)} = \frac{G_F m_c^2}{\sqrt{2}\pi\alpha_{QED}} x^2 = (5.7 \pm 1.4) \times 10^{-5} x^2 , \tag{94}$$

*) Note that this limit (>7 GeV) is only valid if the mass of the top quark is sufficiently low [410].

where G_F is the Fermi coupling constant, $m_c = (1.5 \pm 0.3)$ GeV the current mass of the charmed quark, and α_{QED} the QED coupling constant.

The signature of a long-lived standard axion in radiative J/ψ decays would be a single photon of beam energy. The Crystal Ball Collaboration [212] has conducted a search for this topology and found no evidence, corresponding to the upper limit

$$B(J/\psi \to \gamma a) < 1.4 \times 10^{-5} \tag{95}$$

at the 90% confidence level. The equivalent limit of $x < 0.6$ rules out a value of $x = 3.0 \pm 0.3$ found earlier [215].

For the decays of the Υ(9460), eq. (94) has to be modified by replacing x^2 by $1/x^2$. Consequently, the prediction $B(J/\psi \to \gamma a) \times B(\Upsilon \to \gamma a) = (1.8 \pm 0.4) \times 10^{-9}$ [216], where QCD radiative corrections have been included, is independent of the unknown parameter x. Experimentally [216] one determines the limit $B(J/\psi \to \gamma a) \times B(\Upsilon \to \gamma a) < 0.2 \times 10^{-9}$, which clearly rules out the standard axion. One should note, however, that the non-standard axions (e.g. "invisible axions" [219]) are not affected by this investigation.

6. Radiative J/ψ decays

It is the radiative decays of the J/ψ in which glueballs are expected to be seen if they exist. The decay

$$J/\psi \to \gamma + X, \tag{96}$$

as shown to lowest order in fig. 57a, is ideally suited to scan for glueballs in the mass region up to 3 GeV. The diagram in fig. 57b is considered to be suppressed. The decay $J/\psi \to \gamma\pi^0$, in which the photon must couple as an octet to the light quark final state, is more than an order of magnitude weaker than $J/\psi \to \gamma\eta$ or $\gamma\eta'$ and provides a lower limit to the contribution of the diagram of fig. 57b.

A fairly reliable estimate of the fraction of radiative decays to all decays of the J/ψ can be made following the perturbative approach of section 2.1 using some experimental input in addition. The leptonic branching fractions contributing to the purely electromagnetic diagram of fig. 4b are measured to be $(6.9 \pm 0.9)\%$ [14, 23], identical for $J/\psi \to \mu^+\mu^-$ and $J/\psi \to e^+e^-$. Assuming lepton universality, the error is reduced to $0.9/\sqrt{2}\% = 0.64\%$. Quark pair production via one-photon annihilation following fig. 4b can be readily deduced using the off-resonance measurement of $R = \sigma(e^+e^- \to \text{hadrons})/\sigma(e^+e^- \to \mu\mu) = 2.59 \pm 0.17$ at 3 GeV [25].

The three-gluon decay of fig. 4a can be inferred from the QCD formula of eq. (7) by introducing the

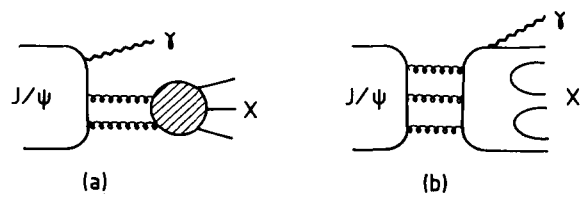

Fig. 57. Radiative J/ψ decay. Decay diagrams in lowest order showing photon emission from the initial state (a) and final state (b) quark line, respectively.

measured value for $\Gamma(J/\psi \to \ell^+\ell^-)$. We neglect terms like m_q^2/M_ψ^2 and assume the $c\bar{c}$ system to be non-relativistic.

In the same we we relate $\Gamma(J/\psi \to \gamma gg)$ to the leptonic decay width using eq. (10),

$$\Gamma(J/\psi \to \gamma gg) = \frac{8}{9\pi}(\pi^2 - 9)\frac{\alpha_s^2}{\alpha}\Gamma(J/\psi \to \ell^+\ell^-)(1 + 10.3\alpha_s/\pi)(1 - 5.8\alpha_s/\pi)\,. \tag{97}$$

Finally, we use the measured branching ratio [230] for the transition $J/\psi \to \gamma\eta_c$, which is $(1.27 \pm 0.36)\%$. Assuming that the decays of fig. 4 total 100% of all J/ψ decays, i.e.,

$$B(J/\psi \to ee, \mu\mu) + B(J/\psi \to q\bar{q})_{elm} + B(J/\psi \to 3g) + B(J/\psi \to \gamma gg) + B(J/\psi \to \gamma\eta_c) = 1\,,$$

one finds, substituting numbers and using the lowest-order formulae only,

$$(6.9 \pm 0.64) \times 10^{-2}\left[2 + (2.59 \pm 0.17) + \frac{5}{18\pi}(\pi^2 - 9)\frac{\alpha_s^3}{\alpha^2}\left(1 + \frac{16}{5}\frac{\alpha}{\alpha_s}\right)\right] + (1.27 \pm 0.36) \times 10^{-2} = 1\,. \tag{98}$$

Solving this cubic equation for α_s yields $\alpha_s = 0.181 \pm 0.008$ and

$$B(J/\psi \to \gamma gg)_{\text{lowest order}} = (7.6 \pm 0.7)\% \tag{99}$$

for the radiative J/ψ branching fraction. One must check if this result is stable with respect to higher orders of perturbation theory and the assumption that the $c\bar{c}$ system is non-relativistic. Introducing the first-order corrections [16] results in a 12% smaller value for α_s (0.16 ± 0.007) and a branching fraction of $B(J/\psi \to \gamma gg) = (6.5 \pm 0.6)\%$, indicating that eq. (99) appears to be relatively stable with respect to higher-order QCD corrections.

One also must worry about the renormalization scheme dependence. Above estimates are based on the $\overline{\text{MS}}$ scheme. Another choice is the "scheme of effective charges" [220], which chooses α_s such that the second order adds zero correction to the result, but not necessarily the orders higher than two. In this scheme $\alpha_s = 0.15 \pm 0.01$ and the same radiative branching fraction as in the first-order calculation with the $\overline{\text{MS}}$ scheme is obtained.

In order to remove reliance on the assumption of a non-relativistic $c\bar{c}$ system one may use only the *ratio* of the γgg and ggg partial widths, $\Gamma_{\gamma gg}/\Gamma_{ggg}$, and the sum of their branching fractions, which amounts to roughly $(68 \pm 4)\%$. The strong coupling constant can then be computed using the standard QCD formula

$$\alpha_s(M_\psi^2) = \frac{12\pi}{(33 - 2n_f)\ln(M_\psi^2/\Lambda^2)}\,, \tag{100}$$

which, with $\Lambda = (200 \pm 100)$ MeV, yields $\alpha_s = 0.21 \pm 0.04$. With this value of α_s, $B(J/\psi \to \gamma gg)$ can be calculated from eq. (11) of section 2.1 and from the sum of the branching ratios for γgg and ggg to be $(6.8 \pm 1.4)\%$ in lowest-order and $(4.9 \pm 1.0)\%$ in first-order QCD.

Summarizing these estimates one can reliably state that

$$B(J/\psi \to \gamma gg) = (6 \pm 2)\%\,. \tag{101}$$

6.1. The inclusive photon spectrum

The inclusive photon spectrum $J/\psi \to \gamma + X$ has been measured by the Lead Glass Wall [221] and Mark II [222] Collaborations. Such a measurement is very difficult, especially in the low $x = 2E_\gamma/M_\psi$ range, due to $\pi^0 \to \gamma\gamma$ and $\eta \to \gamma\gamma$ decays in processes which are not radiative J/ψ decays but can mistakenly be identified as such. Mark II has therefore statistically subtracted events involving π^0 and η decays in the inclusive photon spectrum. The result is shown in fig. 58. The subtraction procedure has large systematic errors for $x \leq 0.6$, i.e., $M_X > 2$ GeV. The integrated branching fraction for $x > 0.6$ is [222] $B(J/\psi \to \gamma + X) = (4.1 \pm 0.8)\%$. Comparison with the perturbative QCD prediction [223] is done by the solid line. The data are clearly softer than the theoretical expectation near $x = 1$, although the integral for $x > 0.6$ is the same ($\approx 5\%$).

Crystal Ball [224] has analysed an inclusive photon spectrum with much larger statistics and a superior photon resolution (fig. 59). Resonance production is observed near the end point of the spectrum, which is, however, not renormalized. The difficulty in obtaining an absolute cross section lies in the knowledge of the photon efficiency associated with the low-multiplicity final states of resonances, many of which are unknown. Figures 59 and 58 are thus not directly comparable. The better resolution and higher statistics of Crystal Ball allows one to identify structures in the inclusive distribution which are labeled in fig. 59. Masses below the η' mass are cut out by the analysis procedure.

The spin decomposition of the two-gluon system X recoiling against the radiative photon in $J/\psi \to \gamma gg$ has been calculated by Billoire et al. [226] and Körner et al. [227]. They obtain the spin parity decomposition of the two-gluon system as a function of mass. Billoire et al. [226] assume the gluons to be massless. This assumption forbids the production of spin 1^+ and $(\text{odd})^-$ gg systems due to Yang's theorem [228]. In their calculations the spin 0^+ and 0^- contributions are identical and fairly large. Remarkably, the dominant contribution is $J^P = 2^+$, especially at small invariant gg masses, which is understood from the structure of the Ore–Powell matrix element for this decay [229]. The spectra are shown in fig. 60a.

Körner et al. [227] have calculated the spectrum by assuming the approximation of non-relativistic, weakly bound, $q\bar{q}$ systems. The meson wave functions at the origin are the only unknowns and are obtained from the measured electromagnetic widths of the J/ψ and the light quark mesons, respectively. To first order in perturbative QCD the diagrams are calculated without assuming the gluons to be

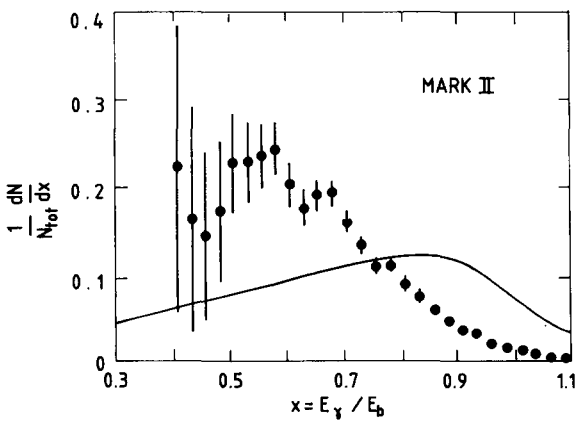

Fig. 58. The inclusive photon distribution from the J/ψ as obtained by Mark II [222]. The solid line is the result of a perturbative QCD calculation with the experimental resolution for this process folded in.

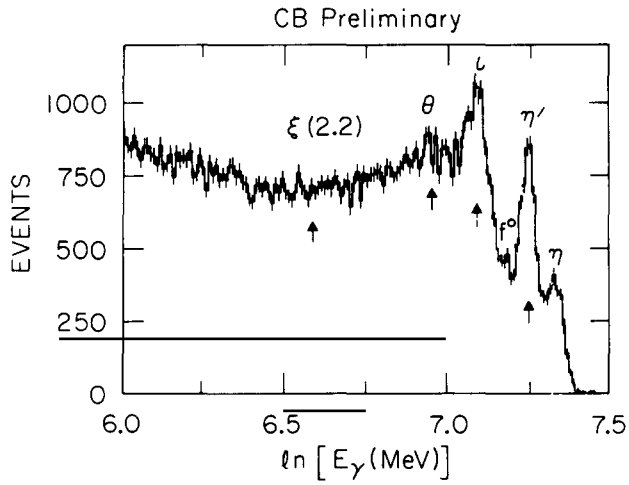

Fig. 59. The inclusive photon distribution as obtained by Crystal Ball. The distribution is not normalized. The particle names label the regions where these resonances should appear. The logarithm of the photon energy is plotted to obtain constant resolution along this axis.

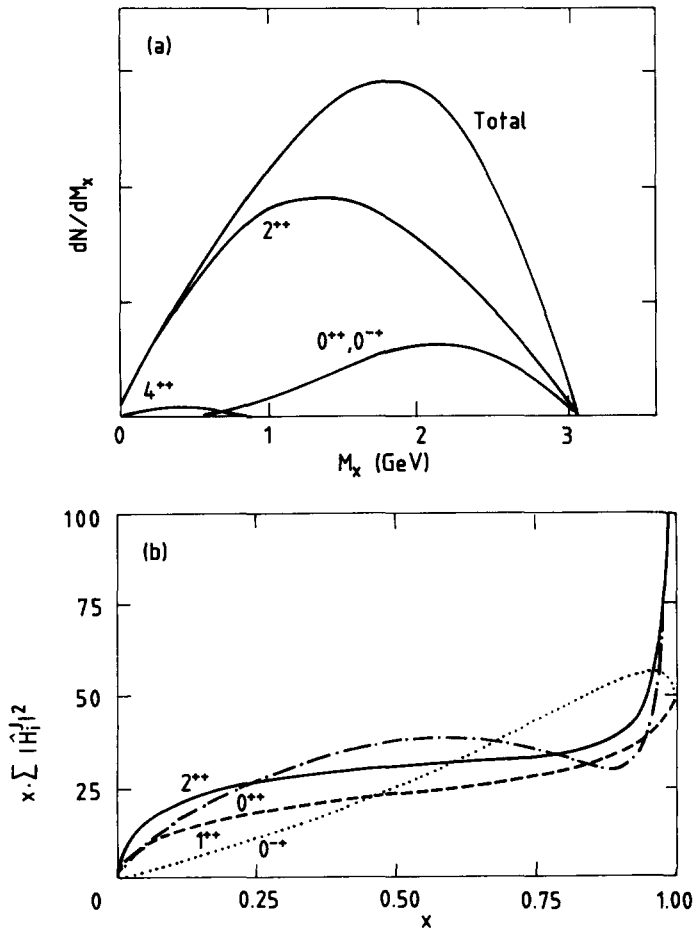

Fig. 60. Perturbative QCD calculation for $J/\psi \rightarrow \gamma gg$. (a) Spin parity content of the gg system as a function of gg invariant mass (from ref. [226]). (b) Summed squares of the reduced helicity amplitudes as a function of $x = 1 - (m_{gg}/m_\psi)^2$ (from ref. [227]).

on-shell, such that spin 1 states are no longer forbidden. The relative contributions of the four different spin parities are shown in fig. 60b.

It is evident from fig. 59 that not every resonance seen in a radiative decay of the J/ψ is necessarily a glueball candidate. Other possibilities have already been outlined in chapter 2. We therefore start with the discussion of the radiative production of those mesons which are most likely composed of a quark–antiquark pair.

6.2. *The M1 transition* $J/\psi \to \gamma\eta_c$

The $^1S_0$, $J^{PC} = 0^{-+}$ state of the charmonium family, the η_c, was found in the inclusive photon spectrum from the ψ' and J/ψ by Crystall Ball [230] and in exclusive hadronic decays by Mark II [231]. The evidence for the η_c in the inclusive γ spectrum of Crystal Ball is shown in fig. 61.

Mass, width and branching fraction from this measurement are

$$m(\eta_c) = 2984 \pm 5\,\text{MeV}\,, \qquad \Gamma(\eta_c) = 11.5^{+4.5}_{-4.0}\,\text{MeV}\,,$$
$$B(J/\psi \to \gamma\eta_c) = (1.27 \pm 0.36) \times 10^{-2}\,. \tag{102}$$

Since then a number of decay modes of the η_c have been measured including the decay to φφ [232], which allows a unique measurement of the 0^- spin parity and has established the η_c to be the $^1S_0$ state

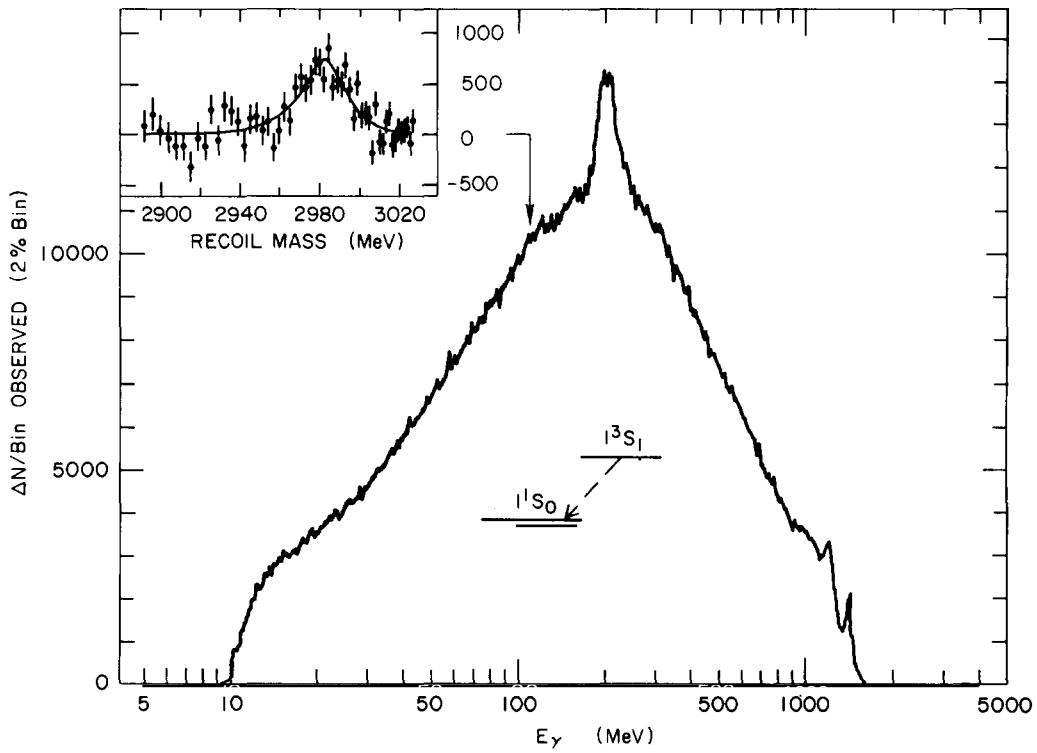

Fig. 61. Evidence for the η_c in the inclusive γ spectrum at the J/ψ. The peak at 200 MeV arises from charged particles not tagged by the tracking system. The peaks at the end point of the spectrum are from $J/\psi \to \gamma\eta'$ and $J/\psi \to \gamma\eta(1440)$. The signals due to $J/\psi \to \gamma\eta$ and $J/\psi \to \gamma\pi^0$ have been removed by cuts. The insert displays the background subtracted η_c region (from ref. [247]).

of the charmonium family. We only list here the experimental results (table 28) without going into further detail of the physics involved. The interested reader is referred to refs. [234] and [237] and references therein.

6.3. Radiative production of $q\bar{q}$ mesons

6.3.1. The decay $J/\psi \to \gamma$ + pseudoscalar

Of the pseudoscalar ground state nonet the η, η', and the π^0 can be produced in the radiative decay $J/\psi \to \gamma$ + pseudoscalar. The physical states $\eta(549)$ and $\eta'(958)$ are mixtures of the SU(3) singlet η_1 and the octet η_8 as a consequence of nonet symmetry breaking. The relation between the mass and the SU(3) eigenstates is given by [14]

$$\eta(549) = \eta_8 \cos\theta_P - \eta_1 \sin\theta_P ,$$
$$\eta'(938) = \eta_8 \sin\theta_P + \eta_1 \cos\theta_P , \qquad (103)$$

Table 28
Decay branching ratios of the $\eta_c(2980)$. The measured product branching fractions have been corrected using the Crystal Ball values for $B(J/\psi \to \gamma\eta_c)$ and $B(\psi' \to \gamma\eta_c)$ [247], respectively, and have been corrected for isospin where necessary.

Decay mode	$B(\eta_c \to X)$ (%)	Reference
$K^*(892)\bar{K}^*(892)$	0.9 ± 0.5	Mark III [234]
	0.55 ± 0.18	DM2 [124]
$a_0(980)\pi$	$<1.0/B(a_0(980) \to \eta\pi)$	Mark III [234]
$a_2(1320)\pi$	<2.0	Mark III [234]
$f_2(1270)\eta$	<1.1	Mark III [234]
$\eta\pi\pi$	3.6 ± 2.4	Crystal Ball [230]
	5.4 ± 1.3	Mark III [234]
$\eta'\pi\pi$	4.1 ± 1.3	Mark III [234]
$K\bar{K}\pi$	16^{+11}_{-7}	Mark II [231]
	4.8 ± 1.1	Mark III [234]
	5.9 ± 1.4	DM2 [235]
$K\bar{K}\eta$	<3.1	Mark III [234]
$K^{*0}(892)K^-\pi^+ + c.c.$	2.0 ± 0.5	Mark III [234]
$\pi^+\pi^-\pi^+\pi^-$	$2.0^{+1.5}_{-0.9}$	Mark II [231]
	1.3 ± 0.5	Mark III [234]
	$1.05 \pm 0.17 \pm 0.16$	DM2 [235]
$\pi^+\pi^-K^+K^-$	$1.4^{+2.1}_{-0.9}$	Mark II [231]
	2.1 ± 0.3	Mark III [234]
$\pi^+\pi^-p\bar{p}$	<2.3	Mark II [231]
$p\bar{p}$	$0.29^{+0.3}_{-0.16}$	Mark II [231]
	0.11 ± 0.06	Mark III [234]
	$0.146 \pm 0.04 \pm 0.03$	DM2 [204]
$\Lambda\bar{\Lambda}$	<0.63	Mark II [231]
	<0.32	DM2 [359]
$\phi\phi$	$0.8 \pm 0.2 \pm 0.25$	Mark III [232, 234]
	$0.31 \pm 0.07 \pm 0.04$	DM2 [233]
$\rho\rho$	$2.6 \pm 0.8 \pm 0.5$	DM2 [236]
$\omega\phi$	<0.13	Mark III [352]
$\omega\omega$	<0.31	Mark III [234]
	<0.7	DM2 [351]
$\gamma\gamma$	0.06 ± 0.03	world average [131]

where θ_P is the pseudoscalar mixing angle. The physical states diagonalize the mass squared matrix

$$M^2 = \begin{pmatrix} M_{11}^2 & M_{18}^2 \\ M_{18}^2 & M_{88}^2 \end{pmatrix}, \tag{104}$$

where $M_{88}^2 = \frac{1}{3}(4m_K^2 - m_\pi^2)$ and M_{11}^2, M_{18}^2 include the sum and the difference of m_π^2 and m_K^2, respectively [239]. Writing down the quadratic Gell-Mann–Okubo mass formula [238] as

$$\tan^2\theta_P = (M_{88}^2 - m_\eta^2)/(m_{\eta'}^2 - M_{88}^2) \tag{105}$$

yields $\theta_P \approx \pm 10°$. SU(3) breaking or higher-order effects [240] increase θ_P to ~20°. The pseudoscalar nonet is *not* ideally mixed, i.e., both η and η' contain u, d, s quarks in contrast, e.g., to the ideally mixed vector mesons, where the $\phi(1020)$ is an almost pure $s\bar{s}$ meson while the ω is devoid of strange quarks. For ideal mixing the mixing angle is 35.3° or $\tan\theta_{ideal} = 1/\sqrt{2}$. Defining

$$\eta_1 = (u\bar{u} + d\bar{d} + s\bar{s})/\sqrt{3}\,, \qquad \eta_8 = (u\bar{u} + d\bar{d} - 2s\bar{s})/\sqrt{6} \tag{106}$$

leads to a negative mixing angle, $\theta_P < 0$.

The experimental estimate of the value of θ_P has changed in the recent past with respect to the long assumed value of $-10°$, obtained from the GMO mass formula (105), due to more precise recent measurements in various areas. Gilman and Kauffman [241] have analysed experimental data from various reactions and found consistency of *all* data with a mixing angle of

$$\theta_P \approx -20°\,. \tag{107}$$

The fact that the η is so much heavier than its isotriplet partner π^0 and that the η–η' mixing is not ideal is often referred to as the essence of the "U(1) problem" [242]. This, plus the fact that the η' is produced in radiative J/ψ decays with a rather large branching fraction, has raised the possibility that the η' might have a sizeable gluonic component mixed into its wave function. A study of the η–η' system in radiative and non-radiative J/ψ decays is therefore of considerable interest (see also section 5.3.2).

6.3.1.1. $J/\psi \to \gamma\eta$ *and* $J/\psi \to \gamma\eta'$. The decays $J/\psi \to \gamma\eta$ and $J/\psi \to \gamma\eta'$ have been measured by DASP [107], the DESY–Heidelberg group [244], Mark II [246], Crystal Ball [247–249], Mark III [250, 251], and DM2 [110]. The measured branching ratios are given in table 29.

Figure 62a,b shows the measured mass distributions with evidence for η and η'. From the branching fractions measured by the Crystal Ball group one finds the ratio [247]

$$\Gamma(J/\psi \to \gamma\eta')/\Gamma(J/\psi \to \gamma\eta) = 4.7 \pm 0.6\,. \tag{108}$$

The decay rate $\Gamma(J/\psi \to \gamma + \text{pseudoscalar})$ can be calculated using perturbation theory [227, 252],

$$\Gamma(J/\psi \to \gamma + P) = \tfrac{1}{6}(\tfrac{2}{3})^2 \alpha_s^4 \alpha Q_c^2 \frac{1}{M_\psi^3} \left(\frac{4R_\psi(0)}{\sqrt{4\pi M_\psi}}\right)^2 \left(\frac{4R_P(0)}{\sqrt{4\pi M_P}}\right)^2 x|H^P(x)|^2\,. \tag{109}$$

Table 29
Branching ratios for the decays $J/\psi \to \gamma + \{\eta, \eta', \pi^0\}$. The branching fractions are corrected for unobserved decay modes using 4.25 keV for the $\gamma\gamma$ width of the η' [131]. Γ has been calculated using (74 ± 8) keV for the total width of the J/ψ [23, 99].

Decay	Detected mode	$B(J/\psi \to \gamma X)$	Γ (eV)	Reference
$J/\psi \to \gamma\pi^0$	$\pi^0 \to \gamma\gamma$	$(7.3 \pm 4.7) \times 10^{-5}$	5.4 ± 3.5	DASP [67]
	$\pi^0 \to \gamma\gamma$	$(3.6 \pm 1.1 \pm 0.7) \times 10^{-5}$	$2.7 \pm 0.9 \pm 0.6$	C.B. [247, 248]
	$\pi^0 \to \gamma\gamma$	$(2.2 \pm 0.4 \pm 0.3) \times 10^{-5}$	$1.6 \pm 0.3 \pm 0.3$	DM2 [243]
		$(2.4 \pm 0.5) \times 10^{-5}$	1.8 ± 0.4	⟨average⟩
$J/\psi \to \gamma\eta$	$\eta \to \gamma\gamma$	$(8.2 \pm 1.0) \times 10^{-4}$	60.7 ± 9.9	DASP [67]
	$\eta \to \gamma\gamma$	$(13 \pm 4) \times 10^{-4}$	97 ± 31	Desy-HD [244]
	$\eta \to \gamma\gamma$	$(8.8 \pm 0.8 \pm 1.1) \times 10^{-4}$	$65.1 \pm 9.2 \pm 10.8$	C.B. [247]
	$\eta \to \gamma\gamma$	$(8.5 \pm 0.5 \pm 1.3) \times 10^{-4}$	$62.9 \pm 7.7 \pm 11.8$	DM2 [243]
	$\eta \to 3\pi^0$	$(10.1 \pm 0.6 \pm 1.6) \times 10^{-4}$	$74.7 \pm 9.2 \pm 14.3$	DM2 [249]
	$\eta \to \gamma\pi^+\pi^-$	$(9.1 \pm 2.2 \pm 1.6) \times 10^{-4}$	$67.3 \pm 17.8 \pm 13.9$	Mark III [251]
		$(8.8 \pm 0.6) \times 10^{-4}$	65.1 ± 8.3	⟨average⟩
$J/\psi \to \gamma\eta'$	$\eta' \to \eta\pi^+\pi^-$	$(3.9 \pm 1.0 \pm 1.1) \times 10^{-3}$	$289 \pm 80 \pm 87$	C.B. [247]
	$\eta' \to \eta\pi^0\pi^0$	$(4.2 \pm 0.6 \pm 0.6) \times 10^{-3}$	$311 \pm 56 \pm 56$	C.B. [247]
	$\eta' \to \gamma\rho^0$	$(4.1 \pm 0.4 \pm 0.6) \times 10^{-3}$	$303 \pm 44 \pm 55$	C.B. [247]
	$\eta' \to \gamma\gamma$	$(4.4 \pm 0.9 \pm 0.5) \times 10^{-3}$	$326 \pm 75 \pm 51$	C.B. [247]
	$\eta' \to \gamma\rho^0$	$(2.4 \pm 0.7) \times 10^{-3}$	178 ± 55	Desy-HD [244]
	$\eta' \to \gamma\rho^0$	$(4.7 \pm 0.2 \pm 0.7) \times 10^{-3}$	$348 \pm 40 \pm 64$	Mark III [251]
	$\eta' \to \gamma\rho^0$	$(4.4 \pm 0.3 \pm 0.7) \times 10^{-3}$	$310 \pm 37 \pm 62$	DM2 [245]
	$\eta' \to \eta\pi^+\pi^-$	$(4.6 \pm 0.4 \pm 0.7) \times 10^{-3}$	$340 \pm 47 \pm 64$	Mark III [251]
	$\eta' \to \gamma\gamma$	$(3.1 \pm 1.2) \times 10^{-3}$	229 ± 90	DASP [67]
	$\eta' \to \gamma\gamma$	$(4.7 \pm 0.4 \pm 0.9) \times 10^{-3}$	$348 \pm 48 \pm 77$	DM2 [243]
		$(4.0 \pm 0.3) \times 10^{-3}$	296 ± 39	⟨average⟩

Here $R_\psi(0)$ and $R_P(0)$ are the wave functions of the J/ψ and the pseudoscalar with mass M_P at the origin. Q_c is the charge of the charm quark. The reduced pseudoscalar helicity amplitude $H^P(x)$ depends on $x = 1 - (M_P/M_\psi)^2$; numerically $xH^P(x) \approx 55$ for $M_P = m_{\eta'}$. The wave functions $R_\psi(0)$ and $R_P(0)$ are obtained from $\Gamma(J/\psi \to e^+e^-)$ [eq. (3) of chapter 2] and $\Gamma(P \to \gamma\gamma)$, respectively, with $R^2(0) = |\psi(0)|^2 \cdot 4\pi$. One finds

$$\Gamma(J/\psi \to e^+e^-) = \frac{4\alpha^2 Q_c^2}{M_\psi^2} R_\psi^2(0)\,, \tag{110}$$

$$\Gamma(P \to \gamma\gamma) = \frac{12\alpha^2 \langle Q^2 \rangle_P^2}{m_P^2} R_P^2(0)\,, \tag{111}$$

where, e.g., for $P = \eta'$ and using $\theta_P = -20°$

$$\langle Q^2 \rangle_{\eta'} = \langle Q^2 \rangle_1 \cos\theta_P + \langle Q^2 \rangle_8 \sin\theta_P = 0.315\,. \tag{112}$$

Following ref. [227] one obtains $\Gamma(J/\psi \to \gamma\eta')$ by multiplying (109) with the SU(3) factor $3\cos^2\theta_P$ and using the lowest-order QCD formula for α_s with $\Lambda = 100$ MeV. The result, $\Gamma(J/\psi \to \gamma\eta') = 213$ eV, is in reasonable agreement with the experimental average of (296 ± 39) eV. In the same model, however, the prediction for $\Gamma(J/\psi \to \gamma\eta)$ is disastrously small. Either or both of the two assumptions, to use

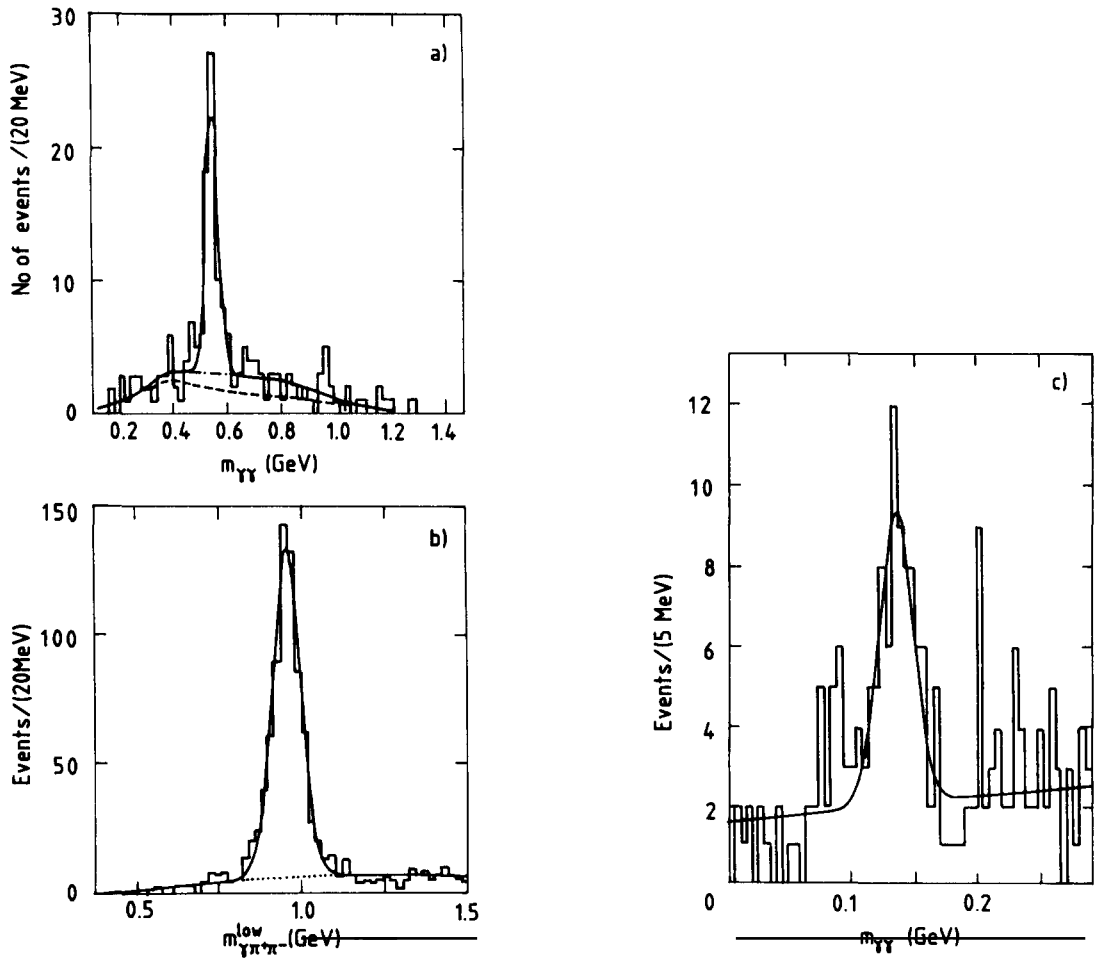

Fig. 62. Evidence for η, η' and π^0 in $J/\psi \to \gamma + X$. (a) $\gamma\gamma$ invariant mass from $J/\psi \to 3\gamma$ (DASP) [107], (b) $\gamma\pi^+\pi^-$ invariant mass from $J/\psi \to \gamma\pi^+\pi^-$ (Crystal Ball) [247], and (c) $\gamma\gamma$ invariant mass from $J/\psi \to 3\gamma$ (DM2) [110].

first-order perturbation theory and a non-relativistic description for the $\eta(549)$, must be invalid. If, on the other hand, one assumes SU(3) invariance, $R^2_\eta(0) = R^2_{\eta'}(0)$, then

$$\frac{\Gamma(J/\psi \to \gamma\eta')}{\Gamma(J/\psi \to \gamma\eta)} \approx \left(\frac{\alpha_s(m^2_{\eta'})}{\alpha_s(m^2_\eta)}\right)^4 \cos^2\theta_P \frac{m_\eta}{m_{\eta'}} = 5\,,$$

which again is in good agreement with the data [see eq. (108)].

Other models have been built [253, 254] to tackle the large $\Gamma(\eta')/\Gamma(\eta)$ ratio in (108). Some calculations indicate a large "glue" admixture to the η' wave function which is not present in the η. In connection with QCD sum rules Novikov et al. [253] predict various values for $\Gamma(\eta')/\Gamma(\eta)$ between 3.7 and 4.0. Fritzsch and Jackson [254] allow small admixtures of η and η' to the wave function of the η_c. In turn the η, η' obtain some $c\bar{c}$ admixture in their wave functions. The η', being more SU(3) singlet than the η, then has a larger $c\bar{c}$ component and hence a larger production rate from the J/ψ. All

theoretical predictions agree well with the experimental observations. An early analysis of J/ψ decays to *vector* plus *pseudoscalar* mesons suggested [121, 199] in fact that the η′ might have a sizeable glueball component, a result that seemed to be contradicted by γγ data [259]. The analysis of ref. [199] did, however, not account for the effect of doubly OZI suppressed decays (DOZI). A more recent analysis [256], based on twice the amount of data, includes the DOZI diagrams and agrees with the conclusions obtained from γγ experiments. Both, γγ data and J/ψ data, point towards a value of $\theta_P \approx -20°$ and find the gluon component in the η or η′ wave functions to be consistent with zero. In the case of the η′, however, the errors are large (see also section 5.3.2).

6.3.1.2. $J/\psi \to \gamma\pi^0$. The branching ratio for the isospin violating decay, $J/\psi \to \gamma\pi^0$, is more than one order of magnitude smaller than for $J/\psi \to \gamma\eta$, $\gamma\eta'$ (cf. table 29). Because the π^0 is a pure SU(3) octet state the decay cannot proceed through the diagram of fig. 57a but must radiate the photon off the final state quark line (fig. 57b).

To measure the decay sequence $J/\psi \to \gamma\pi^0$, $\pi^0 \to \gamma\gamma$, requires the experiment to trigger on neutral particles only. This measurement has been done by DASP [107], Crystal Ball [248], and DM2 [110]. Figure 62c shows the invariant γγ mass distribution for the DM2 data. The average partial width $\Gamma(J/\psi \to \gamma\pi^0) = (1.9 \pm 0.4)$ eV is in fair agreement with the vector meson dominance prediction

$$\Gamma(J/\psi \to \gamma\pi^0) \approx (e^2/f_\rho^2)\Gamma(J/\psi \to \rho^0\pi^0) \approx \tfrac{1}{250}\Gamma(J/\psi \to \rho^0\pi^0) \approx 1 \text{ eV}.$$

Alternatively, following Fritzsch and Jackson [254], the small branching ratio for $J/\psi \to \gamma\pi^0$ could indicate that a $c\bar{c}$ component in the wave functions of η, η′ is responsible for a strong coupling. There is no such component in the SU(3) octet state π^0 and hence a much weaker coupling is expected.

6.3.2. The decay $J/\psi \to \gamma$ + *tensor*

The central members of the $J^{PC} = 2^{++}$, $L = 1$ tensor nonet are the $f_2(1270)$ and the $f_2'(1525)$ (cf. fig. 5). The radiative decay $J/\psi \to \gamma f_2(1270)$ has been observed by many experiments [260–262, 264–266]. The results of the individual measurements are summarized in table 30.

Figure 63 shows the invariant ππ mass distributions from $J/\psi \to \gamma\pi^0\pi^0$ obtained by the Crystal Ball Collaboration and from $J/\psi \to \gamma\pi^+\pi^-$ as measured by DM2. Both distributions show a pronounced $f_2(1270)$ signal as well as indications for the $f_2(1720)$ and a structure around 2.1 GeV. The $\gamma\pi^+\pi^-$ channel suffers from a large background contribution from $J/\psi \to \rho^0\pi^0$, $\pi^0 \to \gamma\gamma$, where one of the π^0 decay photons escapes detection. This reaction is also responsible for the large ρ peak in fig. 63b. Note that there is no evidence for an $f_0(975)$ signal in $J/\psi \to \gamma\pi\pi$ (see section 6.3.3).

The $f_2'(1525)$ has been studied in $J/\psi \to \gamma K^+K^-$ and $\gamma K_S^0 K_S^0$ [110, 264, 265]. The measured branching fractions are also included in table 30. In fig. 64 the $f_2'(1525)$ peak is seen together with the $f_2(1720)$ as observed by the Mark III experiment using 2.7×10^6 J/ψ decays.

As a consequence of the non-ideal mixing of $f_2(1270)$ and $f_2'(1525)$ one expects that

$$R = \frac{B(J/\psi \to \gamma f_2'(1525))}{B(J/\psi \to \gamma f_2(1270))} = \left|\frac{\sqrt{2}X_{f'} + Y_{f'}}{\sqrt{2}X_f + Y_f}\right|^2 \left(\frac{p_{f'}}{p_f}\right)^3 = 0.26, \tag{113}$$

assuming $X_{f'} \approx -Y_f \approx -0.12$ and $X_f \approx Y_{f'} \approx 1$ [256] for the non-strange and strange quark fractions of the two states as suggested by γγ experiments [131]. Using the average for the branching ratios and estimating that $B(f_2'(1525) \to K\bar{K}) \geq 0.70$ [269] one finds

Table 30
Branching ratios for the decays $J/\psi \to \gamma + \{f_2(1270), f_2'(1525)\}$. The DASP value, denoted by ( )[a], depends on the assumed multipole of the photon transition and has not been used in the determination of the average.

Experiment	Decay mode	$B(J/\psi \to \gamma f_2(1270))$ (units of 10^{-3})	$x = A_1/A_0$	$y = A_2/A_0$	ϕ_x	ϕ_y
PLUTO [260]	$\pi^+\pi^-$	2.0 ± 0.3	0.6 ± 0.3	$0.3^{+0.6}_{-1.6}$		
DASP [261]	$\pi^+\pi^-$	$\begin{pmatrix} 0.9 \pm 0.3 \\ 1.5 \pm 0.4 \end{pmatrix}$ [a]				
Mark II [264]	$\pi^+\pi^-$	1.3 ± 0.3	0.81 ± 0.16	0.02 ± 0.15		
Mark III [265]	$\pi^+\pi^-$	$1.36 \pm 0.08 \pm 0.23$	0.94 ± 0.10	0.06 ± 0.11	0.4 ± 0.7	-0.1 ± 2.2
DM2 [266]	$\pi^+\pi^-$	$1.32 \pm 0.05 \pm 0.20$	0.83 ± 0.06	0.01 ± 0.06	0.9 ± 0.3	0 fixed
C.B. [262]	$\pi^0\pi^0$	$1.48 \pm 0.25 \pm 0.30$	0.88 ± 0.13	0.04 ± 0.19		
DM2 [243]	$\pi^0\pi^0$	$0.81 \pm 0.09 \pm 0.21$				
⟨average⟩	$\pi\pi$	1.31 ± 0.11	0.85 ± 0.05	0.02 ± 0.05	0.8 ± 0.3	-0.1 ± 2.2
Experiment	Decay mode	$B(J/\psi \to \gamma f_2'(1525)) \times B(f_2'(1525) \to K\bar{K})$ (units of 10^{-3})	$x = A_1/A_0$	$y = A_2/A_0$	ϕ_x	ϕ_y
Mark II [264]	K^+K^-	$0.18 \pm 0.06 \pm 0.10$				
Mark III [265]	K^+K^-	$0.60 \pm 0.14 \pm 0.12$	0.63 ± 0.10	0.17 ± 0.20	≈ 0	≈ 0
Mark III [265]	$K_S^0K_S^0$	$0.38 \pm 0.14 \pm 0.10$				
DM2 [267]	K^+K^-	$0.50 \pm 0.12 \pm 0.08$	1.08 ± 0.10	0.19 ± 0.11		
DM2 [267]	$K_S^0K_S^0$	$0.40 \pm 0.04 \pm 0.08$				
⟨average⟩	$K\bar{K}$	0.38 ± 0.06	0.86 ± 0.07	0.19 ± 0.10		
C.B. [249]	$\eta\eta$	$0.19 \pm 0.08 \pm 0.05$				
DM2 [243]	$\eta\eta$	$0.18 \pm 0.03 \pm 0.06$				
Mark III [313]	$\eta\eta$	$0.08 \pm 0.04 \pm 0.02$				
⟨average⟩	$\eta\eta$	0.12 ± 0.04				
Mark III [313]	$\pi^+\pi^-$	$0.026^{+0.020+0.08}_{-0.015-0.01}$				

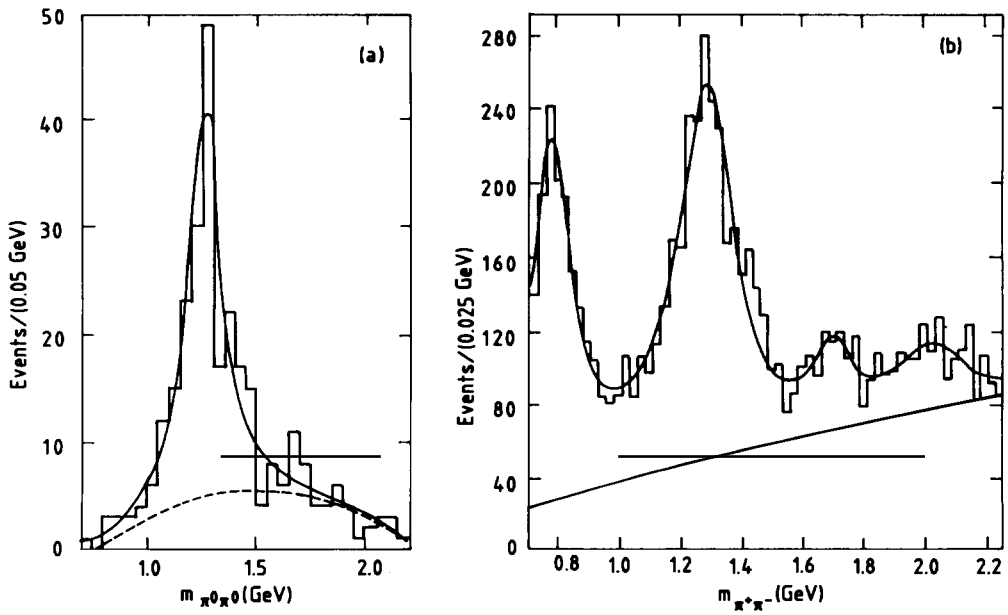

Fig. 63. Evidence for $f_2(1270)$ production in radiative J/ψ decays. ππ invariant mass distributions of (a) $J/\psi \to \gamma\pi^0\pi^0$ (Crystal Ball) and (b) $J/\psi \to \gamma\pi^+\pi^-$ (DM2), showing evidence for $f_2(1270)$, and possibly $f_2(1720)$ and $f_4(2030)$. The peak at low masses in (b) is due to $J/\psi \to \rho\pi$ background.

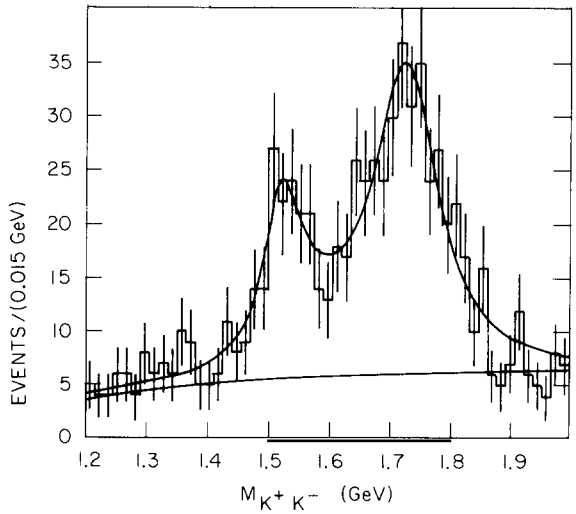

Fig. 64. $K\bar{K}$ invariant mass distribution from $J/\psi \to \gamma K^+K^-$ (Mark III). Evidence for $f_2'(1525)$ and $f_2(1720)$ ("theta") production is given. The curve represents a fit with two coherent Breit-Wigner amplitudes [265].

$$0.24 \pm 0.05 \leq R_{exp} \leq 0.34 \pm 0.07\,, \tag{114}$$

in excellent agreement with (113). Early measurements by DASP [261], PLUTO [260], and Mark II [264] showed much smaller values for R_{exp}, but the data on $f_2'(1525)$ production were sparse.

Although $f_2(1270)$ and $f_2'(1525)$ are well established members of the 2^{++} $q\bar{q}$ nonet it is important to measure the spin and polarization with which they are produced in J/ψ decays. First, the spin determination can be used as a check on the spin analysis for the glueball candidate $f_2(1720)$ (see section 6.4.2), since the events from the decay $J/\psi \to \gamma f_2'(1525) \to \gamma K\bar{K}$ are almost identical to those from $J/\psi \to \gamma f_2(1720) \to \gamma K\bar{K}$. Secondly, a direct comparison of spin and polarization of $f_2(1270)$, $f_2'(1525)$, and $f_2(1720)$ should aid in deciding on whether the $f_2(1720)$ is a member of a 2^{++} $q\bar{q}$ nonet or is rather something else.

To determine the spin and parity as well as the polarization with which the tensor meson states $f_2(1270)$ and $f_2'(1525)$ are produced one must examine the angular distributions of the reaction $J/\psi \to \gamma X$, $X \to \pi\pi$ or $K\bar{K}$. The J/ψ is produced with an incoherent mixture of $J_z = \pm 1$ states, where J_z is the spin projection of the J/ψ onto the beam axis. The angular distribution for the decay sequence $J/\psi \to \gamma X$, $X \to \pi\pi$, where X is a spin 2^+ resonance, is then given by

$$\begin{aligned} W_2(\Omega) = {} & \tfrac{1}{4}(3\cos^2\theta_\pi - 1)^2(1 + \cos^2\theta_\gamma) + \tfrac{1}{4}\sqrt{3}x \cos\phi_x (3\cos^2\theta_\pi - 1)\sin 2\theta_\pi \sin 2\theta_\gamma \cos\phi_\pi \\ & + \tfrac{1}{4}\sqrt{6}y \cos\phi_y (3\cos^2\theta_\pi - 1)\sin^2\theta_\pi \sin^2\theta_\gamma \cos 2\phi_\pi + 3x^2 \sin^2\theta_\pi \cos^2\theta_\pi \sin^2\theta_\gamma \\ & - \tfrac{3}{8}\sqrt{2}xy \cos(\phi_y - \phi_x)\sin^2\theta_\pi \sin 2\theta_\pi \sin 2\theta_\gamma \cos\phi_\pi + \tfrac{3}{8}y^2 \sin^4\theta_\pi (1 + \cos^2\theta_\gamma)\,, \end{aligned}$$

where θ_π, ϕ_π are the polar and azimuthal angles of the pions in the X helicity frame and θ_γ is the polar angle of the radiative photon in the laboratory frame. The state X can be produced with five different helicities, ± 2, ± 1, 0, leading to three independent, complex helicity amplitudes A_2, A_1, A_0. We define $A_1/A_0 = x\,e^{i\phi_x}$ and $A_2/A_0 = y\,e^{i\phi_y}$ to parametrize this dependence.

The polarization is then determined by an acceptance corrected fit to the angular distributions with the four parameters x, y, ϕ_x, ϕ_y and the spin is determined by comparing the likelihood values for different spin hypotheses.

Analyses to measure the polarization of $f_2(1270)$ and $f_2'(1525)$ have been performed with great dedication by PLUTO [260], Mark II [264], Crystal Ball [262], Mark III [265], and DM2 [266]. Their results are included in table 30. Mark III and DM2 have abandoned the convenient assumption that the helicity amplitudes, A_0, A_1, A_2, are (relatively) real, i.e., x, y are real. This generalization had been demanded by Körner et al. [270], noting that it is not justified to assume x and y to be real, although explicit calculations showed that the relative phases of the helicity amplitudes are close to zero. The theoretical predictions of ref. [270] and others are compared to the experimental average in table 31.

The contour lines of the maximum likelihood fits are shown in fig. 65 for the three $J^P = 2^{++}$ states $f_2(1270)$, $f_2'(1525)$, and $f_2(1720)$. The measured phases ϕ_x, ϕ_y of $f_2(1270)$ and $f_2'(1525)$ are found to be consistent with 0 by Mark III. DM2 finds a non-zero ϕ_x for $f_2(1270)$, fixing $\phi_y = 0$ because it is poorly constrained by the data. The discrepancy between theory and experiment most evidently lies in the value for y, which for both $f_2(1270)$ and $f_2'(1525)$ is measured to be close to 0 while the theoretical calculations require a large value around 0.5. In the perturbative calculation both x and y strongly depend on the mass ratio M_T/M_ψ, where M_T is the tensor meson mass. For $M_T/M_\psi \to 0$ the tensor meson is produced in a helicity zero state, i.e., $x = y = 0$. $M_T/M_\psi \to 1$ corresponds to an electric dipole (E1) radiation pattern resulting in $(x, y) \to (\sqrt{3}, \sqrt{6})$ (cf. table 31). For any other value of M_T/M_ψ the calculation would always yield [271] $x \approx y$, clearly inconsistent with the experimental measurements.

In order to explain the data some other concept needs to be introduced to suppress the helicity 2 amplitude A_2. Attempts have been made to achieve this [272] by requiring a large glueball component in the $f_2(1270)$, $f_2'(1525)$ wave functions. This does not seem tenable in light of analyses that are more sensitive to glueball admixtures in $f_2(1270)$ and $f_2'(1525)$ [274, 275]. These analyses find that both states are perfectly consistent with being pure members of the 2^{++} $q\bar{q}$ nonet (see also section 5.3.4).

A more heuristic approach has been proposed by Close [273], suggesting that, in the limit $M_T/M_\psi \to 0$, x could be different from zero while $y \approx 0$ if one no longer assumes that the gg intermediate state is quasi-real. A mixture of E1 and M2 multipoles would then suggest $x = \sqrt{2/3}$ in quite surprising agreement with the experiments (cf. table 31). A measurement of the radiative

Table 31
Results on $f_2(1270)$ and $f_2'(1525)$ polarization. The experimental measurements are compared to theoretical predictions from several authors.

Reference	$x = A_1/A_0$	$y = A_2/A_0$	ϕ_x	ϕ_y
		$f_2(1270)$		
experimental average	0.85 ± 0.05	0.02 ± 0.05	$46° \pm 17°$	$-6° \pm 126°$
Krammer [271]	0.76	0.54		
Körner et al. [270]	0.77	0.55	2°	4°
Li and Shen [272]	0.66	0.04		
Close [273]	0.87	0.0		
		$f_2'(1525)$		
experimental average	0.86 ± 0.07	0.19 ± 0.10	≈ 0	≈ 0
Krammer [271]	0.88	0.70		
Körner [270]	0.90	0.72	1.3°	2.4°
E1 transition	$\sqrt{3}$	$\sqrt{6}$		
M2 transition	$\frac{1}{3}$	$-\frac{1}{3}\sqrt{2}$		
E3 transition	$-\frac{2}{3}$	$\frac{1}{6}$		

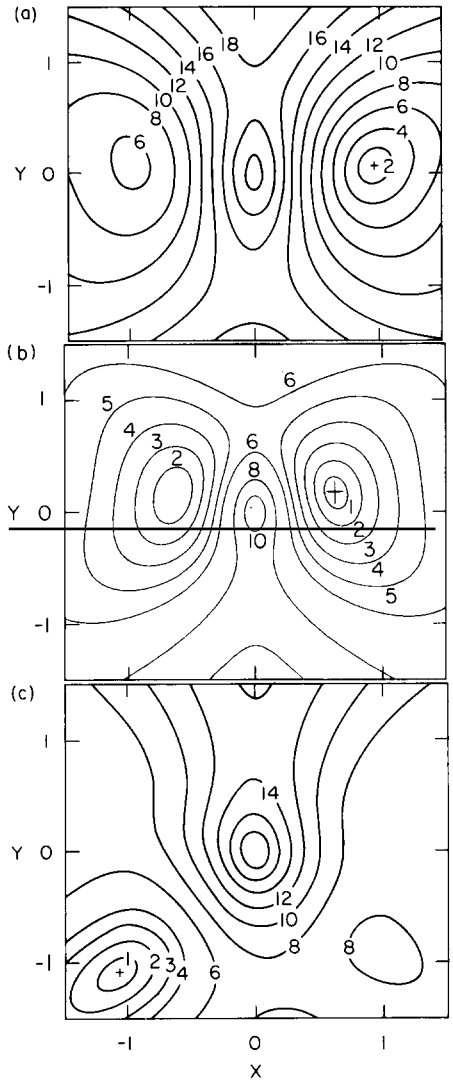

Fig. 65. Contour plots of polarization fits to tensor states. (a) $f_2(1270)$, (b) $f_2'(1525)$, and (c) $f_2(1720)$. The data are from Mark III [265]. $x = |A_1/A_0|$, $y = |A_2/A_0|$, with A_i the production helicity amplitudes. The lines indicate regions of equal likelihood. The maximum of the likelihood function is marked by a cross.

transition to the $f_2(1270)$ from the heavier Υ(9460), for which the limit $M_T/M_\psi \to 0$ is clearly justified, would certainly help to understand the validity range of the calculations.

It should be noted at this point that the polarization pattern for the third tensor state in this energy range, the "theta"/$f_2(1270)$, is very different from the pattern $(x, y) \approx (1, 0)$ of $f_2(1270)$ and $f_2'(1525)$ (see fig. 65c). This point is further discussed in chapter 7.

6.3.3. *The decay* $J/\psi \to \gamma +$ *scalar*

Data on radiative decays to scalar resonances are scarce. Neither the $f_0(975)$ nor the $f_0(1300)$ have been observed in radiative transitions from the J/ψ. Scalar gluonium, which is expected in the mass region below 1.5 GeV, has so far also escaped detection (see section 7.4).

The $f_0(1300)$ is a poorly defined object, which makes a meaningful determination of an upper limit on its radiative production difficult. For the $f_0(975)$, an upper limit has been given by Mark III [265],

$$B(J/\psi \to \gamma f_0(975)) \cdot B(f_0(975) \to \pi\pi) < 7 \times 10^{-5} \quad \text{at 90\% C.L.}, \tag{116}$$

where the two pions have been detected in their charged mode. The preferred decay mode to search for scalar states, however, is $J/\psi \to \gamma\pi^0\pi^0$. This final state is much cleaner than $J/\psi \to \gamma\pi^+\pi^-$ due to the absence of background from $J/\psi \to \rho^0\pi^0$, which forbids a sensible study in the charged mode below 1 GeV. The "all neutral" final state is best measured by the Crystal Ball experiment which is dedicated to the detection of photons. The $\pi^0\pi^0$ invariant mass spectrum is shown in fig. 110 of section 7.4. In the mass range between 0.5 GeV and 1 GeV the limit

$$B(J/\psi \to \gamma X) \cdot B(X \to \pi^0\pi^0) < 1.3 \times 10^{-5} \quad \text{at 90\% C.L.} \tag{117}$$

has been obtained [258] for states narrower than 100 MeV. There are no limits for masses below 0.5 GeV. A recent Mark III reanalysis of $J/\psi \to \gamma\pi^+\pi^-$ and $J/\psi \to \gamma K\bar{K}$ [313], however, shows consistency with scalar behaviour just above threshold. The indication of a—possibly scalar—shoulder on the high-mass side of the $f_2(1270)$ in $J/\psi \to \gamma\pi^+\pi^-$ is discussed in section 7.4.

6.3.4. The decay $J/\psi \to \gamma$ + axial vector

Of the axial-vector meson nonets with $J^{PC} = 1^{++}$ and 1^{+-} only the C-even one can be reached through the radiative J/ψ decay. Candidates for the 1^{++} isoscalar states are the $f_1(1285)$, as the very likely candidate for the mostly non-strange member of the nonet, and even two candidates—the $f_1(1420)$ and the recently confirmed $f_1(1530)$—for the mostly strange state. Note that these are already too many states to be assigned to the 1^{++} ground state nonet but none of them is considered as a candidate for gluonium.

Rosner [225] suggested two possible "non-exotic" explanations, (a) that the $f_1(1530)$ is identical to the $f_1(1420)$, but shifted in mass as a result of the production process kinematics, or (b) that the $K\bar{K}\pi$ system forms a "molecule" in which all three Dalitz plot bands overlap and the $K\pi$, $\bar{K}\pi$ and $K\bar{K}$ subsystems resonate to form a K^*, $\bar{K}^*$ or $a_0(980)$. Such a simultaneous overlap occurs at

$$M = (2m_{K^*}^2 + m_{a_0(980)}^2 - 2m_K^2 - m_\pi^2)^{1/2} \approx 1435 \text{ MeV}.$$

If the $K\bar{K}$ system is in an s wave and $K\pi$, $\bar{K}\pi$ are in relative p waves, the $K\bar{K}\pi$ system will naturally have $J^{PC} = 1^{++}$.

The $f_1(1530)$ has finally been established by the LASS group [154] in the reaction $K^-p \to \Lambda + K_S^0K^\pm\pi^\mp$, where the $s\bar{s}$ state of the 1^{++} multiplet is expected to be seen. The $f_1(1420)$, on the other hand, does no longer appeal as a pure $s\bar{s}$ state given its absence in K^-p scattering and some evidence for its production in the hadronic decay $J/\psi \to \omega K\bar{K}\pi$ [156] (see sections 5.3.5 and 7.2). In the same vein the $f_1(1285)$ is observed in association with a ϕ in hadronic J/ψ decays [142, 283] (section 5.3.5), giving rise to the conclusion that the 1^{++} nonet is probably not ideally mixed. One should also observe $J/\psi \to \phi f_1(1530)$ if the $f_1(1530)$ really is an $s\bar{s}$ state (see section 5.3.5.2).

Regardless of whether the $f_1(1420)$ points to new physics or not, one may search for 1^{++} states in radiative J/ψ decays. Yang's theorem [228] forbids the production of spin-1 mesons if the production process is mediated via two on-shell gluons (cf. fig. 57a). However, Körner et al. [227, 276] have

predicted quite a substantial rate for $J/\psi \to \gamma + \{1^{++}\}$ in a model in which highly virtual gluons play an important role. Using perturbation theory and non-relativistic approximations they calculate that

$$\Gamma(J/\psi \to \gamma + A) = \alpha_s^4 \alpha Q_c^2 \frac{256}{9\pi^2} \frac{|R_\psi(0)|^2}{M_\psi^4} \frac{|R_A(0)|^2}{m_A^3} x \sum_i |H_i^A(x)|^2 , \tag{118}$$

where A stands for axial vector. The other symbols are the same as in eq. (109).

In this model [227] the overall magnitude for $\{1^{++}\}$ is expected to be of the same order as for $\{0^{++}\}$ and $\{2^{++}\}$ as indicated in fig. 60. For ideal mixing the authors predict explicitly

$$B\left(J/\psi \to \gamma + \left\{ \begin{matrix} (u\bar{u} + d\bar{d})/\sqrt{2} \\ s\bar{s} \end{matrix} \right\}_{1^{++}}\right) = \left\{ \begin{matrix} 1.0 \\ 0.3 \end{matrix} \right\} \times 10^{-3} , \tag{119}$$

where $f_1(1285)$ and $f_1(1530)$ masses, respectively, have been assumed. The model has an intrinsic uncertainty of a factor of 2 [227].

On the experimental side one has searched for radiative production of 1^{++} mesons in 4π, $K\bar{K}\pi$, and $\eta\pi\pi$ final states. Lacking the experimental knowledge of the decomposition of the spin parity content in the invariant mass spectra one can never be sure whether the axial-vector states $f_1(1285)$ and $f_1(1420)$ or the candidates for radially excited pseudoscalar states, $\eta(1275)$ and $\eta(1400)$, or even parts of both, are actually seen in the data. Arguments that spin-1 states are suppressed due to Yang's theorem [228] have to be traded off against the reasoning that radially excited $q\bar{q}$ states should have smaller production rates than their ground state partners.

Using their full statistics sample of 8.6×10^6 J/ψ decays DM2 [280] observe a small but clean signal at 1280 GeV in $J/\psi \to \gamma\pi^+\pi^-\pi^+\pi^-$ (see fig. 66b), which they interpret as the $f_1(1285)$. The decay actually proceeds via a $\rho^0\pi^+\pi^-$ intermediate state, resulting in a branching fraction of [280]

$$B(J/\psi \to \gamma f_1(1285)) \cdot B(f_1(1285) \to \rho^0\pi^+\pi^-) = (0.34 \pm 0.08 \pm 0.05) \times 10^{-4} , \tag{120}$$

which is larger by about a factor 2.5 than the prediction (eq. 119) if one corrects for isospin and unobserved decay modes of the $f_1(1285)$. The $f_1(1420)$ and $f_1(1530)$ would, even if they had unexpectedly large couplings to 4π, hide under the enormous background from $J/\psi \to \gamma\rho\rho$ and $J/\psi \to 5\pi$ reactions, which show other prominent states in this mass region (see section 6.4.5.1).

The $\gamma K\bar{K}\pi$ final state is overwhelmed by the 0^{-+} "iota"/$\eta(1440)$ in the 1.4 to 1.6 GeV mass region. Recent developments indicate [277, 278] that the $\eta(1440)$ could accommodate more than just one state although no clear evidence for a 1^{++} contribution prevails in absence of a full isobar analysis (see section 6.4.1). It would, however, not be surprising if the $f_1(1420)$ or the $f_1(1530)$ had a small contribution to the $\gamma K\bar{K}\pi$ final state under the "iota". Recent analyses of large-statistics data samples show an indication of the $f_1(1285)$ below the $\eta(1440)$ signal (fig. 75 in section 6.4.1.1).

The $\gamma\eta\pi\pi$ final state seems more promising for a search for 1^{++} states (see section 6.4.4). Crystal Ball [281], Mark III [282], and DM2 [283] have analysed this interesting channel. The $\eta\pi\pi$ invariant mass distribution is shown in fig. 66a and in fig. 67, where the mass of at least one $\eta\pi$ subsystem is required to be consistent with the $a_0(980)$.

The parameters of the 1.28 GeV peak are consistent with the 1^{++} $f_1(1285)$ but could also be identified with the pseudoscalar $\eta(1275)$. The peak at 1.39 GeV is probably not an axial-vector state because if fits better to the recently observed [159, 279] pseudoscalar $\eta(1400)$ as mentioned above. The

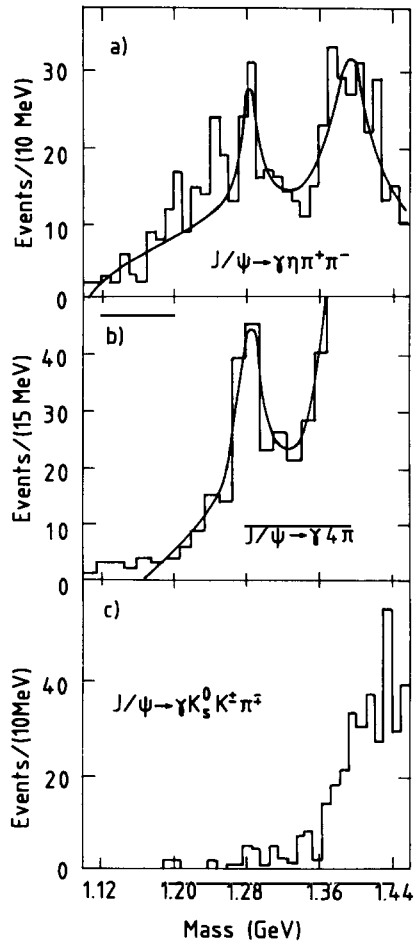

Fig. 66. Evidence for the $f_1(1285)$ production in radiative J/ψ decays. (a) ηππ, (b) 4π, and (c) $K\bar{K}\pi$ invariant mass distributions (DM2 [280]). A clean signal around 1285 MeV is evident in (b) and an indication of a signal in (a). Only a hint of a $f_1(1285)$ signal is observed in (c).

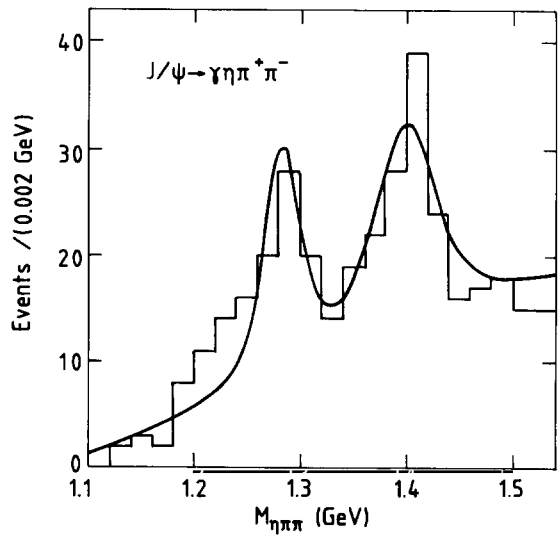

Fig. 67. ηππ invariant mass distribution of $J/\psi \to \gamma\eta\pi^+\pi^-$, $\eta \to \pi^+\pi^-\pi^0$. A cut $|m_{\eta\pi\pi} - 0.983| < 0.05$ GeV has been imposed. Only the mass region below 1.55 GeV is displayed (Mark III).

branching ratios for the 1.28 GeV and 1.38 GeV states are [282] (see also table 40 in section 6.4.4)

$$B(J/\psi \to \gamma X(1280)) \cdot B(X(1280) \to a_0(980)^{\pm}\pi^{\mp}) \cdot B(a_0(980)^{\pm} \to \eta\pi^{\pm}) = (3.2 \pm 1.1 \pm 0.3) \times 10^{-4}, \quad (121)$$

$$B(J/\psi \to \gamma X(1390)) \cdot B(X(1390) \to a_0(980)^{\pm}\pi^{\mp}) \cdot B(a_0(980)^{\pm} \to \eta\pi^{\pm}) = (5.2 \pm 1.8 \pm 0.5) \times 10^{-4}. \quad (122)$$

The $f_1(1530)$ may well be part of the structure at ~1.6 GeV (fig. 88 in section 6.4.4), although nothing firm can be said without a spin determination.

It should be mentioned in this context that a spin-1 state with positive C parity is observed in the

reaction $\gamma\gamma^* \to K\bar{K}\pi$ [131, 284, 285], where one of the photons has $Q^2 \neq 0$ such that $\gamma\gamma$ production of spin 1 states is no longer forbidden by Yang's theorem. The corresponding mass plot is shown in fig. 68. The Q^2 dependence of the production rate indicates that the spin of the observed signal at mass ~1.42 GeV is one [284, 285]. This resonance is consistent with being the $f_1(1420)$, in particular since the TPC/2γ analysis slightly favours positive parity for this state [131], which, if true, would challenge Chanowitz's hypothesis of a hybrid 1^{-+} state [48, 162] at this mass.

If one identifies the $f_1(1420)$ with the $s\bar{s}$ member of the 1^{++} nonet, as has been done traditionally, the ratio of $\gamma\gamma$ partial widths*) for $f_1(1285)$ and $f_1(1420)$ yields a mixing angle of $\theta_A = (49^{+5}_{-8})°$, not too far from the ideal mixing value of 35.3°. When comparing this value with the expectation from the GMO quadratic mass formula (105) one finds a peculiarity. The $I = 1/2$ states with strangeness are no C, G eigenstates. The $K_1(1280)$, the mass eigenstate of the 1^{+-} $q\bar{q}$ nonet (cf. fig. 5), and the $K_1(1400)$, mass eigenstate of the 1^{++} nonet, can mix to form the C, G eigenstates Q_+ and Q_-. The mixing angle ϕ_K is close to 45°. An experimental evaluation [288] yields $m_{Q_+} = (1.31 \pm 0.015)$ GeV and $m_{Q_-} = (1.37 \pm 0.02)$ GeV. The quadratic GMO mass formula, substituting particle names for *squared* masses, then yields

$$\tan^2\theta_A = \frac{4Q_+ - 3f_1' - a_1(1270)}{3f_1(1285) - 4Q_+ + a_1(1270)} \tag{123}$$

for the axial-vector mixing angle. Apart from some uncertainty on the exact value of the $a_1(1270)$ mass [289] it is not clear whether the $f_1(1420)$ or the $f_1(1530)$ should be used for f_1' in (123). Using $f_1(1420)$ results in $\theta_A \approx 59°$, in fair agreement with the ratio of the $\gamma\gamma$ widths, while using $f_1(1530)$ yields $\theta_A \approx 68°$.

The problem of assigning $f_1(1285)$, $f_1(1420)$ and/or $f_1(1530)$ to states in the 1^{++} nonet of $q\bar{q}$ states has still not been uniquely solved. Neither of them seems to be a pure $(u\bar{u} + d\bar{d})/\sqrt{2}$ or $s\bar{s}$ state, respectively, although a mixing angle of ~50° is not far from ideal. If the $f_1(1530)$ is assumed to be the f_1' state a non-strange fraction of $|X|^2 = 29.6\%$ and a strange fraction of $|Y|^2 = 70.4\%$ is obtained using the formula of eq. (59) in section 5.3.2. The observation of the $f_1(1420)$ in the direct decay of the J/ψ in association with an ω [156]—but not with a φ—also casts some doubt on a pure $s\bar{s}$ assignment. This may partly be due to the effect of doubly OZI violating diagrams (section 5.3.5.2). The absence of a signal in $K^-p \to K^\pm K_S^0 \pi^\mp \Lambda$ scattering [154] also renders an $s\bar{s}$ assignment of the $f_1(1420)$ unlikely.

6.4. The new resonances

6.4.1. The "iota"/η(1440)

The "iota" or η(1440) is *the* candidate for the 0^{-+} glueball. To properly introduce this resonance, if it is only one, one would have to go through a long list of confusing facts and contradicting experiments [161]. Recent reviews have been given by Palano [290] and Chung [362]. Let us recall a few points only.

- The η(1440) has been mistaken for a long time, and may be still is, for the "E(1420)"/$f_1(1420)$ [291]. In order not to confuse the issue any further we define here the $f_1(1420)$ to be the isospin 0 state of a 1^{++} $q\bar{q}$ nonet and the η(1440) to be a state with $J^{PC} = 0^{-+}$.
- There are one, two, or even more states observed to decay into $K\bar{K}\pi$ and/or $\eta\pi\pi$ in the mass region between 1.40 and 1.47 GeV. Different results were obtained on whether the decay proceeds via

*) The quantity to be used for this evaluation is $(m^2/Q^2)\Gamma_{\gamma\gamma}$. [287] (see also Olsson [131]).

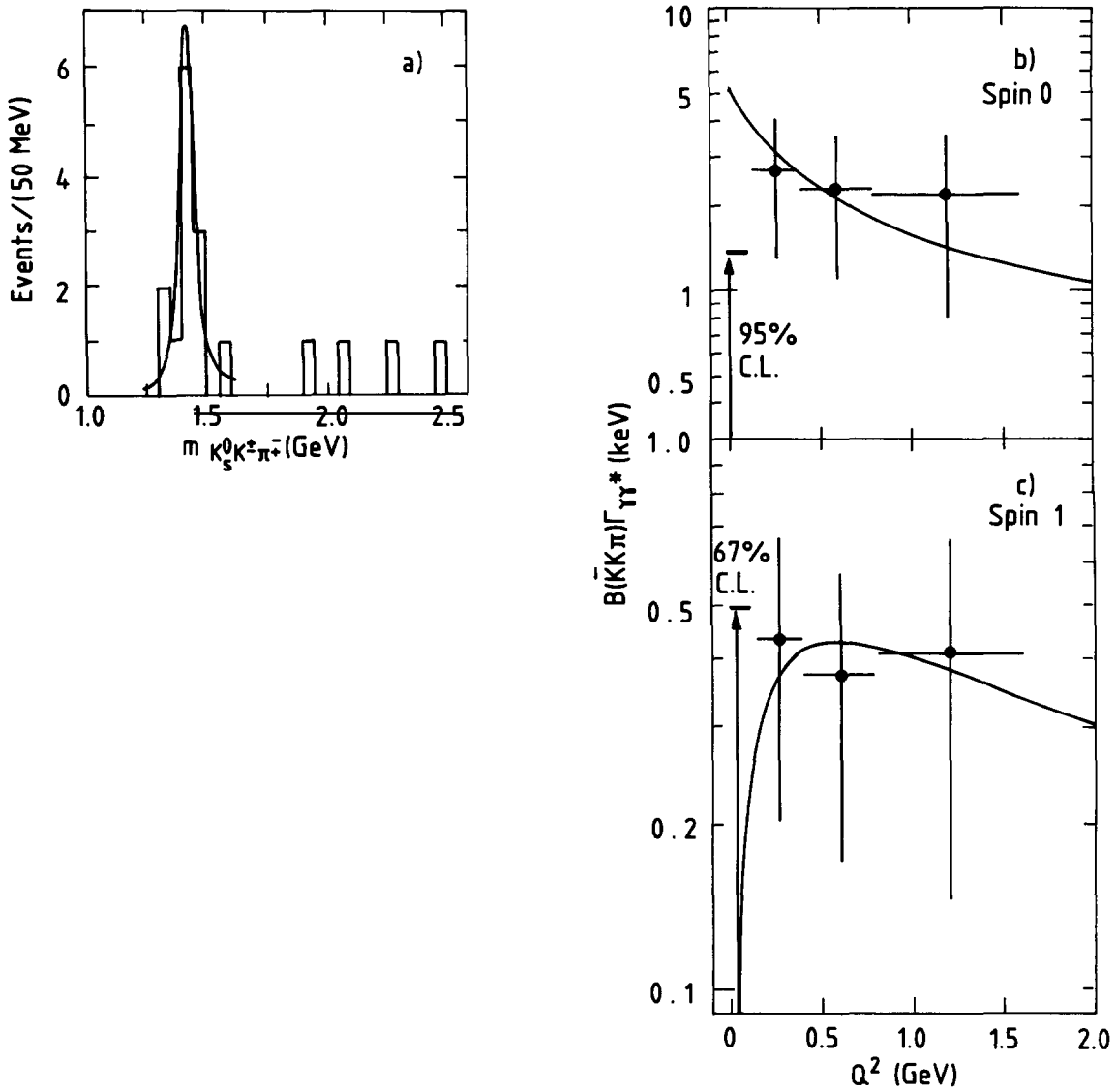

Fig. 68. Evidence for $f_1(1420)$ in $\gamma\gamma$ collisions. (a) Invariant $K\bar{K}\pi$ mass distribution from $\gamma\gamma^* \to K^0_S K^\pm \pi^\mp$ (TPC/2γ). (b), (c) From the Q^2 dependence of the $\gamma\gamma$ width the spin is determined to be one.

$a_0(980)\pi$ or $K^*\bar{K}$ intermediate states. No experiment has identified beyond doubt more than just one resonance at a time in this mass region, although there is a possible indication of a multi-resonance structure in radiative J/ψ decays [277] and $\pi^- p \to K^+ \bar{K}^0 \pi^- n$ reactions [411].

• Some experiments find spin 0^{-+}. Since enough candidate states exist for the 0^{-+} ground state and first radial excitation multiplets, any additional 0^{-+} state is potentially of an exotic nature. Other experiments find $J^{PC} = 1^{++}$ ($f_1(1420)$). A state with these quantum numbers would most likely be a $q\bar{q}$ state. In the light of new data from hadronic J/ψ decays and from $K^- p$ scattering experiments (see sections 5.3.5.2 and 7.2) it is, however, not safe to conclude that the $f_1(1420)$ is the mostly $s\bar{s}$ state of the 1^{++} $q\bar{q}$ ground state nonet [269].

Below we concentrate on the experimental facts of the η(1440) as observed in radiative decays of the J/ψ.

6.4.1.1. Discovery and $K\bar{K}\pi$ *decay.* A resonance, distinct from the $f_1(1420)$ because of its 0^- spin parity, has been discovered by Mark II at SPEAR. Figure 69 shows the discovery of the η(1440) by Mark II (a), (b) and the measurement from Crystal Ball (c) in which the spin was found to be 0^-. In both experiments the width was measured to be much narrower than in successive experiments due to a cut that was applied prematurely by requiring the invariant mass of the $K\bar{K}$ system to be below some value around 1.1 GeV ("delta cut"). Figure 70 shows the signal in the three different $K\bar{K}\pi$ decay modes as seen by Mark III. All measurements are summarized in table 32.

The spin analysis performed by the Crystal Ball group [294] is an isobar analysis with the partial waves (1) $K\bar{K}\pi$ phase space, (2) $a_0(980)\pi^0$, 0^-, (3) $a_0(980)\pi^0$, 1^+, (4) $K^*\bar{K}$ + c.c., 0^-, (5) $K^*\bar{K}$ + c.c., 1^+. $J^P = 0^+$ is not allowed for a decay into three pseudoscalars. The result of the maximum likelihood fits is shown in fig. 71 for the three dominant amplitudes. The Crystal Ball group concluded [294] that the η(1440) is a state with $J^{PC} = 0^{-+}$ decaying dominantly into $a_0(980)\pi$. Figure 71a also shows, however, that 50% of the signal is attributed to the phase space channel, much more than can be accounted for by background.

The 0^- spin measurement of Crystal Ball has been confirmed [110, 251]. The conclusion that the η(1440) decays via $a_0(980)\pi$, however, is not unequivocally accepted. This question is a difficult one

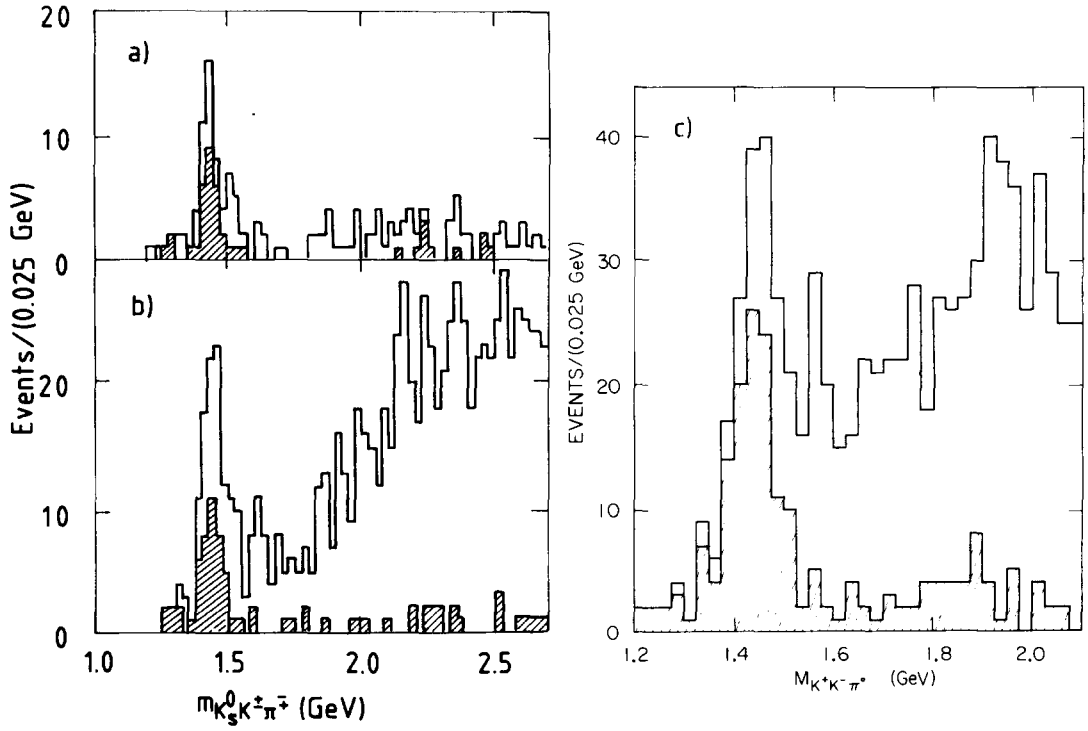

Fig. 69. Observation of the η(1440) by Mark II and Crystal Ball. (a) Mark II, radiative photon detection required, (b) Mark II, photon detection not required. The events in the shaded region have $m_{K\bar{K}} < 1.05$ GeV ("delta cut"). (c) Crystal Ball, events in the shaded region have $m_{K\bar{K}} < 1.125$ GeV.

Table 32
Branching ratios for the decay $J/\psi \to \gamma +$ "iota"/$\eta(1440)$. The measured branching fractions have been multiplied by the appropriate isospin factors to obtain $B(\psi \to \gamma\iota) \cdot B(\iota \to K\bar{K}\pi)$, where ι stands for "iota"/$\eta(1440)$. For isospin 0 of the $\eta(1440)$ the predicted ratios are $K_S^0K^\pm\pi^\mp : K^+K^-\pi^0 : K_S^0K_S^0\pi^0 = \frac{1}{3} : \frac{1}{6} : \frac{1}{12}$. [a] indicates that a cut on the $K\bar{K}$ mass ("delta cut") has been applied (see text). These measurements were left out in the determination of the average.

Experiment	Decay mode	Mass (MeV)	Width (MeV)	$B(J/\psi \to \gamma\iota) \cdot B(\iota \to K\bar{K}\pi)$ (units of 10^{-3})
Mark II [293][a]	$K_S^0K^\pm\pi^\mp$	1440^{+10}_{-15}	50^{+30}_{-20}	4.3 ± 1.7
C.B. [294][a]	$K^+K^-\pi^0$	1440^{+20}_{-15}	55^{+20}_{-30}	$4.0 \pm 0.7 \pm 1.0$
Mark III [145]	$K_S^0K^\pm\pi^\mp$	$1456 \pm 5 \pm 6$	$95 \pm 10 \pm 15$	$5.0 \pm 0.3 \pm 0.8$
Mark III [145]	$K^+K^-\pi^0$	$1461 \pm 5 \pm 5$	$101 \pm 10 \pm 10$	$4.9 \pm 0.25 \pm 0.8$
Mark III [251]	$K_S^0K_S^0\pi^0$			$3.6 \pm 1.6 \pm 1.8$
DM2 [110]	$K_S^0K^\pm\pi^\mp$	$1460 \pm 3 \pm 8$	$100 \pm 12 \pm 15$	$4.1 \pm 0.6 \pm 0.9$
DM2 [110]	$K^+K^-\pi^0$	1451.5 ± 3	97 ± 10	$4.1 \pm 0.54 \pm 0.6$
⟨average⟩		1454 ± 3	98 ± 7	4.5 ± 0.4

because the decay $\eta(1440) \to K^*\bar{K}$ is close to the kinematic limit. Figure 72 shows the Dalitz plot for $\eta(1440) \to K\bar{K}\pi$ for the low- and the high-mass region, respectively. For a 0^- state which decays into $K^*\bar{K}$ angular momentum conservation requires the K* to be produced with helicity 0. This leads to a $\cos^2\theta$ distribution of the K* decay products, producing a node-type accumulation of events in the two K* bands. The $K\bar{K}$ invariant mass distribution for "iota" events is shown in fig. 73. In the lower-mass region close to the kinematic limit it seems hard to distinguish between the isobars of the two decay modes, K*(892) and $a_0(980)$.

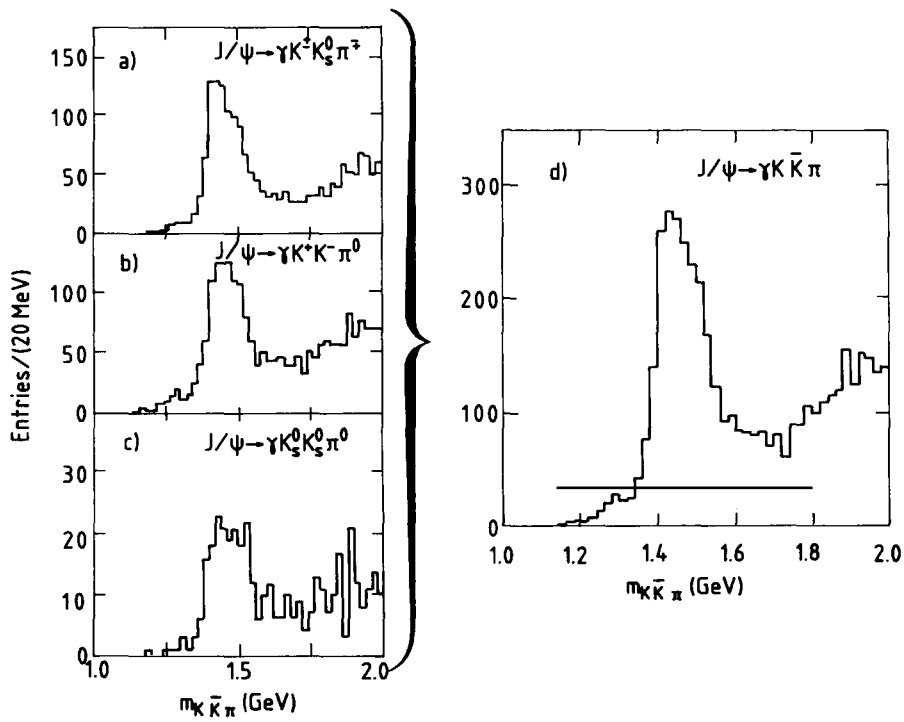

Fig. 70. Observation of the $\eta(1440)$ in $K\bar{K}\pi$. (a) $J/\psi \to \gamma K^\pm K_S^0\pi^\mp$, (b) $J/\psi \to \gamma K^+K^-\pi^0$, (c) $J/\psi \to \gamma K_S^0K_S^0\pi^0$, and (d) the sum of the three (Mark III [145]).

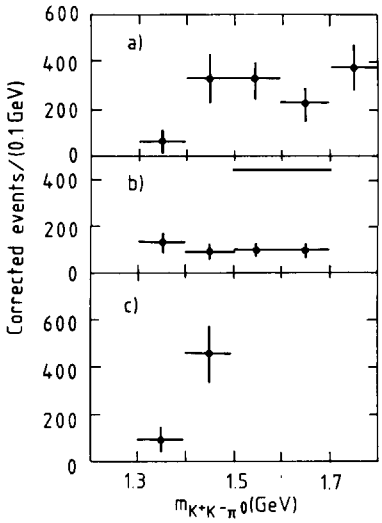

Fig. 71. Partial wave contributions to $J/\psi \to K^+K^-\pi^0$. The different contributions are plotted as a function of the $K\bar{K}\pi$ mass for (a) $K\bar{K}\pi$ phase space, (b) $K^*\bar{K}$ with $J^P = 1^+$, and (c) $a_0(980)\pi$ with $J^P = 0^-$ (Crystal Ball [294]).

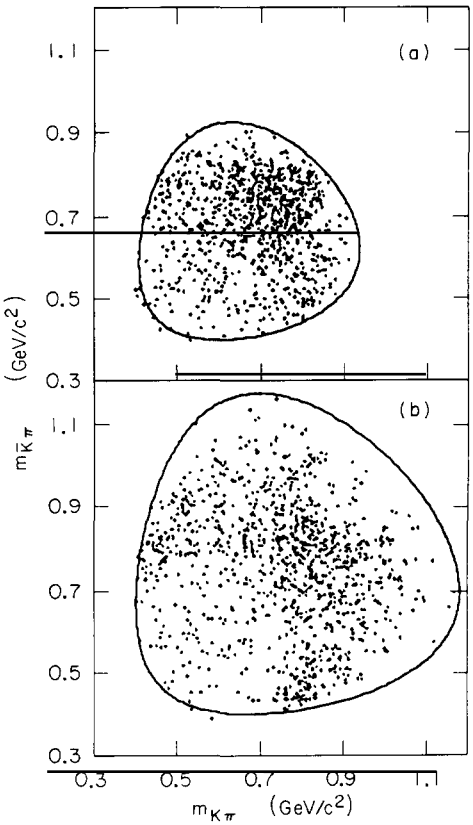

Fig. 72. Dalitz plot distribution of events in the η(1440) mass region (a) for $1360 \leq m_{K\bar{K}\pi} \leq 1460$ MeV, (b) for $1460 \leq m_{K\bar{K}\pi} \leq 1580$ MeV (Mark III [145]).

In addition, the $a_0(980)$ is a state which is not well understood, either. This isovector state with $J^{PC} = 0^{++}$ decays mainly to $\eta\pi$. Its mass is below $K\bar{K}$ threshold and its decay into $K\bar{K}$ is a non-trivial phenomenon. According to some phenomenological analyses [143] the true width of the $a_0(980)$ may be as large as 300 MeV and it may not be a simple $q\bar{q}$ state.

Possible interference effects between different intermediate states or coupled channels may also be important in the η(1440) decay. In the higher-mass region the K*(892) bands are more clearly visible. An upper limit on $K^*\bar{K}$ production is obtained from [251]

$$B(\eta(1440) \to K^*\bar{K} + \text{c.c.})/B(\eta(1440) \to K\bar{K}\pi) < 0.35 \quad \text{at } 90\% \text{ C.L.}. \tag{124}$$

For the $f_1(1420)$ the $K^*\bar{K}$ fraction is larger than 50% according to all experiments and is even close to 100% in the experiment with the largest data sample [292]. Therefore, the Dalitz plot distributions of η(1440) and $f_1(1420)$ are very different from each other.

In the spin analyses of Mark III and DM2 the difficulty of a proper treatment of intermediate state isobars in the η(1440) decay was avoided by employing the three-body helicity formalism [295] for $\eta(1440) \to K\bar{K}\pi$. This method is largely independent of the actual decay sequence. But also in these analyses the "iota" was treated as a single resonance.

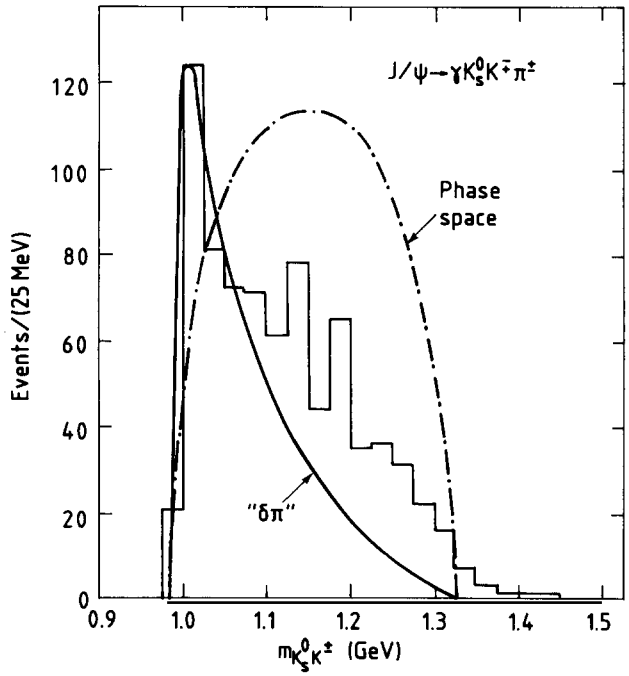

Fig. 73. $K\bar{K}$ submass distribution for η(1440) decays. Invariant $K\bar{K}$ mass distribution for events with $1.3 \leq m_{K\bar{K}\pi} \leq 1.6$ (DM2). The curves show the expectation from pure three-body phase space (dash-dotted line) and "$a_0(980)\pi$" production (solid line).

Out of the three angles that describe the decay, the azimuthal angle of the "iota" decay plane is not very suitable to discriminate $J^P = 1^+$ from 0^- [251]. The two other angles are θ_γ, the polar angle of the radiative photon measured with respect to the positron direction, and β, the polar angle of the normal to the η(1440) decay plane in the $K\bar{K}\pi$ rest frame measured with respect to the $K\bar{K}\pi$ momentum direction. Figure 74 shows the cos θ_γ and cos β distributions for events from $\eta(1440) \rightarrow K_S^0 K^\pm \pi^\mp$ in the Mark III detector [251]. Integrating over cos θ_γ or cos β, respectively, one expects a behaviour like

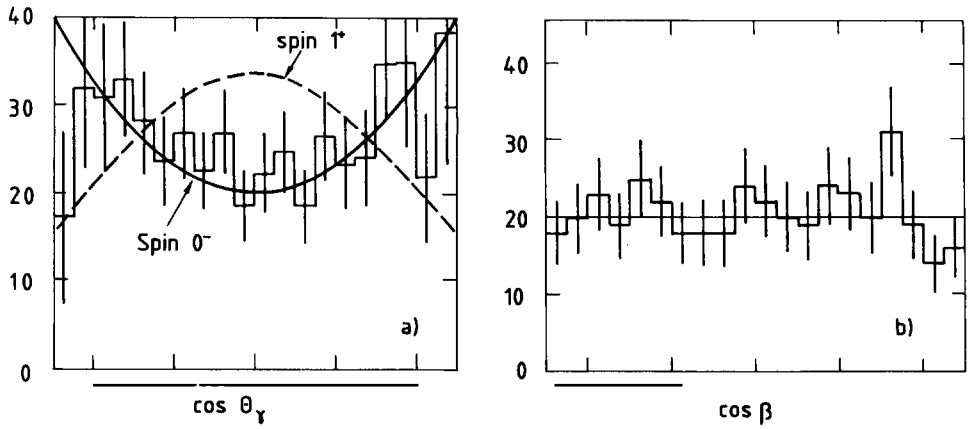

Fig. 74. η(1440) three-body spin analysis. (a) Distribution of cos θ_γ corrected for average acceptance. Superimposed are the predictions for $J^P = 0^-$ (solid line) and for $J^P = 1^+$ with a parameter choice that makes cos β uniform (dashed line). (b) cos β distribution from $\eta(1440) \rightarrow K\bar{K}\pi$. The detector acceptance is flat in this angle.

$$
\begin{aligned}
0^-\!: \quad & \frac{dN}{d\cos\theta_\gamma} \sim (1+\cos^2\theta_\gamma)\,, \quad \frac{dN}{d\cos\beta} \sim \text{uniform}\,, \\
1^+\!: \quad & \frac{dN}{d\cos\theta_\gamma} \sim 1+2x^2+(1-2x^2)\cos^2\theta_\gamma\,, \quad \frac{dN}{d\cos\beta} \sim 2x^2+(2-x^2)\sin^2\beta\,.
\end{aligned} \tag{125}
$$

The ratio of helicity 1 to helicity 0 amplitudes, x, is a free parameter in the fit. In order to fit $\cos\beta$ with the $J^P = 1^+$ hypothesis, $x^2 \sim 2$ is required. With this value for x, however, the $J^P = 1^+$ hypothesis does not fit $\cos\theta_\gamma$, as shown in fig. 74. The spin 1^+ hypothesis cannot simultaneously fit both angular distributions. The likelihood ratios of spins 1^+ and 1^- relative to 0^- are $L(1^+)/L(0^-) \approx 3\times10^{-4}$ and $L(1^-)/L(0^-) \approx 8\times10^{-7}$ [251]. Of course, the acceptance calculation, which is necessary to correct the angular distributions for detection efficiencies, is not independent of the assumed intermediate state isobar in the $\eta(1440)$ decay. The choice of the decay sequence, $a_0(980)\pi$ or $K^*\bar{K}$, slightly changes the likelihood ratios but does not alter the conclusion that the "iota" spin parity is dominantly 0^- [251]. A smaller spin 1 component especially at low masses is, however, not excluded.

The branching fraction $B(J/\psi\to\gamma\eta(1440))\cdot B(\eta(1440)\to K\bar{K}\pi) \approx 4.5\times10^{-3}$ is by far the largest branching ratio of all radiative J/ψ decays that proceed via the annihilation of the $c\bar{c}$ system into gluons. The only radiative decay with a larger branching fraction, the charmonium M1 transition $J/\psi\to\gamma\eta_c$, does not require the quarks to annihilate. Of comparable strength to $J/\psi\to\gamma\eta(1440)$ is only $J/\psi\to\gamma\eta'$, while the decay $J/\psi\to\gamma f_2(1270)$ is about 1/4 as copious as $\gamma\eta(1440)$. This suggests a large SU(3) singlet component in the $\eta(1440)$ and has thus been one of the strongest arguments that the $\eta(1440)$ might be a glueball.

On the other hand, there are also some disturbing facts. It is surprising that the $K\bar{K}\pi$ decay is the only one established so far. Especially if the $\eta(1440)$ were a glueball one would expect other decay modes as well. If, in particular, $\eta(1440)\to K\bar{K}\pi$ proceeds via $\eta(1440)\to a_0(980)\pi$ then one would expect to also find $\eta(1440)\to a_0(980)\pi\to\eta\pi\pi$. This final state has been studied (see section 6.4.4), but no $\eta(1440)$ signal has been found. As an upper limit one obtains [296]

$$
B(J/\psi\to\gamma\eta(1440))\cdot B(\eta(1440)\to\eta\pi\pi) < 8.8\times10^{-4} \quad \text{at } 90\% \text{ C.L.}\,, \tag{126}
$$

which implies that

$$
B(\eta(1440)\to\eta\pi\pi)/B(\eta(1440)\to K\bar{K}\pi) < 0.20\,. \tag{127}
$$

The very limited data on the $a_0(980)$ branching fractions [14, 147] point to a value of ~10 for the ratio in (127) and hence

$$
B(J/\psi\to\gamma\eta(1440))\cdot B(\eta(1440)\to a_0(980)\pi) \approx 4.5\times10^{-2}\,, \tag{128}
$$

which contradicts the data by more than an order of magnitude. As a consequence one would have to conclude that the $a_0(980)$ is not likely to be present as an intermediate state in the decay $\eta(1440)\to K\bar{K}\pi$.

Weinstein et al. [297] have argued that the $a_0(980)$ may be formed in a final state interaction between K and $\bar{K}$ and propose that it is a $qq\bar{q}\bar{q}$ molecule. With this hypothesis they claim to fit the Dalitz plot data from Mark III reasonably well [297]. The actual decay sequence could then be a $\eta(1440)\to K\bar{K}\pi$

three-body decay, or $\eta(1440) \to K^*\bar{K}$ with the $a_0(980)$ being produced by the final state potential $V_{K\bar{K}}$ that acts upon the $K\bar{K}$ system. This is an attractive theoretical ansatz to explain the $a_0(980)$ problem in the $\eta(1440)$ decay because it could explain that the $a_0(980)$ can be present in the reaction $\eta(1440) \to K\bar{K}\pi$ while it is absent in $\eta(1440) \to \eta\pi\pi$.

Recent studies of Mark III [277, 278] revealed evidence that the "iota" structure observed in $J/\psi \to \gamma K\bar{K}\pi$ may in fact be more than just one resonance, thus offering the possibility to unify the so far puzzling observations from different production processes. The study was motivated by the observation that a fit with a single Breit–Wigner curve does not describe the "iota" structure well (fig. 75a). In trying several possibilities a good description of the data was obtained by two methods. In fig. 75b the data have been fit by two interfering Breit–Wigner amplitudes yielding a χ^2 probability of 58% [277] compared to 1.4×10^{-13} for the single Breit–Wigner case. With this fit the "iota" structure would have to be understood as two 0^{-+} states with parameters

$$\begin{aligned} m_{\text{low}} &= (1409 \pm 5)\,\text{MeV}\,, \qquad \Gamma_{\text{low}} = (69 \pm 11)\,\text{MeV}\,, \\ m_{\text{high}} &= (1499 \pm 9)\,\text{MeV}\,, \qquad \Gamma_{\text{high}} = (138 \pm 25)\,\text{MeV}\,. \end{aligned} \tag{129}$$

The second alternative is an ansatz which allows the $a_0(980)\pi$ and $K^*\bar{K}$ decay channels of the $\eta(1440)$ to be coupled. The result of this fit is shown in fig. 75c. The χ^2 probability obtained is 47%. If the two-state interpretation holds one may identify the lower-mass state with the $\eta(1400)$. The state at ~1500 MeV would have to be examined for being conventional $q\bar{q}$ or not. Indications also exist [277] that the isobar decomposition of the "iota" structure varies as a function of mass, containing more $a_0(980)\pi$ at lower and more $K^*\bar{K}$ + c.c. at higher masses. A definitive answer to this question could come from a full isobar analysis with coupled channels and the possibility of several interfering states. This would also reveal any possible 1^{++} component under the "iota" as suggested by Meshkov, Palmer and Pinsky [298]. Until this is settled we continue to refer to the entire "iota" structure by the label $\eta(1440)$. From the three-body analysis of the spin determination of the $\eta(1440)$ it seems clear in any case that the dominant—but perhaps not the only—spin contribution is pseudoscalar.

6.4.1.2. The search for radiative decays of the "iota". The "iota"/$\eta(1440)$ has been the subject of many ideas and model calculations that were put forward to understand the nature of this state. Among these the hypotheses that the "iota" might be a glueball, a radially excited $q\bar{q}$ state, or a hybrid state are the ones most often mentioned. One way to study differences between ordinary mesons and other objects is the pattern of their decay modes.

A very popular question in this context is if a glueball can decay radiatively and how large a radiative width would be expected for a glueball as compared to a radial $q\bar{q}$ excitation. Naively, one would expect that a pure glueball has no photon coupling. In fact, the opposite seems to be true. Radiative decays of glueballs are possible, mediated by an intermediate state containing quarks, or by a quark admixture into the glueball wave function. The calculations show that the $\eta(1440)$ may have a substantial radiative width if it is a glueball. Conversely, only a relatively small width is expected for a radially excited $(q\bar{q})'_R$ pseudoscalar state [300], for which, in the non-relativistic limit, the wave function is orthogonal to the ground state wave function leading to a vanishing M1 transition amplitude. A large suppression is still expected in the relativistic case. Predictions of various theoretical calculations for $\Gamma(\eta(1440) \to \gamma\rho^0)$ are given in table 33. The bag model predictions all settle around a radiative width of

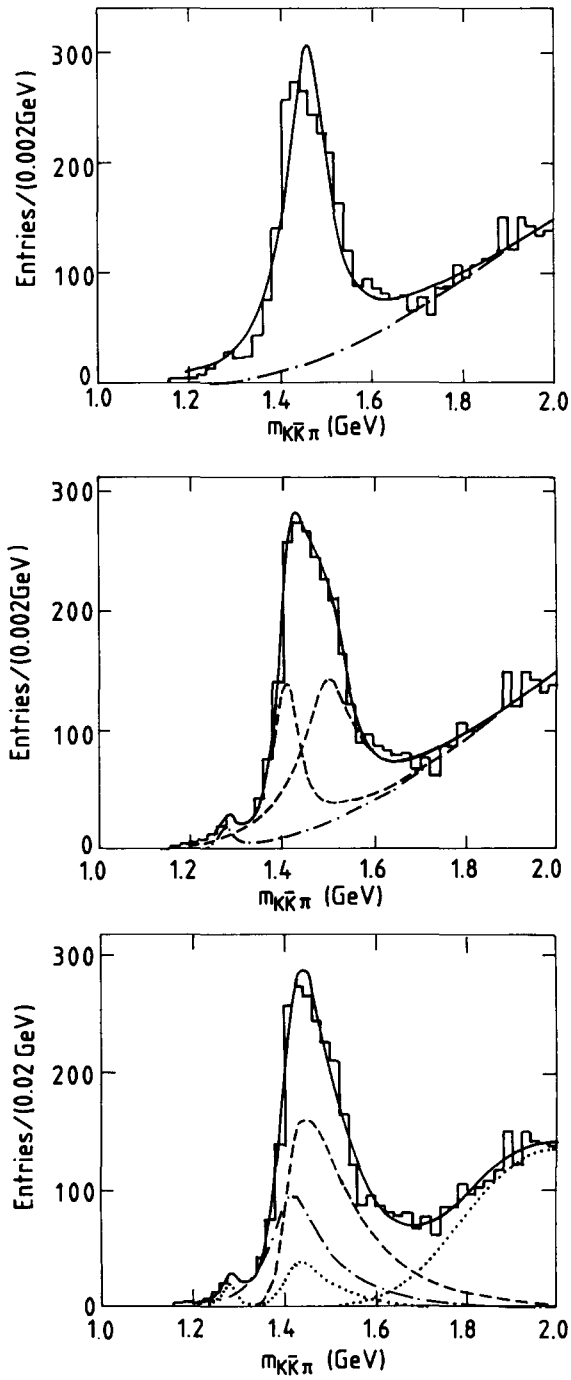

Fig. 75. Fit to the $K\bar{K}\pi$ invariant mass spectrum assuming several hypotheses. Fit with (a) a single Breit–Wigner resonance, (b) two interfering Breit–Wigner amplitudes, and (c) a coupled channel Breit–Wigner. In (b) and (c) a Breit–Wigner amplitude for the $f_1(1285)$ has also been included.

Table 33
Theoretical expectations for $\eta(1440)\to\gamma\rho^0$

Model	Reference	$\Gamma(\eta(1440)\to\gamma\rho^0)$ (MeV)
Bag model: η,η', glue mixing	[301]	0.43
Bag model: $q\bar{q}$,$q\bar{q}g$ mixing	[302]	≤1.5
Bag model: η,η', glue mixing plus q–g coupling	[300]	0.4–1.6
Bag model: pseudoscalar meson dominance	[305]	0.213–0.413
Pole model using data from $J/\psi\to\gamma$ + pseudoscalar	[309]	3.5
η,η', glue mixing model	[306]	0.02
η,η', glue mixing model	[307]	1.72
η,η', glue mixing model with anomalous couplings	[304]	4.2
effective Lagrangian using chiral symmetry	[303]	2.5
non-relativistic $q\bar{q}$ model, harmonic oscillator	[308]	0.42

the order of 1 MeV. Large uncertainties come from the amount of mixing introduced into the "iota" wave function.

The radiative decay $\eta(1440)\to\gamma\rho^0$ has been searched for by Crystal Ball [299], Mark III [251], and DM2 [110] in the process $J/\psi\to\gamma\gamma\rho^0$, $\rho^0\to\pi^+\pi^-$. The event selection is helped by the fact that for the vast majority of events the γ radiated from the J/ψ deposits a larger energy in the electromagnetic calorimeter than the γ radiated from the produced state X, allowing one to distinguish the two from the start and to reduce combinatorial background.

The results of the three experiments are consistent in that they observe a peak at a mass about 1–2 standard deviations lower than the mean value of the "iota" structure and a width of about 150 MeV. The $\gamma\rho$ invariant mass distribution is shown in fig. 76. It is possible that the $\eta(1275)$ or $f_1(1285)$ are contributing to the lower side of the resonance (see fig. 76b). To minimize their contribution Mark III has excluded the mass region below 1.3 GeV in the resonance fit, which results in a slightly higher mass value for X(~1400) (cf. table 34).

An analysis of the $\gamma\rho$ decay angular distributions agrees with a spin 0^- interpretation but spin 1^+ cannot be excluded. The measured parameters are listed in table 34. The average branching ratio is

$$B(J/\psi\to\gamma X)\cdot B(X\to\gamma\rho^0)=(1.0\pm0.18)\times10^{-4}\,. \tag{130}$$

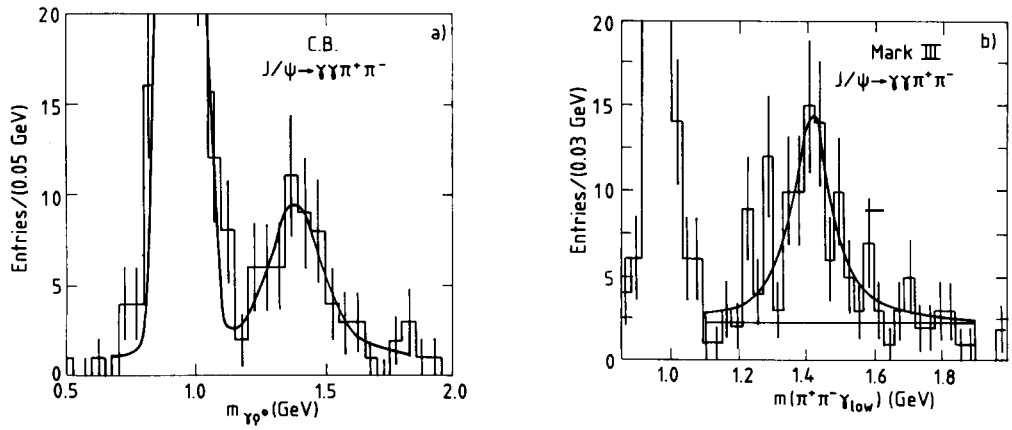

Fig. 76. Search for $\eta(1440)\to\gamma\rho$. Invariant $\gamma\pi\pi$ mass distributions from (a) Crystal Ball [299] and (b) Mark III [251] of the reaction $J/\psi\to\gamma\gamma\pi^+\pi^-$.

Table 34
Measurements on $\eta(1440) \to \gamma + V$

Decay mode	Mass (MeV)	Width (MeV)	$B(J/\psi \to \gamma\iota) \cdot B(\iota \to \gamma V)$ (units of 10^{-4})	Experiment
$X(1400) \to \gamma\rho^0$	$1420 \pm 15 \pm 20$	$133 \pm 55 \pm 30$	$1.0 \pm 0.2 \pm 0.2$	Mark III [251]
	1390 ± 25	185^{+110}_{-80}	$1.9 \pm 0.5 \pm 0.4$	Crystal Ball [299]
	1401 ± 18	174 ± 44	$0.9 \pm 0.2 \pm 0.14$	DM2 [110]
	1403 ± 13	163 ± 34	1.02 ± 0.18	⟨average⟩
$\eta(1440) \to \gamma\omega$			<2.3	Mark III [251]
$\eta(1440) \to \gamma\phi$			<1.6	Mark III [251]

The interpretation of the experimental observations presents some difficulties because there are several possibilities. The γρ signal, if simply identified with the "iota", would clearly support the glueball interpretation for this state according to table 33. The persistently observed lower mass value, however, demands an identification with either the η(1400) or with the lower part of the "iota" structure (cf. section 6.4.1.1), if they are not the same. The observed partial width $\Gamma(X(1400) \to \gamma\rho) \sim 1.0\,\text{MeV}$ would probably be in conflict with the theoretical expectations, if the η(1400) were to be identified as a radially excited pseudoscalar meson state. Repeating the analysis with twice the statistics [310] should help to clarify some of these questions.

The coupling of a glueball to two photons is expected to be very weak. The two-photon decay of the η(1440) is still unobserved. The present upper limit is [311]

$$\Gamma(\eta(1440) \to \gamma\gamma) \cdot B(\eta(1440) \to K\bar{K}\pi) < 1.6\,\text{keV} \quad (95\%\ \text{C.L.})\,. \tag{131}$$

Relating this limit to the γρ decay via vector dominance one predicts that

$$\Gamma(\eta(1440) \to \gamma\rho) \approx \frac{f_\rho^2}{e^2} \cdot 2 \cdot 0.376 \cdot \Gamma(\eta(1440) \to \gamma\gamma) < \frac{0.3}{B(\eta(1440) \to K\bar{K}\pi)}\,\text{MeV}\,. \tag{132}$$

In the evaluation the contribution of phase space has been included and a value of $f_\rho^2/e^2 \approx 250$ has been assumed. This is barely compatible with the experimental result (130). In a more sophisticated, but not principally different, approach Chanowitz [312] derives for the ratio of γγ and γρ widths

$$\Gamma(\eta(1440) \to \gamma\gamma)/\Gamma(\eta(1440) \to \gamma\rho \to \gamma\pi\pi) = 0.625(1 - m_\rho^2/m_{\eta(1440)}^2)^3(1.34e/f_\rho)^2 G(x)^2\,, \tag{133}$$

with $G(x) = (1 + 0.51x)/(1 + x)$. x is proportional to the mixing between the singlet and octet decay amplitudes,

$$x = \tan\theta_{\eta(1440)} \frac{A(\{8\} \to \gamma\rho)}{A(\{1\} \to \gamma\rho)}\,.$$

The value of x is a priori unknown. Attempts to constrain x lead to the conclusion that (133) would be inconsistent with experiment if the entire γρ signal is identified with the "iota". Meshkov et al. [367] have pointed out that with just the right mixture of $u\bar{u}$, $d\bar{d}$ and $s\bar{s}$ the γγ coupling vanishes altogether and so must γρ if it is related by vector dominance.

For $\eta(1440) \to \gamma\omega$, $\gamma\phi$ ref. [312] predicts that

$$\Gamma(\eta(1440) \to \gamma\omega) = 0.085\Gamma(\eta(1440) \to \gamma\rho)\,,$$

$$\Gamma(\eta(1440) \to \gamma\phi)^{*} = 0.063\left(\frac{1-2x}{1+x}\right)^{2}\Gamma(\eta(1440) \to \gamma\rho)\,, \tag{134}$$

which has to be compared to the "naive" expectation of $\Gamma_{\gamma\rho} : \Gamma_{\gamma\omega} : \Gamma_{\gamma\phi} = 9 : 1 : 2$ if X is a $q\bar{q}$ state which decays in a flavour independent way. The experimental upper limits are included in table 34.

6.4.2. *The "theta"* / $f_2(1720)$

6.4.2.1. Discovery and $K\bar{K}$ *decay.* The $f_2(1720)$ was first observed by the Crystal Ball Collaboration [263] in the process $J/\psi \to \gamma\eta\eta$, $\eta \to \gamma\gamma$, based on a data sample of 2.2×10^6 J/ψ decays. The invariant $\eta\eta$ mass distribution is shown in fig. 77a for events which were kinematically fitted with five constraints. Due to the limited statistics it is not possible to decide from fig. 77a whether the $f_2(1720)$ peak also contains the $f_2'(1525)$ on its low-mass side. The measured resonance parameters and branching fractions are shown in table 35.

C parity, parity and spin of the $f_2(1720)$ are even since it is produced in a radiative decay from the J/ψ and because of its $\eta\eta$ decay mode ($J^P = 0^+, 2^+, 4^+, \ldots$). The angular distributions follow the form

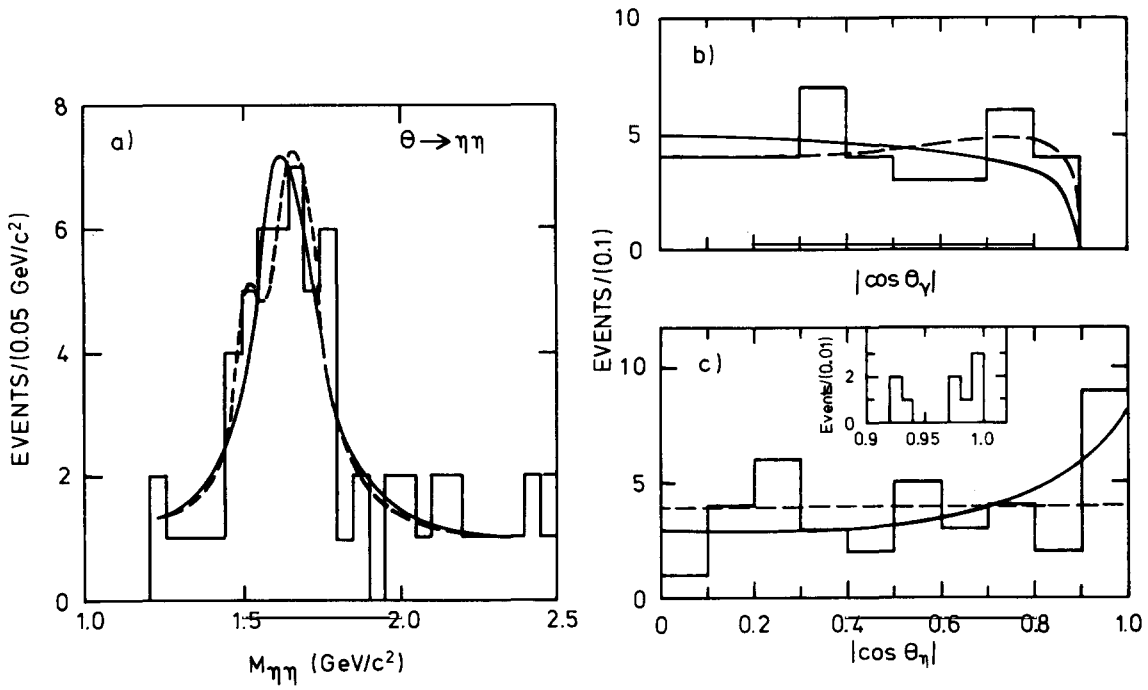

Fig. 77. Discovery and spin determination of the $f_2(1720)$. (a) $\eta\eta$ invariant mass distribution as observed by Crystal Ball. The superimposed curves represent fits assuming no $f_2'(1525)$ (solid line) and $f_2'(1525)$ contributions (dashed line). (b) $|\cos\theta_\gamma|$ and (c) $|\cos\theta_\eta|$ distributions for $J/\psi \to \gamma f_2(1720)$, $f_2(1720) \to \eta\eta$. The solid curves are best-fit distributions for spin 2. The dashed lines represent the expectations for spin 0. The inset is an enlarged view of the highest bin.

Table 35
Resonance parameters and product branching fractions of the "theta"/$f_2(1720)$. The measured branching fraction products have been multiplied by the respective isospin factors assuming $I=0$ to obtain $B(J/\psi\to\gamma f_2(1720))\cdot B(f_2(1720)\to\eta\eta, K\bar{K}, \pi\pi)$. The $\eta\eta$ branching fractions are obtained assuming a contribution of the $f_2'(1525)$ to the mass spectrum. Measurements indicated by [a)] were not used in the determination of the average.

Decay mode	Mass (MeV)	Width (MeV)	Branching fraction (units of 10^{-4})	Reference
$\eta\eta$	1640 ± 50	220^{+100}_{-70}	$4.9\pm1.4\pm1.0$	Crystal Ball [263][a)]
$\eta\eta$	1720 fixed	130 fixed	$2.6\pm0.8\pm0.7$	Crystal Ball [249]
$\eta\eta$	fixed	fixed	$1.3\pm0.4\pm0.3$	DM2 [243]
$\eta\eta$	fixed	fixed	$2.0\pm0.6\pm0.8$	Mark III [313]
$\eta\eta$			1.6 ± 0.4	⟨average⟩
K^+K^-	1700 ± 30	156 ± 20	$12.0\pm1.8\pm5.0$	Mark II [264]
K^+K^-	$1720\pm10\pm10$	130 ± 20	$9.6\pm1.2\pm1.8$	Mark III [265]
K^+K^-	1707 ± 10	166 ± 33	$9.2\pm1.4\pm1.4$	DM2 [267]
$K_S^0K_S^0$	1720 fixed	130 fixed	$9.0\pm2.4\pm2.2$	Mark III [265]
$K_S^0K_S^0$	1711 ± 9	173 ± 22	$10.4\pm1.2\pm1.6$	DM2 [267]
$K\bar{K}$	1711 ± 6	153 ± 11	9.7 ± 1.1	⟨average⟩
$\pi^0\pi^0$			$2.3\pm0.7\pm0.8$	Crystal Ball [249]
$\pi^0\pi^0$			$2.2\pm0.4\pm0.6$	DM2 [243]
$\pi^+\pi^-$			<3.2	Mark II [264][a)]
$\pi^+\pi^-$			$1.47\pm0.24\pm0.71$	Mark III [313]
$\pi^+\pi^-$	1693 ± 13	124 ± 24	$1.55\pm0.24\pm0.23$	DM2 [266]
$\pi\pi$			1.68 ± 0.27	⟨average⟩

$$W(\theta_\gamma, \theta_\eta, \phi_\eta) = 1+\cos^2\theta_\gamma \quad \text{for spin } 0\,, \tag{135}$$

and a form as given in eq. (115) for spin 2.

In the spin analysis performed by the Crystal Ball group [263] a maximum likelihood fit to the three angles θ_γ, θ_η, ϕ_η yielded a probability of only 4.5% for the $f_2(1720)$ having spin 0 relative to spin 2 and hence established a new tensor meson in addition to $f_2(1270)$ and $f_2'(1525)$ in that mass region. The distributions of $\cos\theta_\gamma$ and $\cos\theta_\eta$ are shown in fig. 77b and c. It is obvious from fig. 77c that the spin measurement is largely dependent on the excess of events in the last bin of the $|\cos\theta_\eta|$ distribution. There is no evidence that these events are anomalous, however.

The Mark II [264], Mark III [265], and DM2 [267] experiments observe the $f_2(1720)$ in the $K\bar{K}$ final state. Figure 78 shows the K^+K^- invariant mass distribution as observed by Mark II. Figure 79 displays the K^+K^- and $K_S^0K_S^0$ invariant mass distributions as observed by DM2 based on a sample of 8.6×10^6 J/ψ decays. Mark III data on the same channel are shown in section 6.4.3 (fig. 80). The $f_2'(1525)$ and $f_2(1720)$ are very well separated showing distinct peaks. The parameters measured by the experiments are included in table 35.

The spin 2^{++} assignment for the $f_2(1720)$ has been confirmed by Mark III [265], who find it preferred over spin 0 with 99.9% probability. DM2 finds equal likelihoods for spin 2 and spin 0 [110].

It is interesting to note from table 36 that the $f_2(1720)$ is produced with a polarization quite different from that of the 2^{++} states $f_2(1270)$ and $f_2'(1525)$ (see fig. 65c). While $f_2(1270)$ and $f_2'(1525)$, being well-established members of the 2^{++} nonet, have $(x, y)\approx(1, 0)$, the new state $f_2(1720)$ has $x\approx y\approx -1$. It has been argued [314] that this polarization pattern is not inconsistent with the glueball hypothesis of

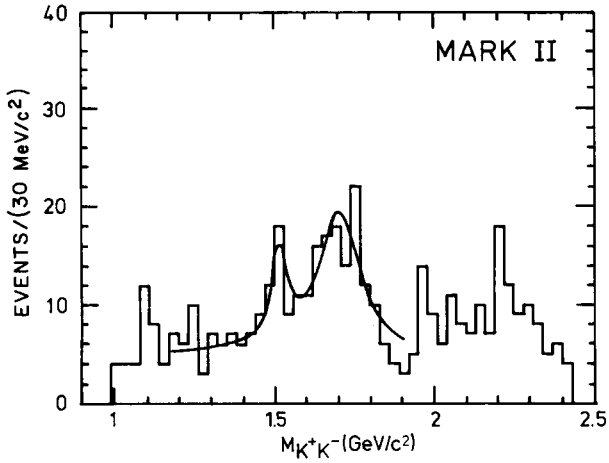

Fig. 78. Evidence for $f_2(1720)$ in $J/\psi \to \gamma K\bar{K}$. Invariant K^+K^- mass distribution from $J/\psi \to \gamma K^+K^-$ as observed by Mark II. The superimposed curve represents a fit including the $f_2'(1525)$.

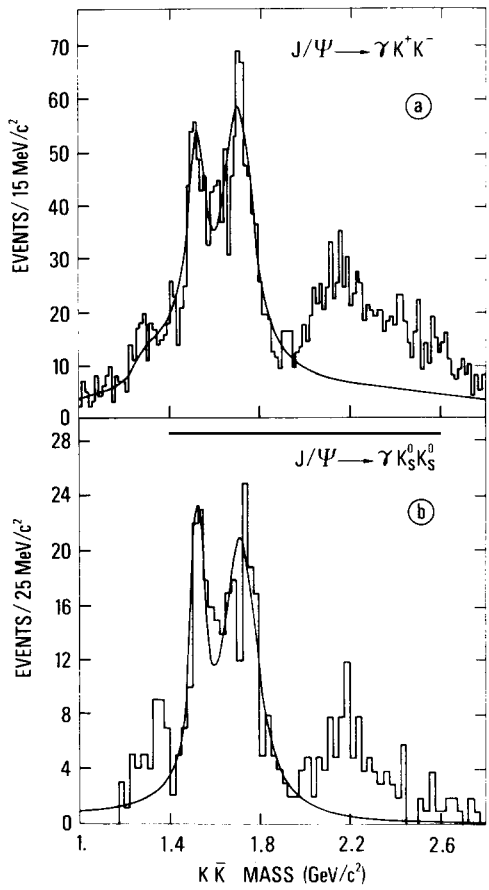

Fig. 79. High-statistics $K\bar{K}$ invariant mass spectra. (a) K^+K^- and (b) $K_S^0K_S^0$ invariant mass distributions from $J/\psi \to \gamma K\bar{K}$ as observed by DM2. The superimposed curves represent fits with two incoherent Breit–Wigner amplitudes.

Table 36
Polarization parameters of the "theta"/$f_2(1720)$

Decay mode	x	y	ϕ_x	ϕ_y	Reference
$\eta\eta$	0.87 ± 0.2	-0.64 ± 0.39			C.B. [263]
K^+K^-	-1.07 ± 0.2	-1.09 ± 0.25	0.6 ± 0.6	-0.1 ± 0.5	Mark III [265]
K^+K^-	-1.3 ± 0.14	-1.1 ± 0.18	0.0 ± 1.4	1.3 ± 0.3	DM2 [110]

the $f_2(1720)$. Li, Shen and Liu [314] have shown that the $f_2(1720)$ can only be fitted by a small d wave component in addition to a major s wave component in the wave function.

6.4.2.2. The $\pi\pi$ decay. The $\pi\pi$ invariant mass distributions of fig. 63 and fig. 110 show evidence for two other peaks being consistent in mass and width with the $f_2(1720)$ and possibly the $f_4(2030)$. A conclusive spin determination has not yet been performed due to significant background from $J/\psi \to \rho\pi$ events and from the tail of the $f_2(1270)$. However, the distribution of $\cos\theta^*_\pi$, the angle of the π^+ in the $\pi^+\pi^-$ rest frame, as well as the values obtained for the helicity parameters, x and y, assuming spin 2, are quite similar for $f_2(1720) \to K^+K^-$ and $f_2(1720) \to \pi^+\pi^-$ [313]. The product branching fraction for the $\pi\pi$ decay of the $f_2(1720)$ is included in table 35. The 2.1 GeV peak is described in section 6.4.3.

If one identifies the $\pi\pi$ peak at ~1.7 GeV with the $f_2(1720)$ one finds from table 35

$$\pi\pi : K\bar{K} : \eta\eta \approx 0.17 \pm 0.05 : 1 : 0.17 \pm 0.03 , \tag{136}$$

using the average experimental values. Equation (136) is different from the expectation for an $SU(3)_{\text{flavour}}$ symmetric decay, for which ratios of $\pi\pi : K\bar{K} : \eta\eta = 2 : 1 : 0.2$ are predicted including d wave phase space corrections.

6.4.2.3. Search for other decay modes. The speculations that the $f_2(1720)$ is not a traditional $q\bar{q}$ state have led to many predictions for other decay modes. Except for the $K\bar{K}$, $\pi\pi$, and $\eta\eta$ modes, no other decays have been observed despite some indication [333, 334] (see section 7.3) that the so far observed decay modes might represent only a fraction of the total.

Lipkin [323, 324] has pointed out decay modes which are particularly useful to test whether the $f_2(1720)$ could be a glueball. To the extent that the pseudoscalar nonet obeys nonet symmetry, i.e., η and η' represent the $\{1\}$ and $\{8\}$ $I = 0$ states of this nonet, respectively, the $\eta\eta'$ system is an octet into which a SU(3) singlet state cannot decay. The decay of an SU(3) singlet with even C parity to $K^*\bar{K}$ is forbidden by G_V parity, the analog of G parity for V spin. The SU(3) singlet component of $K^*\bar{K}$ is odd under C.

Close [325] has extended the selection rules given in refs. [323, 324]. He obtains

$$B(G \to \eta\eta) \geq \tfrac{1}{2} B(G \to K^+K^-) , \tag{137}$$

$$B(G \to \eta\eta') \leq \tfrac{1}{2}[B(G \to \eta'\eta') + B(G \to \eta\eta)] . \tag{138}$$

Intrinsic glue in the η or η', on the other hand, could substantially enhance the $\eta\eta'$ decay of a glueball.

In particular Gershtein et al. [326] have suggested that

$$2 \leq B(G \to \eta\eta')/B(G \to \eta\eta) \leq 3.7 \tag{139}$$

for a glueball decay.

Upper limits obtained for $f_2(1720)$ decays into various channels are listed in table 37.

6.4.2.4. Phenomenology of the "theta". In order to study the question whether the $f_2(1720)$ can be accommodated in a $J^{PC} = 2^{++}$ $q\bar{q}$ multiplet one has to compare the $f_2(1720)$ characteristics with those of the $f_2(1270)$ and the $f_2'(1525)$. The ground state 2^{++} nonet is complete and well established (cf. fig. 5). The $f_2(1720)$ would then have to be the radially excited partner of the central members of that multiplet, for which candidate states already exist, the $f_2(1810)$ [315] and the $f_2(1410)$ [316].

The 4^{++} state $f_4(2030)$ is considered an orbital excitation of the $f_2(1270)$ with orbital angular momentum $L = 3$. A potential model suggests [317] a similar mass scale for the $L = 3$, $J^{PC} = 2^{++}$ excitation of the $f_2(1270)$. The orbitally excited $f_2'(1525)$ is also not expected to lie in the 1.7 GeV mass range, rendering such an interpretation for the $f_2(1720)$ unlikely.

Other explanations and interpretations of the $f_2(1720)$, such as $q\bar{q}g$ hybrid states [54, 318], four quark states [134, 319, 320], or glueballs [225], have been suggested. If the $f_2(1720)$ were a hybrid, four accompanying nonets are predicted in the mass region of interest. A $q\bar{q}$ pair with orbital angular momentum $L = 0$ plus a (TE) gluon results in $J^{PC} = 1^{--}$, $(0, 1, 2)^{-+}$ nonets (see section 2.4). A $f_2(1720)$-like 2^{++} state requires an excited $q\bar{q}$ state plus a (TM) gluon. Chanowitz and Sharpe [54] suggest that such a state exists in the 1.9 to 2.3 GeV mass region with a $K^*\bar{K}^*$ decay signature. In general they find that in the $q\bar{q}$ + (TM) gluon case strange quarks are greatly favoured. To identify the $f_2(1720)$ with such an excited $q\bar{q}g$ state seems difficult because the predicted mass is too high. It is also not very appealing to predict excited $q\bar{q}g$ states before any ground state hybrid has been found.

Four-quark $qq\bar{q}\bar{q}$ states tend to "fall apart" into two mesons and are thus expected to be very wide objects unless the "fall apart" mode is forbidden because the state has a mass below the "fall apart" threshold. Chanowitz [319] suggests that the $f_2(1720)$ could be a $(u\bar{u} = d\bar{d})s\bar{s}$ state, which would like to "fall apart" into $K^*\bar{K}$ or $\phi\omega$ if its mass were not too low. The only other significant decay modes should be $K\bar{K}$ and $\eta\eta$ with $\Gamma(f_2(1720) \to K\bar{K}) > 2\Gamma(f_2(1720) \to \eta\eta)$. The observed $f_2(1720) \to \pi\pi$ decay and the non-observation of $f_2(1720) \to K^*\bar{K}$, which is not far below threshold, clearly represent problems for a four-quark interpretation of the $f_2(1720)$. Weinstein and Isgur [321] have calculated, using a four-body Schrödinger equation, that only the 0^{++} $qq\bar{q}\bar{q}$ state is stable. This casts additional doubt on a possible four-quark interpretation for the $f_2(1720)$.

The most exciting interpretation of the $f_2(1720)$ of course is the glueball hypothesis. This possibility is discussed in section 7.3.

Table 37
Upper limits on product branching fractions for the "theta"/$f_2(1720)$

Decay mode	$B(J/\psi \to \gamma f_2(1720)) \cdot B(f_2(1720) \to X)$	Reference
$\rho\rho$	$< 2.4 \times 10^{-4}$	DM2 [346]
$\omega\omega$	$< 2.4 \times 10^{-4}$	Mark III [350]
$K^*\bar{K}^*$	$< 4.5 \times 10^{-4}$	Mark III [265]
$\eta\eta'$	$< 2.1 \times 10^{-4}$	Mark III [265]
$K\bar{K}\pi$	$< 2.5 \times 10^{-4}$	Mark III [265]

6.4.3. The 2.2 GeV mass region and the ξ(2230)

The mass region around 2.2 GeV shows interesting structures in the radiative decays $J/\psi \to \gamma\pi\pi$, $\gamma K\bar{K}$, and $\gamma 4\pi$.

In $J/\psi \to \gamma\pi\pi$ a peak is observed (fig. 63) which is consistent in mass and width with the 4^{++} $q\bar{q}$ state $f_4(2030)$. The measured parameters are listed in table 38. The signal to background ratio is small and could cast some doubt on the interpretation given by the experiments.

The DM2 Collaboration also claims observation [346] of a signal at 2.12 GeV in the reaction $J/\psi \to \gamma 4\pi$. As evident from fig. 89, structure is indeed observed above a large background from $J/\psi \to 5\pi$ events. The signal seems to be mainly due to $J/\psi \to \gamma\rho^0\rho^0$. A partial wave analysis, performed to the entire spectrum (see section 6.4.5.1), attributes this structure to the pseudoscalar channel but also splits the signal, leaving the question of an ultimate assignment of this structure unanswered. The branching fraction is given in table 41.

Among the states discovered by the "third generation" experiments operating at the J/ψ, the ξ(2230) [Particle Data Group name X(2220)] has raised the largest excitement but is also regarded as the most controversial with regard to its experimental evidence. Let us summarize the facts.

The Mark III Collaboration has published the observation of a narrow resonance at a mass of 2.23 GeV produced in radiative J/ψ decay and decaying into K^+K^- and $K_S^0K_S^0$ [329]. The evidence for this state on top of a wider structure is shown in fig. 80.

The explicit parameters for the ξ(2230) are, in the K^+K^- mode,

$$m(\xi) = (2.230 \pm 0.006 \pm 0.014)\ \text{GeV}, \qquad \Gamma(\xi) = (0.026^{+0.020}_{-0.016} \pm 0.017)\ \text{GeV},$$

$$B(J/\psi \to \gamma\xi) \cdot B(\xi(2230) \to K^+K^-) = (4.2^{+1.7}_{-1.4} \pm 0.8) \times 10^{-5},$$

and in the $K_S^0K_S^0$ mode,

$$m(\xi) = (2.232 \pm 0.007 \pm 0.007)\ \text{GeV}, \qquad \Gamma(\xi) = (0.018^{+0.023}_{-0.015} \pm 0.010)\ \text{GeV},$$

$$B(J/\psi \to \gamma\xi) \cdot B(\xi \to K_S^0K_S^0) = (3.1^{+1.6}_{-1.3} \pm 0.7) \times 10^{-5}.$$

Table 38
Measured parameters of the X(2100) in radiative J/ψ decays. The branching fractions are given for ππ, $K\bar{K}$, ηη, ρρ, correcting for isospin assuming $I = 0$ for the X(2100).

Decay mode	Mass (MeV)	Width (MeV)	$B(J/\psi \to \gamma X(2100)) \cdot B(X \to f)$ (units of 10^{-4})	Reference
$\pi^+\pi^-$	2038 ± 30	304 ± 60	$2.4 \pm 0.4 \pm 0.4$	DM2 [266]
$\pi^+\pi^-$	$2083 \pm 8 \pm 30$	$147 \pm 20^{+75}_{-50}$	$3.0 \pm 0.5 \pm 0.9$	Mark III [313]
$\pi^0\pi^0$			$2.8 \pm 0.7 \pm 1.0$	C.B. [249]
$K_S^0K_S^0$	2197 ± 17	201 ± 51	≈6.0	DM2 [267]
$K_S^0K_S^0$	$2183 \pm 40 \pm 50$	$413 \pm 66 \pm 100$	$7.4 \pm 1.2 \pm 2.0$	Mark III [313]
K^+K^-	$2136 \pm 11 \pm 70$	$240 \pm 25 \pm 100$	$4.6 \pm 1.2 \pm 1.2$	Mark III [313]
ηη			$1.6 \pm 0.7 \pm 0.7$	Mark III [313]
ρρ	2107 ± 9	244 ± 23	$11.7 \pm 0.3 \pm 2.7$	DM2 [346]

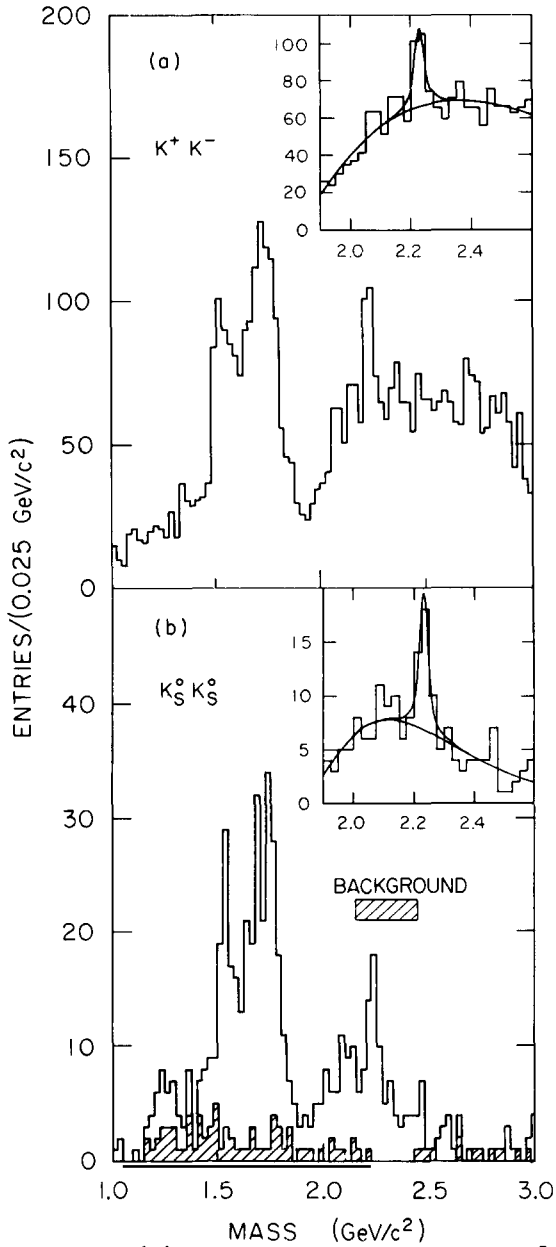

Fig. 80. Evidence for the ξ(2230). (a) K^+K^- and (b) $K^0_SK^0_S$ invariant mass distributions from $J/\psi \to \gamma K\bar{K}$ as observed by Mark III [329] based on 5.8×10^6 J/ψ decays. The four-pion background is shown hatched in (b). Fits to the 1.9–2.6 GeV mass region are displayed in the insets.

The ratio of the branching fractions is consistent with the ξ(2230) being an isoscalar. The statistical significance is stated as 4.5σ and 3.6σ for $K\bar{K}$ and $K^0_SK^0_S$, respectively, based on the total Mark III data sample of 5.8×10^6 J/ψ.

Although the signal is seen by Mark III in two different $K\bar{K}$ decay channels, DM2, based on 8.7×10^6 J/ψ, reports no evidence for the ξ(2230) in either decay mode. The corresponding $K\bar{K}$ invariant mass distributions are shown in fig. 79. Depending on the width assumed for this state the

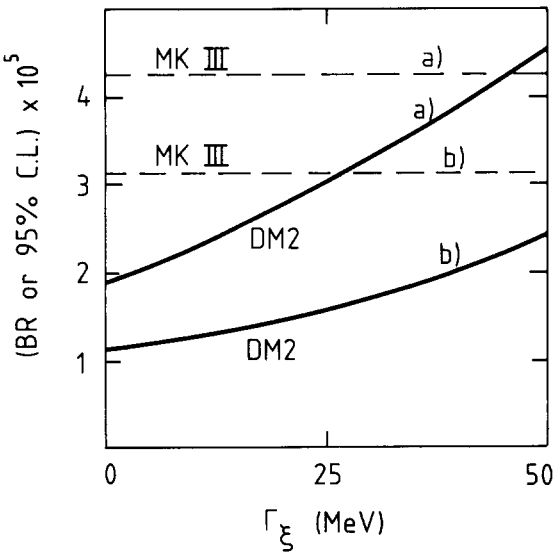

Fig. 81. Upper limits for the ξ(2230) as a function of the width. The limits are obtained from the DM2 collaboration [267] for $J/\psi \to \gamma K^+K^-$ (solid line a) and for $J/\psi \to \gamma K_S^0 K_S^0$ (solid line b). The dashed lines are the values for the product branching ratio as measured by Mark III [329] for both modes, respectively. The two experiments are consistent only for $\Gamma > 50$ GeV.

DM2 upper limit [267] varies as shown in fig. 81. The two experiments are not consistent with each other for width values below ~50 MeV.

To what extent the two experiments really disagree is not entirely clear. The analysis of the K^+K^- channel relies crucially on the TOF measurement distinguishing kaons from pions at momenta above 1 GeV and on the ability to reduce background from $J/\psi \to \rho\pi^0$ and $J/\psi \to \pi^0 K^+K^-$ in which the π^0 decays asymmetrically and one photon escapes undetected. The latter is dominated by $J/\psi \to K^*\bar{K}$ and produces a smooth background under the signal region. This background can in principle be reduced by cutting on the K* bands of the Dalitz plot, but this also reduces the signal. DM2 has demonstrated [267] that after subtraction of this background the K^+K^- and $K_S^0K_S^0$ invariant mass distributions are in reasonable agreement in shape and magnitude. In the $\gamma K_S^0 K_S^0$ mode no such background exists due to C parity conservation. The ability to measure this channel merely depends on the $K_S^0 \to \pi^+\pi^-$ identification capability, which is about the same in both detectors. The TOF resolution of the Mark III detector is superior ($\sigma \sim 190$ ps) to that of DM2 ($\sigma \sim 540$ ps) (cf. table 7). This could serve as an explanation for the K^+K^- mode. Given the even larger statistics of DM2 it seems, however, hard to understand the discrepancy in the $K_S^0K_S^0$ channel.

DM2 and Mark III do agree, in fact, in that they both observe a relatively wide structure in the 2.2 GeV region (fig. 79 and fig. 80), on top of which Mark III claims the observation of the ξ(2230). This structure cannot entirely be explained by background, especially in $J/\psi \to \gamma K_S^0 K_S^0$. A fit to the $K_S^0K_S^0$ mass spectrum of DM2 (fig. 79b) with three Breit–Wigner amplitudes for $f_2'(1525)$, $f_2(1720)$ and the 2.2 GeV structure yields $m_{X(2.2)} = (2197 \pm 17)$ MeV, $\Gamma_{X(2.2)} = (201 \pm 51)$ MeV and a branching ratio product of $B(J/\psi \to \gamma X(2.2)) \cdot B(X(2.2) \to K_S^0K_S^0) \approx 1.5 \times 10^{-4}$ [267]. Fitting the Mark III data [313] with five Breit–Wigner amplitudes (fig. 82), i.e. two resonances in the 2.2 GeV region, reveals the ξ(2230) plus an indication of the X(2100) with resonance parameters as given in table 38.

The Dalitz plots for the Mark III data are shown in fig. 83, where diagonal bands corresponding to

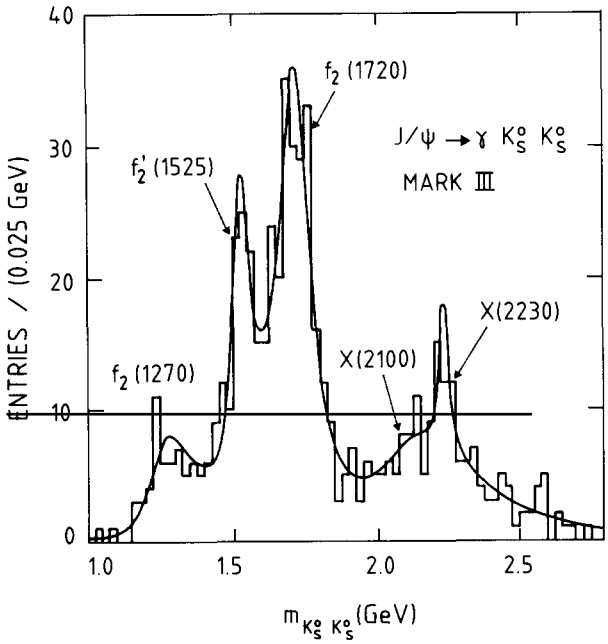

Fig. 82. Fit to the $K\bar{K}$ mass spectrum with five Breit-Wigner amplitudes. The data are from $J/\psi \to \gamma K_S^0 K_S^0$ as obtained by Mark III [313]. Note that the mass distribution is not identical to fig. 80b due to different analysis cuts in ref. [313].

the states $f_2'(1525)$, $f_2(1720)$, and perhaps $\xi(2230)$ are visible together with the two K* bands. It has been checked that the signal does not arise from $K^*\bar{K}$ or $e^+e^-\gamma$ backgrounds.

A spin analysis similar to the one described for the $f_2(1270)$ in section 6.3.2 has been performed by the Mark III group using the cleaner $K_S^0K_S^0$ sample. The analysis assigns a spin greater than or equal to 2 to the $\xi(2230)$ [313]. Figure 84 shows distributions of $\cos\theta_K^*$, where θ_K^* is the polar angle of a K_S^0 in the $K\bar{K}$ rest frame with respect to the photon direction, for events from $f_2'(1525)$, $f_2(1720)$, and $\xi(2230)$, respectively. Because the $K_S^0K_S^0$ system can only have even spin and positive parity the $\xi(2230)$ must have $J^{PC} = 2^{++}, 4^{++}, \ldots$. This is unfortunately not an existence proof of the $\xi(2230)$ because the structure at ~2.2 GeV underneath the $\xi(2230)$, which is observed by both experiments, also shows a non-flat $\cos\theta_K^*$ distribution.

Evidences for resonance peaks with similar parameters have been reported in the literature. The GAMS Collaboration has observed [331] a narrow structure in the $\eta\eta'$ invariant mass spectrum of the $\pi^- p \to \eta\eta' + n$ reaction at 38 and 100 GeV beam energy with parameters similar to the ones of the $\xi(2230)$. The $\eta\eta'$ decay implies $I^G = 0^+$. For the spin of this structure the angular distributions suggest $J^P \geq 2^+$. Some evidence for a 2^{++} $K_S^0K_S^0$ structure at 2.23 GeV and about 80 MeV wide comes from the MSS ITEP group [332]. A detailed comparison with the data in the same channel taken at BNL [333] is yet to be made.

The LASS Collaboration [334] also reported a signal at ~2.2 GeV decaying into $K_S^0K_S^0$ and K^+K^- in the reaction $K^- p \to \Lambda + K\bar{K}$ at 11 GeV. Figure 85 shows the invariant $K_S^0K_S^0$ mass distribution of the LASS data normalized and superimposed to the same distribution of the Mark III data. The K^+K^- channels are not easily comparable because of the large N* diffractive background in the LASS data. A moment analysis done by LASS [334] prefers spin 4^{+4} for this state.

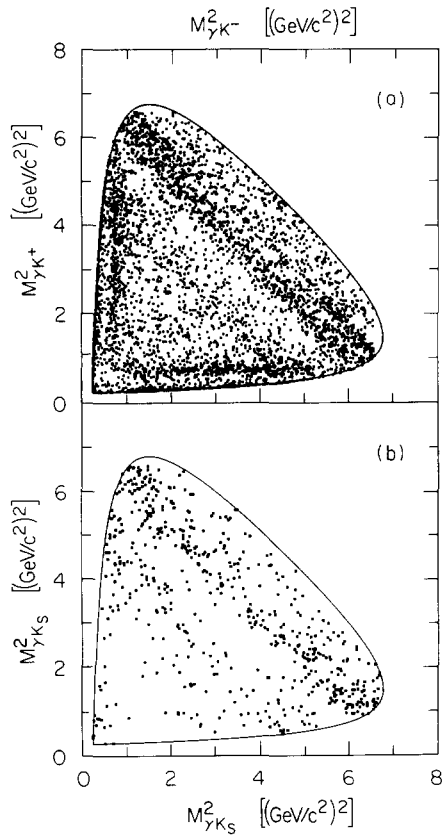

Fig. 83. Dalitz plots for $J/\psi \to \gamma K\bar{K}$. (a) $J/\psi \to \gamma K^+K^-$, (b) $J/\psi \to \gamma K^0_S K^0_S$, diagonal bands due to the $f_2'(1525)$, $f_2(1720)$, and perhaps $\xi(2230)$ (Mark III) are evident.

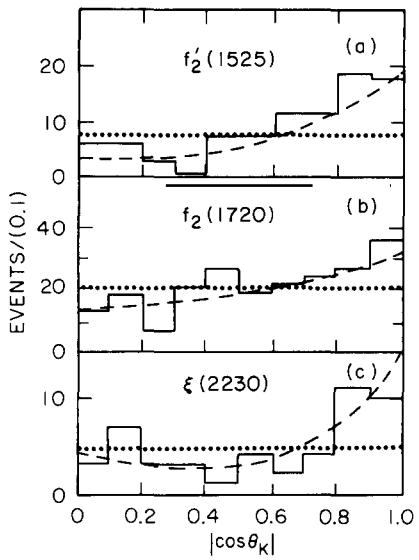

Fig. 84. Distributions of $\cos\theta_K^*$ for events in the $K\bar{K}$ invariant mass regions of (a) 1.42–1.55 GeV ($f_2'(1525)$), (b) 1.62–1.82 GeV ($f_2(1720)$), and (c) 2.18–2.28 GeV ($\xi(2230)$). The histograms are the data, the dotted lines are the Monte Carlo predictions for spin 0, and the dashed lines are the predictions for spin 2 using the best-fit values for the helicity amplitude ratios x and y.

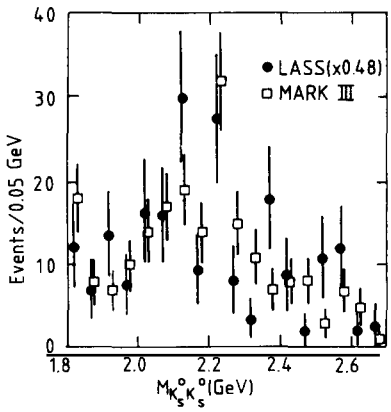

Fig. 85. Comparison of LASS and Mark III $K\bar{K}$ mass spectra. Acceptance corrected $K^0_S K^0_S$ invariant mass distribution of $K^-p \to \Lambda + K^0_S K^0_S$ as observed by LASS (black circles) compared to the same final state produced in radiative J/ψ decay as seen by Mark III (open squares) for invariant masses between 1.8 GeV and 2.7 GeV.

Interpretation of the ξ(2230). The narrow width of the ξ(2230), which is almost consistent with zero, provoked many speculations about the nature of this state, including the hypothesis that the ξ(2230) might be a Higgs particle [335]. Other possible identifications are a glueball or a hybrid state [336], a high-spin $q\bar{q}$ state [337], a narrow $\Lambda\bar{\Lambda}$ bound state [338], or even more exotic possibilities [339].

The Higgs interpretation has become more and more unlikely due to production limits for the ξ from Υ(9640) decays [340] for both the minimal Higgs model as well as for models with two Higgs doublets. Upper limits for other decay modes have been obtained [329]. They are listed in table 39.

The most traditional and also most plausible interpretation of the ξ(2230) is that of a $L = 3$, $^3F_2$ or $^3F_4$ $s\bar{s}$ state [337]. This interpretation is also supported by the LASS measurement [334] in a reaction ideal to search for $s\bar{s}$ states. However, if MSS ITEP [332] and GAMS [331] are both seeing the ξ(2230), the branching ratio into ηη′ is twice as large as into $K\bar{K}$, in contradiction to an expected ratio of $\eta\eta' : K\bar{K} \approx 1 : 3$ or smaller for an $L = 3$ $s\bar{s}$ meson [337], and also at the verge of being inconsistent with the Mark III limit for the ηη′ decay mode [313]. The value for the total width (~60 MeV) expected from the relativistic quark model of Godfrey et al. [337] is at the 2σ variance with the experimental observation.

6.4.4. *The decay* $J/\psi \to \gamma\eta\pi\pi$

The radiative decay $J/\psi \to \gamma\eta\pi\pi$ is interesting for two reasons. First, the observation of the glueball candidate η(1440) in $J/\psi \to \gamma K\bar{K}\pi$ has prompted zealous searches for other decay modes. Since the $K\bar{K}\pi$ final state could actually proceed via $a_0(980)\pi$—a question which is not easily answered in the presence of threshold effects and overlapping K* bands (see section 6.4.1)—it is compelling to search for an η(1440) signal in $J/\psi \to \gamma\eta\pi\pi$ exploiting the fact that the $a_0(980)$ also decays to ηπ. Accepting the ratio of roughly $B(a_0(980) \to K\bar{K}) : B(a_0(980) \to \eta\pi) \simeq 10^{-1}$ [14, 147] one would expect that $B(\eta(1440) \to \eta\pi\pi) > 10B(\eta(1440) \to K\bar{K}\pi)$, provided that the decay proceeds via an $a_0(980)$ intermediate state. Even without an $a_0(980)$-mediated transition in the "iota" decay, Lipkin [323] has predicted comparable $K\bar{K}\pi$ and ηππ couplings for an SU(3) singlet state.

A second domain of the radiative ηππ decay is to explore the production mechanisms of 1^{++} axial-vector mesons. As described in section 6.3.4 there are at least three isoscalar particles which are candidates for the central members of the 1^{++} multiplet, the $f_1(1285)$, the $f_1(1420)$, and the $f_1(1530)$, all three with possible or established ηππ decay modes.

Analyses of $J/\psi \to \gamma\eta\pi\pi$, with $\eta \to \gamma\gamma$ or $\eta \to \pi^+\pi^-\pi^0$, have been performed by Crystal Ball [281], Mark III [282], and DM2 [283] in final states with three photons and two or four charged pions,

Table 39
Upper limits on branching ratios for the ξ(2230)

Decay mode	$B(J/\psi \to \gamma\xi) \cdot B(\xi \to X)$	Reference
$\xi \to \mu^+\mu^-$	$<5 \times 10^{-6}$	Mark III [329]
$\xi \to \pi\pi$	$<2 \times 10^{-5}$	Mark III [329]
$\xi \to K^*\bar{K}$	$<2.5 \times 10^{-4}$	Mark III [329]
$\xi \to K^*\bar{K}^*$	$<3 \times 10^{-4}$	Mark III [329]
$\xi \to \eta\eta$	$<7 \times 10^{-5}$	Mark III [313]
$\xi \to \eta\eta'$	$<8 \times 10^{-5}$	Mark III [313]
$\xi \to p\bar{p}$	$<2 \times 10^{-5}$	Mark III [329]
$\xi \to \phi\phi$	$<5.5 \times 10^{-5}$	Mark III [348]
$\xi \to \omega\phi$	$<5.9 \times 10^{-5}$	Mark III [348]

respectively. The event selection proceeds as usual by applying kinematic fits (4C or 5C using the η mass constraint) to the signal reaction, after standard cuts have been made. The $\eta\pi\pi$ invariant mass distribution obtained in this way is shown in fig. 86. The salient features are (a) an extremely clean η' signal (see also section 6.3.1.1), (b) evidence for an η_c at 2980 GeV, and (c) an interesting mass region between 1 and 2 GeV with a complex structure probably due to several resonances.

The $\eta\pi\pi$ decay proceeds via $a_0(980)\pi$ as can be seen from fig. 87 showing the $\eta\pi^+$ projection of the $\eta\pi\pi$ Dalitz plot with clear evidence for $a_0(980)$ production. After demanding that $m_{\eta\pi}$ is within 50 MeV of the nominal $a_0(980)$ mass, the $\eta\pi\pi$ invariant mass spectrum is shown in fig. 88 for masses above 1 GeV. At least four structures can be identified: (a) at 1280 MeV, most likely the $f_1(1285)$ or the $\eta(1275)$, (b) at ~1400 MeV, probably to be identified with the $\eta(1400)$ and less convincingly the $f_1(1420)$, (c) at ~1600 MeV, and (d) at ~1900 MeV. The mass resolution in this mass region is typically 20 MeV for Mark III and DM2. The first two structures have already been discussed in section 6.3.4. To really identify these structures a phase shift analysis will prove essential. The mass distribution shows no obvious sign for a "iota"/$\eta(1440)$ signal. However, interference effects between different decay modes of the $\eta(1440)$ [309] or the existence of "sub"states hiding under the "iota" structure could lead to the observed effect. Again, a full partial wave analysis has to be performed. The same statement is true for the $f_1(1420)$. The high-mass region between 1.5 GeV and 2.0 GeV shows a pattern which is very similar to the one observed in $J/\psi \to \gamma 4\pi$ (see section 6.4.5.1). In this decay a dominantly pseudoscalar ($J^P = 0^-$) $\rho\rho$ component is found. The branching fractions obtained from the different experiments are listed in table 40.

6.4.5. *Radiative production of vector meson pairs*

Enhancements in *vector–vector* final states with masses below 3 GeV have been observed in hadronic interactions [341, 342] and photon–photon collisions [343]. All of these observations have two features in common. First, the observed *vector–vector* invariant mass distributions are either difficult to free

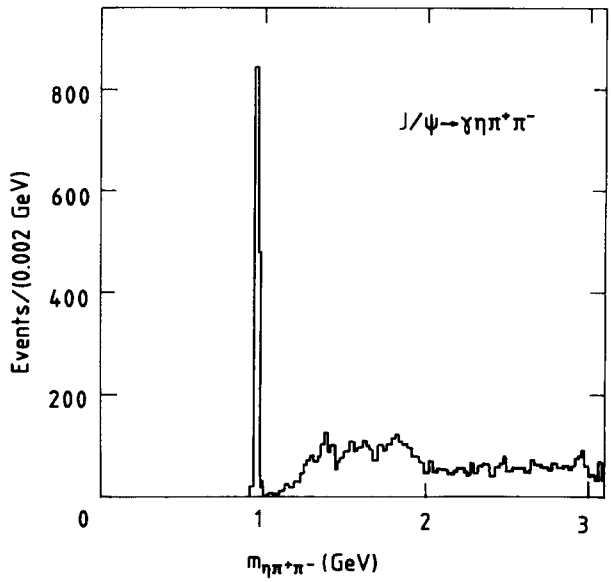

Fig. 86. Radiative decay to the $\eta\pi\pi$ final state. Invariant $\eta\pi\pi$ mass distribution from $J/\psi \to \gamma\eta\pi^+\pi^-$ for masses between 0 and 3.1 GeV (Mark III [282]). The η is observed in its $\gamma\gamma$ decay mode.

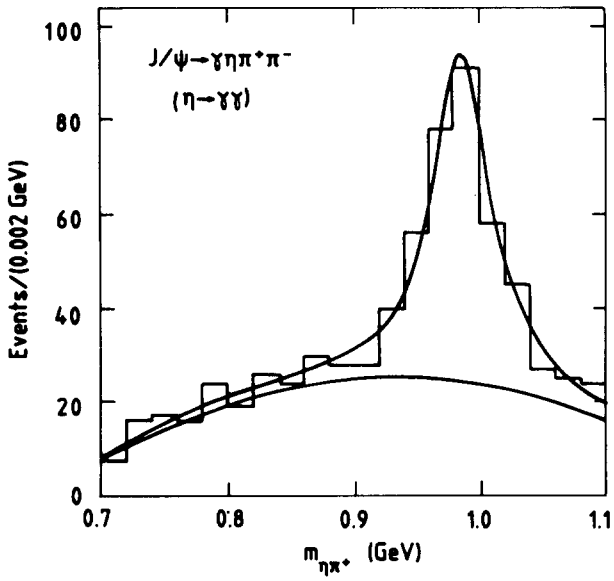

Fig. 87. $\eta\pi^+$ projection of the $\eta\pi\pi$ Dalitz plot from $J/\psi \to \gamma\eta\pi^+\pi^-$. The curve is a Breit-Wigner fit to the $a_0(980)$.

from background ($\rho\rho$), have small statistics ($\omega\omega$, $\phi\phi$), or exhibit complicated structures ($\phi\phi$). Secondly, the reported signals have always provoked speculations about interesting threshold effects or resonance production of $q\bar{q}$, $q\bar{q}q\bar{q}$, $q\bar{q}g$, or gg bound states.

In radiative J/ψ decays the situation is similar. In the large-statistics data samples of Mark III and DM2 the production of all ground state *vector–vector* pairs have been observed in radiative decays: $J/\psi \to \gamma + \{\rho\rho, \omega\omega, \omega\phi, \phi\phi, K^*\bar{K}^*\}$.

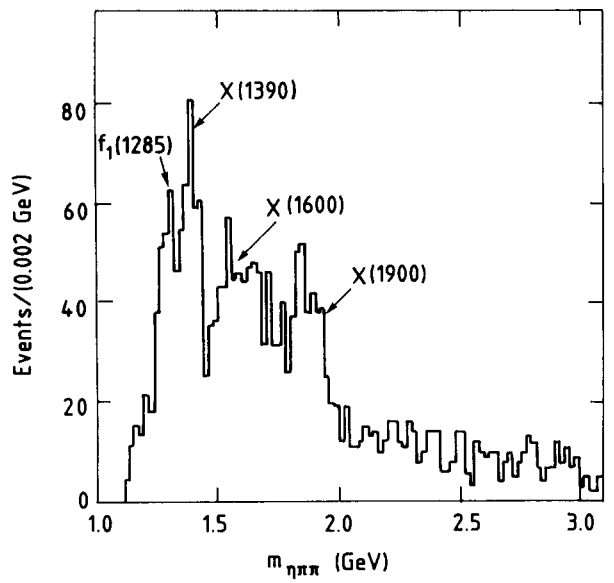

Fig. 88. $\eta\pi^+\pi^-$ invariant mass distribution after a $a_0(980)$ cut (see text).

Table 40
Branching ratios for the decay $J/\psi \to \gamma\eta\pi\pi$. In [a] the branching fractions using the average values of the decays involving $\eta \to \gamma\gamma$ and $\eta \to 3\pi$ are quoted.

Experiment	Branching ratio or 90% C.L. upper limit
Crystal Ball [281]	$B(J/\psi \to \gamma\eta\pi^+\pi^-) = (3.5 \pm 0.3 \pm 0.7) \times 10^{-3}$ $B(J/\psi \to \gamma\eta\pi^0\pi^0) = (2.3 \pm 0.3 \pm 0.7) \times 10^{-3}$
Mark III [282][a]	$B(J/\psi \to \gamma X(1280)) \cdot B(X(1280) \to a_0(980)^{\pm}\pi^{\mp}) \cdot B(a_0(980)^{\pm} \to \eta\pi^{\pm}) = (3.2 \pm 1.1 \pm 0.3) \times 10^{-4}$ $B(J/\psi \to \gamma X(1400)) \cdot B(X(1400) \to a_0(980)^{\pm}\pi^{\mp}) \cdot B(a_0(980)^{\pm} \to \eta\pi^{\pm}) = (5.2 \pm 1.8 \pm 0.5) \times 10^{-4}$
DM2 [283]	$B(J/\psi \to \gamma X(1400)) \cdot B(X(1400) \to \eta\pi^+\pi^-) = (4.1 \pm 0.3 \pm 1.0) \times 10^{-4}$

6.4.5.1. The decay $J/\psi \to \gamma\rho\rho$. The decay $J/\psi \to \gamma\rho^0\rho^0$ has first been observed by Mark II [344]. The $\rho^0\rho^0$ invariant mass distribution is dominated by a structure centred at about 1.65 GeV. Initially it was appealing to identify this structure with the $f_2(1720)$, which would increase the total observed branching fraction for $J/\psi \to \gamma f_2(1720)$ and hence make a glueball interpretation of the $f_2(1720)$ even more pressing. The fact that resonant structures in $\gamma\gamma \to \rho^0\rho^0$ have been observed [343] in the same mass region (1.4–2.0 GeV) with preferred spin assignments of 0^{++} or 2^{++} offered another link to believe that a single resonance was responsible for all these observations.

Mark III [345] and DM2 [346] have measured $J/\psi \to \gamma 4\pi$ with large-statistics samples of 5.8 and 8.6×10^6 J/ψ, respectively. Mark III has analysed both $\gamma\pi^+\pi^-\pi^+\pi^-$ and $\gamma\pi^+\pi^-\pi^0\pi^0$ decays. After kinematic fits are applied both final states still suffer a large contamination from $J/\psi \to 5\pi$ events. This background can only be subtracted on a statistical basis but not event by event. The technique used for this subtraction is mentioned as a typical analysis technique in section 3.4.

Figure 89 shows the 4π invariant mass distribution of events from $J/\psi \to \gamma(\pi^0) + \pi^+\pi^-\pi^+\pi^-$ from the DM2 analysis. Figure 90 shows the 4π invariant mass distributions as observed by Mark III for both final states after a statistical subtraction of the smooth background from $J/\psi \to \pi^0 4\pi$. The striking features of these spectra are resonant structures at ~1.55 GeV, ~1.8 GeV and perhaps ~2.1 GeV. In addition, a peak at 1.28 GeV, possibly the $f_1(1285)$, and the η_c show up in these spectra (fig. 89a).

Despite the large background contamination the statistical significance of these structures is quite remarkable and information on the spin content can be obtained for instance by means of a multi-channel likelihood spin parity analysis [345, 346], where the background can be filtered out. Such analyses show that the dominant component of the spectrum below 2 GeV is due to $J/\psi \to \gamma\rho\rho$ with spin parity 0^- of the ρρ system in which the two ρ's appear in a relative p wave.

A more transparent, but of course less powerful, way to demonstrate this fact is obtained by examining the behaviour of the angle χ between the decay planes of the two possible $\rho \to \pi\pi$ combinations measured in the ρρ rest frame. This angle provides a unique signature for even spin and odd parity [347] and has been used to determine the spin of the η_c [232]. For spin parity 0^-, in particular, the distribution of this angle takes the simple form

$$dN/d\chi \sim \sin^2\chi \,. \tag{140}$$

The distribution of χ is shown in fig. 91 for the Mark III data below 2 GeV and for the 5π background process. A large $\sin^2\chi$ component is evident. The fraction of $\sin^2\chi$ can be fitted for in bins of $m_{4\pi}$. The result of such a fit is shown in fig. 89b as the shaded region. Both peaks below 2 GeV are also present in the pseudoscalar component, but only the 1.55 GeV peak seems to be almost pure 0^-. The structure at

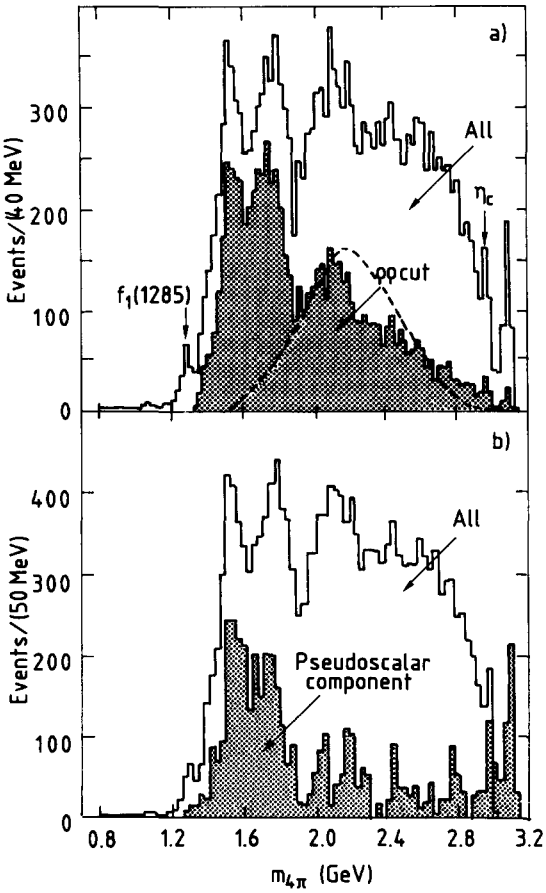

Fig. 89. Radiative ρρ production. Invariant 4π mass spectrum from $J/\psi \to \gamma(\pi^0) + \pi^+\pi^-\pi^+\pi^-$ (DM2, using 8.6×10^6 J/ψ). In (a) the shaded spectrum is obtained after applying a cut to enhance the ρρ component. In (b) the shaded region is the pseudoscalar component obtained from a fit to the angle χ described in the next. The dashed curve represents the expected shape of the spectrum for a p wave phase space distribution of $J/\psi \to \gamma\rho\rho$.

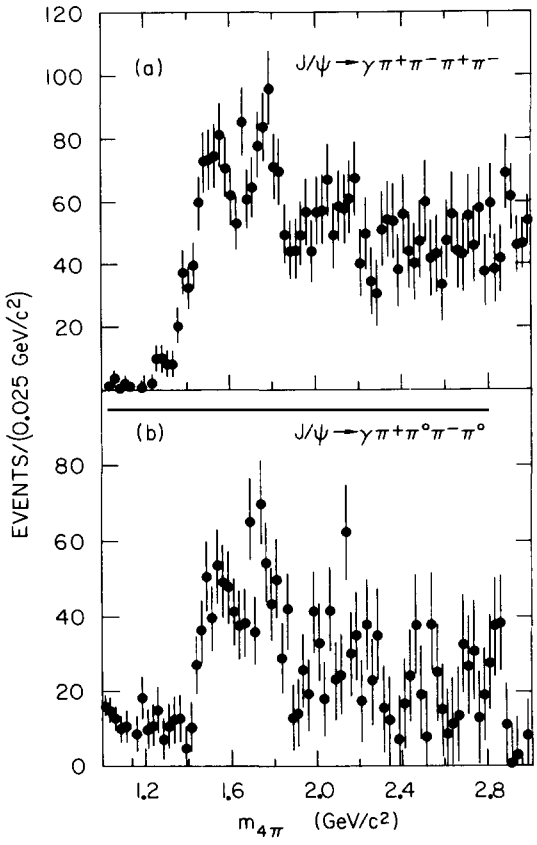

Fig. 90. Background subtracted invariant 4π mass spectrum, (a) from $J/\psi \to \gamma\pi^+\pi^-\pi^+\pi^-$ and (b) from $J/\psi \to \gamma\pi^+\pi^-\pi^0\pi^0$ (Mark III, using 2.7×10^6 J/ψ).

~1.8 GeV may contain a scalar component at its high side and is not necessarily only one state. Clearly the observed behaviour is not at all compatible with phase space production of $J/\psi \to \rho\rho$ (cf. fig. 89a). The structure at ~2.1 GeV does not exhibit such a clear signature and may also consist of more than just one state (see section 6.4.3). The branching fractions for the various reactions are listed in table 41.

The spin parity analysis renders it difficult to assign any of the observed structures to the 2^{++} state $f_2(1720)$ or the tensor states reported by Etkin et al. [342]. Upper limits are included in table 41.

The appearance of yet another pseudoscalar resonance with a sizeable production cross section and a mass just above the η(1440) is quite surprising. The p wave production renders an interpretation as a threshold effect unlikely unless introduced by a dynamical rescattering effect [356]. Attempts have been made to assign the 1.55 GeV peak to the η(1440) in an analysis using coupled channels [349] (see section 6.4.6.1).

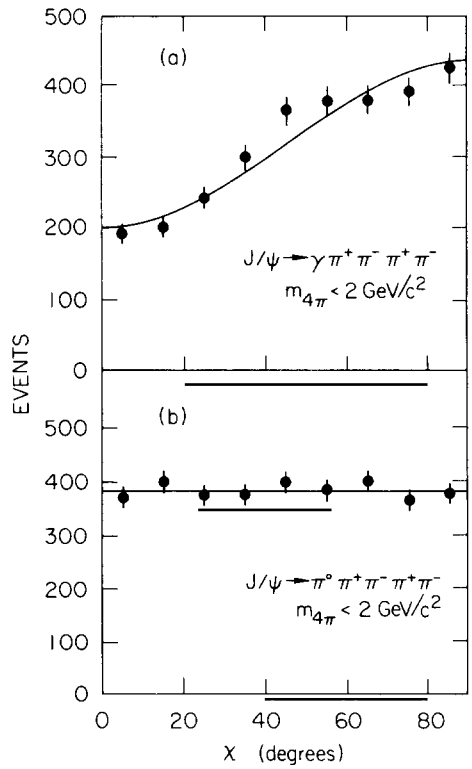

Fig. 91. Evidence for dominant 0^- spin parity of the ρρ system. Distributions of χ, the angle between the ρ decay planes for events below 2 GeV (a) from $J/\psi \to \gamma\pi^+\pi^-\pi^+\pi^-$ including 5π background, and (b) from $J/\psi \to 5\pi$ only. The curves are fits with (a) $a + b\sin^2\chi$ and (b) a constant (Mark III [345]).

Table 41
Branching ratios for the decay $J/\psi \to \gamma\rho\rho \to \gamma 4\pi$. Isospin correction factors have been applied assuming isospin conservation and an isosinglet hypothesis, wherever appropriate.

Experiment	Branching ratio or 90% C.L. upper limit	
Mark III [345]	$B(J/\psi \to \gamma\pi^+\pi^-\pi^+\pi^-) = (6.4 \pm 0.2 \pm 0.8) \times 10^{-3}$	for $m_{4\pi} < 3$ GeV
	$B(J/\psi \to \gamma\pi^+\pi^-\pi^+\pi^-) = (3.05 \pm 0.08 \pm 0.45) \times 10^{-3}$	for $m_{4\pi} < 2$ GeV
	$B(J/\psi \to \gamma\pi^+\pi^0\pi^-\pi^0) = (8.3 \pm 0.2 \pm 3.1) \times 10^{-3}$	for $m_{4\pi} < 2$ GeV
	$B(J/\psi \to \gamma X_{0^-}) \cdot B(X_{0^-} \to \rho\rho) = (4.7 \pm 0.3 \pm 0.9) \times 10^{-3}$	for $m_{4\pi} < 2$ GeV
	$B(J/\psi \to \gamma f_2(1720)) \cdot B(f_2(1720) \to \rho\rho) < 5.5 \times 10^{-4}$	
	$B(J/\psi \to \gamma g_T(2.1\text{–}2.4)) \cdot B(g_T(2.1\text{–}2.4) \to \rho\rho) < 6.0 \times 10^{-4}$	
DM2 [346]	$B(J/\psi \to \gamma\pi^+\pi^-\pi^+\pi^-) = (4.32 \pm 0.14 \pm 0.73) \times 10^{-3}$	for $m_{4\pi} < 3$ GeV
	$B(J/\psi \to \gamma\pi^+\pi^-\pi^+\pi^-) = (2.08 \pm 0.13 \pm 0.35) \times 10^{-3}$	for $m_{4\pi} < 2$ GeV
	$B(J/\psi \to \gamma\rho\rho)_{0^-} = (7.2 \pm 0.3 \pm 1.2) \times 10^{-3}$	
	$B(J/\psi \to \gamma X_{0^-}(1.5)) \cdot B(X(1.5) \to \rho\rho) = (3.3 \pm 0.12 \pm 0.8) \times 10^{-3}$	
	$B(J/\psi \to \gamma X_{0^-}(1.8)) \cdot B(X(1.8) \to \rho\rho) = (2.1 \pm 0.3 \pm 0.6) \times 10^{-4}$	
	$B(J/\psi \to \gamma X_{0^-}(2.1)) \cdot B(X(2.1) \to \rho\rho) = (1.2 \pm 0.03 \pm 0.3) \times 10^{-3}$	
	$B(J/\psi \to \gamma f_1(1285)) \cdot B(f_1(1285) \to \rho^0\pi^+\pi^-) = (3.4 \pm 0.8 \pm 0.5) \times 10^{-5}$	
	$B(J/\psi \to \gamma f_2(1720)) \cdot B(f_2(1720) \to \rho\rho) < 2.4 \times 10^{-4}$	
	$B(J/\psi \to \gamma g_T(2.0\text{–}2.45)) \cdot B(g_T(2.0\text{–}2.45) \to \rho\rho) < 2.7 \times 10^{-4}$	

6.4.5.2. The decay $J/\psi \to \gamma\omega\omega$. The process $J/\psi \to \gamma\omega\omega$ with $\omega \to \pi^+\pi^-\pi^0$ has been observed by Mark III [350] and DM2 [351] in final states with four charged pions and five photons. The detection and analysis of so many particles in the final state is experimentally not easy. The constraint imposed by the narrowness of the ω helps to extract an ωω signal from combinatorial and ω4π backgrounds. The fact that the decays $J/\psi \to \omega\omega$ and $J/\psi \to \pi^0\omega\omega$ are forbidden by *C* parity allows one to identify the radiative process $J/\psi \to \gamma\omega\omega$.

The ωω invariant mass distribution is shown in fig. 92. The spectrum features a shape quite different from the expectation of s wave or p wave phase space (fig. 92b). It shows a resonant-like structure at low ωω masses just above threshold, similar to $J/\psi \to \gamma\rho\rho$. Due to the lower statistics a possible two-peak structure as in the ρρ case cannot be resolved. The branching fractions for ωω production are given in table 42.

The spin parity of the ωω system has been analysed [350, 351] by exploiting the information contained in the orientation of the angle between the ω decay planes [347] and by performing multi-channel likelihood analyses similar to the one employed for the ρρ system. Clear evidence for 0^- spin parity for ωω invariant masses below 2 GeV is found. The distribution of χ, the angle between the two ω decay planes, is displayed in fig. 93 for events with ωω masses below 2 GeV. Upper limits for

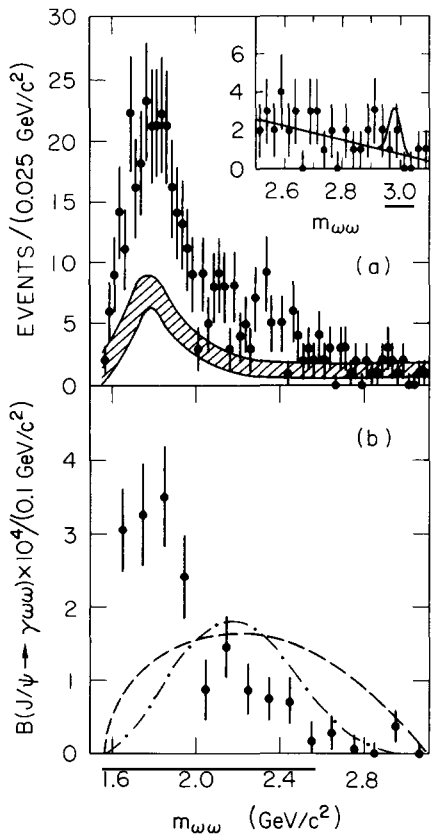

Fig. 92. Radiative ωω production. (a) Invariant ωω mass distribution (Mark III). The band represents the background. The inset displays the mass region from 2.5 to 3.1 GeV with the 90% C.L. curve of the η_c superimposed. (b) $B(J/\psi \to \gamma\omega\omega)$ as a function of $m_{\omega\omega}$. The curves represent s wave (dashed) and p wave (dash-dotted) phase space.

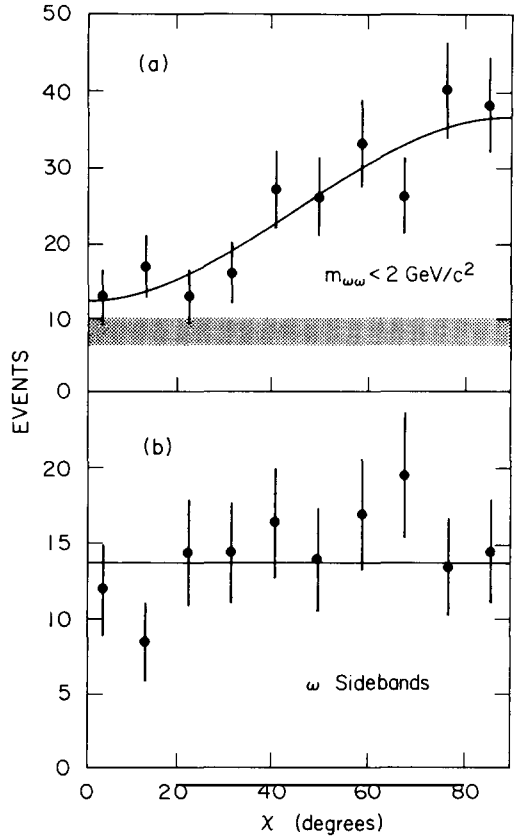

Fig. 93. Evidence for dominant 0^- spin parity of the ωω system. Distributions of χ, the angle between the ω decay planes for (a) $m_{\omega\omega} < 2$ GeV and (b) ω sideband events. The curves are fits with (a) $a + b \sin^2\chi$ and (b) a constant. The magnitude of a flat background is indicated by the band in (a) (Mark III [350]).

Table 42
Branching ratios for the decay $J/\psi \to \gamma\omega\omega$

Experiment	Branching ratio or 90% C.L. upper limit
Mark III [350]	$B(J/\psi \to \gamma\omega\omega) = (1.76 \pm 0.09 \pm 0.45) \times 10^{-3}$
	$B(J/\psi \to \gamma\omega\omega) = (1.22 \pm 0.07 \pm 0.31) \times 10^{-3}$ for $m_{\omega\omega} < 2$ GeV
	$B(J/\psi \to \gamma f_2(1720)) \cdot B(f_2(1720) \to \omega\omega) < 2.4 \times 10^{-4}$
	$B(J/\psi \to \gamma g_T(2.1\text{–}2.4)) \cdot B(g_T(2.1\text{–}2.4) \to \omega\omega) < 2.6 \times 10^{-4}$
DM2 [351]	$B(J/\psi \to \gamma\omega\omega) = (1.42 \pm 0.20 \pm 0.42) \times 10^{-3}$
	$B(J/\psi \to \gamma\omega\omega) = (1.06 \pm 0.16 \pm 0.32) \times 10^{-3}$ for $m_{\omega\omega} < 2$ GeV
	$B(J/\psi \to \gamma g_T(2.0\text{–}2.5)) \cdot B(g_T(2.0\text{–}2.5) \to \omega\omega) < 1.3 \times 10^{-4}$

$J^P = 2^+$ production at the $f_2(1720)$ mass and the mass region above 2 GeV, where 2^+ $\phi\phi$ production has been observed in hadronic decays [342], are included in table 42.

6.4.5.3. The decay $J/\psi \to \gamma\omega\phi$. The OZI violating radiative decay $J/\psi \to \gamma\omega\phi$ has been observed by Mark III [352] in the $\gamma K^+K^-\pi^+\pi^-\pi^0$ final state using 5.8×10^6 J/ψ decays. The invariant $\omega\phi$ mass distribution is shown in fig. 94. The statistical significance is marginal and no resonance structures are evident. The branching fraction is

$$B(J/\psi \to \gamma\omega\phi) = (1.40 \pm 0.25 \pm 0.28) \times 10^{-4}. \tag{141}$$

An upper limit for the ξ(2230) corresponds to the value

$$B(J/\psi \to \gamma\xi(2230)) \cdot B(\xi(2230) \to \omega\phi) < 0.6 \times 10^{-4} \quad \text{at 90\% C.L.} \tag{142}$$

The observation of $J/\psi \to \gamma\omega\phi$ clearly shows the importance of the doubly OZI violating amplitude, which amounts to 0.3 to 0.5 of the allowed singly disconnected amplitude.

6.4.5.4. The decay $J/\psi \to \gamma\phi\phi$. The decays $J/\psi \to \gamma K^+K^-K^+K^-$ and $J/\psi \to \gamma K^+K^-K_S^0K_L^0$ have been analysed to search for $J/\psi \to \gamma\phi\phi$ [353, 354]. This decay mode has been used to determine the η_c spin parity [232]. However, the detection efficiency for a clean observation of the γ4K final state decreases

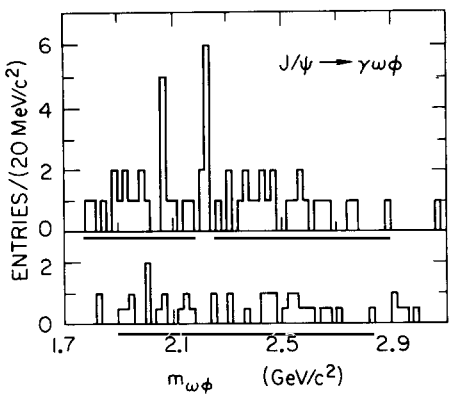

Fig. 94. Radiative ωφ production. Invariant ωφ mass distribution (Mark III [352]) for the ω signal region (top) and ω sidebands (bottom).

rapidly towards smaller $m_{\phi\phi}$. By exploiting the abilities of the detector to its limits, relaxing the kaon identification criteria, and by using kinematic fits with only one constraint (1C), one can recuperate part of the events lost by inefficiencies. Both DM2 [353] and Mark III [354] have done this. The resulting $\phi\phi$ invariant mass distributions are shown in fig. 95.

Apart from the η_c, which is observed by both groups [232, 235], a low-mass structure around 2.2 GeV is evident. The total $\phi\phi$ production branching fraction is [353]

$$B(J/\psi \to \gamma\phi\phi) = (3.1 \pm 0.3 \pm 0.6) \times 10^{-4} . \tag{143}$$

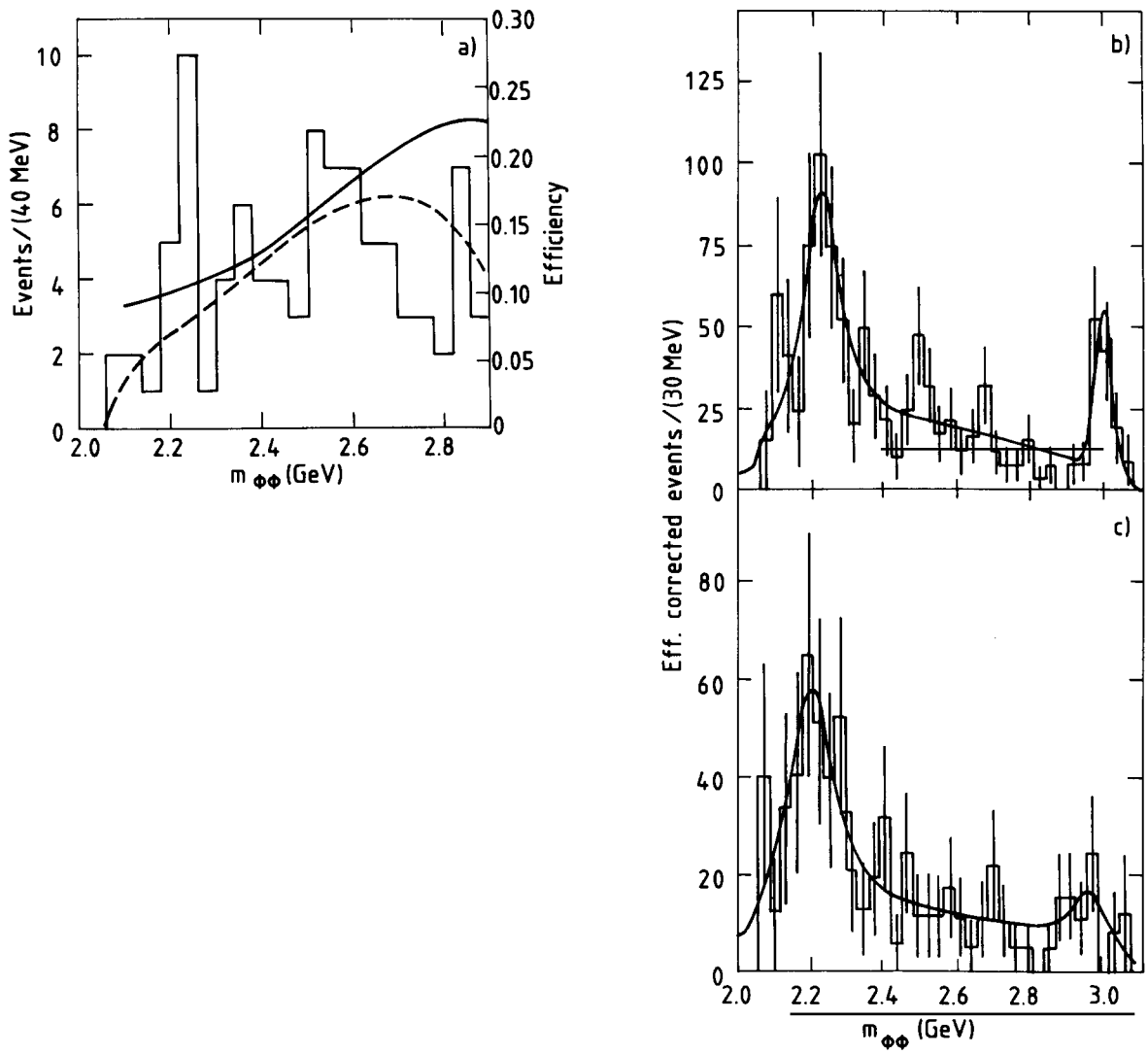

Fig. 95. Radiative $\phi\phi$ production. Invariant $\phi\phi$ mass distributions from $J/\omega \to \gamma\phi\phi$. (a) $J/\psi \to \gamma K^+K^-K^+K^-$ (DM2), (b) $J/\psi \to \gamma K^+K^-K^+K^-$ (Mark III), corrected for efficiency, (c) $J/\psi \to \gamma K^+K^-K_S^0K_L^0$ (Mark III), corrected for efficiency. In (a) the curves represent the detection efficiency (solid line) and the expectation from $\gamma\phi\phi$ phase space (dashed line). In (b) and (c) the curves are fits to the efficiency corrected distributions with two Breit–Wigner resonances [X(2.2) and η_c] plus phase space.

For the peak at 2.2 GeV ($\Gamma \sim 100$ MeV) one obtains*)

$$B(J/\psi \to \gamma X(2.2)) \cdot B(X(2.2) \to \phi\phi) = (3.2 \pm 0.5 \pm 0.6) \times 10^{-4} \quad \text{(Mark III)}. \tag{144}$$

Despite the much too large width of the X(2.2) peak it is tempting to assign the $\xi(2230)$ to this observation. A spin parity investigation, however, [353, 354] prefers spin parity 0^- for this structure. While this would rule out the identification of the $\xi(2230)$ [329] with this state—the $\xi(2230)$, decaying to $K\bar{K}$, cannot have odd parity—it is puzzling why the four *vector–vector* final states $\rho\rho$, $\omega\omega$, $\phi\phi$, and $K^*\bar{K}^*$ all show pseudoscalar structures near threshold.

DM2 has also looked for a 2^{++} component in their spin analysis in order to search for $\phi\phi$ signals in the mass region between 2.0 and 2.5 GeV, which have first been reported by Etkin et al. [342]. Although no evidence for resonant structures is obtained they find that after a subtraction of the events coming from X(2.2) the remaining events are compatible with a 2^{++} hypothesis. However, they cannot definitively rule out other assignments. The branching fraction is

$$B(J/\psi \to \gamma + \{\phi\phi\}_{2^{++}}) = (1.8 \pm 0.3 \pm 0.6) \times 10^{-4}. \tag{145}$$

This is in conflict with an upper limit from Mark III, using a fit to the χ angle rather than a multi-channel fit, for which they obtain [348]

$$B(J/\psi \to \gamma + \{\phi\phi\}_{2^{++}}) < 0.86 \times 10^{-4} \quad \text{at 90\% C.L.}, \tag{146}$$

where $\{\phi\phi\}_{2^{++}}$ is the 2^{++} component in the mass region from 2.0 to 2.4 GeV.

6.4.5.5. The decay $J/\psi \to \gamma K^*\bar{K}^*$. The decay $J/\psi \to \gamma K^{*0}\bar{K}^{*0}$ is observed in the $\gamma K^+K^-\pi^+\pi^-$ final state [355]. Similar to the $\rho^0\rho^0$ case large backgrounds which cannot be discriminated on an event by event basis cause a major experimental difficulty. Here the main background comes from $J/\psi \to K^*(892)K^*(1430) \to K^+K^-\pi^+\pi^-\pi^0$, where one of the π^0 decay photons escapes detection. These background events can be reduced by sophisticated kinematic fitting to several hypotheses keeping only the particle combination with the best fit χ^2. Also possible is a statistical background subtraction from the final spectrum as described in section 3.4.

The invariant $K^{*0}\bar{K}^{*0}$ mass distribution is shown in fig. 96. The measured branching fraction is [355]

$$B(J/\psi \to \gamma K^{*0}\bar{K}^{*0}) = (2.8 \pm 1 \pm 4) \times 10^{-3}. \tag{147}$$

A preliminary investigation of the distribution of χ, the angle between the K* decay planes, also points to a pseudoscalar structure just above $K^*\bar{K}^*$ threshold similar to the observations made in the $J/\psi \to \gamma$ vector–vector decays described in the previous sections.

6.4.6. The pseudoscalar puzzle in radiative J/ψ *decays*

The discovery of pseudoscalar structures in $J/\psi \to \gamma$ vector–vector decays with relatively large branching fraction has created a puzzling situation [349]. With the reported evidence for the $\eta(1400)$ [279] the pseudoscalar sector of $q\bar{q}$ states is the best known to date. More than enough pseudoscalar

*) Average of Mark III data on $\gamma K^+K^-K^+K^-$ and $\gamma K^+K^-K_S^0K_L^0$ [354].

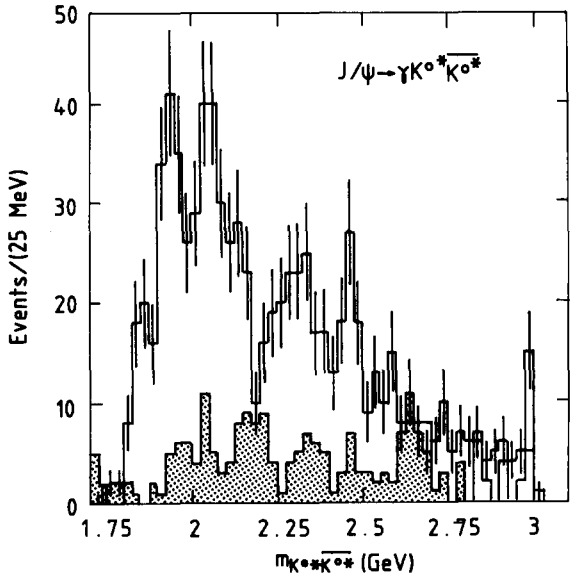

Fig. 96. Radiative $K^*\bar{K}^*$ production. $K^{*0}\bar{K}^{*0}$ mass distribution for events from $J/\psi \to \gamma K^+K^-\pi^+\pi^-$. The dotted spectrum represents the background. The data are from Mark III [355].

states to fill the ground state and radial excited state multiplets are established. In addition, yet unassigned pseudoscalar states and structures have been reported. They are:

the "iota"/$\eta(1440)$ (BR $\sim 5 \times 10^{-3}$),

the 0^- structures at ~1.55 GeV, ~1.8 GeV, ~2.1 GeV in $J/\psi \to \gamma\rho\rho$ (BR $\sim 10^{-3}$),

the 0^- structure below 2 GeV in $J/\psi \to \gamma\omega\omega$ (BR $\sim 10^{-3}$),

the 0^- structure below 2 GeV in $J/\psi \to \gamma K^*\bar{K}^*$ (BR $\sim 10^{-3}$),

the 0^- structure at ~2.2 GeV in $J/\psi \to \gamma\phi\phi$ (BR $\sim 3 \times 10^{-3}$),

the various peaks in the $\eta\pi\pi$ invariant mass distribution with as yet unknown spin parities (BR $\sim 3 \times 10^{-3}$).

Not all of these can possibly be explained as conventional $q\bar{q}$ states, especially since the second radial excitation states are expected to be heavier than ~2 GeV. Apart from this the $J/\psi \to \gamma X$ production rate for a radially excited state is expected to be suppressed as compared to the ground state [300, 308]. It seems therefore unlikely that the large branching ratio states $\eta(1440)$ and the pseudoscalar structures in $J/\psi \to \gamma VV$, $V = \rho$, ω are $q\bar{q}$ states. It seems also far fetched to believe that they are all different new objects, may be even different pseudoscalar glueballs.

Attempts to clarify this situation have been made. A possible description of part of the data in terms of coupled channels is described in the following section. Another approach, interpreting the measured spin characteristics by a quark–quark rescattering effect is discussed in ref. [356].

6.4.6.1. A coupled channel analysis of "iota" decays. An attempt has been made [349] to interpret the data on $J/\psi \to \gamma K\bar{K}\pi$, $\gamma\rho\rho$, $\gamma\omega\omega$, and $\gamma\gamma\rho$ jointly in an analysis with coupled channels. This has also been suggested by Achasov and Shestakov [357] in a similar approach. The key feature of this analysis is to describe the 0^- states in $J/\psi \to \gamma\rho\rho$ and $\gamma\omega\omega$ at threshold with one underlying state, the "iota". The different masses and widths measured in the various channels then arise from phase space differences

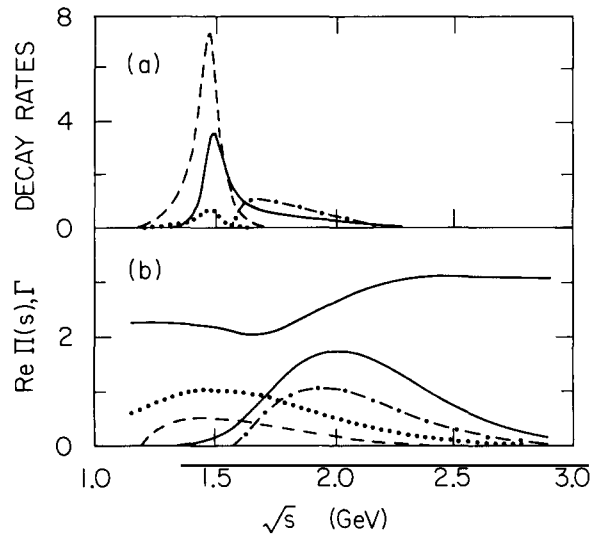

Fig. 97. The effect of coupled channels on decay rates and partial widths. (a) Coupled channel Breit–Wigner amplitude squared for the channels $K\bar{K}\pi$ (dashed), ρρ (solid), ωω (dashed–dotted), and γρ (dotted) in arbitrary units. (b) Re $\Pi(s)$ (upper curve) and Γ_i, the partial widths, as a function of $\sqrt{s}$. The curve for $\Gamma_{\gamma\rho}$ (dotted line) has been multiplied by 100.

and coupled channel effects. The details of this approach are described in ref. [349]. The mass distributions of four channels are fitted with this ansatz. The "iota" pole position, its total width in the $K\bar{K}\pi$ decay mode, and the ratios of coupling constants are the parameters of the fit. Figure 97 shows the expected resonance shapes of the four channels in question. Figure 98 shows the result of a joint fit superimposed on the Mark III data on the four channels after background subtraction for ωω and γρ and after correcting for relative efficiencies.

The ~1.55 GeV peak of the ρρ(4π) mass spectrum can be explained by a resonance (the "iota"?) below ρρ threshold. Another resonance, which is assumed not to couple to $K\bar{K}\pi$ but to ρρ, ωω, and γρ,

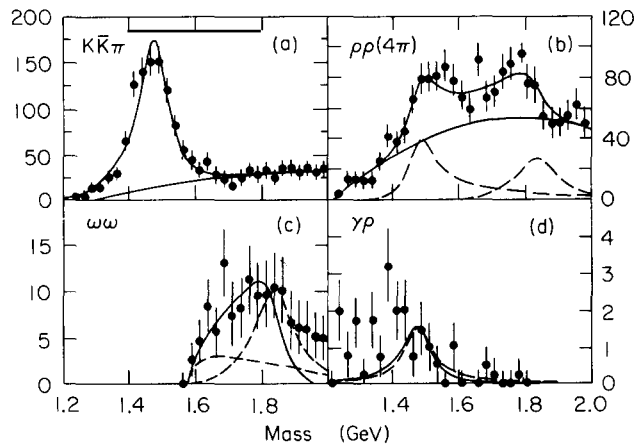

Fig. 98. Coupled channel fits to four decay channels. Invariant mass distributions for (a) $K\bar{K}\pi$, (b) 4π representing ρρ (≈50%), (c) ωω and (d) γρ (Mark III), corrected for relative efficiencies (arbitrary units, 0.025 GeV bins). The curves represent the result of a fit with coupled channels.

must be included to explain the ρρ(4π) spectrum. With this ansatz the ρρ and ωω spectra can be roughly described. The ratio of ρρ to ωω coupling constants is predicted by SU(3) to be three; the fit yields 5.0 ± 0.7, in reasonable agreement. The shape of the γρ mass spectrum is not well reproduced. The absence of phase space effects near threshold in this channel requires the peak of the Breit–Wigner curve to be at the same position as for the $K\bar{K}\pi$ channel, i.e., ~1.46 GeV. Furthermore, vector dominance predicts a ratio of $f_\rho^2/e^2 \cdot \frac{3}{2} \approx 400$ for the ratio of ρρ to γρ couplings. The fit requires 3300 ± 600. If the γρ signal were to be identified with the η(1440)*), this large coupling ratio would certainly cause some inconsistency.

The following approximate branching ratios result from the coupled channel analysis [349]:

$$B(J/\psi \to \gamma\eta(1440)) \cdot B(\eta(1440) \to \rho\rho) \approx (1.5 \pm 0.2) \times 10^{-3} ,$$

$$B(J/\psi \to \gamma\eta(1440)) \cdot B(\eta(1440) \to \omega\omega) \approx (0.3 \pm 0.1) \times 10^{-3} , \tag{148}$$

$$B(J/\psi \to \gamma X(1800)) \cdot B(X(1800) \to \rho\rho) \approx (1.0 \pm 0.2) \times 10^{-3} ,$$

where X(1800) is the ~1.8 GeV enhancement in the ρρ mass spectrum. Using the average value for $J/\psi \to \gamma\eta(1440) \to K\bar{K}\pi$ one arrives at a total production fraction, summing $K\bar{K}\pi$, ρρ and ωω, of

$$B(J/\psi \to \gamma\eta(1440)) = (6.3 \pm 0.5) \times 10^{-3} . \tag{149}$$

The coupled channel analysis provides a first hint that the branching fraction to the "iota" may be even larger than deduced from the $K\bar{K}\pi$ channel alone and that decays to non-strange final states, which can restore flavour symmetry of "iota" decays, might exist.

We would like to point out two "caveats", i.e. inconsistencies, that must be solved before the above conclusions from the coupled channel fits can be regarded as solid.

1. The upper limit for γγ production of the η(1440) is [358]

$$\Gamma(\eta(1440) \to \gamma\gamma) \cdot B(\eta(1440) \to K\bar{K}\pi) < 1.6\,\text{keV} . \tag{150}$$

Using vector dominance for the ρρ/γγ couplings one safely predicts from (148) a γγ width of the order of 0.1 keV. However, ρρ phase space decreases by more than two orders of magnitude in the region between 1.55 and 1.4 GeV. Taking this into account at 1.46 GeV, the best present estimate of the "iota" mass, the above 0.1 keV must be multiplied by a factor 100 ± 50, which is above the experimental upper limit for $\Gamma(\eta(1440) \to \gamma\gamma)$.

2. The ηππ invariant mass distribution of $J/\psi \to \gamma\eta\pi^+\pi^-$ (fig. 88) shows—apart from the low-mass peaks near 1280 and 1400 MeV—an additional two-peak structure at ~1.6 GeV and ~1.85 GeV with mass and width values close to the ones observed in $J/\psi \to \gamma\rho\rho$. A spin parity analysis of the ηππ spectrum has unfortunately not yet been done. Let us, notwithstanding other possibilities, assume that the ηππ and ρρ structure have the same origin. Since the ηππ decay does not suffer any strong phase space suppression one would have to conclude that the ηππ structure cannot be due to the "iota". The 1.5 GeV peaks in ρρ and ηππ must therefore either come from different states with about the same mass and width values or come from the same resonance which then cannot be the "iota".

*) Note that is this is still a question which is experimentally unsolved.

Table 43
Radiative final states containing baryons. The results have been averaged assuming uncorrelated errors. Upper limits are given at the 90% C.L.

Final state	Branching ratio (units of 10^{-4})	Experiment
$p\bar{p}$	$3.8 \pm 0.7 \pm 0.7$	Mark II [185]
	$4.89 \pm 0.24 \pm 0.43$	Mark III [189]
	$3.3 \pm 0.3 \pm 0.7$	DM2 [359]
	4.3 ± 0.4	⟨average⟩
$p\bar{p}\pi^+\pi^-$	<7.9	Mark II [185]
$\Lambda\bar{\Lambda}$	<1.3	DM2 [186]

Summarizing we conclude that the coupled channel analysis reveals a possibility to understand the puzzle of too many pseudoscalar states. Despite some obvious deficiencies and potential problems of this ansatz it is an appealing approach to describe the tantalizing wealth of data. An attempt to decompose the spin parity content of the $\eta\pi\pi$ mass spectrum would surely help to clarify the facts. Refined analyses with coupled channels using more than twice the statistics are in progress [310, 351].

6.5. Radiative decays to baryon–antibaryon pairs

The Mark I [184], Mark II [185], Mark III [189], and DM2 [186, 359] Collaborations have investigated radiative J/ψ decays leading to baryonic final states (see table 43). The study of $J/\psi \to \gamma p\bar{p}$ decays is an interesting area to explore the spectra of mesons and baryonia [360], which decay to baryons in the 2 to 3 GeV mass range, with excellent mass resolution (≈7 MeV). Figure 99 shows the $p\bar{p}$ mass spectra obtained by DM2 [359] and Mark III [189] in $J/\psi \to \gamma p\bar{p}$.

Apart from a small η_c signal (see table 28), the $p\bar{p}$ mass spectra do not show any statistically significant signs for additional narrow structures. In particular no signal is apparent in the ξ(2230) mass region (see table 39 for an upper limit). Taking into account the drop in efficiency at low $p\bar{p}$ mass, the spectra show enhancements at threshold.

Calculations [223] based on lowest-order perturbative QCD predict similar shapes but underestimate the rate.

It has been suggested that the ξ(2230) is a $\Lambda\bar{\Lambda}$ bound state [338]. When searching for radiative $\Lambda\bar{\Lambda}$ production the observed [186] $\Lambda\bar{\Lambda}$ mass spectrum (not shown) contains only a few events below 3 GeV, which are difficult to attribute to the radiative $J/\psi \to \gamma\Lambda\bar{\Lambda}$ decay because of the presence of several background processes involving photons. Upper limits for the excitation of $\eta_c(2980)$ and ξ(2200) are included in table 28 and table 39, respectively.

7. The quest of glueballs

The non-abelian nature of QCD together with QCD inspired models have lead to the general belief that bound states of gluons should exist. Where are these glueballs and how can they be found?

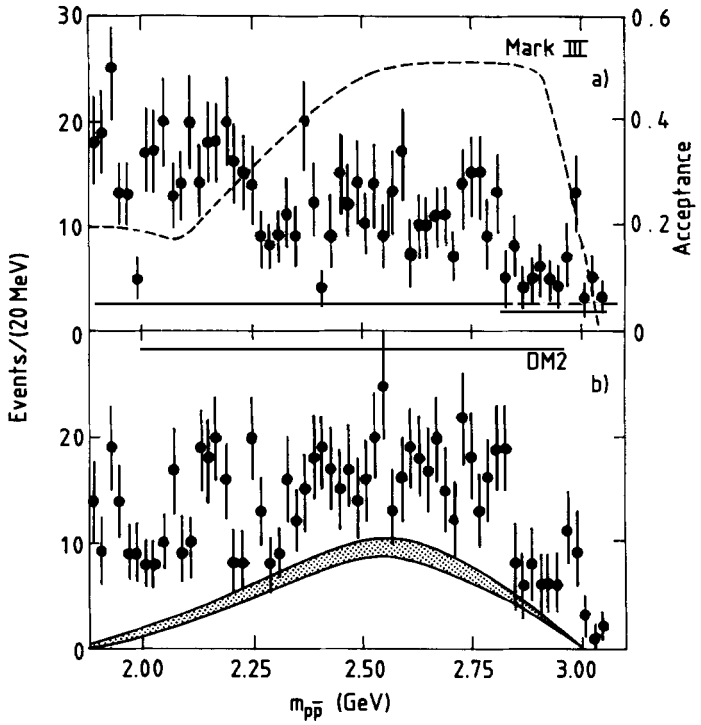

Fig. 99. $p\bar{p}$ invariant mass spectra in radiative J/ψ decays. Shown are $p\bar{p}$ mass distributions obtained by (a) Mark III and (b) DM2. In (a) the efficiency for $p\bar{p}$ pairs is indicated by the dashed line. The band in (b) represents the background remaining from $J/\psi \to p\bar{p}\pi^0$ decays.

Today's hadron spectroscopy is largely motivated by the search for glueballs and other exotics. A complete understanding of ordinary mesons is a necessary condition for a systematic approach to the problem. Only a reasonably complete understanding of all the available data will reveal any conclusive evidence for glueballs.

The J/ψ radiative decays are commonly regarded as *the* hunting ground for glueballs. Nevertheless, to write about glueball spectroscopy solely based on results from J/ψ decays would not only be incomplete and biased but would also do injustice to the beautiful data available from hadro- and photoproduction [361, 362] and from photon–photon [363] experiments. On the other hand, it is much beyond the scope of this report to cover all aspects of glueball spectroscopy.

We will therefore proceed along the following line. We take the point of view that the lowest lying gluonium states ($J^{PC} = 0^{++}$, 0^{-+}, 2^{++}), which are expected to have masses accessible in J/ψ decays, *must*, if they exist, at some level be observable in radiative decays of the J/ψ (fig. 57). We will try to specify features, mostly qualitative or semi-quantitative in nature, that are expected to be characteristic for glueballs and are suited to distinguish them from ordinary mesons. Since the spectroscopy of the light quark mesons is dominated by the valence quarks there is reason to hope that also a simple-minded view of gluonium states may be qualitatively correct [48]. We then point out possible candidates for the three gluonium spin states in question and discuss the arguments supporting or weakening their glueball identity. Only here will we incorporate information from other, non-J/ψ decay, experiments and will indicate which valuable pieces of information are still missing. It will be impossible to always mark off gluonium against gg–$q\bar{q}$ mixtures, $q\bar{q}g$ hybrids, or other more exotic possibilities, in the

arguments; we will therefore concentrate on arguments that support the case against a $q\bar{q}$ state hypothesis. Following these lines we hope to be able to convince the reader that very strong candidates for the 0^{-+} and 2^{++} glueball states have been observed in radiative J/ψ decays and that the search for the scalar glueball is also promising.

7.1. Glueballs versus $q\bar{q}$ mesons

In the discussion of radiative decays we have seen that in almost every final state studied, previously unobserved phenomena have been discovered, new states which naturally have to be considered also as glueball candidates. However, the production of a state in radiative decays of the J/ψ does not necessarily mean that it is made of gluonic matter. After all, well-established $q\bar{q}$ resonances have also been seen in this "glue enriched" environment.

Lacking precise predictions either for masses and widths or for production and decay characteristics of "glueballs", which would be invaluable to identify these objects, one has to rely on qualitative guidance in the search for glueball candidates. In the following list of qualitative arguments for glueball searches we start from the assumption that the diagram of fig. 4c is dominant in radiative J/ψ decays. That is, the photon is radiated off from the initial state quark line and the $c\bar{c}$ system annihilates into two gluons. With this assumption one can identify the following guidelines for gluonium searches:

1. Glueballs with masses accessible in radiative J/ψ decays are expected to be copiously produced compared to the production of pure $q\bar{q}$ states. To set the scale, η and η′, which appear to have no strong gluonic components [131, 121], are produced in radiative J/ψ decays with branching fractions of about 0.1% and 0.4%, respectively. Note that the η′ is mostly an $SU(3)_{flavour}$ singlet.

2. Gluons do not carry quark flavour because they are singlets with respect to $SU(3)_{flavour}$. The decays of gluon bound states therefore should—apart from SU(3) breaking effects—proceed in a flavour-symmetric way. While this is true for the gluon–quark couplings, the actual decay rates will depend on the available phase space and possible dynamical effects (see section 2.4).

3. Gluons do not couple to photons, at least not without forming an intermediate $q\bar{q}$ state. Notwithstanding the possibility that mixing of gluonium and $q\bar{q}$ mesons may confuse a quantitative conclusion the absence or strong suppression of a candidate state in photon–photon collisions together with a large production rate in radiative J/ψ decays provides a strong constraint on the nature of the state.

4. Glueball production in hadronic decays of the J/ψ (fig. 100b) is expected to be suppressed with respect to $q\bar{q}$ meson production when the singly OZI disconnected diagram of fig. 100a (SOZI) represents the dominant contribution. For $q\bar{q}$ states the doubly OZI disconnected diagram of fig. 100c (DOZI) is strongly suppressed compared to the SOZI diagram. A direct comparison of the radiative production of a state X with its hadronic production in $J/\psi \rightarrow \{\omega, \phi\} + X$ proves to be an excellent tool to probe the quark/gluon content of a candidate state X.

5. Finally, the complete understanding of the $q\bar{q}$ sector, the ground state and excited $q\bar{q}$ meson nonets, is essential to fully reveal the non-$q\bar{q}$ nature of a gluonium candidate state. If there is no vacant place left in the SU(3) $q\bar{q}$ multiplets for a given J^P, the gluonium hypothesis for a new state has to be taken more seriously.

In the following text, we shall use these points to discuss the candidates for pseudoscalar, tensor and scalar gluonium.

In the previous sections, hadronic and radiative J/ψ decays were treated separately, representing different classes of events. A most useful insight into the nature of resonances produced in both kinds

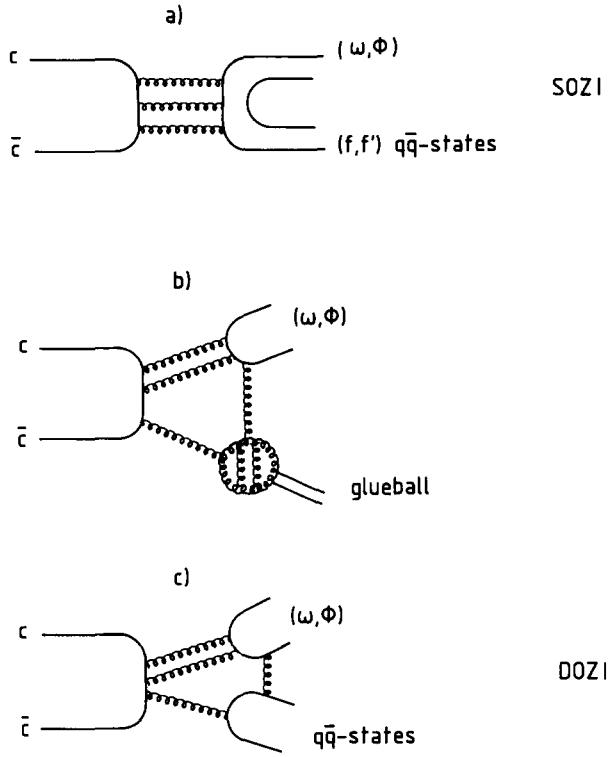

Fig. 100. J/ψ decay diagrams relevant to "glueball hunting". (a) Singly OZI suppressed (SOZI) diagram for $q\bar{q}$ production, dominant for, e.g., $J/\psi \to \omega f$, $J/\psi \to \phi f'$; (b) disconnected diagram for glueball production; (c) doubly OZI suppressed (DOZI) diagram for $q\bar{q}$ production, responsible for, e.g., $J/\psi \to \phi\pi\pi$.

of J/ψ decay processes is obtained by a direct comparison of the invariant mass spectra from

$$J/\psi \to \left\{ \begin{matrix} \gamma \\ \omega \\ \phi \end{matrix} \right\} + X\,, \tag{151}$$

where X represents $\pi\pi$, $K\bar{K}$, $K\bar{K}\pi$, $\eta\pi\pi$, or 4π.

The experimental information necessary for this study is obtained by the Mark III and DM2 Collaborations [142, 372]. The individual reactions are described in their respective sections. The direct comparison of the different reactions is done in fig. 101 to fig. 105, which, in a sense, also summarize the wealth of information on new and old states observed in J/ψ decays.

Ordinary $q\bar{q}$ mesons can be produced in *hadronic* J/ψ decays as shown by the diagrams of fig. 100a and c. The singly disconnected diagram (fig. 100a) is dominant and one may assume it to maintain $SU(3)_{flavour}$ symmetry by relegating $SU(3)_{flavour}$ breaking amplitudes to the corresponding electromagnetic diagram (fig. 4b) or to quark mass effects. Gluonium states can only couple to the outer quark lines through their $q\bar{q}$ admixtures or through diagrams as shown in fig. 100b. The doubly OZI disconnected diagrams (DOZI, fig. 100c) for $q\bar{q}$ production are strongly suppressed with respect to SOZI diagrams (fig. 100a) at least for $q\bar{q}$ nonets which are close to ideally mixed. The contribution of fig. 100b is expected lie in between the two others. For glueballs, Fritzsch and Minkowski [364] have

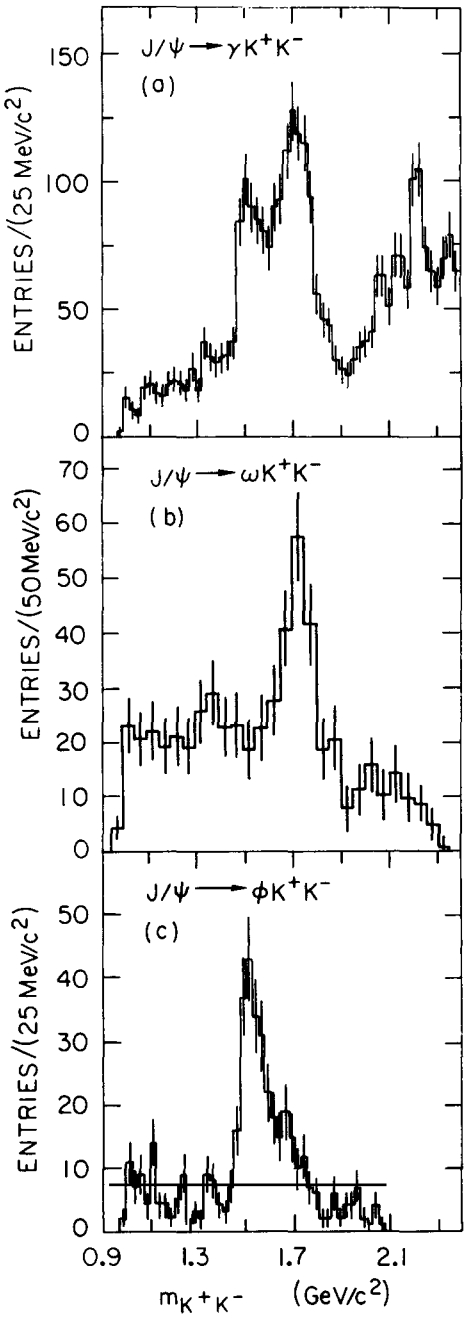

- $f_2'(1525)$, $f_2(1720)$ signals
- structure around 2.2 GeV

- $f_2(1720)$ signal
- no $f_2'(1525)$
- no $\xi(2230)$

- large $f_2'(1525)$
- shoulder due to $f_2(1720)$

Fig. 101. Comparison of $K\bar{K}$ invariant mass spectra. The $K\bar{K}$ system is recoiling against (a) a radiative photon, (b) an ω, and (c) a ϕ. The data are from Mark III.

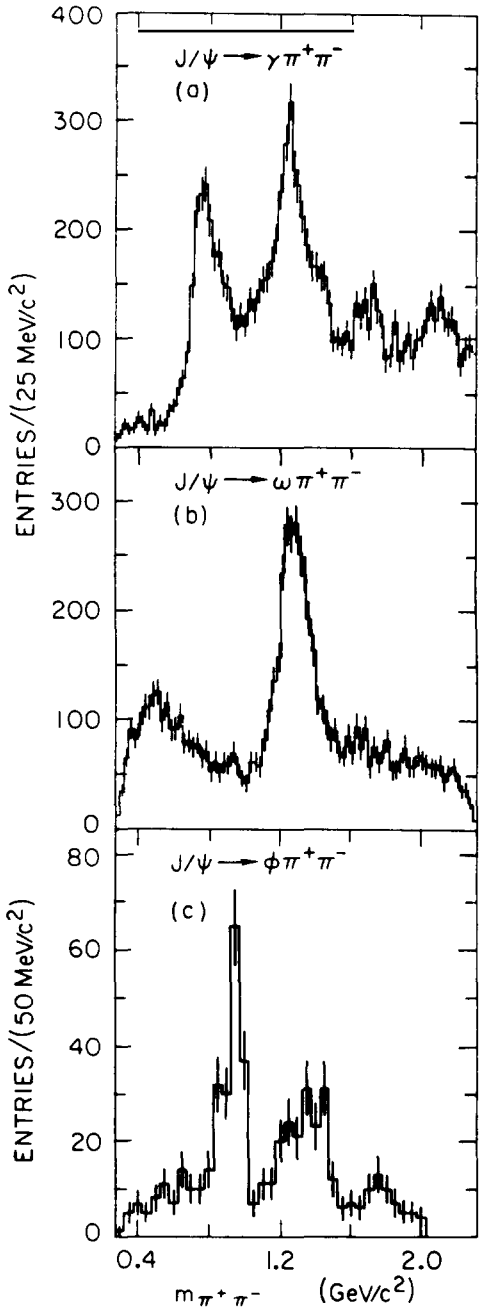

- $f_2(1270)$, $f_2(1720)$, $X(2.1)$ signals
- ρ signal from $J/\psi \to \rho\pi$ background
- high mass shoulder on $f_2(1270)$
- no obvious low mass scalars

- dominant $f_2(1270)$ signal
- broad low mass enhancement
- no $f_2'(1525)$, $f_2(1720)$ peaks
- no $f_2(1270)$ shoulder
- marginal or no $f_0(975)$

- large $f_0(975)$
- small $f_2(1720)$ signal
- structure at 1.2 − 1.5 GeV (may contain $f_2(1270)$)

Fig. 102. Comparison of $\pi\pi$ invariant mass spectra. The $\pi\pi$ system is recoiling against (a) a radiative photon, (b) an ω, and (c) a ϕ. The data are from Mark III.

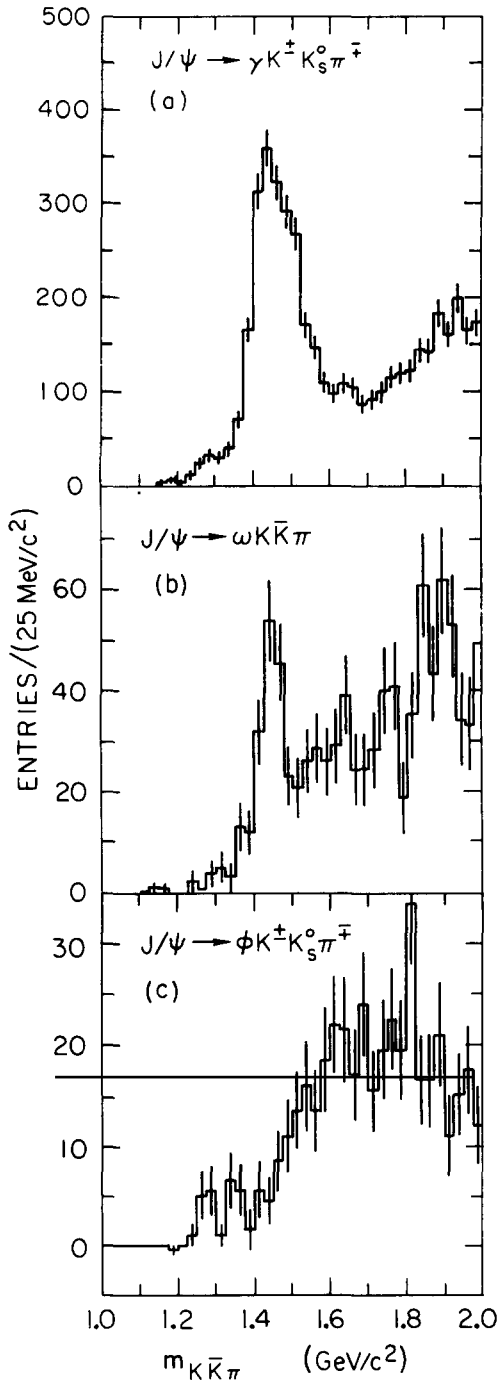

- dominant 'iota' structure
- $f_1(1420)$ signal
- too narrow for 'iota'
- no 'iota' signal
- no $f_1(1420)$
- events in $f_1(1285)$ region

Fig. 103. Comparison of $K\bar{K}\pi$ invariant mass spectra. The $K\bar{K}\pi$ system is recoiling against (a) a radiative photon, (b) an ω, and (c) a φ. The data are from Mark III.

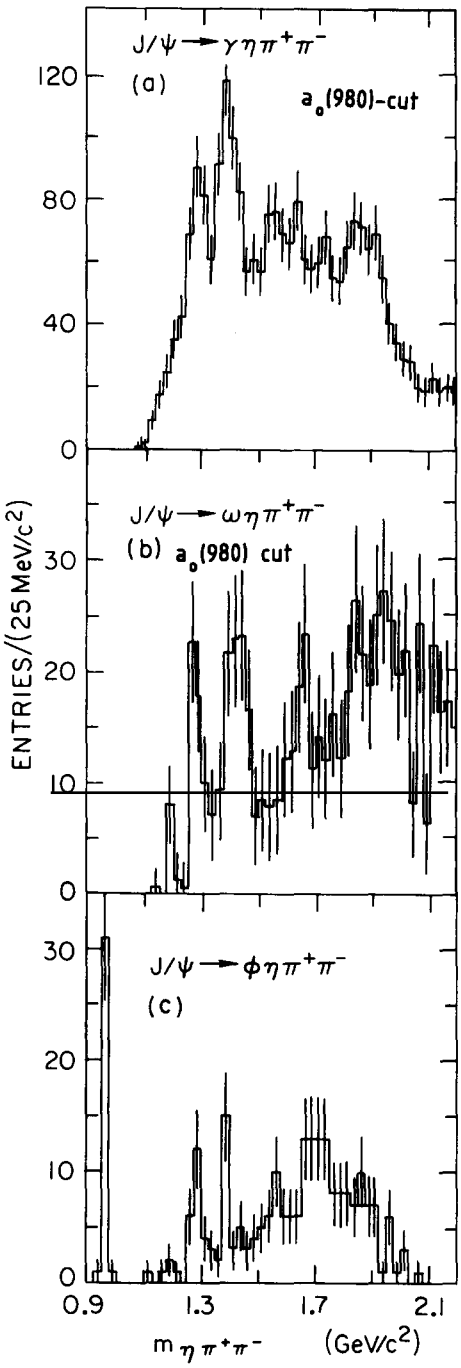

- signals in $f_1(1285)$, $f_1(1420)$ region
- no 'iota' signal
- further structures between 1.5 and 2.0 GeV

- possible $f_1(1285)$ and $f_1(1420)$ signals
- no 'iota' signal

- $f_1(1285)$ signal
- no 'iota' signal

Fig. 104. Comparison of $\eta\pi\pi$ invariant mass spectra. The $\eta\pi\pi$ system is recoiling against (a) a radiative photon, (b) an ω, and (c) a ϕ. $\eta\pi^+$ or $\eta\pi^-$ are required to be in the $a_0(980)$ mass region, except for (c). The data are from Mark III.

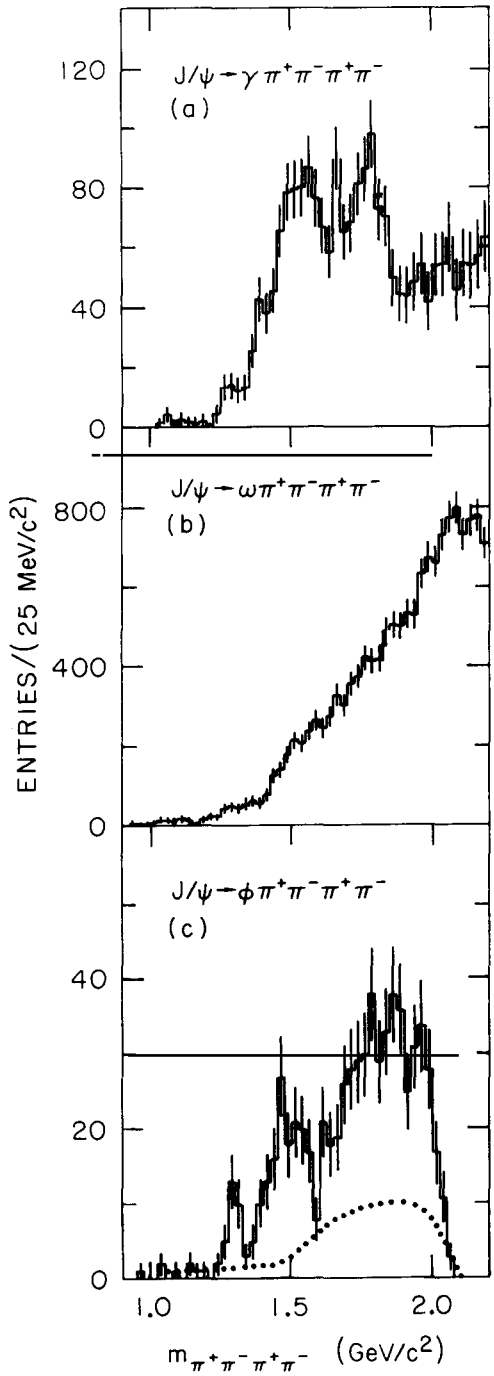

- $J^P = 0^-$ structures at ~1.55 GeV and ~ 1.8 GeV
- small $f_1(1285)$ signal
- no obvious resonant structures
- $f_1(1285)$ signal
- structure at ~1.5 GeV

Fig. 105. Comparison of 4π invariant mass spectra. The 4π system is recoiling against (a) a radiative photon, (b) an ω, and (c) a φ. In (c) the dotted line describes background from events that contain a φ. The data are from Mark III.

argued that the contribution of fig. 100b could even be of the same order of magnitude as that of fig. 100a.

In this context, the hadronic two-body decays containing either an ω or a φ are particularly useful since the vector meson acts as a "tag" of the flavour of the recoiling system, assuming that it is dominated by the diagram of fig. 100a. Expressed more simply, a resonance produced with a "φ" recoil tag should have a large $s\bar{s}$ content and conversely a resonance produced with an "ω" should have a large $u\bar{u} + d\bar{d}$ content.

If one assumes ideal mixing for the vector mesons one can write

$$\phi = |s\bar{s}\rangle = \frac{1}{\sqrt{3}}(\{1\} - \sqrt{2}\{8\}), \qquad \omega = \frac{1}{\sqrt{2}}(|u\bar{u}\rangle + |d\bar{d}\rangle) = \frac{1}{\sqrt{3}}(\sqrt{2}\{1\} + \{8\}),$$

and predict the ratio [371]

$$R_{\text{vector}} = \frac{\Gamma(J/\psi \to \omega X)}{\Gamma(J/\psi \to \phi X)} = 2 \text{ if X is an SU(3) singlet},$$

$$= \tfrac{1}{2} \text{ if X is an SU(3) octet}.$$

R_{vector} and R_γ, defined as

$$R_\gamma = \Gamma(J/\psi \to \gamma X)/\Gamma(J/\psi \to \{\omega, \phi\} + X),$$

provide a semi-quantitative argument in the search for glueballs. A glueball candidate is expected to have $R_{\text{vector}}(G) > 1$ and $R_\gamma(G) \gg 1$.

We have made comments in fig. 101 to fig. 105 on the right-hand side of the figures. These remarks do not always represent experimentally proven facts*) but are merely a possible, perhaps not too unlikely, interpretation of the data. They are necessary to guide the reader through the arguments which follow in the next sections.

Some general remarks are in order:

- While the production rate of η(1440) and $f_2(1720)$ is large in radiative decays, their rate in hadronic decays is suppressed compared to other pseudoscalar and tensor mesons. The comparison reveals possible evidence for the $f_2(1720)$ in the $J/\psi \to \{\omega, \phi\} + K\bar{K}$ reactions and no indication for the η(1440) in reactions other than $J/\psi \to \gamma + K\bar{K}\pi$.
- The production and decay of the $f_2(1720)$ in hadronic J/ψ decays do not show the pattern of nearly ideally mixed $q\bar{q}$ tensor states.
- Interesting phenomena are observed in radiative and OZI-violating hadronic decays in the 1400 MeV and 1500–1900 MeV mass regions. These phenomena are absent in OZI allowed reactions.
- The results on the $f_1(1285)$ and $f_1(1420)$ mass regions in the $K\bar{K}\pi$ and ηππ final states allow interesting speculations but remain inconclusive as long as full spin parity analyses on these spectra are missing.

In the following sections we shall discuss in more detail the three lowest lying glueball states, which are expected to have $J^{PC} = 0^{-+}$, 2^{++}, and 0^{++}. In doing this we shall often refer to the information contained in fig. 101 to fig. 105.

*) This is particularly so because spin parity measurements of the hadronic channels have not yet been performed in each case.

7.2. The 0^- glueball

We start by examining the 0^{-+} $q\bar{q}$ sector. For $J = 0$ there are ground state and radial excitations, but no orbital excitations. The 0^- ground state (1S) nonet is one of the best established $q\bar{q}$ multiplets. Its first radial excitation (2S) is also relatively well known. Eight of the nine members can be assigned to the isotriplet $\pi(1300)$, the strange quartet K(1460), and the $\eta(1275)$ [158, 159], all being established states. A most plausible assignment for the ninth member, the radially excited partner of η or η', is the $\eta(1400)$, observed in the reaction $\pi^- p \to \eta\pi\pi n$ at KEK [279] and in $\pi^- p \to K_S^0 K^+ \pi^- n$ at BNL [373] (cf. fig. 5). This state has been reported earlier by the MPS experiment at BNL [374] in $p\bar{p}$ annihilations at 6.6 GeV and may be even as early as 1963 at CERN [291]. In both cases the 0^{-+} assignment was discredited because of confusing [161] and still not unambiguously resolved controversies among different experiments (see section 6.4.1). The situation is much clearer in the $\eta\pi\pi$ final state. However, the $\eta(1400)$ appears to be mostly a $u\bar{u}$, $d\bar{d}$ state and is also too light to easily comply with most estimates for the mass of the radially excited $s\bar{s}$ state [375]. While it seems unlikely that the $\eta(1400)$ can be identified with the entire "iota"/$\eta(1440)$ structure, it could possibly be assigned to its low-mass portion and also to the 1390 MeV peak in $J/\psi \to \gamma\eta\pi\pi$.

Pseudoscalar resonances that do not easily fit into the 0^{-+} nonets are the "iota"/$\eta(1440)$, the pseudoscalar structures seen at threshold of the γ vector–vector decays, and the higher-mass peaks in the $\eta\pi\pi$ mass distribution.

Arguments that these states are not radial excitations are at hand. The measured branching fractions for these new pseudoscalar resonances are too large to be considered reasonable for a radially excited $q\bar{q}$ state. Frank and O'Donnel [308] estimate that the η_R' would have at least an order of magnitude lower production rate than the ground state η' if no gluonium is admixed. However, in models with large mixing of the $\eta(1440)$ with η and η' the radiative width of the J/ψ to a radial excitation can be substantial due to large cancellations in the amplitudes [376].

We are left with even too many candidates for the 0^- gluonium state. A plausible hypothesis has been outlined in section 6.4.6.1, assigning at least the ~1.55 GeV 0^- state in $\rho\rho$ and the $\omega\omega$ 0^- structure to the "iota". If one accepts this statement, the list of qualitative glueball features turns into an impressive score sheet for the "iota" being a glueball or having at least a large glue component.

It is produced with the largest branching fraction in radiative J/ψ decays, except for the M1 transition within the $c\bar{c}$ family, $J/\psi \to \gamma\eta_c$. This can be seen from fig. 106, where a direct comparison of production rates of various radiative decays is made. Gounaris et al. [377] predict a branching fraction of $B(J/\psi \to \gamma\eta(1440)) \approx 17 \times 10^{-3}$ in a model that assumes the $\eta(1440)$ to be a fairly pure glueball.

Moreover, the "iota" is not seen at all in association with an ω or a ϕ in hadronic J/ψ decays (see fig. 103). This indicates that neither a strong $u\bar{u}$, $d\bar{d}$ nor a strong $s\bar{s}$ component is present.

The "iota" is *not* observed in $\gamma\gamma$ collisions [358]. Expressed as the fractional $u\bar{u}$, $d\bar{d}$ content of the "iota", X_ι, the upper limit of eq. (131) corresponds to $|X_\iota|^2 \leq 0.05$ employing the formula

$$\Gamma(\text{"iota"} \to \gamma\gamma) = (m_{\text{iota}}/m_{\pi^0})^3 \tfrac{25}{9} |X_\iota + \tfrac{1}{5}\sqrt{2} Y_\iota|^2 \Gamma(\pi^0 \to \gamma\gamma)\,, \tag{152}$$

and assuming that either $|X_\iota| \geq |Y_\iota|$ or that X_ι and Y_ι have the same phase as expected by orthogonality with respect to the η wave function. The quantity "stickiness" [365],

$$S_X \propto \frac{\Gamma(J/\psi \to \gamma X)}{\Gamma(X \to \gamma\gamma)} \frac{\text{phase space}(X \to \gamma\gamma)}{\text{phase space}(J/\psi \to \gamma X)}\,, \tag{153}$$

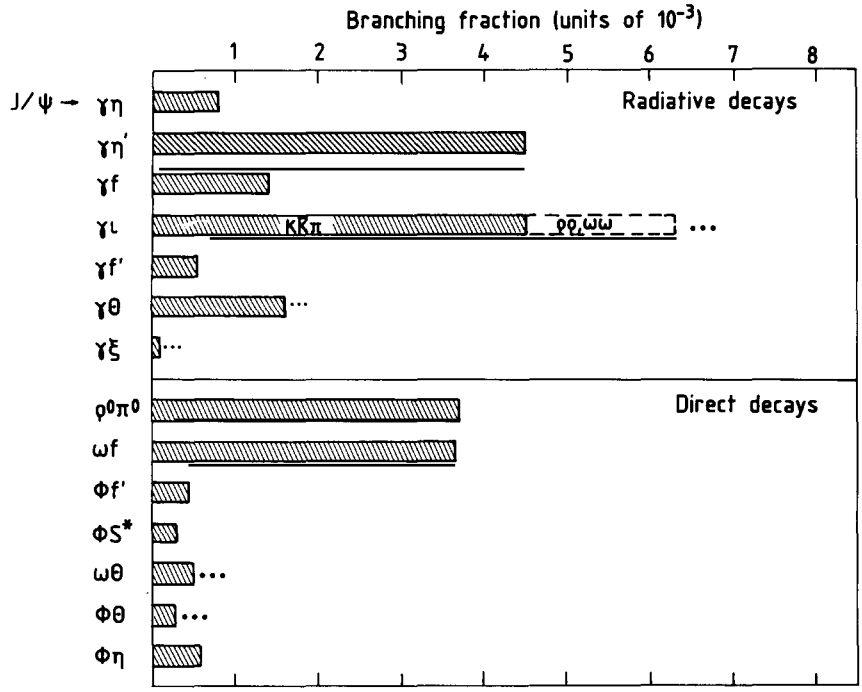

Fig. 106. Production rates for various states in radiative J/ψ decays. The rate for the η(1440) includes the estimates for ρρ and ωω (section 6.4.6.1).

is defined to quantify the comparison of radiative J/ψ production of glueball candidate states with their production in γγ processes. The second factor in (153) compensates for phase space differences and is proportional to $(m_X/p_X^*)^{2l+1}$, where m_X is the mass and p_X^* the momentum of X in the J/ψ rest frame; l is the angular momentum of the production process. Although it may be confused by mixing [366, 367], the quantity S_X provides a useful qualitative comparison on how "sticky" different states of the same J^P are.

For the "iota", the upper limit in (131) results in a "stickiness" value of >60 when normalizing S_X to unity for X = η(549). For comparison, $S_{\eta'} \approx 3.7$. A $q\bar{q}$ state with the wave function $u\bar{u} + d\bar{d} - 5s\bar{s}$, however, would also have no γγ coupling [368, 369], but the η(1440) is unlikely to have such a large $s\bar{s}$ component. In fig. 107, S_X is shown for the various isoscalar resonances produced in J/ψ radiative decays and in γγ reactions.

A drawback for the glueball interpretation of the "iota" always has been that the $K\bar{K}\pi$ decay is the only directly observed decay mode of this state. There are, however, not many final states that a 0^- resonance at ~1.4 GeV can decay to. Decays into ππ or $K\bar{K}$ violate parity. Three-pion decay is forbidden by G parity. Radiative transitions to vector mesons should be suppressed relative to those of groundstate $q\bar{q}$ mesons if the "iota" is indeed a gluonium state. 4π, $K\bar{K}\pi\pi$, ηππ and $K\bar{K}\pi$ are the obvious modes at hand. Also possible in principle are decays into pairs of vector mesons but this can only occur below nominal threshold. In fact, the coupled channel analysis (section 6.4.6.1) suggests that vector–vector decays of the iota do exist. The coupling strength of η(1440) → vector–vector would be much bigger than the actual branching fractions suggest due to the dramatic decrease of the ρρ phase space for lower invariant ρρ masses. The problem stated above, that the $K\bar{K}\pi$ decay might be the only one observed, would then be reduced to the much simpler task to explain why the different "iota" couplings to strange or non-strange final states do not obey exact SU(3) symmetry. Gounaris and

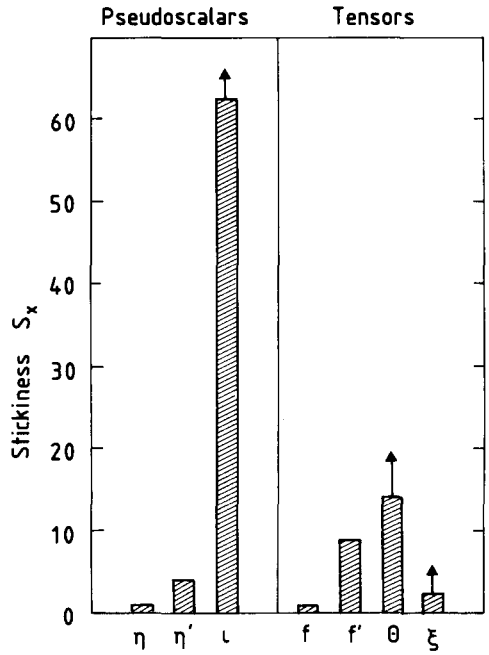

Fig. 107. The stickiness S_X, defined as in eq. (153), for various isoscalar states X observed in J/ψ radiative decays and in γγ reactions. S_X is normalized to the η for pseudoscalar and to the $f_2(1270)$ for tensor states, respectively. The arrows indicate that yet undetected decay modes could increase the value of S_X.

Neufeld [412] point out, however, that the $K\bar{K}\pi$ decay could be the only prominent decay mode if the η(1440) is the lightest 0^- glueball.

Finally, the mass of the η(1440) is consistent with the range expected by lattice gauge theories and other QCD inspired models (see fig. 7 in section 2.4.1).

Summarizing, if one accepts the guide lines for gluonium searches as stated above, the "iota" certainly sticks out as *the* candidate for the 0^{-+} glueball state and should have at least a considerable gluonium component.

7.3. The 2^+ glueball

In this section we shall follow a similar procedure to argue for a candidate for the 2^{++} glueball state. The 2^{++} $q\bar{q}$ sector imposes a much weaker constraint on tensor gluonia than in the 0^{-+} case. Although the ground state nonet is well established [$a_2(1320)$, $K_2^*(1430)$, $f_2(1270)$, $f_2'(1525)$], orbital as well as radial excitations have to be considered, both of which belong to multiplets which are not yet fully established (cf. fig. 5). One would again expect that pure radial excitations are produced with a smaller strength than their ground state partners.

The candidate resonances that come to mind are the $f_2(1720)$ (the "theta") and the, so-called, g_T states [342]. The X(1810), recently observed in hadronic collisions [379], should also be considered. The latter two have only been mentioned in this report in passing for the very reason that these states have not yet been observed in J/ψ decays. In fact, the g_T states have so far only been seen [342]—and partially confirmed—in the process $\pi^- p \to \phi\phi n$ [380]. They are three relatively wide ($\Gamma \sim$ 150–300 MeV) 2^{++} states with masses of $2.011^{+0.062}_{-0.076}$ GeV, 2.297 ± 0.28 GeV, and 2.339 ± 0.055 GeV [381]. These states are produced in a doubly OZI forbidden process and are therefore sometimes

interpreted as glueball states [382]. A major drawback is the fact that they have as yet not been directly observed in $J/\psi \to \gamma\phi\phi$ decays. However, the DM2 data on $J/\psi \to \gamma\phi\phi$ [353] have room for a 2^{++} wave contribution for $m_{\phi\phi} < 2.5$ GeV, which does not, however, show any structure (see also section 6.4.5.4).

There has been some discussion [32] on the ratio of 2^{++} and 0^{++} glueball masses in lattice gauge theories and bag models in the recent past. Most estimates place the 2^{++} state somewhat higher in mass than the 0^{++} state [383]. A mass value above 2 GeV for the lowest 2^{++} gluonium state seems to be too high in any case.

The most promising 2^{++} glueball candidate is the $f_2(1720)$. Its radiative production fraction, $\sim 1.5 \times 10^{-3}$, is relatively large, but still smaller by a factor $\sim 1/3$ than the rate for the $\eta(1440)$. A comparison of the production rates in radiative J/ψ decays is given in fig. 106. The decays of the $f_2(1720)$ show that u, d quarks as well as strange quarks may be involved in the decays. As a qualitative statement this is more appealing for a glueball interpretation of the $f_2(1720)$ than for the $\eta(1440)$, for which the only well-established decay mode is the $K\bar{K}\pi$ decay. On the other hand, for an $SU(3)_{flavour}$ symmetric decay of a flavour singlet state the decay widths obey the ratios

$$\Gamma(\pi\pi) : \Gamma(KK) : \Gamma(\eta\eta) \approx 2 : 1 : 0.2 , \tag{154}$$

taking into account d wave phase space corrections. This pattern is not observed for the $f_2(1720)$ ($\pi\pi : KK : \eta\eta \approx 0.2 : 1 : 0.2$). The possibility of flavour symmetry breaking has been discussed [324, 327]. The conclusion is that SU(3) forbidden decays such as $G \to K^*\bar{K}$ remain forbidden, but SU(3) allowed decays as above may be substantially modified due to the u, d and s quark mass differences. While the violation of a strictly SU(3) symmetric decay pattern has been an argument against a glueball interpretation for several authors [328], it has also provoked explanations that can maintain this interpretation [54–56]. Recent approaches ascribe the suppressed $\pi\pi$ decay mode of the $f_2(1720)$ to a form factor effect [57], or to mixing with non-strange quarks [58] or a certain combination of strange and non-strange quarks [59, 413]. Arguments based on helicity suppression favouring strangeness due to the higher mass of the s quark can also be found [54, 55].

The $f_2(1720)$ has not been observed in $\gamma\gamma$ reactions. The present upper limit is [385, 386]

$$\Gamma(f_2(1720) \to \gamma\gamma) \cdot B(f_2(1720) \to K\bar{K}) < 0.2\,\text{keV} \quad \text{at } 95\% \text{ C.L.} \tag{155}$$

The "stickiness" value, S_{theta}, resulting from this limit is ~17 (cf. fig. 107).

When comparing the radiative production of the $K\bar{K}$ system with the hadronic production recoiling against ω or φ (fig. 101) a peak is observed in $J/\psi \to \omega K^+K^-$ (fig. 101b) and a shoulder on the high-mass side of the $f_2'(1525)$ in $J/\psi \to \phi K^+K^-$ (fig. 101c), both consistent with being due to the $f_2(1720)$. However, this is not a safe assumption since there is evidence for a 0^{++} resonance $f_0(1730)$ [14, 332, 387] in the same mass region. Still, the $f_2(1720)$ production rates would be smaller than those for $\omega f_2(1270)$ or $\phi f_2'(1525)$, respectively, as can be seen from table 44.

If we accept both signals being due to the $f_2(1720)$ and assume that the SOZI diagram of fig. 100a dominates the process, this could indicate that the $f_2(1720)$ has some strange as well as non-strange components. However, also a glueball could be produced in $J/\psi \to \{\omega, \phi\} + G$ following the diagram of fig. 100b, even with a possibly sizeable rate [364]. In this case a glueball state should be expected to be produced in both ω and φ tagged hadronic decays. The value for R_{vector} is 1.2 ± 0.4 (see table 44), as expected for an $SU(3)_{flavour}$ singlet state.

Some help on which diagram is responsible for the observed rates comes from a comparison of the reactions

Table 44
Decay rates and ratios for gluonium candidates and $q\bar{q}$ mesons. The "stickiness" values, which are normalized to η(549) and $f_2(1270)$, have been obtained assuming angular momenta $l = 1$ and $l = 0$ for the production of pseudoscalar and tensor states, respectively. The decay rates are given in keV.

	η	η′	η(1440)→KK̄π	
$\Gamma(J/\psi\to\gamma X)$	0.065 ± 0.008	0.296 ± 0.039	0.333 ± 0.050	
$\Gamma(J/\psi\to\omega X)$	0.113 ± 0.015	0.013 ± 0.002	–	
$\Gamma(J/\psi\to\phi X)$	0.048 ± 0.006	0.026 ± 0.004	<0.016	
$\Gamma(X\to\gamma\gamma)$	0.524 ± 0.031	4.25 ± 0.19	<1.6	
S_X	1.00 ± 0.14	3.7 ± 0.5	>60	
R_V	2.4 ± 0.4	0.5 ± 0.1	–	
R_γ	0.6 ± 0.1	11.4 ± 2.3	>21	
	$f_2(1270)$	$f_2'(1525)\to K\bar{K}$	$f_2(1720)\to K\bar{K}$	$\xi(2230)\to K\bar{K}$
$\Gamma(J/\psi\to\gamma X)$	0.096 ± 0.013	0.028 ± 0.005	0.072 ± 0.011	0.006 ± 0.003
$\Gamma(J/\psi\to\omega X)$	0.307 ± 0.050	<0.009	0.031 ± 0.008	–
$\Gamma(J/\psi\to\phi X)$	<0.027	0.040 ± 0.007	0.026 ± 0.004	–
$\Gamma(X\to\gamma\gamma)$	2.84 ± 0.16	0.10 ± 0.02	<0.2	<0.2
S_X	1.00 ± 0.15	11.0 ± 3.0	>17.1	>2.8
R_V	>9.5	<0.3	1.2 ± 0.4	–
R_γ	0.31 ± 0.07	0.70 ± 0.18	2.3 ± 0.7	–

$$J/\psi\to\gamma + K\bar{K} \tag{156}$$

and

$$K^-p\to\Lambda + K\bar{K}\,. \tag{157}$$

The kaon induced reaction is believed to proceed as shown in fig. 108, where the presence of the Λ tags the production of an $s\bar{s}$ quark pair. This diagram can describe the production of an $s\bar{s}$ state, but not that of a glueball. While K^+K^- can couple to all spin states, $K_S^0K_S^0$ is restricted to even spin states only.

The LASS group has made a comparison of their data [334] on reaction (157) with the Mark III data on reaction (156). Figure 109 shows the LASS data normalized to, and superimposed onto, the $K_S^0K_S^0$ invariant mass distribution from J/ψ radiative decays. It is striking to see an almost identical shape of both data sets for the $f_2'(1525)$ but, while the Mark III data exhibit the $f_2(1720)$ as a second, even larger peak in this distribution, there is no indication of such a state from the LASS data with an eight times larger event sample. Compelling as this is for ruling out the $f_2(1720)$ as a standard $s\bar{s}$ state like the $f_2'(1525)$, there is a problem to understand why K^-p scattering does not produce the $f_2(1720)$ despite the fact that the KK̄ decay is, so far, the most prominent decay mode of this state [333, 334, 388]. Either the one-kaon exchange diagram is suppressed for some reason [389]*) or the $f_2(1720)\to K\bar{K}$ coupling is actually much smaller than commonly believed, leaving many more decay modes yet to be discovered.

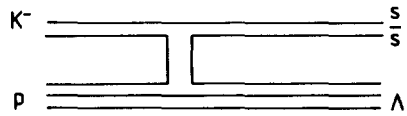

Fig. 108. Quark line diagram for $J/\psi\to\Lambda + K\bar{K}$.

*) There have been indications of problems with the one-kaon exchange picture; see ref. [389].

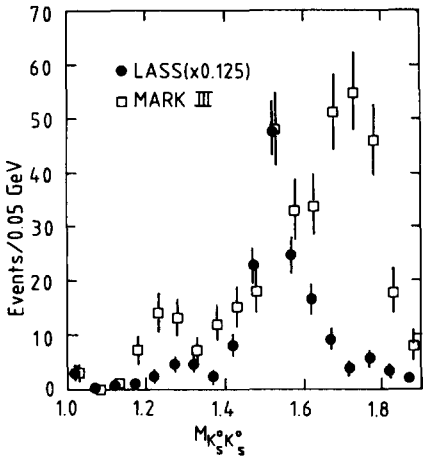

Fig. 109. Comparison of LASS and Mark III $K\bar{K}$ spectra. Acceptance corrected $K_S^0K_S^0$ invariant mass distribution of $K^-p\to\Lambda+K_S^0K_S^0$ as observed by LASS (black circles) compared to the same final state produced in radiative J/ψ decay as seen by Mark III (open squares) for invariant masses below 1.9 GeV.

Some weak evidence for $f_2(1720)$ production in $\pi^-p\to\pi^+(K^+K^-)p$ and $pp\to p(K^+K^-)p$, where the kaon system is centrally produced, has been reported [390] with no definite spin determination. A partial wave analysis of $\pi^-p\to K_S^0K_S^0n$ by the MSS ITEP group [332] reveals a 2^{++} d wave state at the mass of the $f_2(1720)$ but with a too narrow width. Longacre et al. [333] have globally fit $\pi\pi$, $\eta\eta$ and $K\bar{K}$ final states obtained in $\pi\pi$ and $K\bar{K}$ scattering as well as from radiative J/ψ decays. Their fit results in a surprisingly small $K\bar{K}$ branching fraction of the $f_2(1720)$ $[B(f_2(1720)\to K\bar{K})=0.38^{+0.09}_{-0.19}]$. An even smaller $K\bar{K}$ branching fraction would be inferred if the new LASS data were included [48]. This in turn would mean that the actual J/ψ production fraction of the $f_2(1720)$ may be larger than presently known, boosting a glueball interpretation of the $f_2(1720)$ even further.

The conclusion that the $f_2(1720)$ is not dominantly a $q\bar{q}$ state is also underlined by the notion that the close to ideal mixing in the f–f′ system would very likely be disturbed by another nearby 2^{++} $q\bar{q}$ state.

Despite the still standing possibility that the $f_2(1720)$ has some quarkonium admixture, similar arguments as used to call the "iota" an excellent 0^{-+} glueball candidate would assign the "theta"/$f_2(1720)$ to the 2^{++} candidate of the glueball spectrum. Rosner [225] has pointed out that the $f_2(1720)$ is a good candidate for the first physical particle lying on the Pomeranchuk trajectory or Pomeron [391] proposed to explain the approximate constancy of total cross sections at high energies. A plausible parametrization [225] of this trajectory is

$$J(M^2)=1+0.44M^2\,. \tag{158}$$

Based on (158) one expects a $J^P=2^{++}$ particle around 1.5 GeV, which could mix with the $f_2'(1525)$ [58, 392] to gain in mass. Models to understand the "Pomeron" as a "glue-ring" [393] or a "two-gluon exchange" mechanism [394] have been proposed some time ago.

7.4. *Where does the scalar glueball hide?*

The 0^{++} gluonium state turns out to be the experimentally most difficult one to find. Theoretically it is a very attractive one since it is predicted to be the lowest in mass of the states of the glueball

spectrum according to most models. There seems to be consensus [383] that the scalar glueball should have a mass $m_{0^{++}} \approx 1.0$–1.5 GeV [395, 396, 383]. Masses as low as 0.6 GeV are also found [33]. The width of the scalar glueball is even more uncertain. Both, narrow [397] and very wide [398] width expectations are found in the literature.

Peaks and structures with 0^{++} spin parity have been reported in the past, mostly in hadronic production processes. We list some of them below.

- A $J^P = 0^{++}$ state called $f_0(1590)$ with a mass of (1592 ± 25) MeV and a width of (210 ± 40) MeV [378] is found by GAMS in $\eta\eta$, $\eta\eta'$, and $4\pi^0$ [379] final states of π^- p collisions [399]. This state is also seen in central hadron collisions [400] where a glueball would be expected to show up.
- The GAMS experiment [401] also reports evidence for a narrow state at a mass (1755 ± 8) MeV and a width of less than 50 MeV in the $\eta\eta$ final state. The preferred spin assignment is again 0^{++}.
- Au, Morgan and Pennington [137] have analysed data on central di-meson production from the AFS experiment at the ISR. In a coupled channel analysis of $I = 0$, s wave $\pi\pi$ and $K\bar{K}$ final states they find three resonances around 1 GeV, $S_1(991)$, $S_2(988)$ and $\varepsilon(900)$, where the naive quark model expects at most two. They argue that the $S_1(991)$ is a plausible candidate for the scalar glueball.
- In this context, the well-known $f_0(975)$ (the former S*) deserves mentioning. Both the $f_0(975)$ and its isovector partner, the $a_0(980)$, have been puzzling states for a long time. Identification as $q\bar{q}$ states has proven to be difficult. More exotic alternatives, such as four-quark states [134] or loosely bound $K\bar{K}$ molecules [135] have been suggested. It can also not be excluded that the $f_0(975)$ might have a sizeable scalar glueball component [138]. In the same vein one should consider the $f_0(1300)$ as a possible candidate for scalar gluonium although it is usually assigned to the non-strange $I = 0$ state of the scalar multiplet with dominant $\pi\pi$ coupling (see fig. 5). Both, $f_0(975)$ and $f_0(1300)$, have not yet been identified in radiative J/ψ decays.
- Several indications for other scalar resonance production below 2 GeV have been reported [139, 333, 345], obtained mostly as a result of complicated analyses with several partial waves or coupled channels. We shall not address the details of these pieces of evidence here.

Let us come back to the context of J/ψ decays and our guideline that at some level all gluonium states should be observable in the glue-enriched environment of J/ψ decays. Places to look for scalar gluonium are final states of $\pi\pi$, $K\bar{K}$, $\eta\eta$ and $\eta\eta'$ in hard gluon channels such as radiative decays or strongly Zweig suppressed hadronic decays. The statistics of $\eta\eta$ and $\eta\eta'$ final states in radiative J/ψ decays are still too scarce to be conclusive (see section 6.4.2). The $K\bar{K}$ channel has already been exhaustively discussed in the context of the tensor glueball search. The most promising final state seems to be the $\pi\pi$ channel (see section 6.3.3).

Examination of fig. 102a shows, apart from the features already discussed, a peak at 2.1 GeV which is consistent with the $f_4(2030)$ and a shoulder on the high-mass side of the $f_2(1270)$. The $f_0(975)$ is not observed (section 6.3.3). Figure 110a shows the $\pi\pi$ invariant mass distribution of $J/\psi \to \gamma\pi^0\pi^0$ obtained from Crystal Ball [249], which does not suffer background from $J/\psi \to \rho\pi$ as does the charged mode. Also here the superimposed fit cannot account for an excess of events on the high-mass side of the $f_2(1270)$ although the statistics is not as convincing as in the charged mode (fig. 110b). Interference with the $f_2'(1525) \to \pi\pi$ decay would provide a more conventional explanation for this phenomenon (see below).

A recent investigation [313] of the angular distributions of events from $J/\psi \to \gamma\pi\pi$ and $J/\psi \to \gamma K\bar{K}$ just above threshold finds agreement with a scalar behaviour. If background contributions can be excluded this is the first observation of scalar production in radiative J/ψ decays.

Other promising channels to look into are doubly Zweig forbidden decays such as $J/\psi \to \phi\pi\pi$ or

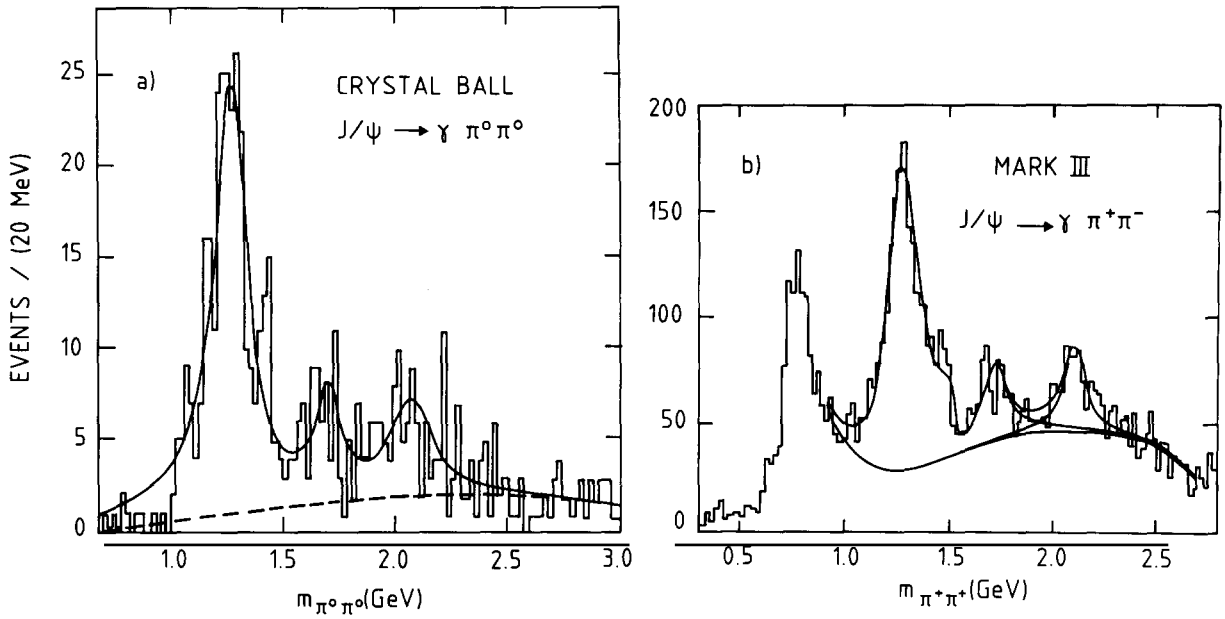

Fig. 110. $\pi\pi$ invariant mass distributions for $J/\psi \to \gamma\pi\pi$. (a) $\pi^0\pi^0$ mass distribution as obtained by Crystal Ball [249]. (b) $\pi^+\pi^+$ mass distribution as obtained by Mark III [348] using a sample of 5.8×10^6 J/ψ decays. In (a) the spectrum is fitted with three Breit–Wigner amplitudes, in (b) four interfering amplitudes have been allowed to accommodate the unusual shape of the $f_2(1270)$.

$\phi 4\pi$, as emphasized by Lindenbaum [402]. Figure 102c shows a clear $f_0(975)$ and possibly a $f_2(1720)$ signal at the high end of the $\pi\pi$ invariant mass distribution. The bump in the centre does not follow an exact Breit–Wigner resonance shape and is probably not just one state. Although there is likely to be some $f_2(1270)$ contribution, this structure is unlikely to be entirely due to the $f_2(1270)$ (see section 5.3.3). Note that ordinary $q\bar{q}$ states are suppressed in this Zweig forbidden decay. The DM2 group [126] has investigated this bump more closely as described in section 5.3.4. A change in the shape of the angular distribution of $\cos\theta^*_\pi$, the angle of the π^+ in the $\pi\pi$ centre of mass system, is clearly observed when one compares this distribution for events from the $f_2(1270)$ mass region with events from the mass region above (fig. 36). Qualitatively the data are consistent with a change from spin 2 to spin 0 when moving from the lower to the upper part of this enhancement.

The $\pi\pi$ mass spectrum of $J/\psi \to \omega\pi\pi$ in fig. 102b also shows, apart from the $f_2(1270)$, a mysterious bump with mass around 300 to 400 MeV and few hundred MeV wide. This phenomenon has been observed by every experiment analysing the $\omega\pi\pi$ final state. Several attempts to reveal a resonant behaviour of the structure have been made. DM2 [403] has performed an empirical fit with a Breit–Wigner curve distorted by phase space. The fit requires a mass of (278 ± 36) MeV and a width of (588 ± 88) MeV. Inspection of the angular distributions indicates deviations from a pure s wave. No experiment has as yet convincingly proven the nature of this structure. See section 5.5 for a possible non-resonant explanation of this phenomenon.

An indication of a $f_0(975)$ is also present in the same mass spectrum (fig. 102b). This would imply that the $f_0(975)$ possesses couplings of the about the same strength [403] to both s quarks (tag with ϕ) and u, d quarks (tag with ω), a feature that also a glueball would show.

It is tempting to associate the shoulder of the $f_2(1270)$ in $J/\psi \to \gamma\pi\pi$ with the possibly scalar part of the central structure in $J/\psi \to \phi\pi\pi$. If this identification holds, it would certainly produce a most

interesting hypothesis for a scalar glueball candidate. If one introduces a narrow state at ~1420 MeV [266], the $\pi\pi$ mass distribution of $\gamma\pi\pi$ in fig. 102a is well fitted. In the same reference (DM2) it is stated, however, that this additional narrow resonance cannot well explain the $\phi\pi\pi$ data. An alternative description for the shoulder in fig. 102a is also possible by allowing for interference of $f_2(1270)$ and $f_2'(1525)$ in $J/\psi \to \gamma\pi\pi$ [266]. The curve in fig. 110b corresponds to a fit with four Breit–Wigner amplitudes being allowed to interfere [348]. The shoulder of the $f_2(1270)$ is reproduced by interference of $f_2(1270)$ and $f_2'(1525)$. The obtained $f_2'(1525) \to \pi\pi$ branching fraction corresponds to a 30° tensor meson mixing angle in agreement with recent 2γ measurements and Gell-Mann–Okubo mass relationships. It remains to be seen by future experiments (see section 8.2), whether an interference effect or a new state is the correct explanation for this shoulder.

Until the time that many events are taken, the quest of the scalar glueball in J/ψ decays will keep experimenters excited.

8. Summary and outlook

In this report we have tried to review the wealth of information obtained through intense studies of J/ψ decays for more than 13 years. The discovery of the narrow J/ψ resonance has been a great surprise, promising new and interesting physics. The detailed studies of J/ψ decays have kept this promise.

In the area of radiative decays at least two candidates for gluonic bound states, the "iota"/η (1440) and the "theta"/$f_2(1720)$, have been discovered and many decay modes have been studied. Although both states appeal as glueball candidates, a unique interpretation has yet to be obtained. The measurements of the hadronic J/ψ decays to meson pairs have already reached a level at which the analysis in terms of $SU(3)_{flavour}$ conserving and $SU(3)_{flavour}$ violating amplitudes is possible. Much can be learned from these studies about light quark systems and possible gluonium admixtures. The detailed comparison of hadronic and radiative decays is the key to determine quarkonic and gluonic elements of the states in question.

In general, the investigations of J/ψ decays yielded more information about light quark systems than of charm by making use of the J/ψ as a well defined "factory" for mesons and baryons. The emphasis for future experiments must be to extend the systematic measurements of two-body hadronic decays and of radiative decays to a level at which quantitative statements on the properties of $q\bar{q}$ mesons and exotic states can be made. Some facts and ideas relevant to future studies of J/ψ decays are discussed in the following two sections.

8.1. What fraction of J/ψ decays has been seen?

As discussed in section 2.1, direct hadronic, electromagnetic, and radiative decays represent roughly 65%, 14%, and 7% of the total J/ψ decay rate, respectively. It is an interesting exercise to estimate how much of this rate has been measured in exclusive studies of J/ψ decays.

In table 45 the measured branching ratios for hadronic decays in final states containing pions, kaons, and protons are listed. From the measurements of charged final states the total contribution to the J/ψ hadronic decay rate can be estimated by employing isospin arguments [167]. In addition, some of the measured J/ψ decays that proceed via resonant intermediate states lead to topologies not compiled in table 45 (i.e. final states containing η's). Their contribution is estimated to be greater than $(1.1 \pm$

Table 45
Topological branching ratios of hadronic decays. Branching ratios into general modes computed from the observation of one particular charge state of that mode. The average values were taken from the compilation of the Particle Data Group [14]. The range of the correction factor is calculated assuming all allowed isospin combinations in the final state [167]. Theoretically one expects that roughly 65% of all J/ψ decays are hadronic decays.

General mode	Observed mode	B(observed) (%)	Isospin factor	B(general) (%)
3π	$\pi^+\pi^-\pi^0$	1.50 ± 0.15	1	1.50 ± 0.15
5π	$2(\pi^+\pi^-)\pi^0$	3.42 ± 0.31	$\frac{2}{3}$	5.10 ± 0.45
7π	$3(\pi^+\pi^-)\pi^0$	2.86 ± 0.55	$\frac{1}{3} \rightarrow \frac{8}{15}$	$5.36 \pm 1.03 \rightarrow 8.58 \pm 1.65$
9π	$4(\pi^+\pi^-)\pi^0$	0.90 ± 0.30	$0 \rightarrow \frac{16}{35}$	$>2.0 \pm 0.7$
$K\bar{K}\pi$	$K\bar{K}\pi$	0.61 ± 0.10	1	0.61 ± 0.10
$K\bar{K}2\pi$	$K^+K^-\pi^+\pi^-$	0.72 ± 0.23	$\frac{1}{6} \rightarrow \frac{1}{3}$	$2.2 \pm 0.7 \rightarrow 4.3 \pm 1.4$
$K\bar{K}3\pi$	$K^+K^-\pi^+\pi^-\pi^0$	1.2 ± 0.3	$\frac{1}{15} \rightarrow \frac{1}{2}$	$2.4 \pm 0.6 \rightarrow 18.0 \pm 4.5$
$K\bar{K}4\pi$	$K^+K^-2(\pi^+\pi^-)$	0.31 ± 0.13	$0 \rightarrow \frac{4}{15}$	$>1.2 \pm 0.5$
$2(K\bar{K})$	$K^+K^-K^+K^-$	0.07 ± 0.03	$0 \rightarrow \frac{1}{3}$	$>0.21 \pm 0.09$
$N\bar{N}$	$p\bar{p}$	0.220 ± 0.012	$\frac{1}{2}$	0.440 ± 0.024
$N\bar{N}\pi$	$p\bar{p}\pi^0$	0.1093 ± 0.095	$\frac{1}{6}$	0.656 ± 0.055
$N\bar{N}2\pi$	$p\bar{p}\pi^+\pi^-$	0.60 ± 0.05	$\frac{1}{6} \rightarrow \frac{1}{3}$	$1.80 \pm 0.14 \rightarrow 3.60 \pm 0.29$
$N\bar{N}3\pi$	$p\bar{p}\pi^+\pi^-\pi^0$	0.233 ± 0.087	$\frac{1}{15} \rightarrow \frac{1}{2}$	$0.47 \pm 0.17 \rightarrow 3.50 \pm 1.30$
Σ				$>25.1 \pm 1.8$

0.2)%. Thus a minimum of $(25.1 \pm 1.8)\%$ of J/ψ decays can be accounted for by exclusively reconstructed hadronic decays. Using a statistical model, in which all available isospin states are populated according to their statistical weights [404], one further calculates that $(34.8 \pm 2.8)\%$, roughly half of all hadronic decays, have already been measured in exclusive reactions.*) The difference between the two estimates may arise from higher multiplicities,**) decay modes involving η's and/or photons, and strong decays violating generalized $\mathcal{C}$ parity.

Table 46 shows a similar compilation for the radiative decays. For some topological final states, where no value for the total branching ratio can be found in the literature, a lower limit for the decay rate has been estimated by summing over the branching ratios of resonances leading to the particular final state. Similar to the case of the hadronic decays, one finds that roughly half of all radiative decays can be accounted for by exclusively reconstructed topologies.

8.2. *Outlook for the Beijing storage ring (BEPC)*

The unique experimental conditions, the variety of interesting physical processes, and the prospect of event samples an order of magnitude larger than currently available, will guarantee continuing interest in the physics of J/ψ decays at e^+e^- storage rings at least for another decade. It is expected that the BEPC storage ring in Beijing reaches a peak luminosity of $5 \times 10^{30}\,cm^{-2}\,s^{-1}$ and features an energy spread of $\Delta E \approx 0.6$ MeV. Both values are by far superior to those obtained with SPEAR and DCI (see table 5) and may translate into an order of magnitude higher J/ψ event rates, such that total event samples of 100 million events and more are not outside reach. In the context of $b\bar{b}$ factories, multi-bunch double-storage rings with high luminosity have been proposed [407] that are based on

*) To simplify the argument, we assume here that the contribution of the electromagnetic diagram to the topologies studied is negligible.

**) Using smooth multiplicity curves, one can estimate that higher multiplicities contribute about 6% to the unaccounted J/ψ decays [405].

Table 46
Radiative decay branching ratios. Summary of branching ratios of radiative decays into mutually exclusive final states of pseudoscalar mesons, vector mesons, and baryons. In the case of the $\gamma\pi\pi$, $\gamma K\bar{K}$, and $\gamma K\bar{K}\pi$ final states a lower limit for the total decay rate has been estimated by taking the sum over the resonant subprocesses. To extrapolate from the measured $\gamma 2(\pi^+\pi^-)$ rate to the total $\gamma 4\pi$ rate, isospin factors of 1/3 and 4/9 have been assumed, corresponding to the cases where the $\pi^+\pi^-$ subsystems have $I=1$ and $I=0$, respectively. Note, that it has been shown (see section 6.4.5.1) that these decays mainly proceed via $\gamma\rho\rho$ and $\gamma\rho\pi\pi$ intermediate states. Theoretically one estimates [see eq. (101)] that $B(J/\psi\rightarrow\gamma+X)=(600\pm200)\times10^{-4}$.

Final state	Branching ratio (units of 10^{-4})	References and remarks
$\gamma\pi^0$	0.24 ± 0.05	table 29
$\gamma\eta$	8.8 ± 0.6	table 29
$\gamma\eta'$	40 ± 3	table 29
$\gamma 2\pi$	$>8.0\pm1.1$	table 30, table 35, and table 38; from $\gamma\{f_2(1270), f_2(1720), X(2100)\}$
$\gamma\eta\eta$	7.3 ± 2.3	[406]
$\gamma\eta\eta'$	5.7 ± 2.7	[406]
$\gamma K\bar{K}$	11.8 ± 1.3	table 30 and table 35; from $\gamma\{f_2'(1525), f_2(1720)\}$
$\gamma\omega\omega$	16 ± 3	[350, 351]
$\gamma\omega\phi$	1.4 ± 0.4	[352]
$\gamma\phi\phi$	3.1 ± 0.7	[353]
$\gamma\eta\pi\pi$	35 ± 11	[281]; contribution of η' excluded
$\gamma K\bar{K}\pi$	$>45\pm4$	table 32; from $\iota\rightarrow K\bar{K}\pi$
$\gamma 4\pi$	$144\pm18\rightarrow192\pm24$	[345]; from $\gamma 2(\pi^+\pi^-)$
$\gamma N\bar{N}$	7.6 ± 2.0	[185]; from $\gamma p\bar{p}$
Σ	$>318\pm22$	

available accelerator technology. A similar concept applied to the J/ψ energy range could lead to event samples of as many as 10^{10} J/ψ decays [408].

The difficulty in identifying gluonia is due to a large extent to the great complexity of the particle spectrum in the 1–2.5 GeV mass regions, where glueballs are expected to occur. In addition to $q\bar{q}$ multiplets, hybrid and four-quark states may exist, often overlapping in mass, and sometimes mixing with each other. This means that gluonic states cannot be treated in isolation; it is necessary to understand the particle spectrum as a complete entity in order to understand its components. This insight determines the physics program of hadron spectroscopy in the coming years. High-statistics experiments at the J/ψ are a well-suited exercise if the efforts to study its decays in a systematic way are continued and a search for rare effects pointing to exotic behaviour is initiated.

In particular, the study of meson multiplets, by comparing J/ψ decays into meson pairs, has to be completed and extended to lesser known nonets; all radiatively accessible final states have to be investigated and as a whole compared to the inclusively measured radiative photon spectrum. In general this will require partial wave analyses to identify the spin of the resonances involved, so that current ambiguities in the interpretation of the results can be settled. In particular, this is true for the interpretation of radiative decays, where, e.g., the complex structures in the $\eta\pi\pi$ and 4π systems can only be disentangled if large data samples are available.

Some of the results covered in this report have been a matter of controversy or lacked statistical significance. In particular, the question of the $\xi(2230)$ will most likely be settled at BEPC.

A completely new field, that has only started to be addressed [126] in J/ψ decays, is the search for exotic final states with spin parity combinations not allowed by the quark model. These states are

Table 47
Some final states suited to search for exotic particles

J^{PC}	Decay channels
0^{--}, 2^{+-}	$\{\omega, \phi\} + \{\pi, \eta, \eta'\}$
1^{-+}, 3^{-+}	$\pi + \{\eta, \eta', f, f'\}$, $\eta\eta'$, $\rho\rho$, $\omega\omega$, $\phi\phi$

present in glueball, hybrid and four-quark models. Recent hints for such objects [409] should initiate a similar search in J/ψ decays. A list of simple final states that exotic particles can decay to is shown in table 47.

Acknowledgements

We would like to thank our colleagues from the Mark III and DM2 Collaborations for their help in preparing this paper. In particular we are grateful to A. Falvard, P. Henrard, B. Jean-Marie, and T. Burnett for corrections and clarifications that resulted from their careful reading of the manuscript. We would also like to thank J. Field and M. Chanowitz for discussions on the physics of J/ψ decays and W. Dunwoodie for a critical examination of fig. 5. Finally we want to thank Mme. A. Coudert for the timely preparation of the figures.

References

[1] B.J. Bjorken and S.L. Glashow, Phys. Lett. 11 (1964) 255.
[2] M. Gell-Mann and Y. Ne'eman, The Eightfold Way (Benjamin, New York, 1964).
[3] S.L. Glashow, J. Iliopoulos and L. Maiani, Phys. Rev. D 2 (1970) 1285.
[4] M.K. Gaillard and B.W. Lee, Phys. Rev. D 10 (1974) 897.
[5] S.C.C. Ting, A discovery story of the J, p. 115; G. Goldhaber, A discovery story of the ψ, p. 131; B. Richter, A discovery story of the ψ and ψ', p. 143; in: Adventures in Experimental Physics, Vol. 5, Epsilon, ed. B. Maglic (World Science Education, Princeton, NJ, 1976); M.E. Riordan, The Hunting of the Quark (Simon and Schuster, New York, 1987).
[6] J.J. Aubert et al., Phys. Rev. Lett. 33 (1974) 1404.
[7] J.E. Augustin et al., Phys. Rev. Lett. 33 (1974) 1406.
[8] C. Bacci et al., Phys. Lett. 33 (1974) 1408.
[9] W. Braunschweig et al., Phys. Lett. B 53 (1974) 393, 491.
[10] G.S. Abrams et al., Phys. Rev. Lett. 33 (1974) 1453.
[11] P.A. Rapidis et al., Phys. Rev. Lett. 39 (1977) 526; W. Braunschweig et al., Phys. Lett. B 57 (1975) 407; J.S. Whittaker et al., Phys. Rev. Lett. 37 (1976) 1596; W. Tanenbaum et al., Phys. Rev. D 17 (1978) 1731.
[12] S. Okubo, Phys. Lett. 5 (1963) 165; G. Zweig, CERN preprints CERN-TH-401, 402, 412 (1964); J. Iizuka, Prog. Theor. Phys. Suppl. 37–38 (1966) 21.
[13] G. Feldman and M. Perl, Phys. Rep. 19 (1975) 234; G. Feldman and M. Perl, Phys. Rep. 33 (1977) 285; R.F. Schwitters and K. Strauch, Annu. Rev. Nucl. Sci. 26 (1976) 89; W. Chinowsky, Annu. Rev. Nucl. Sci. 27 (1977) 393; B. Wiik and G. Wolf, DESY report, DESY 77/01 (1977); Electron positron interactions (Springer, Berlin, 1979); K. Königsmann, Phys. Rep. 139 (1986) 243.
[14] Particle Data Group, Review of Particle Properties, Phys. Lett. B 170 (1986).
[15] T. Appelquist and H.D. Politzer, Phys. Rev. Lett. 34 (1975) 43; T. Appelquist, A. de Rujula, H.D. Politzer and S.L. Glashow, Phys. Rev. Lett. 34 (1975) 365;

M.S. Chanowitz, Phys. Rev. D 12 (1975) 918;
L. Okun and M. Voloshin, ITEP-95 (1976);
T. Appelquist and H.D. Politzer, Phys. Rev. D 12 (1975) 1404;
T. Appelquist, R.M. Barnett and K. Lane, Annu. Rev. Nucl. Sci. 28 (1978) 387.
[16] P.B. Mackenzie and G.P. Lepage, in: AIP Conf. Proc. No. 74, Particles and Fields subseries No. 24 (Tallahassee, 1981) p. 176, eds D.W. Duke and J.F. Owens; Phys. Rev. Lett. 47 (1981) 1244;
G.P. Lepage, in: Proc. 1983 Intern. Symp. on Lepton and Photon Interactions at High Energies (Cornell Univ., Ithaca, NY, 1983), eds D.G. Cassel and D.L. Kreinick.
[17] W. Kwong, J.L. Rosner and C. Quigg, Annu. Rev. Nucl. Part. Sci. 37 (1987) 325.
[18] W. Kwong, P.B. Mackenzie, R. Rosenfeld and J.L. Rosner, Phys. Rev. D 37 (1988) 3210.
[19] S.J. Brodsky, G.P. Lepage and P. Mackenzie, Phys. Rev. D 28 (1983) 228.
[20] R. Barbieri, R. Gatto and E. Remiddi, Phys. Lett. B 106 (1981) 497.
[21] R. Van Royen and V.F. Weisskopf, Nuovo Cimento 50 (1967) 617; 51 (1967) 583.
[22] J. Jauch and F. Rohrlich, Theory of Photons and Electrons (Addison-Wesley, Reading, MA, 1955).
[23] K. Königsmann, in: Proc. 22nd Rencontre de Moriond (Les Arcs, France, 1987), DESY/87-046 (1987); in: Proc. Physics in Collision VI Conf. (Chicago, 1986), DESY/86-136 (1986).
[24] J.P. Alexander, G. Bonvicini, P.S. Drell and R. Frey, Phys. Rev. D 37 (1988) 56.
[25] J.L. Siegrist et al., Phys. Rev. D 26 (1982) 969.
[26] R. Partridge et al., Phys. Rev. Lett. 45 (1980) 1150.
[27] B.W. Lee, in: High Energy Physics and Elementary Particles, lectures presented at the International Centre for Theoretical Physics (Trieste, Italy, 1965), eds C. Fronsdal and A. Salam (International Atomic Energy Agency, Vienna, 1965) p. 371.
[28] W.S. Hou and A. Soni, Phys. Rev. D 29 (1984) 101.
[29] For an introduction to basic models see: E. Leader and N. Predazzi, An Introduction to Gauge Theories and the New Physics (Cambridge Univ., London, 1982);
F.E. Close, An Introduction to Quarks and Partons (Academic Press, London, 1979);
the properties of hadrons in the quark model are, e.g., reviewed in: A.W. Hendry and D.B. Lichtenberg, Fortschr. Phys. 33 (1985) 139; for a comprehensive review of meson spectroscopy see refs. [361, 362].
[30] For early references see: M. Falcioni et al., Phys. Lett. B 110 (1982) 295;
K. Ishikawa, G. Schierholz and M. Teper, Phys. Lett. B 110 (1982) 399;
B. Berg, A. Billoire and C. Rebbi, Ann. Phys. 142 (1982) 185;
see also: T.A. De Grand, Phys. Rev. D 36 (1987) 176, and references therein.
[31] For an introduction to lattice gauge theories see, e.g.: J.B. Kogut, Rev. Mod. Phys. 51 (1979) 659; 55 (1983) 775;
R. Gupta, LA-UR 87-2464 (1987).
[32] B.A. Berg et al., Phys. Rev. Lett. 57 (1986) 400;
K. Ishikawa et al., Z. Phys. C 19 (1983) 327;
J. Koller and P. Baal, Phys. Rev. Lett. 58 (1987) 2511;
R.V. Gavai et al., Phys. Lett. B 190 (1987) 182;
M. Albanese et al., Phys. Lett. B 192 (1987) 163;
S.A. Chin, C. Long and D. Robson, Texas A&M Univ. preprint CTP-TAMU-26/87 (1987);
C. Michael, Liverpool preprint, LTH 189 (1987);
G. Schierholz, in: Intern. Symp. on Field Theory on the Lattice (Seillac, France, 1987), Nucl. Phys. B (Proc. Suppl.) 4 (1988) 11, preprint DESY 87-157 (1987).
[33] P. de Forcrand, G. Schierholz, H. Schneider and M. Teper, Phys. Lett. B 152 (1985) 107; Z. Phys. C 31 (1986) 87.
[34] A. Le Yaouanc, L. Oliver, O. Pène and J.-C. Raynal, Orsay preprint LPTHE-Orsay 88/21 (1988).
[35] M. Albanese et al., Phys. Lett. B 192 (1987) 163.
[36] J.F. Donoghue, K. Johnson and B.A. Li, Phys. Lett. B 99 (1981) 416;
M.S. Chanowitz and S.R. Sharpe, Nucl. Phys. B 222 (1983) 211;
C.E. Carlson, T.H. Hansson and C. Peterson, Phys. Rev. D 30 (1984) 1594.
[37] R. Jaffe, in: Proc. Intern. School of Subnuclear Physics 17 (Erice, 1979), ed. N. Zichichi, p. 99.
[38] T. Barnes, Z. Phys. C 10 (1981) 275;
J.M. Cornwall and A. Soni, Phys. Lett. B 120 (1983) 431.
[39] J. Ellis and J. Lanik, Phys. Lett. B 150 (1985) 289;
M.A. Shifman, Z. Phys. C 9 (1981) 347;
H. Gomm and J. Schechter, Phys. Lett. B 158 (1985) 449.
[40] V.A. Novikov et al., Nucl. Phys. B 191 (1981) 301;
S. Narrison, Z. Phys. C 26 (1984) 209.
[41] N. Isgur and J. Paton, Phys. Rev. D 31 (1985) 2910.
[42] N. Isgur, R. Kokoski and J. Paton, Phys. Rev. Lett. 54 (1985) 869.

[43] R. Jaffe and K. Johnson, Phys. Lett. B 60 (1976) 201;
R. Jaffe, Phys. Rev. D 15 (1977) 267, 281;
R. Jaffe and F. Low, Phys. Rev. D 19 (1979) 2105.
[44] Early references to hybrid states can be found in: D. Horn and J. Mandula, Phys. Rev. D 17 (1982) 898;
P. Hasenfratz et al., Phys. Lett. B 95 (1980) 299;
F. de Viron and J. Weyers, Nucl. Phys. B 185 (1981) 391.
[45] T. Barnes and F. Close, Phys. Lett. B 116 (1982) 365;
M.S. Chanowitz and S.R. Sharpe, Nucl. Phys. B 222 (1983) 211; Phys. Lett. B 132 (1983) 413;
T. Barnes, F. Close and F. de Viron, Nucl. Phys. B 224 (1983) 241;
M. Flensburg, C. Peterson and L. Sköld, Z. Phys. C 22 (1984) 293.
[46] B.A. Campbell, Phys. Lett. B 142 (1984) 291.
[47] I.I. Balitsky, D.I. Dyakonov and A.V. Yung, Phys. Lett. B 111 (1982) 71;
J. Govaerts et al., Phys. Lett. B 128 (1983) 262; Nucl. Phys. B 248 (1984) 1;
J.I. Latorre et al., Z. Phys. C 34 (1987) 347.
[48] M.S. Chanowitz, Berkeley preprint LBL-23437; in: Proc. Second Intern. Conf. on Hadron Spectroscopy (KEK, Tsukuba, Japan, 1987).
[49] B.A. Li and K.F. Liu, Phys. Rev. D 30 (1984) 613; Phys. Lett. B 134 (1984) 128.
[50] M. Fukugita et al., Phys. Lett. B 145 (1984) 93;
J.E. Mandula and N. Papanicolaou, Phys. Lett. B 146 (1984) 422.
[51] R. Petronzio, preprint CERN-TH.4858/87 (1987).
[52] D. Robson, Nucl. Phys. B 130 (1977) 328.
[53] M.S. Chanowitz, in: Proc. 1981 SLAC Summer Institute on Particle Physics; in: Proc. Charm Physics Symp. (Inst. of High Energy Physics, Beijing, China, 1987);
A. Soni, UCLA preprint UCLA-83-TEP-6 (1983).
[54] M.S. Chanowitz and S.R. Sharpe, Nucl. Phys. B 222 (1983) 211.
[55] P. Pascual and R. Tarrach, Phys. Lett. B 113 (1982) 495.
[56] M.S. Chanowitz, in: Proc. XIV Intern. Symp. on Multi-Particle Dynamics at High Energies (Lake Tahoe, 1983), eds P. Yaeger and J.F. Gunion, p. 716.
[57] B.A. Li, Q.X. Shen and K.F. Liu, Phys. Rev. D 35 (1987) 1070.
[58] J.L. Rosner, Phys. Rev. D 24 (1981) 1347;
J.L. Rosner and S.F. Tuan, Phys. Rev. D 27 (1983) 1544.
[59] F. Caruso and E. Predazzi, Z. Phys. C 33 (1987) 569.
[60] SLAC Storage Ring Group, in: Proc. Eighth Intern. Conf. on High Energy Accelerators (CERN, 1971) p. 145;
SPEAR Storage Ring Group, in: Proc. Ninth Intern. Conf. on High Energy Accelerators (SLAC, 1974) p. 37.
[61] F. Amman et al., Lett. Nuovo Cimento 1 (1969) 729; in: Proc. Seventh Intern. Conf. on High Energy Accelerators (Yerevan, 1969) p. 9.
[62] K. Steffen, in: Proc. Seventh Intern. Conf. on High Energy Accelerators (Yerevan, 1969) p. 60;
DESY Storage Ring Group, in: Proc. Ninth Intern. Conf. on High Energy Accelerators (SLAC, 1974) p. 43.
[63] P. Martin, in: Proc. Ninth Intern. Conf. on High Energy Accelerators (Stanford, 1974) p. 49.
[64] W.W. Ash et al., Lett. Nuovo Cimento 11 (1974) 705;
R. Baldini-Celio et al., Lett. Nuovo Cimento 11 (1974) 711;
G. Barbiellini, Lett. Nuovo Cimento 11 (1974) 718.
[65] J.-E. Augustin et al., Phys. Rev. Lett. 34 (1975) 233.
[66] G.S. Abrams et al., Phys. Rev. Lett. 43 (1979) 477, 481;
W. Davies-White et al., Nucl. Instrum. Meth. 160 (1979) 227;
G.S. Abrams et al., IEEE Trans. Nucl. Sci. 25 (1978) 1, 309; 27 (1980) 59.
[67] R. Brandelik et al., Z. Phys. C 1 (1979) 233.
[68] M. Oreglia et al., Phys. Rev. D 25 (1982) 2259;
R. Chestnut et al., IEEE Trans. Nucl. Sci. 26 (1979) 4395;
G.I. Kirkbride et al., IEEE Trans. Nucl. Sci. 26 (1979) 1535;
J. Gaiser et al., IEEE Trans. Nucl. Sci. 26 (1979) 173.
[69] W. Bartel et al., Phys. Lett. B 64 (1976) 483.
[70] L.M. Barkov et al., Nucl. Phys. B 265 (1985) 365.
[71] H.J. Besch et al., Z. Phys. C 8 (1981) 1.
[72] C.J. Biddick et al., Phys. Rev. Lett. 38 (1977) 1324.
[73] E. Hilger et al., Phys. Rev. D 15 (1977) 1324, 1809.
[74] D. Bernstein et al., Nucl. Instrum. Methods 226 (1984) 301, and references quoted therein.
[75] J.-E. Augustin et al., Phys. Scr. 23 (1981) 623.
[76] L. Criegee et al., in: Proc. 1973 Intern. Conf. on Instrum. for High Energy Physics (1973) p. 707;
J. Burmeister et al., Phys. Lett. B 66 (1977) 395.

[77] BEPC Group, in: Proc. 12th Intern. Conf. on High-Energy Accelerators (1983) p. 157.
[78] J.M. Feller et al., IEEE Trans. Nucl. Sci. 25 (1978) 304;
A. Barbaro-Galtieri et al., Phys. Rev. Lett. 39 (1977) 1058.
[79] R.A. Lee, PhD Thesis, SLAC-Report-282 (1985);
C. Edwards et al., Phys. Rev. D 25 (1982) 3065.
[80] T. Himel et al., Phys. Rev. Lett. 45 (1980) 1146.
[81] A.A. Zholenz et al., Phys. Lett. B 96 (1980) 214.
[82] S. Van der Meer, IEEE Trans. Nucl. Sci. 28 (1981) 1994.
[83] C. Baglin et al., Nucl. Phys. B 286 (1987) 592.
[84] Ya.S. Derbenev et al., Part. Accel. 8 (1978) 115.
[85] B. Jean-Marie et al., Phys. Rev. Lett. 36 (1976) 291.
[86] W. Braunschweig et al., Phys. Lett. B 63 (1976) 487.
[87] R. Baldini-Celio et al., Phys. Lett. B 58 (1975) 471.
[88] J.-E. Augustin et al., Phys. Rev. Lett. 34 (1975) 764; SLAC-PUB-1727 (1976).
[89] W. Braunschweig et al., Phys. Lett. B 63 (1976) 115.
[90] G. Gidal et al., Phys. Lett. B. 107 (1981) 153.
[91] B. Alper et al., Nucl. Phys. B 87 (1975) 19.
[92] Whitmore, in: Proc. 19th Intern. Conf. on High Energy Physics (Tokyo, 1978);
V. Karimaki et al., CERN/EP 81-18 (1981).
[93] J.D. Jackson and D.L. Scharre, Nucl. Instrum. Meth. 128 (1975) 13.
[94] E.A. Kuraev and V.S. Fadin, Sov. J. Nucl. Phys. 41 (1985) 466.
[95] M. Greco, G. Pancheri-Srivastava and Y. Srivastava, Nucl. Phys. B 101 (1975) 234; Phys. Lett. B 56 (1975) 367.
[96] F.A. Behrends, C.J.H. Burgers and W.L. van Neerven, Phys. Lett. B 185 (1987) 395.
[97] Y.S. Tsai, SLAC-PUB-3129 (1983).
[98] S.E. Baru et al., Z. Phys. C. 30 (1986) 551.
[99] W. Buchmüller and S. Cooper, MIT preprint MIT-LNS-159 (1987).
[100] M. Bander, B. Klima, U. Maor and D. Silverman, Phys. Rev. D 29 (1984) 2038; Phys. Lett. B 134 (1984) 258.
[101] P. Falkensteiner, D. Flamm and F. Schöberl, Z. Phys. C 23 (1983) 275.
[102] E. Eichten et al., Phys. Rev. D 17 (1978) 3090; D 21 (1980) 203.
[103] S. Jacobs, M.G. Olsson and C. Suchyta III, Phys. Rev. D 33 (1986) 3338.
[104] V.A. Novikov et al., Phys. Rep. 41 (1978) 1;
R.A. Bertelmann, Nucl. Phys. B 204 (1982) 387.
[105] S.N. Gupta, S.F. Radford and W.W. Repko, Phys. Rev. D 26 (1982) 3305; D 30 (1984) 2424.
[106] W. Buchmüller and S.H.H. Tye, Phys. Rev. D 24 (1981) 132.
[107] W. Braunschweig et al., Phys. Lett. B 67 (1977) 243.
[108] R. Barbieri, R. Gatto and E. Remiddi, Phys. Lett. B 106 (1981) 497.
[109] E.D. Bloom and G.W. Peck, Annu. Rev. Nucl. Part. Sci. 33 (1983) 143.
[110] J.-E. Augustin et al., Orsay preprint LAL/85-27 (1985).
[111] A.M. Boyarski et al., Phys. Rev. Lett. 34 (1975) 1357.
[112] R.L. Ford et al., Phys. Rev. Lett. 34 (1975) 604.
[113] A.D. Liberman, in: Proc. Lepton Photon Symp. (Stanford, 1975) p. 55.
[114] C. Bemporad, in: Proc. Lepton Photon Symp. (Standford, 1975) p. 113.
[115] B. Esposito et al., Nuovo Cimento Lett. 14 (1975) 73.
[116] W. Braunschweig et al., Phys. Lett. B 56 (1975) 491.
[117] J.J. Sakurai, Contribution to the Festschrift honoring J. Schwinger, UCLA/78/TEP/20 (1978); in: Schwinger Symp. (1978) p. 300.
[118] S. Okubo, Phys. Rev. D 13 (1976) 1994;
S. Rudaz, Phys. Rev. D 14 (1976) 298;
H. Kowalski and T. Walsh, Phys. Rev. D 14 (1976) 852;
H. Lipkin, Phys. Lett. B 67 (1977) 65.
[119] J.L. Rosner, Phys. Rev. D 27 (1983) 1101.
[120] A. de Rujula, H. Georgi and S.L. Glashow, Phys. Rev. D 12 (1975) 147;
L. Ametller and A. Bramon, Ann. Phys. (NY) 154 (1984) 308.
[121] R.M. Baltrusaitis et al., Phys. Rev. D 32 (1985) 2883.
[122] W. Bartel et al., Phys. Lett. B 64 (1976) 484.
[123] G. Alexander et al., Phys. Lett. B 72 (1978) 493.
[124] A. Falvard, in: Proc. Intern. Europhys. Conf. on High Energy Physics, ed. O. Botner (Uppsala, Sweden, 1987).
[125] H. Jnad, Thesis, Université de Clermont II, Aubiere, France (1987) (in French).
[126] A. Falvard et al., Phys. Rev. D 38 (1988) 2706.

[127] D. Coffman et al., Phys. Rev. D 38 (1988) 2695.
[128] A. Bramon and J. Casulleras, Phys. Lett. B 173 (1986) 97.
[129] S.S. Pinsky, Phys. Rev. D 31 (1985) 1753;
A. Bramon and J. Casulleras, Z. Phys. C 32 (1986) 467.
[130] A. Seiden, in: Proc. VIIth Intern. Workshop on Photon–Photon Collisions (Paris, France, 1986), and Santa Cruz preprint SCIPP 86-58.
[131] J. Olsson, in: Proc. Intern. Symp. on Lepton and Photon Interactions (Hamburg, West Germany, 1987), Nucl. Phys. B (Proc. Suppl.) 3 (1988) 613, and DESY 87-136 (1987).
[132] Particle Data Group, Review of Particle Properties, Rev. Mod. Phys. 56 (1984) p. 151;
N.N. Achasov, S.A. Devyanin and G.N. Shestakov, Sov. Phys. – Usp. 27(3) (1984);
the aspect of two photon decays is discussed, e.g., in: T. Barnes, Phys. Lett. B 165 (1985) 434.
[133] E.P. Shabalin, ITEP-128 preprint (1984);
N.A. Törnqvist, Phys. Rev. Lett. 49 (1982) 624.
[134] R. Jaffe, Phys. Rev. D 15 (1977) 267.
[135] J. Weinstein and N. Isgur, Phys. Rev. Lett. 48 (1982) 659; Phys. Rev. D 27 (1983) 588.
[136] G. Menessier et al., Phys. Lett. B 158 (1985) 153.
[137] K.L. Au, D. Morgan and M.R. Pennington, Phys. Lett. B 167 (1986) 229; Phys. Rev. D 35 (1987) 1633.
[138] S.S. Freyman and A.E. Nazaryan, Yerevan preprint 930(8I)-86 (1986).
[139] M. Svec, J. Physique 46 C2, Suppl. 2 (1985).
[140] G. Gidal et al., Phys. Lett. B 107 (1981) 153.
[141] B. Jean-Marie, in: Proc. XXIIIrd Intern. Conf. on High Energy Physics (Berkeley, CA, 1986), ed. S. Loken (World Scientific, Singapore, 1987).
[142] L. Köpke, in: Proc. XXIIIrd Intern. Conf. on High Energy Physics (Berkeley, CA, 1986), ed. S. Loken (World Scientific, Singapore, 1987), and Santa Cruz preprint SCIPP 86/74.
[143] S.M. Flatté, Phys. Lett. B 63 (1976) 224.
[144] G. Mennessier, Z. Phys. C 16 (1983) 241.
[145] U. Mallik, talk given at the SLAC Summer Institute on Particle Physics (Stanford, 1986), SLAC-PUB-4238 (1987).
[146] N.N. Achasov, S.A. Devyanin and G.N. Shestakov, Sov. J. Nucl. Phys. 32 (1980) 566.
[147] T. Barnes, in: Proc. VIIth Intern. Workshop on Photon–Photon Collisions (Paris, 1986), and Univ. of Toronto preprint UTPT-86-05 (1986).
[148] The possibility of mixing between $f_2(1270)$, $f_2'(1525)$, and $f_2(1720)$ has been discussed in:
H. Schnitzer, Nucl. Phys. B 207 (1982) 131;
J. Rosner, Phys. Rev. D 27 (1983) 1101;
J. Rosner and S.F. Tuan, Phys. Rev. D 27 (1983) 1544;
A. Bramon et al., Z. Phys. C. 28 (1985) 573;
F. Caruso and E. Predazzi, Z. Phys. C 33 (1987) 569.
[149] K. Senba and M. Tanimoto, Phys. Rev. D 26 (1982) 3270.
[150] R. Xu, PhD Thesis, UC Santa Cruz, SCIPP preprint 87/108 (1987) (unpublished).
[151] W. Beusch et al., Phys. Lett. B 25 (1967) 357;
A. Etkin et al., Phys. Rev. D 25 (1982) 1786;
V. Chabaud et al., Nucl. Phys. B 223 (1983) 1;
C. Daum et al., Z. Phys. C 23 (1984) 339.
[152] J.-E. Augustin et al., Z. Phys. C 36 (1987) 369, and references therein.
[153] P. Gavillet et al., Z. Phys. C 16 (1982) 119.
[154] D. Aston et al., Phys. Lett. B 201 (1988) 573.
[155] S. Godfrey and N. Isgur, Phys. Rev. D 32 (1985) 189.
[156] J.J. Becker et al., Phys. Rev. Lett. 59 (1987) 186.
[157] J. Burmester et al., Phys. Lett. B 72 (1977) 135.
[158] N.R. Stanton et al., Phys. Rev. Lett. 42 (1979) 346.
[159] A. Ando et al., Phys. Rev. Lett. 57 (1986) 1296.
[160] H. Grässler et al., Nucl. Phys. B 121 (1977) 189;
S.I. Bitukov et al., Phys. Lett. B 144 (1984) 133.
[161] *Axial-vector*: C. Dionisi et al., Nucl. Phys. B 169 (1980) 1;
T.A. Armstrong et al., Phys. Lett. B 146 (1984) 273;
H. Aihara et al., Phys. Rev. Lett. 57 (1986) 2500;
G. Gidal et al., Phys. Lett. 59 (1987) 2012;
pseudoscalar: P. Baillon et al., Nuovo Cimento 50A (1967) 393;
S.U. Chung et al., Phys. Rev. Lett. 55 (1985) 779;
A. Ando et al., Phys. Rev. Lett. 57 (1986) 1296;
D.F. Reeves et al., Phys. Rev. D 34 (1986) 1960; Phys. Rev. Lett. 57 (1986) 129.

[162] M.S. Chanowitz, Phys. Lett. B 187 (1987) 409.
[163] G. Gidal et al., Phys. Rev. Lett. 59 (1987) 2012.
[164] S.L. Brodsky and G.P. Lepage, Phys. Rev. D 24 (1981) 2848.
[165] G.P. Lepage et al., p. 83; S.L. Brodsky et al., p. 143, and literature quoted therein; in: Proc. Banff Institute on Particles and Fields, eds A.Z. Capri and A.N. Kamal (Plenum, New York, 1983).
[166] L.J. Clavelli and G.W. Intemann, Phys. Rev. D 28 (1983) 2767.
[167] F. Vanucci et al., Phys. Rev. D 15 (1977) 1814.
[168] R.M. Baltrusaitis et al., Phys. Rev. D 32 (1985) 566.
[169] P.M. Ivanov et al., Phys. Lett. B 107 (1981) 297.
[170] B. Jean-Marie, in: Proc. 23rd Intern. Conf. on High Energy Physics (Berkeley, 1986), and Orsay preprint LAL/86-33 (1986).
[171] J. Adler et al., Contributed Paper to 1987 Europhys. Conf. on High Energy Physics (Uppsala, 1987).
[172] S.J. Brodsky and Chueng-Ryong Ji, SLAC-PUB-3747 (1985).
[173] F.E. Close and W.N. Cottingham, Nucl. Phys. B 99 (1975) 61.
[174] L.M. Barkov et al., Nucl. Phys. B 256 (1985) 365;
D. Bisello et al., Orsay preprint LAL 85-15 (1985);
F. Mané et al., Phys. Lett. B 99 (1981) 261;
B. Delcourt et al., Phys. Lett. B 99 (1981) 257;
P.M. Ivanov et al., Phys. Lett. B 107 (1981) 297, and references therein.
[175] L. Martinovic, in: Proc. XXIst Rencontre de Moriond (Les Arcs, France, 1986);
F. Mané et al., Phys. Lett. B 99 (1981) 261;
L.M. Barkov et al., Nucl. Phys. B 256 (1985) 365, and references therein.
[176] J.-E. Augustin et al., in: Proc. XXIst Rencontre de Moriond (Les Arcs, France, 1986) p. 421.
[177] L. Köpke, UC Santa Cruz preprint, SCIPP 86/61 (1986).
[178] H.G. Dosch and D. Gromes, Z. Phys. C 34 (1987) 554.
[179] H.G. Dosch and D. Gromes, Phys. Rev. D 33 (1986) 1378.
[180] G. Karl and S.F. Tuan, Phys. Rev. D 34 (1986) 1629.
[181] G. Karl and W. Roberts, Phys. Lett. B 144 (1984) 263.
[182] W.-S. Hou and A. Soni, Phys. Rev. Lett. 50 (1983) 569;
P.G.O. Freund and Y. Nambu, Phys. Rev. Lett. 34 (1975) 1645;
S.J. Brodsky and G.P. Lepage, Phys. Rev. Lett. 59 (1987) 621.
[183] H.J. Besch et al., Phys. Lett. B 78 (1978) 347.
[184] I. Peruzzi et al., Phys. Rev. D 17 (1978) 2901.
[185] M.W. Eaton et al., Phys. Rev. D 29 (1984) 804.
[186] P. Henrard et al., Nucl. Phys. B 292 (1987) 670.
[187] P. Henrard, PhD Thesis, Université de Clermont II (1987) (in French).
[188] D. Pallin et al., Nucl. Phys. B 292 (1987) 653.
[189] J.S. Brown, PhD Thesis, Univ. of Washington UMI 84-19117-mc (unpublished).
[190] L. Köpke, Talk given at XXIIIrd Intern. Conf. on High Energy Physics (Berkeley, CA, 1986).
[191] M. Claudson, S.L. Glashow and M.B. Wise, Phys. Rev. D 25 (1982) 1345.
[192] C. Carimalo, Int. J. Mod. Phys. A 2 (1987) 249.
[193] N.A. Törnquist, Found. Phys. 11 (1981) 171; Univ. of Helsinki preprint HU-TFT-86-12 (1986) (see also references therein).
[194] A. Einstein, B. Podolski and N. Rosen, Phys. Rev. 47 (1935) 777.
[195] M.H. Tixier, in: Proc. Conf. on Microphysical Reality and Quantum Formalism, eds. A. van der Merwe et al. (Kluwer Academic, 1988) p. 361; DM2 Collab., M.H. Tixier et al., Phys. Lett. B 212 (1988) 523.
[196] J.-G. Körner, Z. Phys. C 33 (1987) 529.
[197] J.-G. Körner and M. Kuroda, Phys. Rev. D 16 (1977) 2165.
[198] S. Meshkov, W.F. Palmer and S.S. Pinsky, DOE/ER/01545-382 (1986);
D. Caldwell, Contributed Paper to XXIIIrd Intern. Conf. on High Energy Physics (Berkeley, CA, 1986).
[199] H.E. Haber and J. Perrier, Phys. Rev. D 32 (1985) 2961.
[200] H. Genz, M. Malvetti and S. Tatur, Phys. Rev. D 31 (1985) 1751.
[201] V.L. Chernyak and I.R. Zhitnitski, Nucl. Phys. B 246 (1984) 52;
M. Fukugita and J. Kwiecinski, Rutherford Lab. preprint RL-79-045 (1979).
[202] R. Sinha and S. Okubo, Phys. Rev. D 30 (1984) 2333.
[203] C. Jarlskog and H. Pillkuhn, Phys. Lett. 20 (1966) 428; B.R. Martin, Phys. Rev. 138B (1965) 1136.
[204] Abdelkar Dekmouche, PhD Thesis, Université de Clermont II (1987) p. 66 (in French).
[205] N. Isgur, Phys. Rev. D 11 (1975) 3236.
[206] M.S. Chanowitz, J/ψ Physics at BEPC, LBL-17930 (1984), Gluonic States at BEPC, LBL-24355 (1987).
[207] J. Ellis, in: Proc. 6th SLAC Summer Institute on Particle Physics, ed. M. Zipf, SLAC-PUB 2177 (1978) p. 69.

[208] T. Goldman and H.E. Haber, Los Alamos preprint LA-UR-83-2323 (1983).
[209] M. Roos, Helsinki preprint HU-TFT 80-5 (1980).
[210] A.D. Linde, JETP Lett. 23 (1976) 64;
S. Weinberg, Phys. Rev. Lett. 36 (1976) 294.
[211] T. Goldman and H.E. Haber, Physica D 15 (1985) 181.
[212] C. Edwards et al., Phys. Rev. Lett. 48 (1982) 903.
[213] S. Weinberg, Phys. Rev. Lett. 40 (1978) 223.
[214] R.D. Peccei and H.R. Quinn, Phys. Rev. Lett. 38 (1977) 1440; Phys. Rev. D 16 (1977) 1791.
[215] H. Faissner et al., Phys. Lett. B 103 (1981) 234.
[216] K. Königsmann, in: Proc. Intern. Symp. on The Production and Decay of Heavy Flavours (Stanford, 1987), and preprint DESY 87-151 (1987).
[217] D.J. Bechis et al., Phys. Rev. Lett. 42 (1979) 1511;
J.L. Vuilleumier et al., Phys. Lett. B 101 (1981) 341;
J. Frère et al., Phys. Lett. B 103 (1981) 129;
M. Wise et al., Phys. Lett. B 103 (1981) 121;
A. Zehnder et al., Phys. Lett. B 104 (1981) 494.
[218] F. Wilczek, Phys. Rev. Lett. 40 (1978) 279.
[219] M. Dine, W. Fischler and M. Srednicki, Phys. Lett. B 104 (1981) 199;
M.B. Wise, H. Georgi and S.L. Glashow, Phys. Rev. Lett. 47 (1981) 402.
[220] A. Grunberg, Phys. Rev. D 29 (1984) 2315.
[221] M.T. Ronan et al., Phys. Rev. Lett. 44 (1980) 367.
[222] G.S. Abrams et al., Phys. Rev. Lett. 44 (1980) 114;
D.L. Scharre et al., Phys. Rev. D 23 (1981) 43.
[223] S.J. Brodsky et al., Phys. Lett. B 73 (1978) 203.
[224] E.D. Bloom, in: Aspen Winter Conf. (1985), and SLAC-PUB-3573 (1985);
E.D. Bloom, J. Physique C3 (1982) 407.
[225] J.L. Rosner, Concluding Talk at Hadron 87, Second Intern. Conf. on Hadron Spectroscopy (KEK, Tsukuba, Japan, 1987), and references therein.
[226] A. Billoire, R. Lacaze, A. Morel and H. Navelet, Phys. Lett. B 80 (1979) 381.
[227] J.G. Körner, J.H. Kühn, M. Krammer and H. Schneider, Nucl. Phys. B 229 (1983) 115.
[228] L.D. Landau, Sov. Phys. - Dokl. 60 (1948) 207;
C.N. Yang, Phys. Rev. 77 (1950) 242.
[229] A. Ore and J.L. Powell, Phys. Rev. 75 (1949) 1696;
M. Krammer and H. Krasemann, XVIIIth Schladming lectures (Schladming, Austria, 1979), Acta Phys. Austr. Suppl. XXI (1979) 259.
[230] R. Partridge et al., Phys. Rev. Lett. 45 (1980) 1150.
[231] T. Himel et al., Phys. Rev. Lett. 45 (1980) 1146.
[232] R.M. Baltrusaitis et al., Phys. Rev. Lett. 52 (1984) 2126.
[233] D. Bisello et al., Phys. Lett. B 179 (1986) 289.
[234] R.M. Baltrusaitis et al., Phys. Rev. D 33 (1986) 629.
[235] B. Jean-Marie, in: Proc. 23rd Intern. Conf. on High Energy Physics (Berkeley, 1986), and Orsay preprint LAL/86-29 (1986).
[236] D. Bisello et al., Phys. Lett. B 200 (1988) 219.
[237] C. Quigg and J.L. Rosner, Phys. Rev. D 16 (1977) 1497.
[238] M. Gell-Mann, CTLS-20, published in: The Eightfold Way (Benjamin, New York, 1964);
S. Okubo, Prog. Theor. Phys. 27 (1962) 949.
[239] For a derivation of the Gell-Mann–Okubo mass formula, see, e.g.: F.E. Close, An Introduction to Quarks and Leptons (Academic Press, London, 1979) pp. 77, 406.
[240] J.F. Donoghue, B.R. Holstein and Y.C.R. Lin, Phys. Rev. Lett. 55 (1985) 2766;
J. Gasser and H. Leutwyler, Nucl. Phys. B 250 (1985) 465;
G. Grunberg, Phys. Lett. B 168 (1986) 141.
[241] F. Gilman and R. Kauffman, Phys. Rev. D 36 (1987) 2761.
[242] S. Weinberg, Phys. Rev. D 11 (1975) 3583;
H. Fritzsch, M. Gell-Mann and H. Leutwyler, Phys. Lett. B 47 (1973) 365;
G.'t Hooft, Phys. Rev. Lett. 37 (1976) 8; Phys. Rev. D 14 (1976) 3432;
R. Crewther, Phys. Lett. B 70 (1977) 349; Riv. Nuovo Cimento 2 (1979) 63.
[243] F. Couchot, PhD Thesis, Université de Paris-Sud, Orsay preprint LAL 87-55 (1987).
[244] W. Bartel et al., Phys. Lett. B 64 (1976) 483; B 66 (1977) 489.
[245] J.-E. Augustin et al., to be published.
[246] D.L. Scharre et al., in: Proc. XIVth Rencontre de Moriond (Les Arcs, France, 1979), and SLAC-PUB-2321.

[247] E.D. Bloom and C.W. Peck, Annu. Rev. Nucl. Part. Sci. 33 (1983) 143.
[248] K. Königsmann, in: Proc. XVIIth Rencontre de Moriond (Les Arcs, France, 1982), and SLAC-PUB-2910 (1982).
[249] R.A. Lee, PhD Thesis, Stanford, SLAC-Report No. 282 (1985).
[250] W. Toki, in: 1983 SLAC Summer Inst., SLAC-Report No. 267 (1983) p. 471.
[251] J.D. Richmann, PhD thesis, Caltech preprint CALT-68-1231 (1985); in: Proc. XXth Rencontre de Moriond (Les Arcs, France, 1985).
[252] B. Guberina and J.H. Kühn, Nuovo Cimento Lett. 32 (1981) 295.
[253] V.A. Novikov et al., Phys. Lett. B 86 (1979) 347; Nucl. Phys. B 165 (1980) 55.
[254] H. Fritzsch and J.D. Jackson, Phys. Lett. B 66 (1977) 365.
[255] H.E. Haber and J. Perrier, Phys. Rev. D 32 (1985) 2961.
[256] A. Seiden, H. Sadrozinski and H. Haber, Phys. Rev. D 38 (1988) 824.
[257] A. Bramon and J. Casulleras, Z. Phys. C 32 (1986) 467.
[258] Quotation without reference in: F. Couchot, Orsay preprint LAL 87-40 (1987).
[259] J.C. Sens, in: Proc. Physics in Collision V Conf. (Autun, France, 1985), and SLAC-PUB-3754 (1985).
[260] G. Alexander et al., Phys. Lett. B 72 (1978) 493; B 76 (1978) 652.
[261] R. Brandelik et al., Phys. Lett. B 74 (1978) 292.
[262] C. Edwards et al., Phys. Rev. D 25 (1982) 3065.
[263] C. Edwards et al., Phys. Rev. Lett. 48 (1982) 458.
[264] M.E.B. Franklin, PhD Thesis, SLAC-Report No. 254 (1982);
D.L. Scharre, in: Proc. 10th Intern. Symp. on Lepton and Photon Interactions at High Energy (Bonn, 1981), ed. W. Pfeil.
[265] R.M. Baltrusaitis et al., Phys. Rev. D 35 (1987) 2077;
K.F. Einsweiler, PhD Thesis, SLAC-Report No. 272 (1984).
[266] J.-E. Augustin et al., Z. Phys. C 36 (1987) 369.
[267] J.-E. Augustin et al., Phys. Rev. Lett. 60 (1988) 2238.
[268] H.J. Lipkin and H.R. Rubinstein, Phys. Lett. B 76 (1978) 324.
[269] L. Montanet, Rep. Prog. Phys. 46 (1983) 337.
[270] J.G. Körner, J.H. Kühn and H. Schneider, Phys. Lett. B 120 (1983) 444.
[271] M. Krammer, Phys. Lett. B 74 (1978) 361.
[272] B.A. Li and Q.X. Shen, Phys. Lett. B 126 (1983) 125.
[273] F.E. Close, Phys. Rev. D 27 (1983) 311.
[274] A. Bramon, R. Casas, J. Casulleras and F. Cornet, Z. Phys. C 28 (1985) 573.
[275] J.J. Becker et al., Contributed Paper to 23rd Intern. Conf. on High Energy Physics (Berkeley, CA, 1986), and SLAC-PUB-4243 (1987).
[276] J. Körner and M. Krammer, Z. Phys. C 16 (1983) 279.
[277] W. Wisniewski, in: Proc. 2nd Intern. Conf. on Hadron Spectroscopy (KEK, Tsukuba, Japan, 1987), and Caltech preprint CALT-68-1446 (1987).
[278] W. Toki, in: Proc. 2nd Intern. Conf. on Hadron Spectroscopy (KEK, Tsukuba, Japan, 1987), and SLAC-PUB-4360 (1987).
[279] T. Tsuru, in: Proc. 2nd Intern. Conf. on Hadron Spectroscopy (KEK, Tsukuba, Japan, 1987).
[280] D. Bisello et al., Contributed Paper to 1987 Intern. Symp. on Lepton and Photon Interactions at High Energies (Hamburg, 1987).
[281] C. Edwards et al., Phys. Rev. Lett. 51 (1983) 859;
C. Newman-Holmes, in: Proc. 21st Intern. Conf. on High Energy Physics (Paris, France, 1982), and SLAC-PUB-2971 (1982);
E.D. Bloom and C.W. Peck, Annu. Rev. Nucl. Part. Sci. 33 (1983) 143.
[282] J. Becker et al., Contributed Paper to 23rd Intern. Conf. on High Energy Physics (Berkeley, 1986), and SLAC-PUB-4246 (1987).
[283] B. Jean-Marie, in: Proc. 23rd Intern. Conf. on High Energy Physics (Berkeley, 1986).
[284] H. Aihara et al., Phys. Rev. Lett. 57 (1986) 2500.
[285] G. Gidal et al., Phys. Rev. Lett. 59 (1987) 2016.
[286] G. Gidal et al., Phys. Rev. Lett. 59 (1987) 2012.
[287] R. Cahn, Phys. Rev. D 35 (1987) 3342;
F.M. Renard, Nuovo Cimento 80A (1984) 1.
[288] C. Daum et al., Nucl. Phys. B 187 (1981) 1.
[289] M.G. Bowler, Phys. Lett. B 182 (1986) 400, and references therein.
[290] A. Palano, in: Proc. XXIInd Rencontre de Moriond (Les Arcs, France, 1987); extended version in CERN-EP/87-92 (1987).
[291] R. Armenteros et al., in: Intern. Conf. on Elementary Particle Physics (Siena, Italy, 1963);
P. Baillon et al., Nuovo Cimento 50A (1967) 393.
[292] T.A. Armstrong et al., Phys. Lett. B 146 (1984) 273; Z. Phys. C 34 (1987) 23.
[293] D.L. Scharre et al., Phys. Lett. B 97 (1980) 329.
[294] C. Edwards et al., Phys. Rev. Lett. 49 (1982) 259.
[295] S. Berman and M. Jacob, Phys. Rev. 139 (1965) B 1023.
[296] J. Becker, PhD Thesis, Univ. of Illinois Report (1984).

[297] M. Frank, N. Isgur, P. O'Donnell and J. Weinstein, Phys. Lett. B 158 (1985) 442; Phys. Rev. D 32 (1985) 2971;
J. Weinstein, Talk given at the APS Annual Meeting Div. Particles and Fields (Eugene, OR, 1985), and UTPT-85-27 (1985).
[298] S. Meshkov, W.F. Palmer and S.S. Pinsky, in: Proc. DPF Meeting (Salt Lake City, UT, 1987), DPF Conf. (1987) p. 520, and NBS preprint 87-0205.
[299] C. Edwards, PhD thesis, Cal Tech preprint CALT-68-1165 (1985).
[300] J.F. Donoghue, Phys. Rev. D 30 (1984) 114.
[301] C.E. Carlson and T.H. Hansson, Nucl. Phys. B 199 (1982) 441.
[302] T. Barnes and F.E. Close, Rutherford preprint RAL-84-055 (1984).
[303] C. Rosenzweig, Syracuse preprint SU-4217-227 (1982).
[304] K. Senba and M. Tanimoto, Nuovo Cimento Lett. 35 (1982) 295.
[305] S. Iwao, Nuovo Cimento Lett. 35 (1982) 209.
[306] F. Caruso et al., Z. Phys. C 30 (1986) 493.
[307] B. Bagchi and A. Lahiri, J. Phys. G 12 (1986) 479.
[308] M. Frank and P. O' Donnell, Phys. Lett. B 144 (1984) 451.
[309] W.F. Palmer and S.S. Pinsky, Phys. Rev. D 27 (1983) 2219;
W.F. Palmer, S.S. Pinsky and C. Bender, Phys. Rev. D 30 (1984) 1002;
W.F. Palmer and S.S. Pinsky, Phys. Rev. D 36 (1987) 1434.
[310] T.H. Burnett, Mark III Collab., private communication.
[311] H. Aihara et al., Phys. Rev. Lett. 57 (1986) 51.
[312] M.S. Chanowitz, Phys. Lett. B 164 (1985) 379.
[313] T. Bolton, PhD Thesis, SLAC-Report (1988), unpublished.
[314] B.F.L. Ward, Phys. Rev. D 33 (1986) 1900;
B.A.Li, Q.X. Shen and K.F. Liu, Phys. Rev. D 35 (1987) 1070.
[315] G. Costa et al., Nucl. Phys. B 175 (1980) 402;
N.M. Cason et al., Phys. Rev. Lett. 48 (1982) 1316.
[316] W. Beusch et al., Phys. Lett. B 25 (1967) 357;
[317] S. Godfrey, R. Kokoski and N. Isgur, Phys. Lett. B 141 (1984) 439.
[318] T. Barnes and F.E. Close, Nucl. Phys. B 224 (1983) 241.
[319] M.S. Chanowitz, in: 1981 Meeting Div. Particles and Fields Am. Phys. Soc. (Santa Cruz, 1981).
[320] B.A. Li and K.F. Liu, Phys. Rev. D 32 (1985) 308.
[321] J. Weinstein and N. Isgur, Phys. Rev. Lett. 48 (1982) 659.
[322] M.A. Shifman, A.I. Vainshtein and V.I. Zakharov, Nucl. Phys. B 147 (1979) 385;
V.A. Novikov et al., Nucl. Phys. B 165 (1980) 67; B 191 (1981) 301.
[323] H.J. Lipkin, Phys. Lett. B 106 (1981) 114.
[324] H.J. Lipkin, Phys. Lett. B 109 (1982) 326.
[325] F.E. Close, in: Proc. XXIInd Rencontre de Moriond (Les Arcs, France, 1987), and RAL preprint RAL-87-040 (1987).
[326] S. Gershtein et al., Z. Phys. C 24 (1984) 305.
[327] P.M. Fishbane et al., NBS preprint 81-0896 (1981).
[328] S. Meskov, in: Intern. Conf. on Meson Spectroscopy (Upton, NY, 1983);
P.M. Fishbane, UCLA preprint UCLA-82-TEP-18 (1982).
[329] R.M. Baltrusaitis et al., Phys. Rev. Lett. 56 (1986) 107.
[330] N. Wermes, in: Proc. XIXth Rencontre de Moriond (La Plagne, France, 1984), and SLAC-PUB-3312 (1984).
[331] D. Alde et al., Phys. Lett. B 177 (1986) 120.
[332] B.V. Bolonkin et al., Nucl. Phys. B 309 (1988) 426.
[333] R.S. Longacre et al., Phys. Lett. B 177 (1986) 223.
[334] D. Aston et al., Nucl. Phys. B 301 (1988) 525; Phys. Lett. B 215 (1988) 199.
[335] H.E. Haber and G.L. Kane, Phys. Lett. B 135 (1984) 196;
R.S. Willey, Phys. Rev. Lett. 52 (1984) 585;
R.M. Barnett et al., Phys. Rev. D 30 (1984) 1529.
[336] M.S. Chanowitz and S.R. Sharpe, Phys. Lett. B 132 (1983) 413;
B.L. Ward, Phys. Rev. D 31 (1985) 2849.
[337] S. Godfrey et al., Phys. Lett. B 141 (1984) 439.
[338] S. Ono et al., Phys. Rev. D 35 (1987) 933.
[339] M. Shatz, Phys. Lett. B 138 (1984) 209;
S. Pakvasa et al., Phys. Lett. B 145 (1984) 135; Phys. Rev. D 31 (1985) 2378.
[340] S. Behrends et al., Phys. Lett. B 137 (1984) 277;
S. Yousseff et al., Phys. Lett. B 139 (1984) 332;
S.E. Baru et al., Contributed paper to Intern. Symp. on Lepton and Photon Interactions (Hamburg, 1987).

[341] A. Bettini et al., Nuovo Cimento 42 (1966) 695;
H. Braun et al., Nucl. Phys. B 30 (1971) 213.
[342] A. Etkin et al., Phys. Rev. Lett. 49 (1982) 1620; Phys. Lett. B 165 (1986) 217.
[343] R. Brandelik et al., Phys. Lett. B 97 (1980) 448;
D.L. Burke et al., Phys. Lett. B. 103 (1981) 153;
M. Althoff et al., Z. Phys. C 16 (1982) 13;
H.J. Behrend et al., Z. Phys. C 21 (1984) 205.
[344] D.L. Burke et al., Phys. Rev. Lett. 49 (1982) 632.
[345] R.M. Baltrusaitis et al., Phys. Rev. D 33 (1986) 1222.
[346] D. Bisello et al., Contributed Paper to 1987 Intern. Symp. on Lepton and Photon Interactions at High Energies (Hamburg, 1987).
[347] N.P. Chang and C.T. Nelson, Phys. Rev. Lett. 40 (1978) 1617;
T.L. Trueman, Phys. Rev. D 18 (1978) 3423.
[348] G. Eigen, in: Intern. School of Physics with Low Energy Antiprotons (Erice, Sicily, 1987), and Caltech preprint CALT-68-1483 (1988).
[349] N. Wermes, in: Proc. Physics in Collision V Conf. (Autun, France, 1985), and SLAC-PUB-3730 (1985).
[350] R.M. Baltrusaitis et al., Phys. Rev. Lett. 55 (1985) 1723.
[351] D. Bisello et al., Phys. Lett. B 192 (1987) 239.
[352] J.J. Becker et al., Contributed Paper to 23rd Intern. Conf. on High Energy Physics (Berkeley, CA, 1986).
[353] D. Bisello et al., Phys. Lett. B 179 (1986) 294.
[354] J. Adler et al., Contributed Paper to 1987 Europhysics Conf. on High Energy Physics (Uppsala, Sweden, 1987).
[355] M. Burchell, in: Proc. XXIIIrd Rencontre de Moriond (Les Arcs, France, 1988).
[356] C.A. Heusch, in: Proc. XXIIIrd Rencontre de Moriond (Les Arcs, France, 1988).
[357] N.N. Achasov and G.H. Shestakov, Phys. Lett. B 156 (1985) 434.
[358] H. Aihara et al., Phys. Rev. Lett. 57 (1986) 51.
[359] P. Henrard, PCCF RI 87-03 (1987); and in: Proc. XXIInd Rencontre de Moriond (Les Arcs, France, 1987).
[360] P.G.O. Freund, F. Waltz and J. Rosner, Nucl. Phys. B 13 (1969) 237.
[361] B. Diekmann, Phys. Rep. 159 (1988) 99, and references therein.
[362] S.U. Chung, preprint BNL 40599 (1987), submitted to Rev. Mod. Phys., and references therein.
[363] H. Kolanoski, Springer Tracts in Modern Physics, Vol. 105 (1984) p. 187;
C. Berger and W. Wagner, Phys. Rep. 146 (1987) 1, and references therein.
[364] H. Fritzsch and P. Minkowski, Nuovo Cimento 30A (1975) 393.
[365] M.S. Chanowitz, in: Proc. 6th Intern. Workshop on Photon–Photon Collisions, ed. R.L. Lander (World Scientific, Singapore, 1984).
[366] H.J. Lipkin, Phys. Lett. B 171 (1986) 301.
[367] S. Meshkov, W.F. Palmer and S.S. Pinsky, in: Proc. XXIInd Rencontre de Moriond (Les Arcs, France, 1987) p. 683, and preprint NBS 87-0557 (1987).
[368] H.J. Lipkin, Phys. Lett. B 171 (1986) 298.
[369] S. Meshkov, in: Proc. Aspen Winter Particle Physics Conf. (1986) p. 87.
[370] V.A. Novikov, M.A. Shifman, A.I. Vainshtein and V.I. Zakharov, Nucl. Phys. B 191 (1981) 301;
A. Soni, Phys. Rev. D 29 (1984) 1424;
M.S. Chanowitz, in: Proc. XIVth Intern. Symp. on Multiparticle Dynamics at High Energies (Lake Tahoe, 1983).
[371] C.A. Heusch, in: XVIIth Intern. Symp. on Multiparticle Dynamics (Seewinkel, Austria, 1986), and UC Santa Cruz preprint SCIPP 86/69 (1986).
[372] B. Jean-Marie, Orsay preprint LAL 86/21 (1986).
[373] S. Protopopescu, in: Proc. 2nd Intern. Conf. on Hadron Spectroscopy (KEK, Tsukuba, Japan, 1987).
[374] D.F. Reeves et al., Phys. Rev. D 34 (1986) 1960.
[375] A recent compilation of model calculations on light quark spectra is: P.J. O'Donnell, in: Workshop on Quarks, Gluons and Hadronic Matter (Cape Town, 1987), and Univ. of Toronto preprint UTPT-87-05 (1987).
[376] J. Field, private communication.
[377] G.J. Gounaris, R. Körgeler and J.E. Paschalis, Phys. Lett. B 186 (1987) 107.
[378] F.G. Binon, Lecture given at Intern. School on Low Energy Antiproton Physics (Erice, Sicily, 1987).
[379] D. Alde et al., Phys. Lett. B 198 (1987) 286.
[380] P.S.L. Booth et al., Nucl. Phys. B 273 (1986) 689;
C. Daum et al., Phys. Lett. B 104 (1981) 246;
T.F. Davenport et al., Phys. Rev. D 33 (1986) 2519.
[381] S.J. Lindenbaum et al., in: Proc. 1987 Europhys. Conf. on High Energy Physics (Uppsala, Sweden, 1987), and preprint BNL-40200.
[382] See, e.g.: S.J. Lindenbaum and R.S. Longacre, Phys. Lett. B 165 (1985) 202, and references therein.
[383] A recent summary of 0^{++} and 2^{++} glueball mass calculations is: C.A. Dominguez, Invited Talk at Intern. Workshop on Quarks, Gluons and Hadronic Matter (Univ. of Cape Town, 1987), and DESY preprint 87-010 (1987).
[384] M. Teper, Phys. Lett. B 185 (1987) 121.

[385] M. Althoff et al., Z. Phys. C 29 (1985) 189.
[386] H. Aihara et al., Phys. Rev. Lett. 57 (1986) 404.
[387] R. Longacre et al., in: Proc. 23rd Intern. Conf. on High Energy Physics (Berkeley, CA, 1986) p. 729.
[388] S.C. Cooper, in: Proc. 23rd Intern. Conf. on High Energy Physics (Berkeley, CA, 1986), and SLAC-PUB-4139 (1986).
[389] G.W. Brandenburg et al., Nucl. Phys. B 104 (1976) 413;
M. Aguilar-Benitez et al., Z. Phys. C 8 (1981) 313.
[390] T. Armstrong et al., Phys. Lett. B 167 (1986) 133.
[391] I.Ya. Pomeranchuk, Zh. Eksp. Teor. Fiz. 30 (1956) 423; 34 (1958) 725 [Sov. Phys. - JETP 3 (1956) 306; 7 (1958) 499];
V.N. Gribov, Zh. Eksp. Teor. Fiz. 41 (1961) 667 [Sov. Phys. - JETP 14 (1962) 478];
G.F. Chew, Rev. Mod. Phys. 34 (1962) 394;
for a review see, e.g.: R.J. Eden, High Energy Collisions of Elementary Particles (Cambridge Univ. Press, 1967).
[392] G. Frye and L. Susskind, Phys. Lett. B 31 (1970) 589.
[393] P.G.O. Freund and Y. Nambu, Phys. Rev. Lett. 34 (1975) 1645.
[394] F.E. Low, Phys. Rev. D 12 (1975) 163;
S. Nussinov, Phys. Rev. Lett. 34 (1975) 1286; Phys. Rev. D 14 (1976) 246.
[395] A. Patel et al., Phys. Rev. Lett. 57 (1986) 1288.
[396] A. Chin and M. Karliner, Phys. Rev. Lett. 58 (1987) 1803.
[397] C.E. Carlson et al., Phys. Lett. B 99 (1981) 353.
[398] P. Pascual and R. Tarrach, Phys. Lett. B 113 (1982) 495;
J. Ellis and J. Lanik, Phys. Lett. B 150 (1985) 289.
[399] F. Binon et al., Nuovo Cimento 78A (1983) 313; 80A (1984) 363; Phys. Lett. B 140 (1984) 264;
D. Alde et al., Nucl. Phys. B 269 (1986) 485.
[400] D. Alde et al., Phys. Lett. B 201 (1987) 160.
[401] D. Alde et al., Phys. Lett. B 182 (1986) 105.
[402] S.J. Lindenbaum, in: Proc. 1985 Europhys. Conf. on High Energy Physics (Bari, Italy, 1985).
[403] B. Jean-Marie, in: Proc. 23rd Intern. Conf. on High Energy Physics (Berkeley, CA, 1986).
[404] A. Pais, Ann. Phys. (NY) 9 (1960) 548.
[405] G.J. Feldman and M.L. Perl, Phys. Rep. 33 (1977) 285.
[406] Mark III Collab., Contributed Paper to 1987 Europhys. Conf. on High Energy Physics (Uppsala, 1987).
[407] R. Eichler et al., Motivation and Design Study for a B-Meson Factory with High Luminosity, SIN preprint PR-86-13 (1986).
[408] J. Kirkby, A τ-Charm Factory at CERN, CERN-EP/87-210 (1987);
J.M. Jowett, CERN preprint CERN LEP-TH/87-56 (1987).
[409] L.G. Landsberg, Serpukov preprint 87-83, submitted to 1987 Europhys. Conf. on High Energy Physics (Uppsala, Sweden, 1987).
[410] E. Gross and E. Duchovni, Phys. Rev. D38 (1988) 2308.
[411] A. Birman et al., Phys. Rev. Lett. 61 (1988) 1557.
[412] G.J. Gounaris and H. Neufeld, Phys. Lett. B 213 (1988) 541;
G.J. Gounaris, Univ. of Thessaloniki preprint UT-TP 88/15 (1988).
[413] K. Ishikawa et al., Phys. Rev. D 37 (1988) 3216.